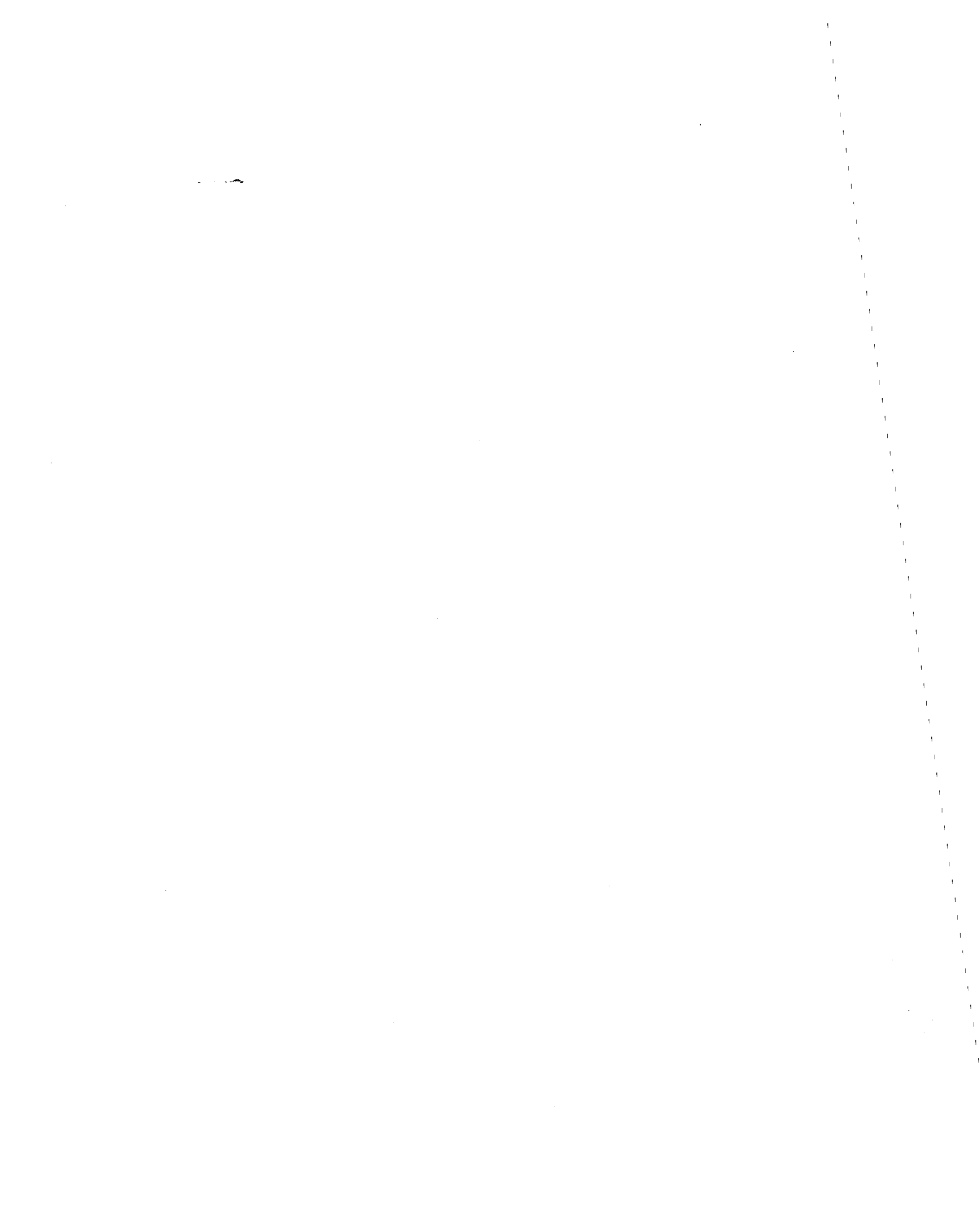


RESPONSE OF MODEL REINFORCED
EARTH WALLS TO SEISMIC LOADING
CONDITIONS

UCLA-ENG-7412
FEBRUARY 1974

G.N. RICHARDSON
K.L. LEE

Report to the
National Science Foundation
Project GI 38983



REPORT DOCUMENTATION PAGE	1. REPORT NO. NSF-RA-E-74-520	2.	3. Recipient's Accession No. PB297749
4. Title and Subtitle Response of Model Reinforced Earth Walls to Seismic Loading Conditions		5. Report Date February 1974	
7. Author(s) C.N. Richardson, K.L. Lee		8. Performing Organization Rept. No. UCLA-ENG 7412	
9. Performing Organization Name and Address University of California Mechanics and Structures Department School of Engineering and Applied Science Los Angeles, California 90024		10. Project/Task/Work Unit No.	
12. Sponsoring Organization Name and Address Engineering and Applied Science (EAS) National Science Foundation 1800 G Street, N.W. Washington, D.C. 20550		11. Contract(C) or Grant(G) No. (C) (G) GI38983	
15. Supplementary Notes		13. Type of Report & Period Covered	
16. Abstract (Limit: 200 words) This report presents the results of ongoing studies aimed at developing a rational design method for reinforced earth retaining walls. The described method is based on results obtained from small laboratory scale walls subjected to horizontal sinusoidal loading with a shaking table. Tests show that the walls respond like a non-linear damped elastic system to the input vibrations. From measurements of the peak tie forces, an empirical design force envelope was developed which is a function only on input acceleration. It is suggested that the design earth pressures for an actual wall subjected to earthquake loading be based on this design force envelope using a base acceleration determined by response spectra modal participation factor techniques. Data are also presented of soil-tie friction under static and vibratory loading. Recommendations are given for calculating the size and spacing of ties including appropriate safety factors. The report is divided into pseudo static studies, vibration studies, and a summary paper.		14.	
17. Document Analysis a. Descriptors Walls Earthquakes Vibration testing Reinforcement (structures) Models Structural engineering Loads (forces) Stressing Earth pressure Forced vibration Earthquake resistant structures b. Identifiers/Open-Ended Terms Seismic response Pseudo static studies c. COSATI Field/Group			
18. Availability Statement NTIS		19. Security Class (This Report) 20. Security Class (This Page) 22. Price PCA13/MF A61	

CAPITAL SYSTEMS GROUP, INC.
6110 EXECUTIVE BOULEVARD
SUITE 250
ROCKVILLE, MARYLAND 20851

Response of Model Reinforced Earth
Walls to Seismic Loading Conditions

by

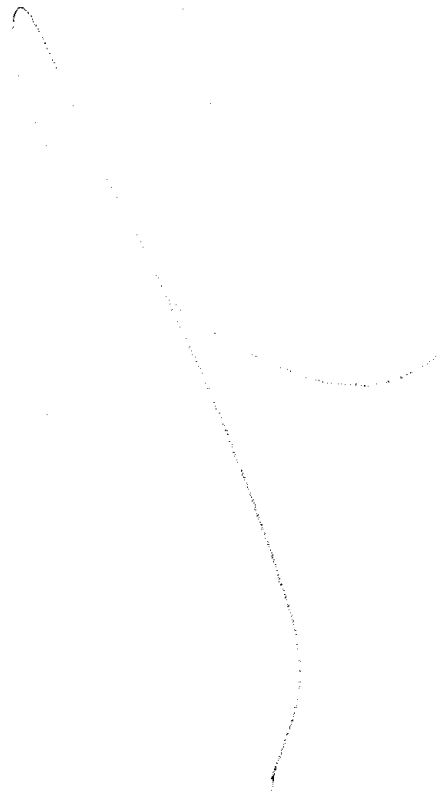
Gregory N. Richardson and Kenneth L. Lee

Report to the
National Science Foundation
Project GI 38983

Principal Investigator: Kenneth L. Lee

Mechanics and Structures Department
School of Engineering and Applied Science
University of California
Los Angeles, California

Any opinions, findings, conclusions
or recommendations expressed in this
publication are those of the author(s)
and do not necessarily reflect the views
of the National Science Foundation.



Foreward

This report presents in three parts, the results of on going studies at UCLA on the subject of Reinforced Earth. Earlier studies at UCLA dealt with the behavior of small, laboratory scale reinforced earth walls during construction. The studies were carried out by two research assistants, Mr. B. D. Adams and Mr. J. J. Vagneron, as part of the requirements for their Master of science degrees at UCLA. The results have been presented in the form of a report to the National Science Foundation and have been summarized in a paper appearing in the November issue of the Journal of the Soil Mechanics and Foundations Division, ASCE. Only static loading was considered in these studies.

Following completion of these static loading studies, preparations were made to extend the investigation to seismic loading conditions, which would eventually lead to a method for designing reinforced earth walls in seismically active areas. As a first step, Mr. Vagneron and Adams carried out some preliminary calculations and experiments involving a pseudo-static approach to the seismic problem. The results of this preliminary study were summarized as an internal laboratory report. It appears as Part I of this report.

During this time a small shaking table was constructed in the Soil Mechanics laboratory for use in carrying out more realistic seismic studies. Mr. Gregory N. Richardson used this shaking table, along with the same box and soil used by Adams and Vagneron, to perform a large number of studies of the response of reinforced earth walls to seismic loading. In addition he performed some preliminary analytical seismic calculations using special computer programs and,

developed a fairly simple preliminary method for designing reinforced earth walls to resist earthquake loading. These studies have been presented to UCLA as a Master of Science thesis, and are presented as Part II of this report.

At the completion of the above mentioned studies, a summary paper was prepared for presentation to a National ASCE meeting in Los Angeles, January 21-25, 1973. In preparation of this paper, it was felt desirable to perform a very few additional tests to clarify some of the previously obtained seismic response data. The significant results of these tests, along with the significant results of the previously mentioned studies are contained in the paper which appears as Part III of this report.

Studies of reinforced earth are continuing at UCLA. Current topics include:

- (i) Improved definition of soil-tie friction.
- (ii) Improved analytical methods of analysis using non-linear finite element techniques for both static and seismic conditions.
- (iii) Preparations for a full scale field test under static and dynamic loading.
- (iv) Reinforced earth slabs over potentially unstable ground.

A major part of the studies reported herein, as well as those currently underway are supported by the National Science Foundation. Grateful appreciation is expressed for this support.

During much of the shaking table studies reported herein, considerable and invaluable assistance was given by Mrs. Kathy Richardson,

wife of the first named author, and by Mr. Bart Patton, Research student at UCLA.

Synopsis

This paper is a summary progress report of ongoing studies at UCLA toward developing a rational design method for reinforced earth retaining walls. The method described herein is based largely on the results obtained from small laboratory scale walls subjected to horizontal sinusoidal seismic loading with a shaking table. The tests showed that the walls responded like a non-linear damped elastic system to the input vibrations. From measurements of the peak tie forces, an empirical design force envelope was developed which is a function only of input acceleration. It is suggested that the design earth pressures for an actual wall subjected to earthquake loading be based on this design force envelope using a base acceleration determined by response spectra modal participation factor techniques. Data are also presented of soil-tie friction under static and vibratory loading. Recommendations are given for calculating the size and spacing of the ties including appropriate factors of safety. The recommendations presented herein are tentative, and must await verification from additional analytical, laboratory and field studies.

Table of Contents

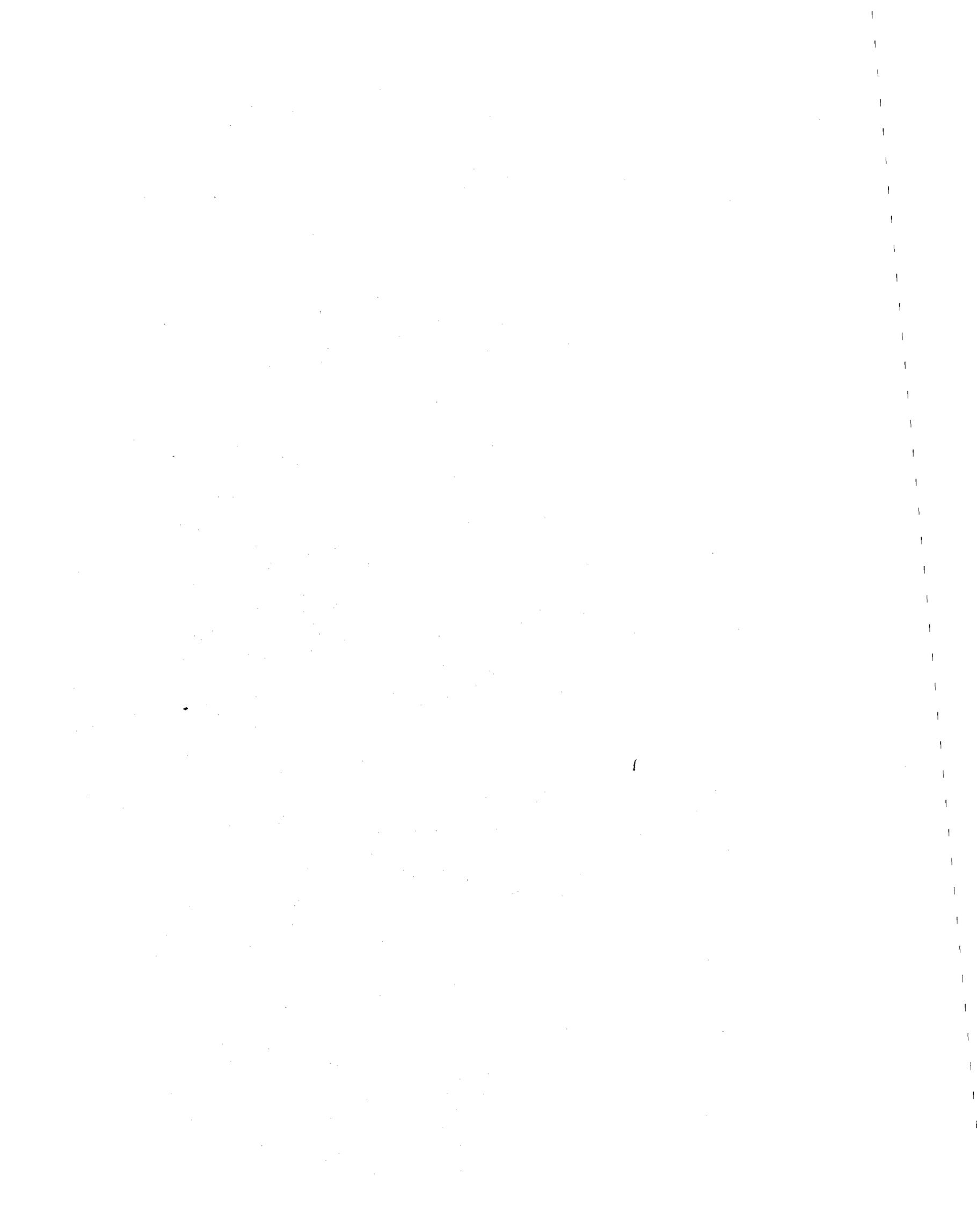
Part I	Pseudo Static Studies by J. J. Vagneron and B. D. Adams
Part II	Vibration Studies by G. N. Richardson
Part III	Summary Paper, Pseudo Static and Vibration Studies by G. N. Richardson and K. L. Lee

X

Part I
Pseudo Static Studies

by

J. J. Vagneron and B. D. Adams



Seismic Stability of Reinforced Earth Walls
Using
Pseudo Static Tilt Up Analyses

by

J. J. Vagneron and B. D. Adams

A Report of a preliminary investigation
of the seismic stability of Reinforced
Earth Retaining Walls by Pseudo
Static Methods

Soil Mechanics Laboratory
Department of Mechanics and Structures
School of Engineering and Applied Science
University of California, Los Angeles

May, 1972

Seismic Stability of Reinforced Earth Retaining Walls
Using Pseudo Static Tilt Up Analyses

by

J. J. Vagneron and B. D. Adams
Research Assistants, Soil Mechanics Laboratory, UCLA

Introduction

At the completion of the studies on reinforced earth walls reported in Ref. 1, it was realized that if such walls were to be built in seismically active areas such as Southern California, they must be designed to be stable under seismic as well as under static conditions. The first approach to this problem was to review the state of the art paper by Seed and Whitman (2) who have summarized the results of pseudo static methods for designing conventional retaining walls. The second step was to perform some additional laboratory tests. As there was no shaking table available at the time, it was decided to use an experimental pseudo-static approach and simulate seismic effects by means of tilting up the box in which a model wall had been previously constructed on a level base. Only a limited number of tests were performed, mostly on an exploratory basis. The results of these studies are summarized in the following pages.

Theoretical Considerations - Pseudo Static Analyses by the Mononobe-Okabe Method

Seed and Whitman (2) have recently reviewed the past historical development and current state-of-the-art procedures for designing retaining walls to resist seismic loads. The oldest and currently most common method of calculating the seismic earth pressures is by

the classical Mononobe-Okabe pseudo static approach. The wall is assumed to yield sufficiently to develop the minimum active earth pressure within a soil wedge as shown on Fig. 1a. From the vibration point of view, the soil within this wedge is assumed to behave as a rigid body so that the accelerations are uniform throughout the mass. Thus the effect of the earthquake is to produce an additional body force $k_h W$ as shown on Fig. 1, where the seismic coefficient $k_h = a/g$, where a is the ground acceleration and g is the acceleration of gravity.

The equilibrium analysis of this force system may be made by the Coulomb method of calculating lateral earth pressures. A general analytical expression for P_{AE} (active + earthquake force) is obtained by writing the equilibrium equation for a trial sliding wedge ABC shown in Fig. 2. The most critical failure plane BC will be found by differentiating P_{AE} with respect to θ . Assuming that the total resulting earth pressure force P_{AE} can be expressed as the result of a pseudo or equivalent fluid pressure which increases linearly with depth, the following expressions are obtained.

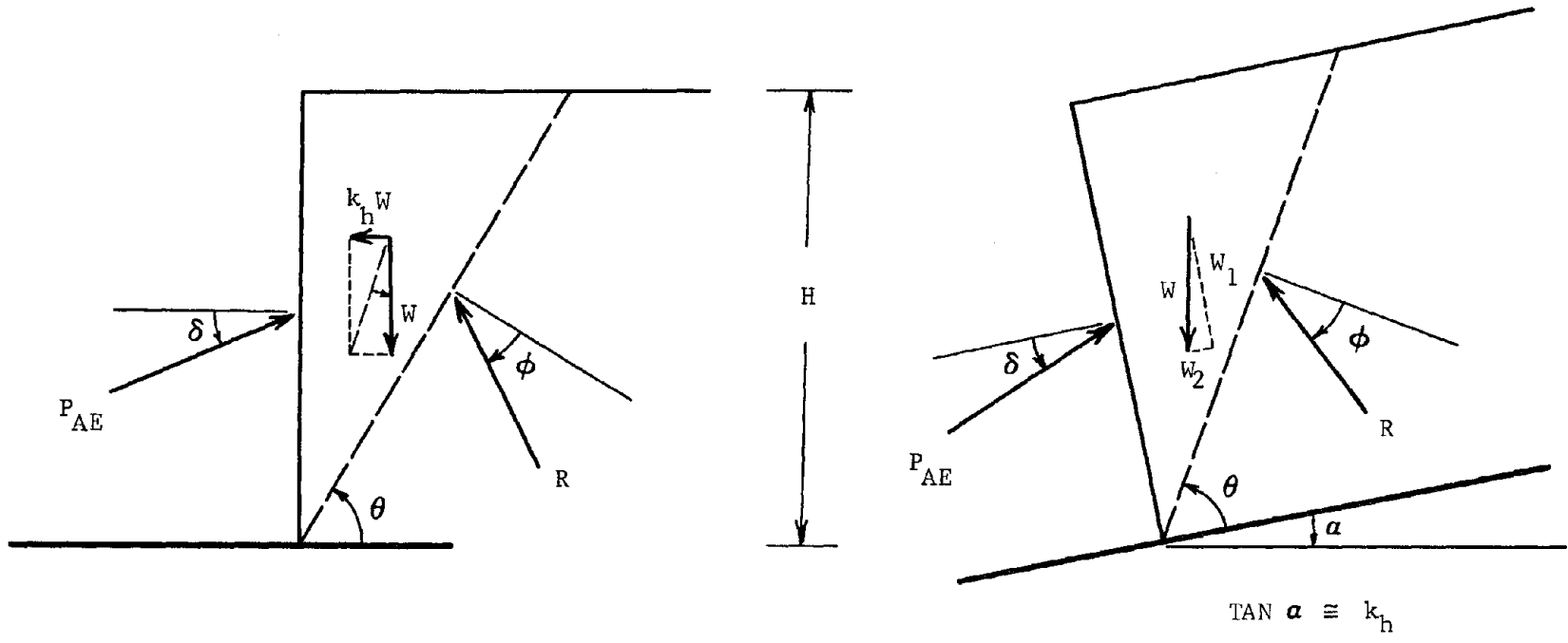
$$P_{AE} = \frac{1}{2} K_{AE} \gamma H^2 \quad (1)$$

where

$$K_{AE} = \frac{\cos^2 (\phi - \mu - \lambda)}{\cos \mu \cos^2 \lambda \cos (\delta + \lambda + \mu) \left[1 + \sqrt{\frac{\sin (\phi + \delta) \sin (\phi - \mu - \beta)}{\cos (\delta + \lambda + \mu) \cos (\beta - \lambda)}} \right]^2}$$

and

$$\mu = \tan^{-1} k_h \quad (2)$$



(A) PSEUDO STATIC

(B) TILT-UP EQUIVALENT

FIGURE 1 PSEUDO STATIC and TILT-UP SEISMIC EARTH PRESSURE ANALYSES

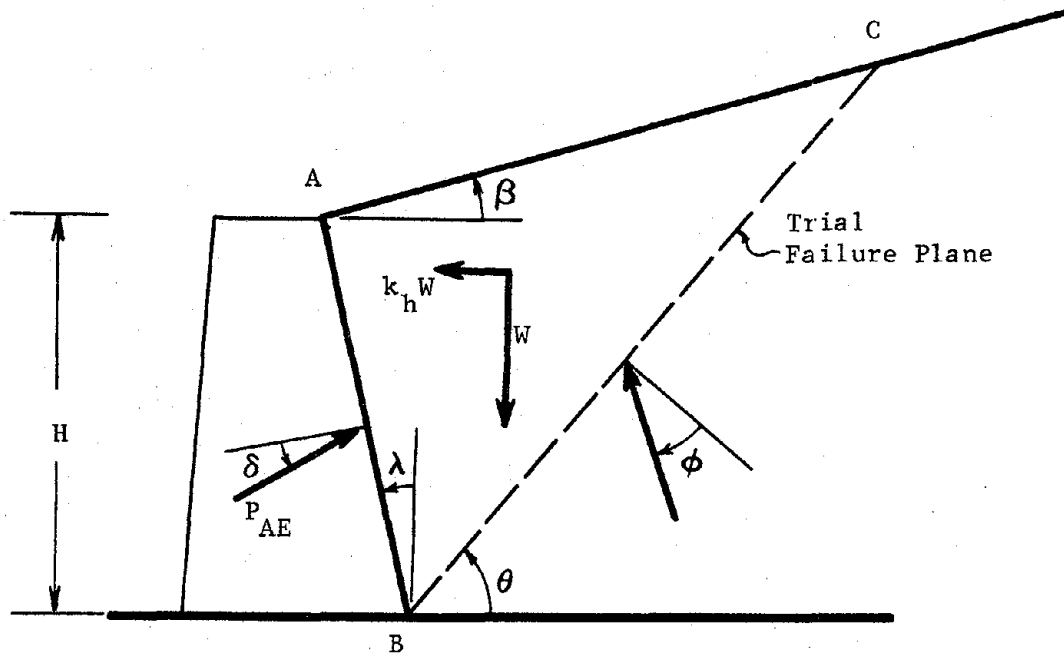


FIGURE 2 QUANTITIES USED IN GENERAL MONONABE-OKABE
PSEUDO STATIC EARTH PRESSURE CALCULATIONS

The meaning of the other symbols are illustrated in Fig. 2.

For the special case of a vertical wall, horizontal backfill and no surcharge, the analysis leads to an involved expression for the slope θ of the most critical failure plane.

$$\sin \theta \cos (\delta + \phi - \theta) \left[k_h \sin(\phi - 2\theta) + \cos(\phi - 2\theta) \right] - \cos(2\theta - \delta - \phi) \left[k_h \cos(\theta - \phi) + \sin(\theta - \phi) \right] = 0 \quad (3)$$

Eq. 3 can only be solved numerically by successive approximations. This has been done for several values of ϕ and δ and the results are shown in Fig. 3. These calculations show that the theoretical position of the failure plane becomes flatter with increasing horizontal seismic coefficient.

Some values of the pseudo-static earth pressure for the special case of vertical wall and horizontal backfill and for various horizontal seismic coefficients are shown in Fig. 4. Note that the horizontal seismic coefficient is defined as

$$(K_{AE})_{\text{Horiz}} = K_{AE} \cos \delta \quad (4)$$

Seed and Whitman have shown that K_{AE} is virtually independent of δ , whereas for low values of k_h , the horizontal component of lateral earth pressure is significantly affected by δ as shown in Fig. 4.

One method of estimating the lateral earth pressures on a reinforced earth wall, which could then be used in designing the ties etc., would be by means of the above described pseudo-static procedure using horizontal earth pressure coefficients and failure wedges as shown in Figs. 3 and 4. Reference to Fig. 4 indicates that for moderate ground accelerations of about 0.3 g, this would lead to tie forces almost double those required for static conditions.

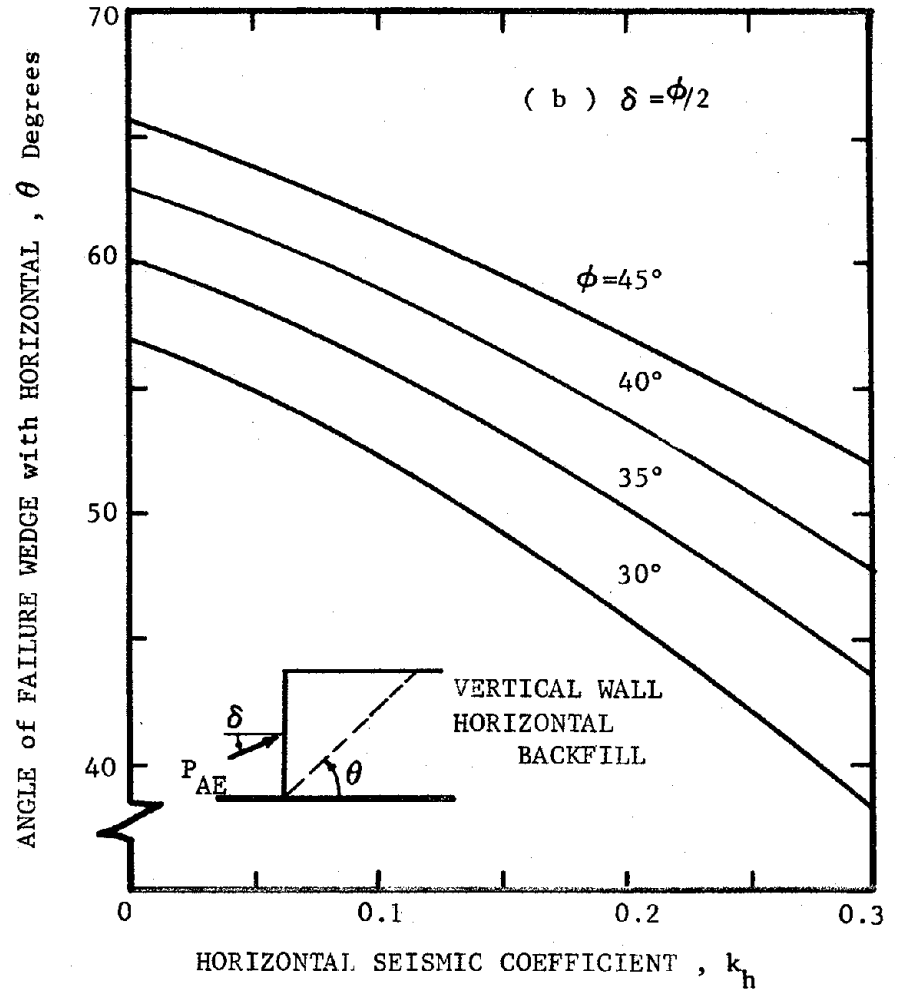
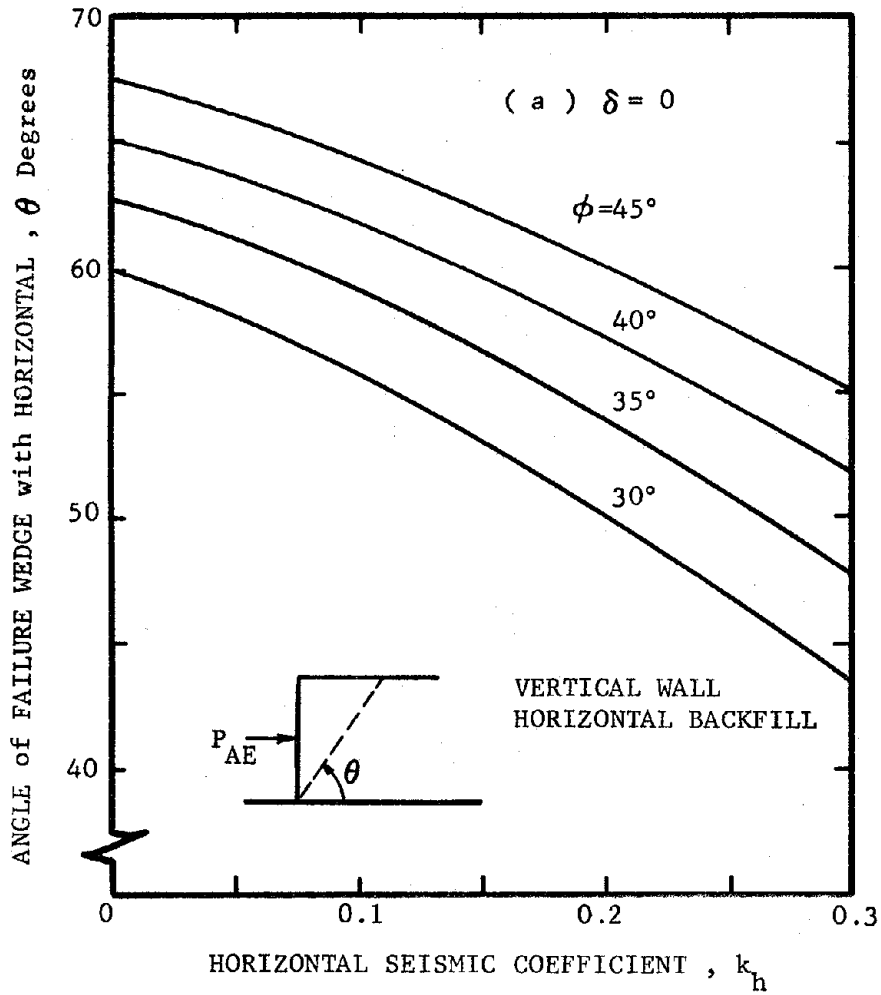


FIGURE 3 THEORETICAL LOCATION OF CRITICAL FAILURE PLANE
 PSEUDO STATIC ANALYSIS

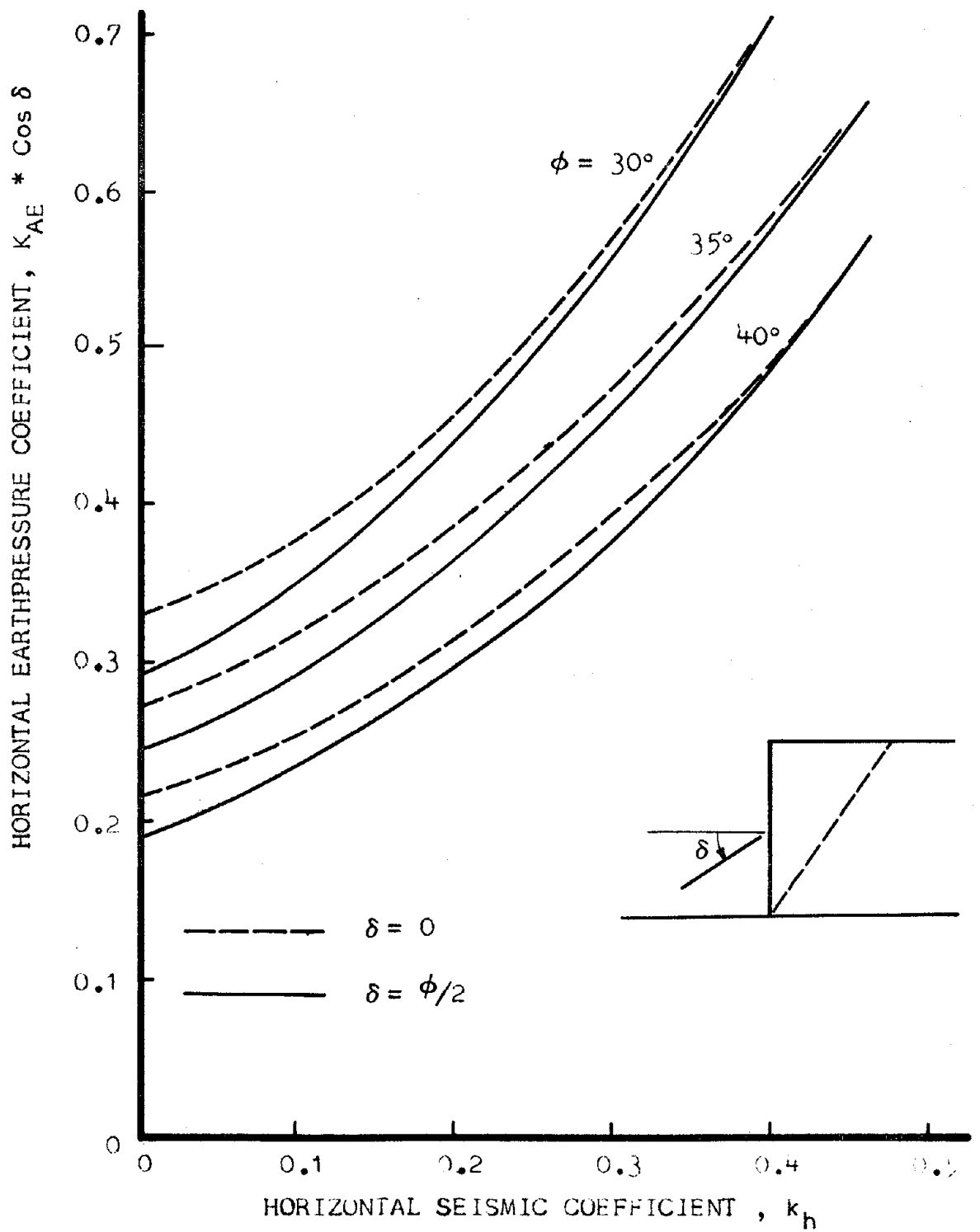


FIGURE 4 THEORETICAL HORIZONTAL EARTH PRESSURE COEFFICIENTS
 PSEUDO STATIC ANALYSIS

Following the static analyses procedures, only the portion of the ties which extend beyond the failure plane are assumed capable of resisting pull out forces. Thus reference to Fig. 3 indicates that the required tie lengths would be considerably greater than for static conditions.

Many model shaking table tests have been performed for conventional and rigid retaining walls, and the results have generally agreed with the Mononobe-Okabe theoretical predictions. However no such tests have been made on reinforced earth walls.

Experimental Studies - Tilt Up Tests

A possible alternative to laboratory shaking table tests is the use of tilt up tests to investigate the seismic behavior of a wall by the pseudo static approach. Such methods have been used by Sultan and Seed (3) to investigate the stability of slopes under static loading. Extension to seismic loading is illustrated in Fig. 1. Tilting the foundation of the wall by a small angle α is approximately equivalent to applying a pseudo static force defined by a horizontal seismic coefficient

$$k_h = \tan \alpha \quad (5)$$

The analogy is as accurate as the assumption that the actual weight of the wedge W is equal to the pseudo weight W_1 normal to the base of the box. For tilt angles less than 18° , the error will be less than 5 percent.

Following the reasoning implied in Fig. 1, tilt up tests were used as a first step in the experimental investigation of the behavior of a reinforced earth wall. The tests were performed using the same

soil, test equipment and construction procedures which were used in the previous laboratory studies (2). The soil was a fine, uniformly graded quartz sand which was deposited by dry raining into the model box. The angle of internal friction at the density of the sand used in the tests was $\phi = 44^\circ$. The model box was 30 in. wide, and 48 in. in length. The skin elements used were 1 in. high curved sections of thin aluminum. The ties were 0.15 in. wide strips of aluminum foil, having a breaking strength of about 536 grams, and a friction angle with the soil of about 31 degrees.

Three tilt up tests were performed. Each test wall was constructed to a predetermined stable height. The rigid base of the box was then tilted slowly until the wall failed. A summary of the test results is shown in Table 1, along with the comparative data from non-tilting tests performed earlier (2). The tilt up tests had significantly longer ties and somewhat closer spacing than required for static stability. The static factors of safety ranged from about 1.12 to 1.65 against a breaking failure, and 2.0 to 2.5 against a pullout failure.

The behavior of the walls during each test was qualitatively similar. As the base was tilted up, the top of the wall moved out. The relative outward tilt just prior to failure ranged from 1.3 to 2.0 percent of the height of the wall. Failure occurred suddenly, but the wall was restrained from large movements so that post-failure conditions could be observed. In each case the failure appeared to be caused by the ties breaking. The broken ties were found in the middle portion of the wall. This is in sharp contrast

to the previous observations from the static tests, where the broken ties were always deep below the lower third point of the wall. Tie force measurements were attempted, but unfortunately, the equipment malfunctioned each time. In one test, good readings were obtained for only the lower ties. Even up to failure, the forces in the lower ties did not approach the ultimate strength of the tie.

From the observations which were made, a value for the horizontal earth pressure coefficient $K_{AE} \cos \delta$ was back calculated for each test at the failure conditions. This calculation was made assuming that the total strength of the wall as defined by P_{AE} at failure would be the same as determined experimentally in the previous static test study (2). Thus knowing P_{AE} for each wall height, the only unknown in Eq. 1 is the seismic earth pressure coefficient.

These back figured values of earth pressure coefficient are shown on Fig. 5. The value for the no-tilt, $\alpha = 0$ case was obtained during the previous testing, and as seen, agrees well with the active earth pressure theory for $\delta = \frac{1}{2} \phi$. The values obtained from the tilt up tests were all lower than predicted by the theory.

Using colored sand marker layers, the location and slope of the outer failure plane was also observed. The measured slopes for the three tilt up and the previous non-tilt up tests are shown on Fig. 6. Again, the non-tilt up data agrees well with the theory. However, the tilt up tests indicate much flatter failure surfaces than predicted.

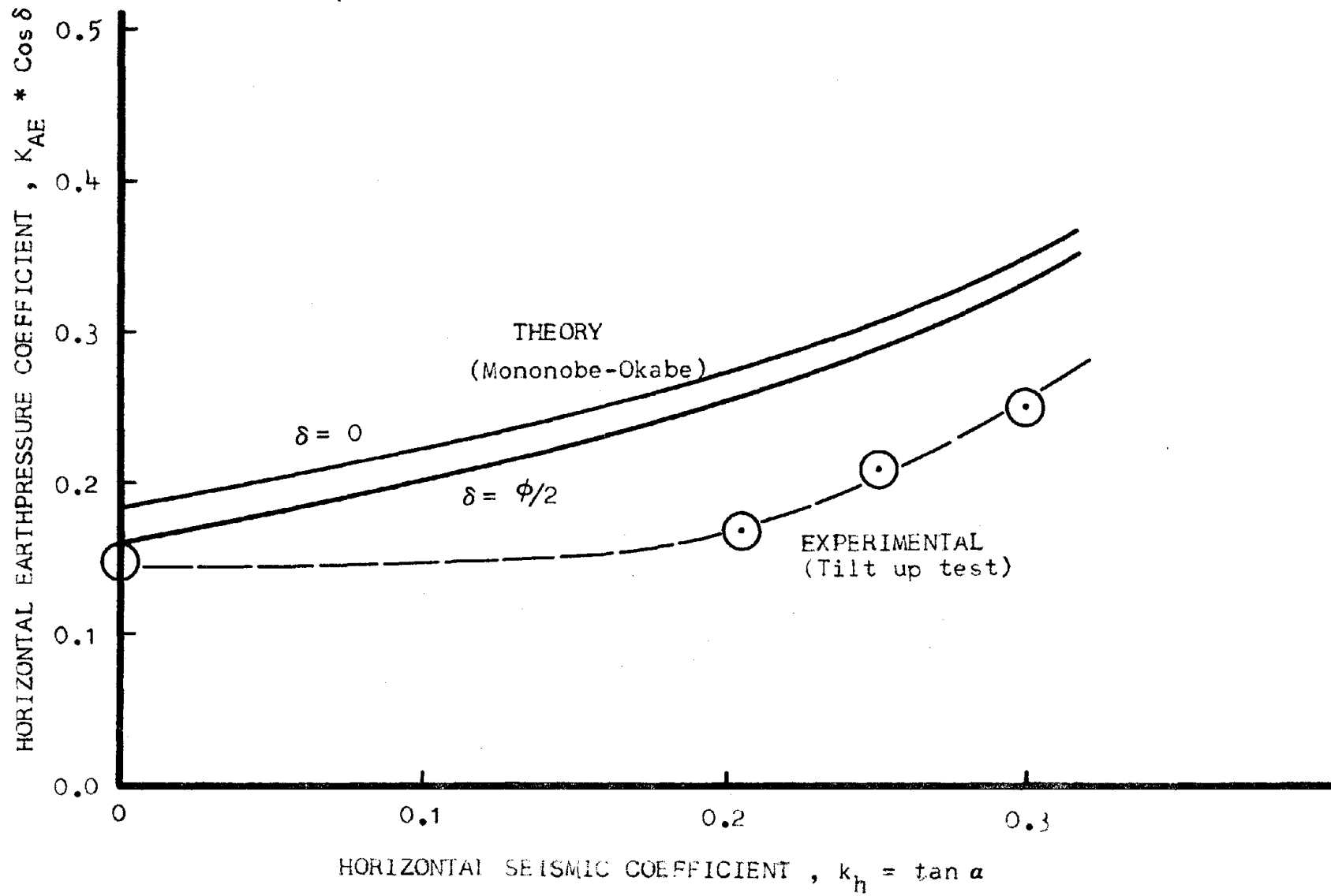


FIGURE 5 PSEUDO STATIC EARTH PRESSURE COEFFICIENTS

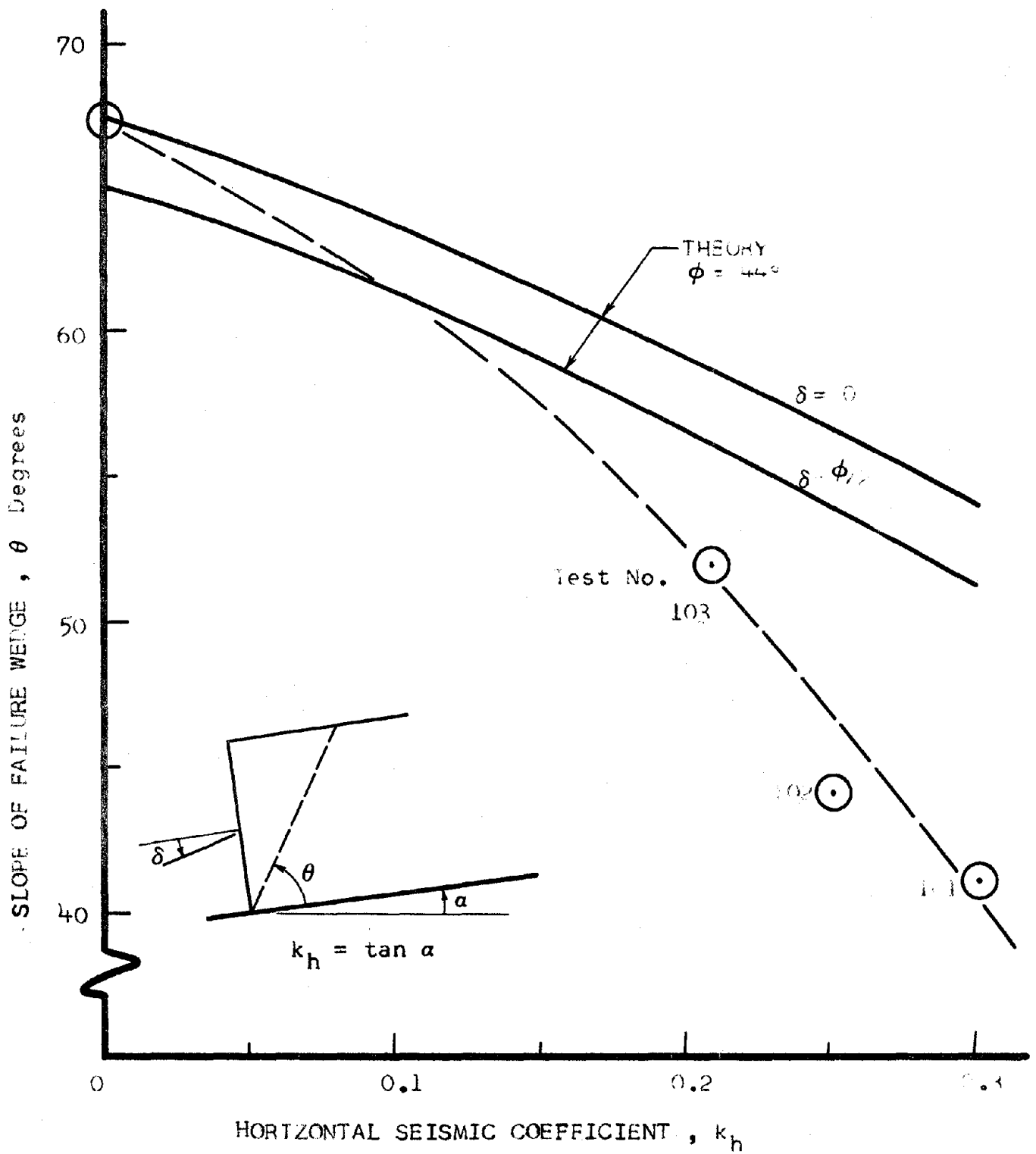


FIGURE 6 INFLUENCE OF PSEUDO STATIC k_h ON THE SLOPE OF THE FAILURE WEDGE

Limitations of the Pseudo Static - Tilt Up Approaches

The above described pseudo static theory and tilt up experimental investigations, while not leading to absolute agreement of numerical values, nevertheless both indicated the similar general trends of the effect of an earthquake on a reinforced earth wall. The earth pressure forces are increased by the seismic loading, especially toward the top of the wall. A larger failure wedge is developed. Thus longer and stronger or more frequent ties are required than for static designs, especially near the top of the wall.

The above described pseudo static methods of investigating the effect of earthquakes on reinforced earth walls have many limitations. Two of the most significant which are apparent at this writing include:

- (i) rigid body motion of the soil in the failure zone rather than damped elastic response
- (ii) continuous, steady, one directional static loading rather than actual cyclic loading

Actual seismic loading will cause the soil behind the wall to respond as a flexible damped elastic structure. The seismic loading will be cyclic, and will have a short and finite duration time. Actual shaking tests are required to investigate the effect of these factors.

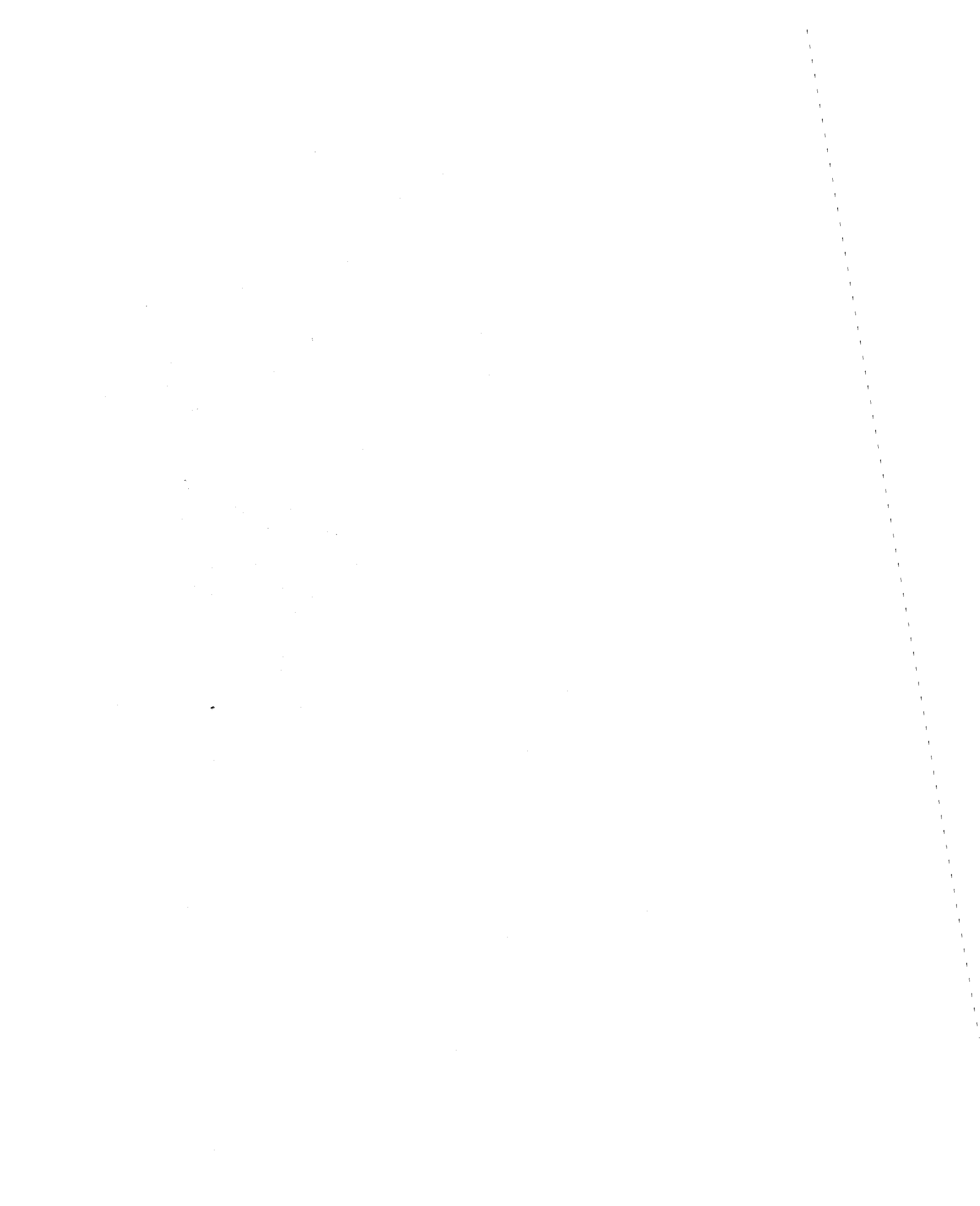
Table 1

Summary of Pseudo Static - Tilt Up Tests

Test No.	Static - No Tilt Tests		Pseudo Static Tilt Up Tests		
	53	Extrapolate	101	102	103
Height - in.	18	18	11	13	16
Length of Ties - in.	12	11	17	20	20
Static - No Tilt FS (a) Tie Breaking (b) Tie Pull Out	1.0 1.1	≅ 1.0 1.0	1.65 2.5	1.38 2.5	1.12 2.0
Tilt up angle, α - deg	0	0	16.5	14	12.5
$k_h = \tan \alpha$	0	0	0.3	0.25	0.21
$K_{AE} \cos \delta$	0.15	0.15	0.25	0.21	0.17
Slope of failure plane θ - deg	67	67	41	44	52

References

1. Lee, Kenneth L., Adams, B. D. and Vagneron, J. J., "Reinforced Earth Walls", Report to the National Science Foundation, UCLA-Eng 7233, April 1972.
2. Seed, H. B. and Whitman, R. V., "Design of Retaining Structures for Dynamic Loads", ASCE Speciality Conference on Lateral Stresses, Cornell University, 1970, pp. 103-147.
3. Sultan, H. A. and Seed, H. B., "Stability of Sloping Core Earth Dams", Journal of the Soil Mechanics and Foundations Division, ASCE, Vol. 93, No. SM4, July 1967, pp. 45-67.



Part II
Vibration Studies

by

G. N. Richardson

UNIVERSITY OF CALIFORNIA

Los Angeles

The Response of Reinforced Earth Walls
to Vibratory Loading

A thesis submitted in partial satisfaction of the
requirements for the degree Master of Science
in Engineering

by

Gregory Neil Richardson

Thesis Committee

C. M. Duke

P. Lade

K. L. Lee, Chairman

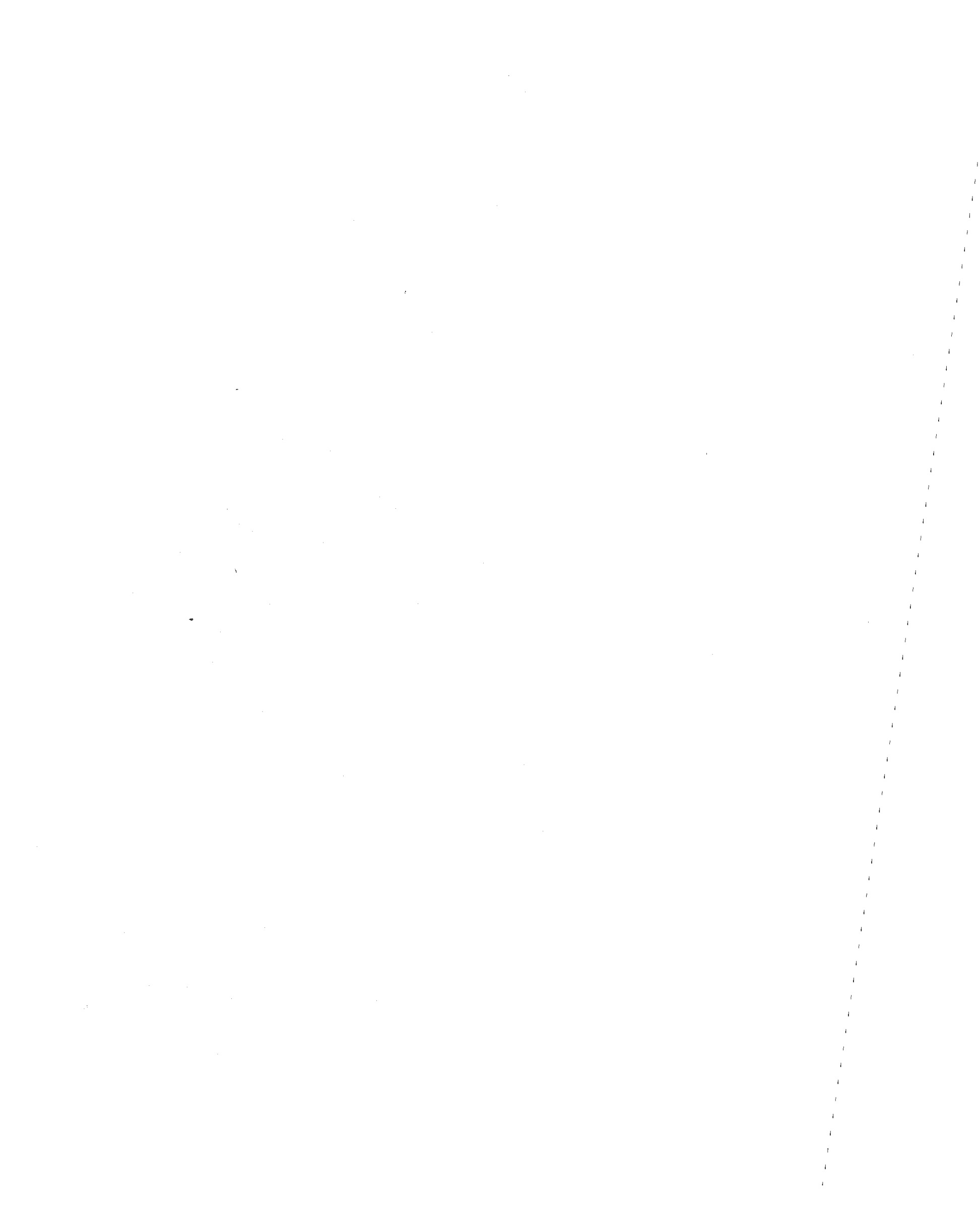


TABLE OF CONTENTS

	<u>Page</u>
LIST OF FIGURES	II-v
LIST OF TABLES	II-ix
ABSTRACT	II-x
CHAPTER 1 INTRODUCTION	
1.1 Reinforced Earth	II-1
1.2 Review of Previous Work	II-3
1.3 The Need for the Investigation of the Dynamic Analysis of Reinforced Earth Walls	II-4
CHAPTER 2 GENERAL THEORY OF REINFORCED EARTH	
2.1 Basic Structural Modeling	II-8
2.2 Possible Failure Modes	II-12
2.3 Static Analysis by Rankine Earth Pressure Theory	II-13
2.4 Static Analysis by Coulomb Earth Pressure Theory	II-18
2.5 Trapezoidal Design Procedure	II-20
CHAPTER 3 TEST EQUIPMENT AND PROCEDURES	
3.1 Dimensional Modeling	II-23
3.2 Reinforced Earth Wall Models	II-26
3.3 Shaking Table	II-32
3.4 Instrumentation	II-35
CHAPTER 4 LABORATORY TEST RESULTS	
4.1 Introduction	II-43
4.2 Series A: Tie Breakage	II-52
4.3 Series B: Tie Pullout	II-63
4.3.1 Series B-1	II-66

	<u>Page</u>
4.3.2 Series B-2	II-80
4.3.3 Series B-3	
4.4 Additional Testing	II-91
4.5 Tie Pullout-Tests	II-111
CHAPTER 5 ANALYTICAL PROCEDURES AND RESULTS	
5.1 Program LEVSFC	II-128
5.2 Finite Element Analysis	II-141
CHAPTER 6 PROPOSED SEISMIC DESIGN PROCEDURE	
6.1 Introduction	II-158
6.2 Equivalent Lateral Earth Pressure	II-159
6.3 Influence of Frequency of Vibration	II-168
6.4 Random Vibration	II-176
6.5 Design Factor of Safety	II-184
6.6 Tie Arrangement Criteria	II-186
6.7 Seismic Design Example	II-190
CHAPTER 7 SUMMARY AND CONCLUSIONS	II-208
REFERENCES	II-215
APPENDIX A: LABORATORY MODEL TESTS	II-218

LIST OF FIGURES

<u>Fig.</u> <u>No.</u>		<u>Page</u>
1.1	Reinforced Earth Wall - Highway 39	II-5
1.2	Major Faults in Southern California	II-6
2.1	Configuration of Structural Components	II-9
2.2	System Forces	II-11
2.3	Rankine Tie Force Calculations	II-15
2.4	Coulomb Theory Variables	II-19
2.5	Trapezoidal Design	II-21
3.1	Ottawa 90 Grain Size Distribution	II-28
3.2	Test Model Box	II-31
3.3	Modifications to Shaking Table	II-33
3.4	MTS Closed-Loop System	II-34
3.5	Acceleration and Displacement Gauges	II-36
3.6	Q-Flex Accelerometer	II-38
3.7	Tie-Tension Gauges	II-39
3.8	Tie-Pullout Device	II-41
4.1	Rankine Static Factor of Safety	II-44
4.2	Basic Terminology	II-50
4.3	Instrumented Tie Failure	II-53
4.4	Tie-Tension Gauge Location	II-55
4.5	Dynamic Tie Fluctuational Force	II-56
4.6	Acceleration Amplification	II-57
4.7	Wall Displacement Record	II-59
4.8	Failure Mechanism	II-60
4.9	Series A-1 Failure Surfaces	II-62

<u>Fig. No.</u>		<u>Page</u>
4.10	Series B Instrumentation	II-64
4.11	Series B Dynamic Tie Tension	II-68
4.12	Tie Tension Measurements, Test No. 3	II-69
4.13	Tie Tension Measurements, Test No. 4	II-71
4.14	Tie Tension Measurements, Test No. 5	II-72
4.15	Failure Mechanism	II-75
4.16	Series B-1 Failure Surfaces	II-77
4.17	Earth Pressure At Rest Design	II-83
4.18	Tie Tension Measurements, Test No. 6	II-84
4.19	Tie Tension Measurements, Test No. 7	II-86
4.20	Failure Wedge Amplification	II-88
4.21	Shear Type Wall Deformation	II-90
4.22	Seismic Design Tie-Force Envelope	II-93
4.23	Tie Tension Measurements, Test No. 8	II-99
4.24	Tie Tension Measurements, Test No. 9	II-100
4.25	Tie Tension Measurements, Test No. 10	II-102
4.26	Tie Tension Measurements, Test No. 11	II-103
4.27	Failure Wedge Analysis	II-106
4.28	Extreme Dynamic Tie Forces verses Seismic Design Envelopes	II-107
4.29	'Pullout' Ties	II-112
4.30	Tie Pullout Record	II-114
4.31	Backwall Pullout	II-115
4.32	Middle-of-Box Pullout	II-116

<u>Fig. No.</u>		<u>Page</u>
4.33	Front-of-Wall Pullout	II-117
4.34	Backwall Pullout Test	II-119
4.35	Middle-of-Box Pullout Test	II-120
4.36	Front-of-Wall Pullout Test	II-121
4.37	Load Deformation Curve From Field Pulling Tests	II-124
4.38	Load Deformation Curve From Field Pulling Tests	II-125
4.39	Summary of Field Pullout Data From Highway 39 Wall	II-126
5.1	Equivalent Damping and Shear Moduli	II-129
5.2	Strain Dependent Moduli	II-131
5.3	Strain Dependent Damping	II-132
5.4	Lumped Mass Model	II-133
5.5	Required Number of Sub-Layers	II-137
5.6	Acceleration Amplification and Shear Deformation	II-138
5.7	Surface Acceleration Amplification	II-140
5.8	Finite Element Model-Series B	II-146
5.9	Surface Accelerations	II-147
5.10	Seismic Tie Forces-Series B	II-148
5.11	Fundamental Periods - Series B	II-152
5.12	Tie Force Along the Ties	II-153
5.13	Finite Element Model-12' Wall	II-154
5.14	Seismic Tie Forces-12' Wall	II-156
6.1	Equivalent Lateral Earth Pressures-Seismic Design Envelopes	II-160
6.2	Comparison of Lateral Earth Pressures	II-162
6.3	Seismic Coefficients	II-164

<u>Fig. No.</u>		<u>Page</u>
6.4	Factored Static Design Envelopes	II-166
6.5	Frequency Response	II-169
6.6	Frequency Corrected-Seismic Design Envelope	II-172
6.7	Extrapolated Frequency Response	II-174
6.8	Chopra-San Fernando Earthquake	II-178
6.9	Pseudo-Acceleration Spectra	II-179
6.10	Modal Participation Factors	II-182
6.11	Reinforced Earth Wall Design Example	II-191
6.12	Design Lateral Earth Pressures-21' Wall	II-194
6.13	Finite Element Model-21' Wall	II-195
6.14	Finite Element Lateral Earth Pressures	II-197
6.15	Seismic Tie Spacing-21' Wall	II-200
6.16	Static Tie Spacing-21' Wall	II-204
6.17	Seismic vs Static Design-21' Wall	II-206

LIST OF TABLES

<u>Table No.</u>		<u>Page</u>
2.1	Possible Failure Modes	II-12
3.1	Dimensional Similitude Requirements	II-24
3.2	Comparison of Dimensional Similitude Ratios	II-25
3.3	Summary of Physical Properties of Model Construction	II-27
4.1	Basic Tie Arrangement and Design Assumptions	II-48
4.2	Series B-1 and B-2 Tie Arrangements	II-81
4.3	Influence of Soil-Tie Friction Angle on the Required Tie Length	II-96
4.4	Series B-1, B-2, and B-3 Tie Arrangements	II-97
4.5	Additional Model Test Tie Arrangements	II-110
5.1	Fundamental Period of Vibration	II-139
6.1	Fundamental Periods	II-180
6.2	Minimum Edge Distance	II-188
6.3	Maximum Tie Spacing for Seismic Loading	II-199
6.4	Maximum Tie Spacing for Static Loading	II-203

INTENTIONALLY BLANK

II-X

ABSTRACT OF THESIS

The Response of Reinforced Earth Walls
to Vibratory Loading

by

Gregory Neil Richardson

Master of Science in Engineering

University of California, Los Angeles, 1973

Professor Kenneth L. Lee, Chairman

Reinforced Earth is a construction material composed primarily of soil, which is strengthened by the introduction of small quantities of bars, rods, or fibers to resist tensile forces that the soil alone is unable to resist. This report deals with the design of Reinforced Earth walls using embedded bars as the reinforcing in the backfill, and subjected to seismic loading.

The first Reinforced Earth retaining wall was constructed in 1966 but it is only since 1972 that a Reinforced Earth wall was constructed in a region of high seismic activity. Because of this, there exist no precedents to guide in the evaluation of the seismic stability of Reinforced Earth walls.

The behavior of Reinforced Earth walls subjected to seismic loading was studied using small models on a shaking table subjected to sinusoidal lateral accelerations. These tests provided measured

values for displacements, accelerations, and the forces in the reinforcing during vibratory loading. In addition, numerical studies were performed using a dynamic finite element program with nonlinear strain dependent modulus and damping properties.

Based on the above studies, a procedure was developed for estimating the lateral earth pressures acting on a Reinforced Earth wall during static and dynamic loading, from which the reinforcing elements could be designed.

To demonstrate the application to field cases, a typical Reinforced Earth wall was designed for the predicted seismic forces from an earthquake accelerogram, 15 seconds long and with a maximum acceleration of 0.2g. For this case the peak spectral acceleration occurred at nearly the same frequency as the fundamental frequency of the wall and therefore the wall was designed for a spectral acceleration of 0.59g. The design required approximately twice the amount of reinforcing of conventional statically designed walls. Based on earlier studies, this would indicate an approximate 20% increase in the total wall cost due to seismic design considerations.

CHAPTER 1 INTRODUCTION

1.1 REINFORCED EARTH

As used in this study, the term "Reinforced Earth" defines a construction material composed primarily of soil, which is strengthened by the introduction of small quantities of bars, rods, or fibers to resist tensile forces that the soil alone is unable to resist. This concept is a corollary of "Reinforced Concrete," where steel bars are introduced to compensate for the low tensile strength of concrete.

Reinforced Earth in its current form, was introduced by a French engineer, Mr. Henri Vidal, about eight years ago, and used most extensively to support highway embankments where retaining walls were previously required (1). The primary advantages of this construction technique are

- 1) greater economy in total job cost,
- 2) the ability to take large deformations, and therefore,
- 3) the ability to use sites with relatively poor foundations.

In addition, since the concept is to strengthen the site material to suit the structure, rather than modifying the structure to suit the site, there is greater flexibility and economy in designing the structure.

Since the construction of the early structures, Reinforced Earth has been repeatedly used to replace conventional structures such as bin walls, quarry walls, bridge abutments, and earth embankments.

In addition to conventional retaining walls, the following uses for Reinforced Earth have also been proposed by Vidal (2):

- 1) structures which will provide for sharp differences in grade between adjoining platforms,
- 2) structures to improve large embankments or to provide a level platform on such an embankment,
- 3) elevated structures such as earth dams, coffer dams, retaining structures,
- 4) vaults and,
- 5) foundation slabs to bridge superstructures over weak foundations or to increase the capacity of individual footings.

1.2 REVIEW OF PREVIOUS WORK

A review of previous investigations of Reinforced Earth is presented in a report by Lee, Adams, and Vagneron (3) and only a brief extract of this review will be presented herein.

Vidal has published a series of articles (1, 2, 4, 5, and 6) that describe actual Reinforced Earth walls and laboratory tests performed on laboratory models one to three feet high. These articles outline a theory for estimating design requirements and describe their application to full scale walls that have been successfully built.

The Japanese National Railway Research Laboratory (7, 8) have performed tests on two scale model walls. The walls were constructed with a theoretical static factor of safety of eight and were tested in a dry and saturated condition. The larger of the test walls, constructed to a scale ten times larger than the smaller wall, was also subjected to forced vibrations using a vibrator mounted at the top of the wall.

"Additional model tests on Reinforced Earth walls are currently being conducted at the University of Lyons under the direction of Professor Guy Sanglerat (9). Other laboratory studies have been, and are currently being conducted at the Laboratoire Central des Ponts et Chaussées in Paris, France, under the direction of Mr. F. Schlosser."

Beaton et al (12) have described the design method and some observed results related to the construction of a full scale wall recently constructed in Southern California, and heavily instrumented to provide research data.

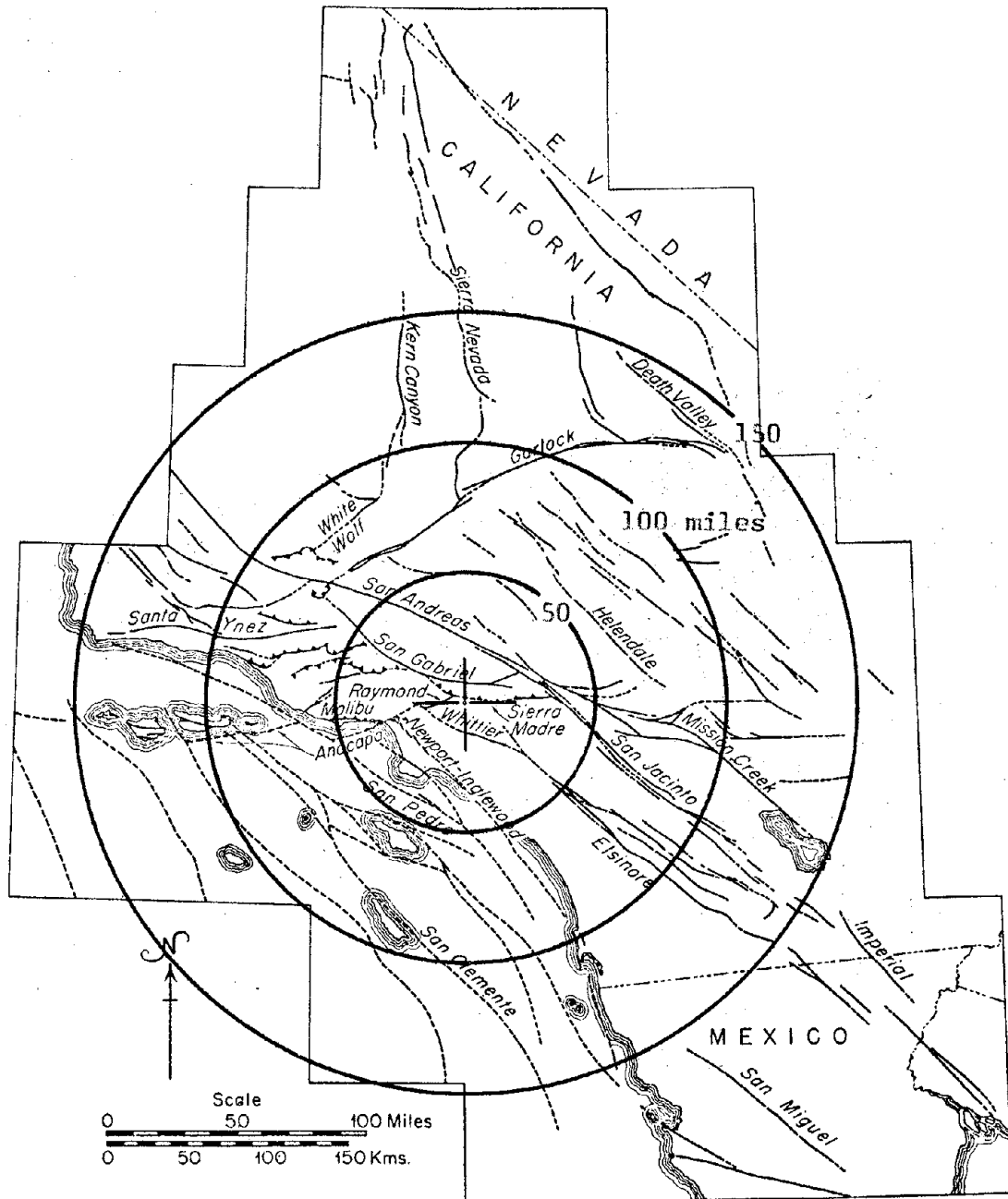


FIGURE 1.2 Map of major faults in southern California (modified from Allen et al, 1965; California Department of Water Resources, 1964a; Emery, 1960; Hill, 1916).

Railways Research Institute (7, 8). These tests were inconclusive in that the walls were built to excessively high factors of safety under static loading, and the dynamic forces were not sufficiently large to cause failure or large deformations. Subsequent tests by the Japanese have studied the possible use of Reinforced Earth to improve the resistance of loose saturated sand to liquefaction from earthquake effects (14). These tests showed that placing a good reinforced earth structure on a foundation of loose saturated sand did not significantly improve the overall behavior as compared with an embankment with no reinforcing on the same loose saturated sand foundation. Thus considerably more research must be performed to fully define the behavior of Reinforced Earth walls under seismic loading conditions.

The studies described herein were undertaken to investigate the seismic behavior of Reinforced Earth walls with dry sand backfill and resting on a firm foundation. The studies were mainly model tests on one ft. high walls built on a laboratory shaking table. A summary of the 21 model tests performed and the conclusions drawn from each test is presented in Appendix A. A few analytical studies were made near the end of the investigation using a dynamic finite element computer program.

CHAPTER 2 GENERAL THEORY OF REINFORCED EARTH WALLS

2.1 BASIC STRUCTURAL MODELING

The analytical and laboratory modeling of any structural system is dependant on an accurate knowledge of and handling of the structural subcomponents that make up the total system. Also intrinsic to the simulation of the total system is a knowledge of the connectivity of the system subcomponents and an accurate knowledge of the forces acting on the total system. Therefore the requisite preliminary steps to any analysis are to determine;

- 1) the structural properties of the subcomponents of the system,
- 2) the connectivity between structural subcomponents, and
- 3) the loads acting on the system.

The total analysis can not be assumed to have any more accuracy than the least accurate preliminary step.

The Reinforced Earth wall structural system considered in these studies is composed of three components:

- 1) cohesionless backfill material with little compaction,
- 2) skin components acting as the face of the wall, and
- 3) tie components embedded in the backfill.

A typical arrangement of these components is shown in Fig. 2.1. The structural modeling of the tie and skin components seperately presents no problem. Modeling of the backfill material is uncertain at best and must consider the inherent non-linearity of most soil properties.

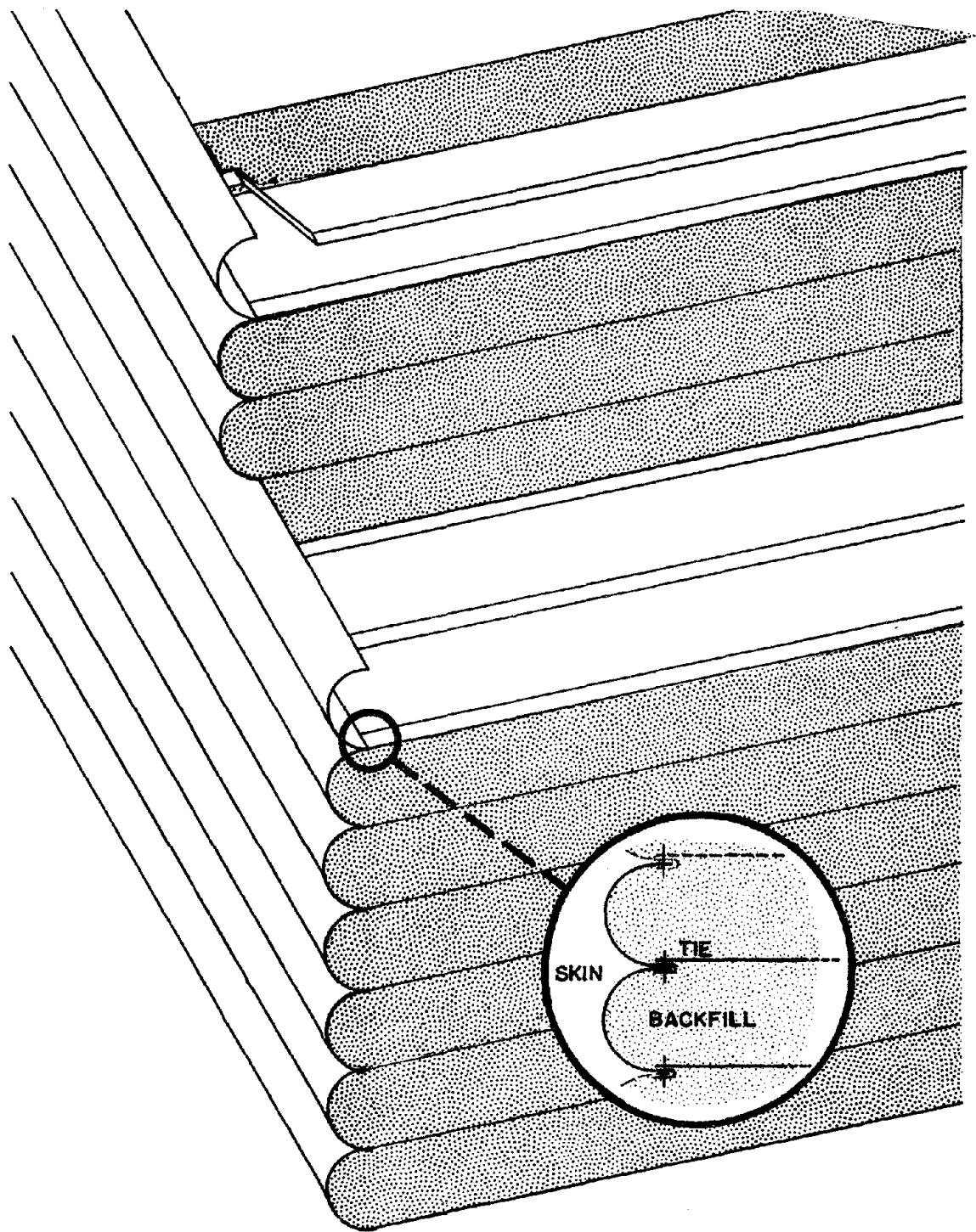


FIGURE 2-1 CONFIGURATION OF
STRUCTURAL COMPONENTS

Examining the connectivity between the components, the only known relationships are that the ties are rigidly attached to the skin components and that the soil component is retarded from lateral expansion by the skin elements. The largest uncertainty in completely defining the connections is prediction of the connectivity between the tie and the soil.

The loads acting on the system include those due to the mass of the backfill, surcharge loads, and possible design service loads. At present only the loads due to the mass of the backfill are included in the analysis. The direct and reactive forces due to the soil mass are shown in Fig. 2.2. The primary unknowns are the relationship between the vertical effective stress, σ_v , and the horizontal effective stress, σ_h , and the soil-tie frictional stress, τ_u .

Thus even from this cursory examination of the structural elements and loads it is easy to realize the difficulty in achieving an accurate analytical model. The structural system is an indeterminate system, of uncertain connectivity and internal loading.

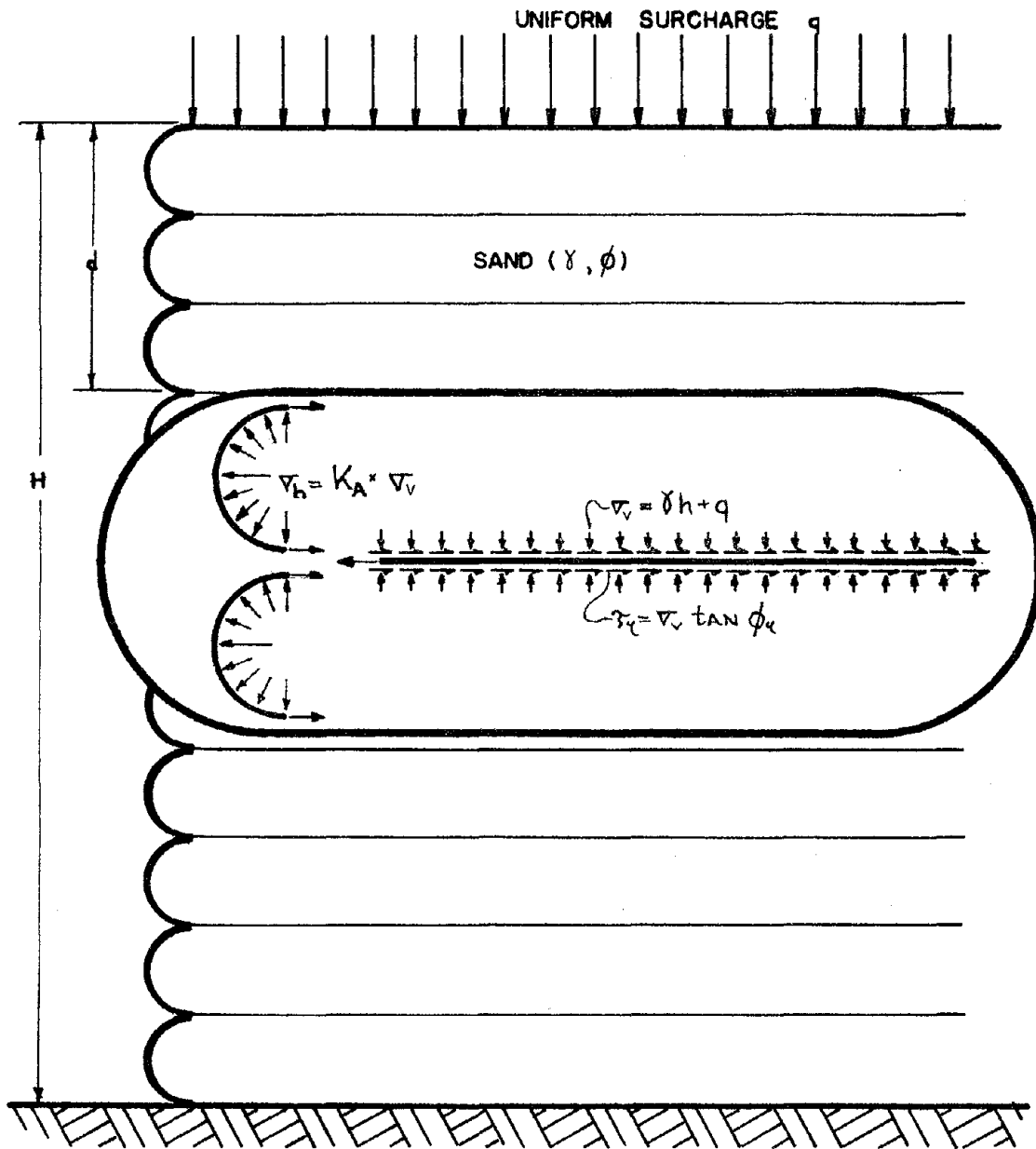


FIGURE 2-2 SYSTEM FORCES

2.2 POSSIBLE FAILURE MODES

The failure of any structural system may be precipitated by the failure of one of its subcomponents, as shown on Fig. 2.2, or the foundation to which the system is attached. The summary of possible failure modes is presented in Table 2.1. This study will only deal with failure modes 1 and 2, Tie breakage and pullout respectively. The design of skin components for tensile and bending forces, and a study of corrosion effect have previously been presented by Lee, et al (3).

Component Failure	Tie Component	1.	tie breakage
		2.	tie pullout
		3.	corrosion of tie
	Skin Component	4.	tensil stress
		5.	bending or buckling
Support Failure		6.	shear or bearing capacity failure of the foundation soil beyond the reinforced zone

2.3 STATIC ANALYSIS BY RANKINE EARTH PRESSURE THEORY

The design of Reinforced Earth walls using Rankine Earth Pressure Theory has been discussed by Lee, Adams, and Vagneron (3). The analysis makes all the assumptions inherent in the Rankine Theory as used in the design of conventional retaining walls. The vertical earth pressure, ∇_v , is given by

$$\nabla_v = \gamma d + q \quad (2.1)$$

and is related to the horizontal pressure, ∇_h , by

$$\nabla_h = K * \nabla_v \quad (2.2)$$

where γ is the unit weight of soil, q is a possible surcharge load, and K is a earth pressure coefficient.

The value of K is dependent on the soil type and density, and on the amount of wall yield. For rigid unyielding walls K will be the coefficient of earth pressure at rest, K_0 . The value of K_0 will normally be 0.5 or less and is usually calculated using an empirical expression presented by Jaky (15):

$$K_0 = 1 - \sin \phi \quad (2.3)$$

where ϕ is the angle of internal friction of the soil. It should also be noted that excessive compaction effort can increase the earth pressure coefficient beyond this value. With increasing wall displacement the earth pressure coefficient is reduced until the minimum active pressure condition is reached. This minimum lateral earth pressure coefficient is given by

$$K_A = \tan^2 (45^\circ - \frac{1}{2}\phi) \quad (2.4)$$

The model tests reported by Lee, et al, (3) used no special compaction other than raining the sand into the box, and the lateral earth pressures deduced from these tests corresponded to a K_A condition. On the other hand the backfill at the instrumented field wall reported by Beaton, et al, (12) used some compaction from passes of construction equipment, and the measured data indicates a K_0 lateral earth pressure condition.

Earth pressures calculated by the Rankine Theory can be expressed as an equivalent hydrostatic force acting on the structure. The amount of force resisted by an individual tie is assumed to equal the lateral pressure at the elevation of the tie acting on the tributary area of the tie. The tributary area, T_A , of a tie is assumed to be that portion of the wall supported by that tie. A sample of this calculation using K_A lateral pressure condition is presented in Fig. 2.3. It should be noted that the apparent drop in the tie force at the base level is due only to the reduced wall areas supported by ties at the base. This figure is based on an uniform horizontal tie spacing of 3 feet for a wall 12 feet in height.

The static factors of safety may be defined as the ratio of the tie resisting force to the Rankine design force. Of particular interest are the static factors of safety against Tie Breakage and Tie Pullout.

For failure due to Tie Breakage, assuming the ties are long enough to prevent pullout, the resisting force is equal to the ultimate tensile strength of the tie as given by

$$F_t = f_u * A \quad (2.5)$$

ST-II

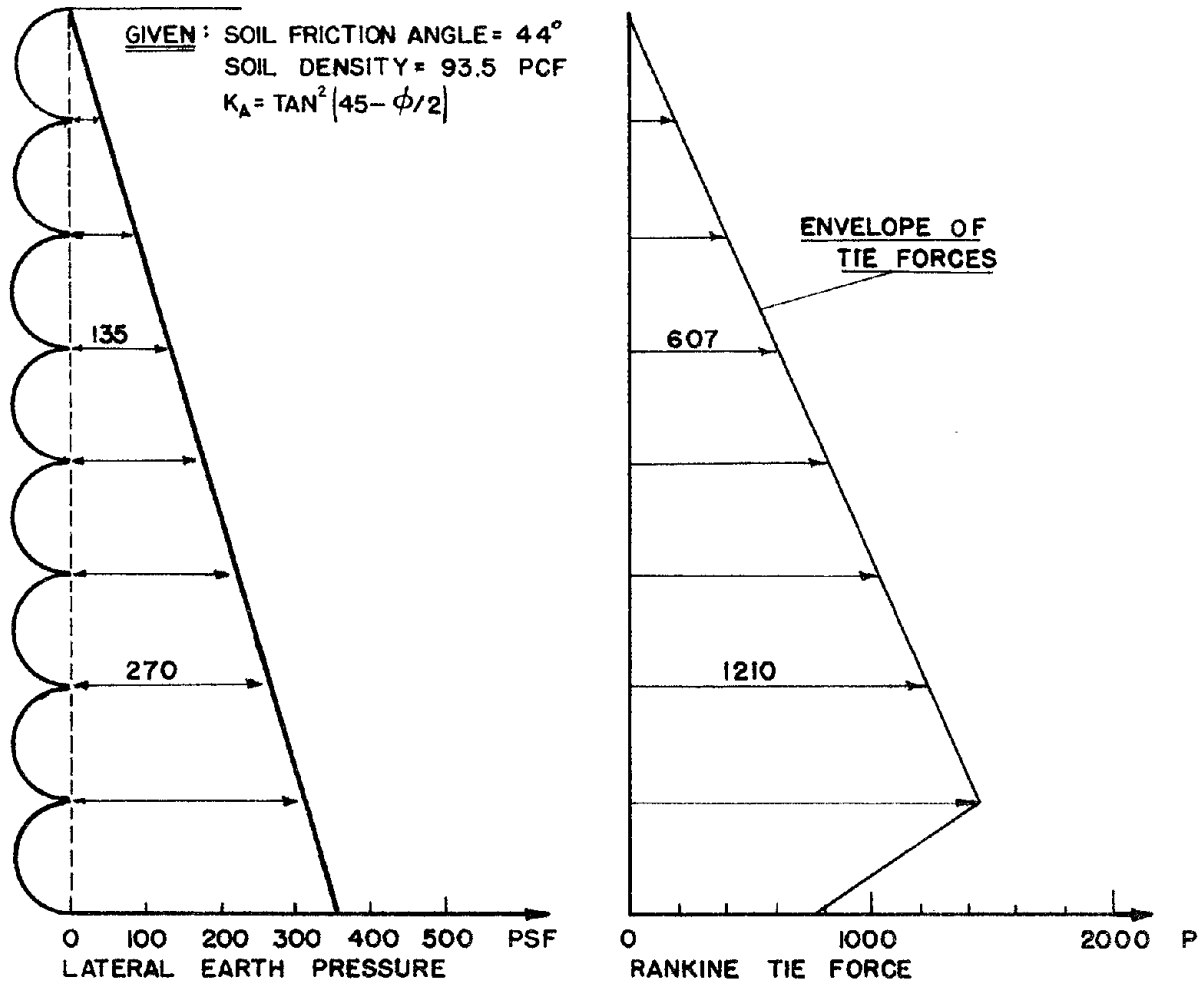


FIGURE 2-3 RANKINE TIE FORCE CALCULATIONS

where f_u is the failure stress of the tie material and A is the cross sectional area of the tie. At each depth where the overburden pressure is defined by ∇_v , the Rankine factor of safety against Tie Breakage may therefore be expressed as

$$F.S. = \frac{F_t}{F_R} = \frac{f_u * A}{K_A * \nabla_v * TA} \quad (2.6)$$

where TA is the tributary area. The factor of safety against Tie Breakage is increased by increasing the tie cross sectional area, A, or decreasing the tie spacing (which decreases the tributary area).

Assuming that the ties are strong enough, the frictional force resisting failure by Tie Pullout is given by

$$F_f = 2 * L_e * w * \tan \phi_u * \nabla_v \quad (2.7)$$

where w is the tie width, L_e is the tie length resisting pullout, and ϕ_u is the frictional angle between the soil and the tie material. Lee, et al. (3) have suggested that L_e should be the length of the tie extending behind the Rankine Active failure wedge in the sand backfill. At each depth when the overburden pressure is defined by

∇_v , the Rankine factor of safety against tie pullout may be expressed by

$$F.S. = \frac{F_f}{F_R} = \frac{2 * L_e * w * \tan \phi_u}{K * TA} \quad (2.8)$$

The factor of safety against Tie Pullout may be increased by increasing the tie length and/or width, increasing the soil-tie friction angle, and by decreasing the tie spacing.

The overall factor of safety for the entire wall is taken as the minimum value of F.S. calculated by Eq. 2.6 and 2.8 for every level

of ties. For constant tie size, spacing, and length, the factor of safety against breaking will be a minimum at the base of the wall and against pullout will be a minimum at the top. Practical designs usually involve changing tie dimensions and spacing at various levels to approach a balanced design. The Reinforced Earth Company recommends using a constant length of ties at all levels of 0.8 times the height of the wall. Lee, et al, (3) suggested an alternative design approach which would allow shorter ties at the top than at the base.

2.4 STATIC ANALYSIS BY COULOMB EARTH PRESSURE THEORY

For the more general static analysis where the assumptions of vertical frictionless walls and level backfill are inapplicable, Lee, Adams, and Vagneron (3) have adapted the Coulomb Earth Pressure Theory. The analysis shares with the Rankine Active analysis the assumptions of a rigid wall and lateral movement of the wall sufficient to bring the backfill into a state of plastic equilibrium.

The Coulomb theory is based upon the equilibrium of the entire failure wedge rather than the equilibrium at each location. Thus the general expression for the sum of the lateral forces acting on a width of the wall equal to the tie spacing, S , is

$$P = \frac{1}{2} K_A'' \left(\gamma + \frac{2q}{h} \right) H^2 * S \quad (2.9)$$

where

$$K_A'' = \frac{\cos^2(\phi - \lambda)}{\cos^2(\lambda) \cos(\lambda + \delta) \left[1 + \sqrt{\frac{\sin(\phi + \delta) \sin(\phi - \theta)}{\cos(\lambda + \delta) \cos(\beta - \lambda)}} \right]^2} \quad (2.10)$$

and q is a possible surcharge load, see Fig. 2.4.

Next the tie forces may be determined by examining the equilibrium of the wall face. The static equilibrium of the wall face may be calculated by

- 1) sum of forces in the horizontal direction, or
- 2) moment equilibrium about the toe of the wall.

Both methods require an assumption to be made on the distribution of lateral earth pressure and tie tensions along the wall.

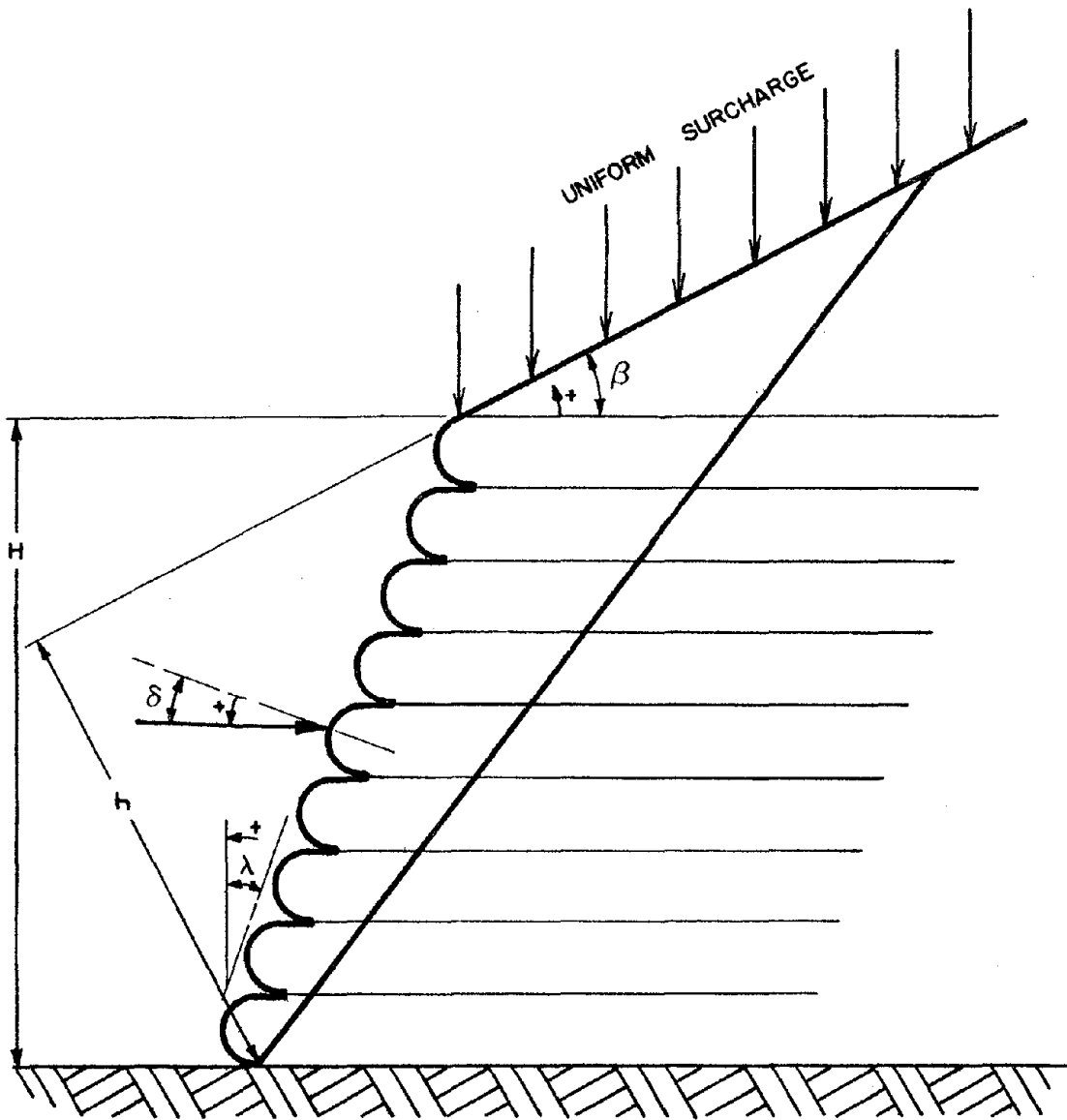


FIGURE 2-4 COULOMB THEORY VARIABLES

2.5 TRAPEZOIDAL DESIGN PROCEDURE

The static design procedure used by the Reinforced Earth Company¹ treats the Reinforced Earth wall as a composite structure acted upon by external loads, as shown in Fig. 2.5. The basic procedure is initially identical to that used in the design of foundations subjected to overturning. The analysis steps are as follows.

- 1) Determine the constant length for all ties
 $D = (0.8 \text{ to } 1.0) H$
- 2) Determine the lateral earth forces acting against the wall structure assuming $K = K_A = \tan^2 (45^\circ - \phi/2)$
- 3) Replace the lateral earth forces with Concentrated loads acting at the force centroids.

$$A_p = \frac{1}{2} K_A \gamma H^2 \quad (2.11)$$

$$A_s = K_A q H \quad (2.12)$$

- 4) Calculate the total vertical forces.

$$V = W_1 + q * D \quad (2.13)$$

- 5) Take moments about the toe, point Θ , to determine the eccentricity.

$$e = \frac{\sum A * d}{V} \quad (2.14)$$

- 6) Calculate the vertical trapezoidal pressure at point Θ .

$$\text{if } e < \frac{D}{6} \text{ then } \sigma_v = \frac{V}{D} \left(1 + \frac{6e}{D} \right) \quad (2.15)$$

$$\text{if } e > \frac{D}{6} \text{ then } \sigma_v = V / (L - 2e) \quad (2.16)$$

1. This procedure is based on actual design calculations given the author by the Reinforced Earth Company for actual walls constructed in Anniston, Alabama and Little Falls, New York.

GIVEN

Soil Density = γ
 Soil Friction Angle = ϕ
 Tie Tributary Area @ i^{th} Level = TA_i

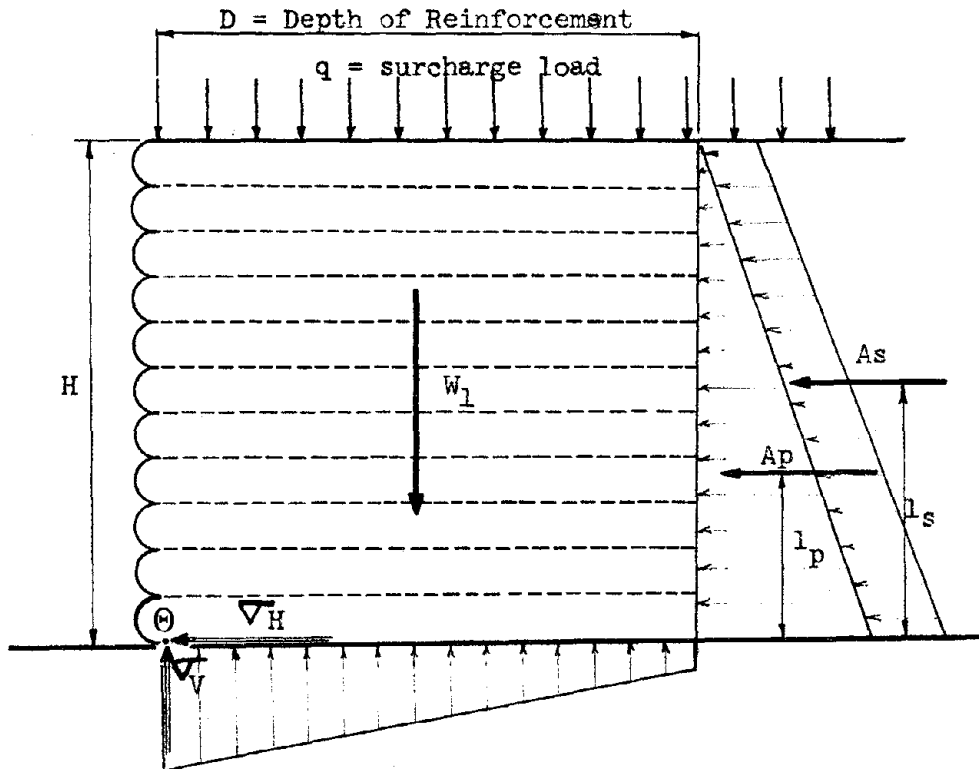


FIGURE 2.5 TRAPEZOIDAL DESIGN

DESIGN STEPS

- 1) Determine Constant Tie Length
- 2) $K_A = \text{Tan}^2 (45 + \phi / 2)$
- 3) $Ap = \frac{1}{2} K_A \gamma H^2$
- 4) $As = K_A qH$
- 5) $V = W_1 + qD$
- 6) Determine eccentricity, taking moments about Θ .

$$e = \frac{Ap * l_p + As * l_s}{V}$$
 If $e < \frac{D}{6}$ then $\nabla_V = \frac{V}{D} * (1 + \frac{6e}{D})$
 If $e > \frac{D}{6}$ then $\nabla_V = V / (D - 2 * e)$
- 7) $\nabla_H = K_A \nabla_V$
- 8) Tie Force at base level =

$$F_b = TA_b * \nabla_H$$
- 9) Design Base Tie
- 10) Repeat for next Tie Level

- 7) Calculate the horizontal pressure acting at point Θ .

$$\sigma_H = K_A \sigma_V \quad (2.17)$$

- 8) Calculate the base tie force using the horizontal base pressure times the tributary area of the base ties.
- 9) Design the base tie for tie pullout and tie failure using Eqs. (2.5) and (2.7).

This procedure is repeated for each level of ties and will produce a static design that is more conservative than that obtained from the Rankine method.

CHAPTER 3 TEST EQUIPMENT AND PROCEDURES

3.1 DIMENSIONAL MODELING

The accuracy of analysis using prototype model testing is dependent on the degree to which requirements for model similitude are met. The use of prototype models is an accepted practice in soil mechanics and similitude requirements have been thoroughly investigated. Model similitude requirements for the case of the seismic response of an earth dam has been presented by Clough and Pirtz (16); these will serve as a guide for this report.

In a structural model intended for dynamic loading, complete similitude is obtained, if there is similarity between the model and prototype, with respect to length, time, and force. These similitudes may be obtained by the following:

- 1) length similitude is obtained by making the model geometrically similar to the prototype,
- 2) time similitude is obtained if every event in the model is made proportional in duration to the corresponding event in the prototype and,
- 3) similitude of forces requires that all forces in the model have a constant ratio to the corresponding forces in the prototype.

Since force is a product of mass and acceleration, involving both length and time, it is only possible to set one or two scales; the remaining scales are calculated by dimensional similitude requirements.

The dimensional similitude requirements as developed by Clough and Pirtz are summarized in Table 3.1, where λ is the geometric scale ratio defined by:

$$\lambda = \frac{\text{model length}}{\text{prototype length}}$$

Table 3.1 Dimensional Similitude Requirements	
Quantity	Required Model/Prototype Ratio
Lengths	λ
Times	$\sqrt{\lambda}$
Accelerations	1
Modulus of Rigidity	λ
Angle of Internal Friction	1

The basic model wall used in this report is 12 inches high and is intended to simulate a typical prototype wall 12 feet high. Thus the Geometric Scale Ratio for this series of test is 1 to 12, or $\lambda = 0.0833$; this is used to insure continuity with past model tests performed on Reinforced Earth walls. Additional physical limitations are imposed on the wall geometry, due to the size limitations of the box constructed to contain the model. To reduce the effect of wave reflection off the back of the box the wall height should be less than one third the model depth. This in effect, limits the model wall to a height less than 13 inches.

For a 12 inch high wall the time scale is $\sqrt{\lambda} = 0.289$. Assuming a typical earthquake has a predominant period of about 0.3 seconds, the simulated model ground motion would have frequency given by

$$f_M = \frac{1}{\text{Period}} = \frac{1}{.3 \times \sqrt{\lambda}} = \frac{1}{.3 \times .286} = 11.6 \text{ cps}$$

In the model, the input ground motion was limited to a continuous

sine wave of only one frequency. All tests in this study used a frequency of 11.6 cps.

For granular soil the modulus of rigidity, G, increases approximately with the square root of confining pressure. For uniform soil conditions the modulus increases linearly with the square root of depth. Thus the modulus or rigidity for the model and prototype are given by

$$G_M = k * (d_m)^{\frac{1}{2}}$$

$$G_p = k * (d_p)^{\frac{1}{2}}$$

and the similitude ratio of the modulus is given by

$$S.R. = \frac{k * (d_m)^{\frac{1}{2}}}{k * (d_p)^{\frac{1}{2}}} = \left(\frac{d_m}{d_p}\right)^{\frac{1}{2}}$$

where

$$\frac{d_m}{d_p} = \lambda$$

and therefore the similitude ratio for the modulus or rigidity is equal to the square root of λ .

A comparison of similitude requirements as outlined by Clough and Pirtz to that used in the reinforced earth model tests is presented in Table 3.2.

Table 3.2 Comparison of Dimensional Similitude Ratios		
Quantity	Clough/Pirtz	Actual Lab.
Lengths	λ	λ
Times	$\sqrt{\lambda}$	$\sqrt{\lambda}$
Accelerations	1	1
Modulus of Rigidity	λ	$\sqrt{\lambda}$
Angle of Internal Friction	1	1

3.2 REINFORCED EARTH WALL MODELS

After a thorough review of model similitude requirements, the next step in the laboratory simulation of a structure was to select and design materials to simulate the structural subcomponents. Two such structural models are used in this report. The first group of tests, Series A, was performed using a model wall with structural subcomponents identical to those used and reported on by Lee, Adams, and Vagneron, (3). This test series was intended to demonstrate the seismic failure of Reinforced Earth walls by tie failure, and to serve as a test vehicle for the design of instrumentation required to monitor dynamic loading. The ties were made of narrow strips of aluminum foil which had a relatively low breaking strength but high soil-tie friction angle. The second group of tests, Series B, was intended to demonstrate failure by tie pullout. It used ties made of smooth plastic strips which had a high breaking strength but low coefficient of friction with the soil. The Series B tests also incorporated some minor changes to improve the design based on knowledge gained from the Series A tests. A summary of the Test model geometry and material properties from the Series A and B tests is presented in Table 3.2.

Soil Backfill. The sand used as backfill material, in both Series A and B tests, was a fine dry crystal silica sand available commercially as Ottawa 90 Sand. The sand backfill was placed by raining from a drop height of 18 inches. The properties of this sand, as previously reported by Lee, et al, (3) are as follows:

Structural Component	Table 3.3 Summary of Physical Properties of Model Construction Materials	
	Test Series A : Tie Failure	Test Series B : Tie Pullout
Tie Component	<u>Aluminum Ties</u> thickness .0005 in. average width .155 in. average strength 1.18 lb.	<u>Mylar Ties</u> thickness .001 in. average width .25 in. average strength 10.0 lb.
Skin Component	<u>Aluminum Skin</u> thickness .012 in. height 1.0 in. shape: 	<u>Aluminum Skin</u> thickness .012 in. height 1.5 in. shape: 
Sand Backfill	<u>Ottawa 90</u> $\gamma_{min} = 81.4 \text{ pcf}$ $\gamma_{max} = 102.5 \text{ pcf}$ $\gamma = 93.5 \text{ pcf (D}_r = 63\%)$	
	$G_s = 2.64$ $D_{50} = .15 \text{ mm}$ $\phi_u = 44$	

II-28

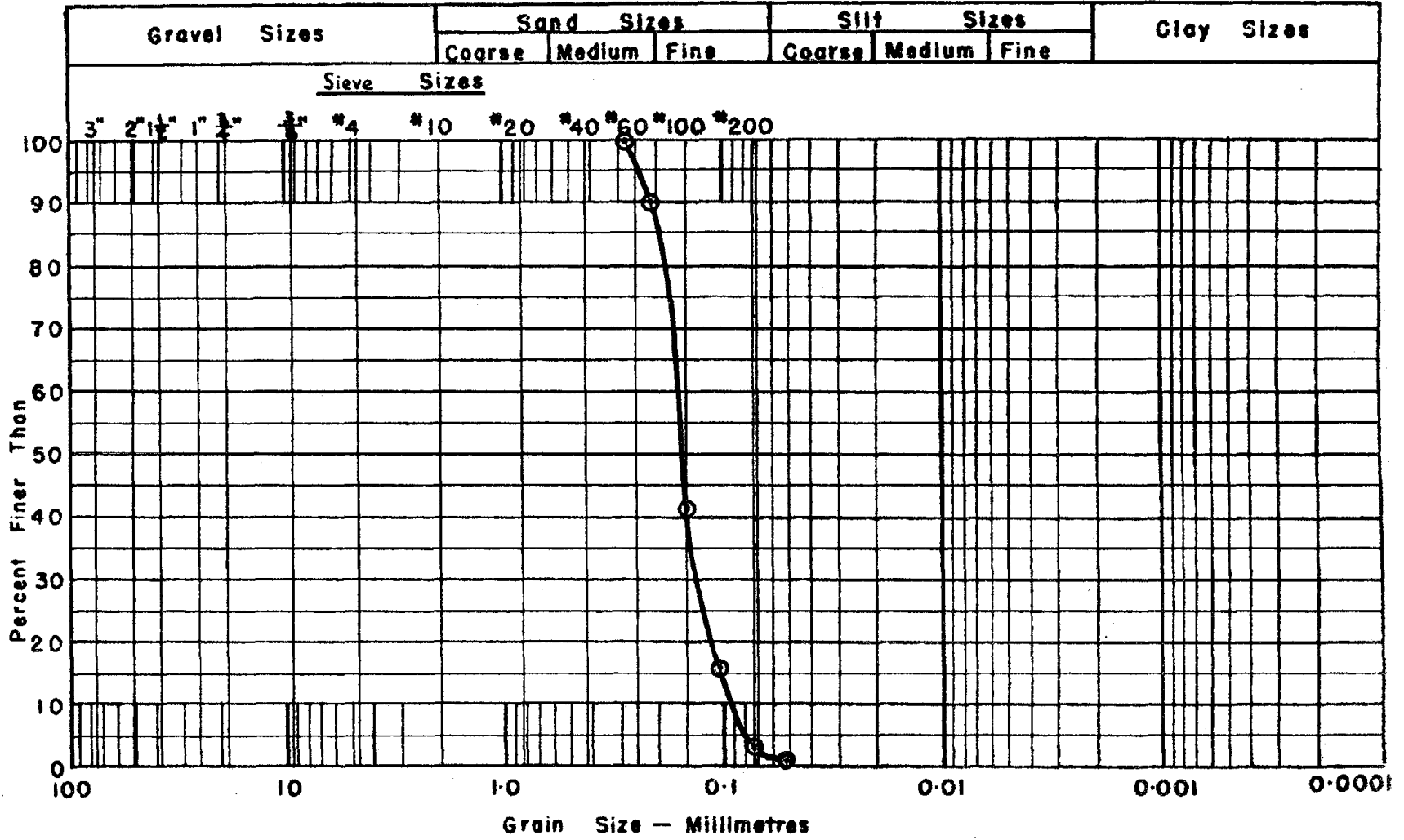


FIGURE 3-1 OTTAWA 90 GRAIN SIZE DISTRIBUTION

- 1) mean grain size $D_{50} = 0.15\text{mm}$,
- 2) dry density of 93.5 PCF,
- 3) relative density $D_r = 63$
- 4) specific gravity = 2.64, and
- 5) a friction angle of 44° , as determined by special direct shear tests at low confining pressures similar to those in the model.

The soil grain size distribution curve is presented in Fig. 3.1.

Tie Material. The ties for test Series A were cut from rolls of aluminum foil. These straps were very fragile and not consistently uniform. The foil thickness was 0.0005 inches, the average width of the ties is 0.155 inches, and the average rupture strength was 1.18 pounds.

The ties for the Series B tests were cut from mylar recording tape which was 0.001 inches thick and 0.25 inches wide. The tape had a rupture strength of 10.0 pounds and an elastic modulus of 3000 Ksi.

Skin Elements. Because this report does not deal with the mode of failure caused by failure of the skin component, the skin elements were not designed using scale similitude. They were designed to be relatively light weight and strong enough to be reusable for successive tests. They were made from thin sheets of aluminum (0.012 inches thick). The Series A tests used curved skin elements resembling the shape used in many actual Reinforced Earth walls (see Fig. 2.1). The Series B tests used flat skin elements which are similar to other Reinforced Earth walls which use precast concrete slabs for the skin.

The skin components for Series A tests were made in two lengths, 12 and 18 inches; and assembled alternately in brick fashion to span the 30 inches inside width of the box. The two parts were joined by lapping the shorter one inside the longer one. Each element

was 1 inch high so that the Series A models were constructed in 1 inch layers.

The Series B skin elements were 1.5 inch wide flat sheets, each spanning the full 30 inch width of the box.

Box for Model. The Reinforced Earth walls were built in a plywood box 30 inches wide, 48 inches long, and 24 inches high, as shown in Fig. 3.2. These dimensions were chosen such that construction of the walls would involve a reasonable amount of sand, and that the width to height ratio of all test walls would be kept higher than 1.25 in order to minimize the effect of side restraints and friction against side walls. In order to provide a cross section viewing port, the box was lined with laminated safety glass.

The depth of the model Reinforced Earth walls was 36 inches for all tests on models 12 inches in height or lower. This provided adequate space at the face of the wall for instrumentation. The depth of models higher than 12 inches was increased to 42 inches, which was the maximum depth possible for this model box.

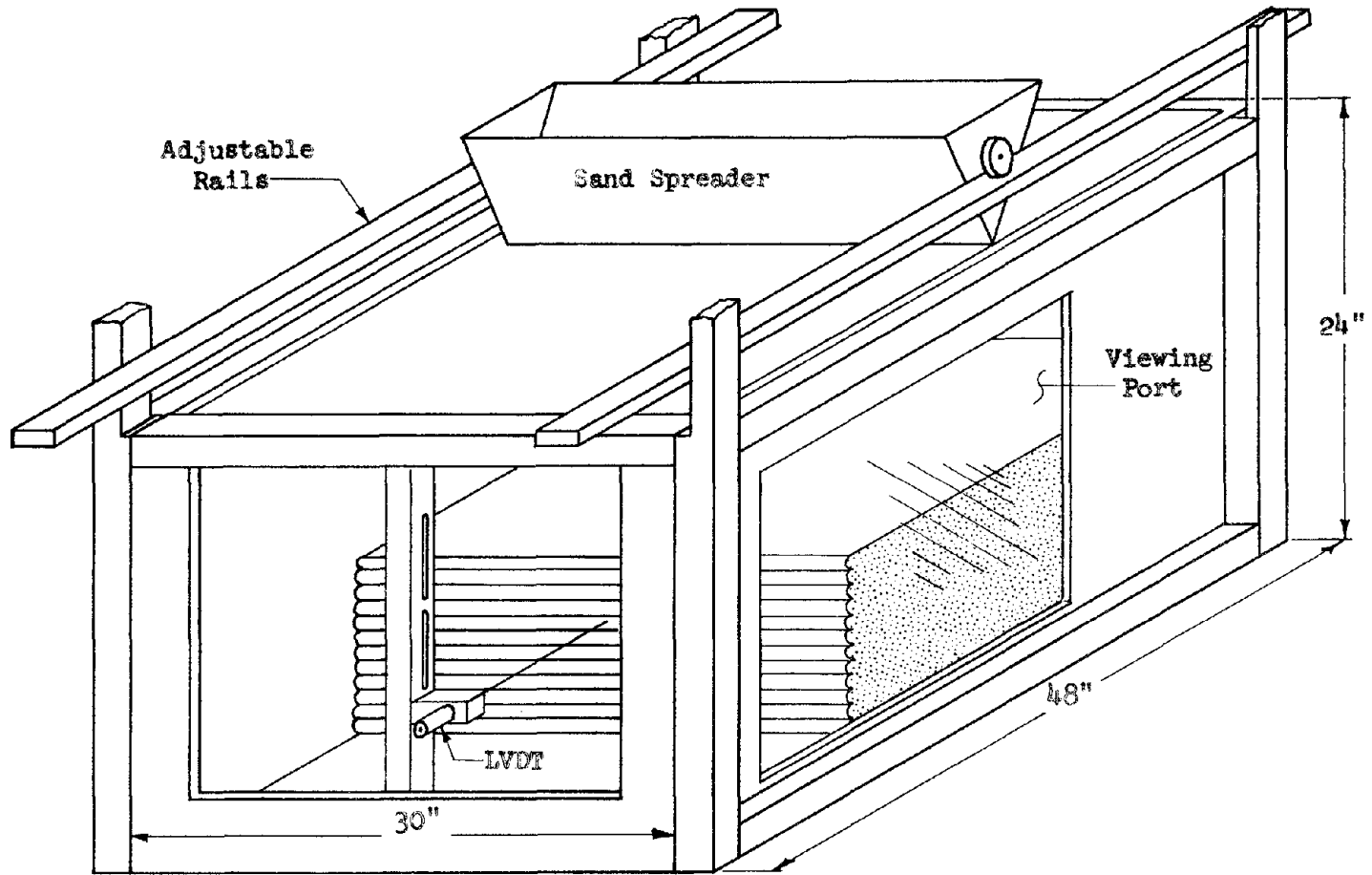


FIGURE 3-2 TEST MODEL BOX

3.3 SHAKING TABLE

To provide the necessary base input motion to the Reinforced Earth model, the model box was mounted on a Shaking Table, designed and built at UCLA by Professor R.B. Matthiesen and Mr. B.D. Adams as a student project. The original design of the table used a steel "table," riding on Teflon pads, mounted in a steel cradle, and powered by mechanical shaker units. For the research presented in this report the Shaking Table was modified to be driven by the Material Test System (MTS), available through the Soil Mechanics Laboratory. The physical layout of the Shaking Table is illustrated by Fig. 3.3.

The MTS system is a closed-loop electro-hydraulic system that provides a high degree of control for the table motion and increases the workable frequency range. The MTS system uses a 5 kip hydraulic actuator serviced by an electrically controlled servo-valve. The servo-valve is controlled through an electrical feed back system that receives an input from preselected electrical gauges. The control flow network for this system is illustrated on Fig. 3.4.

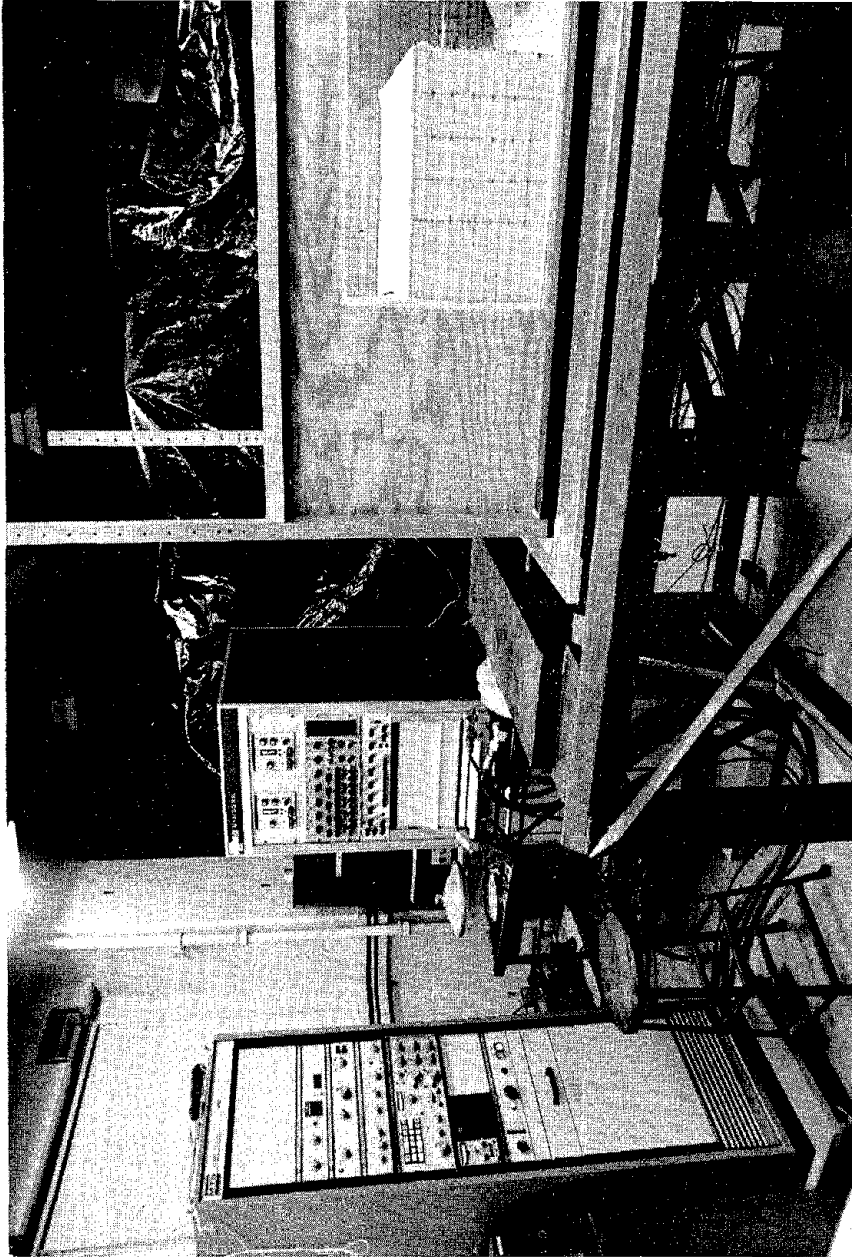
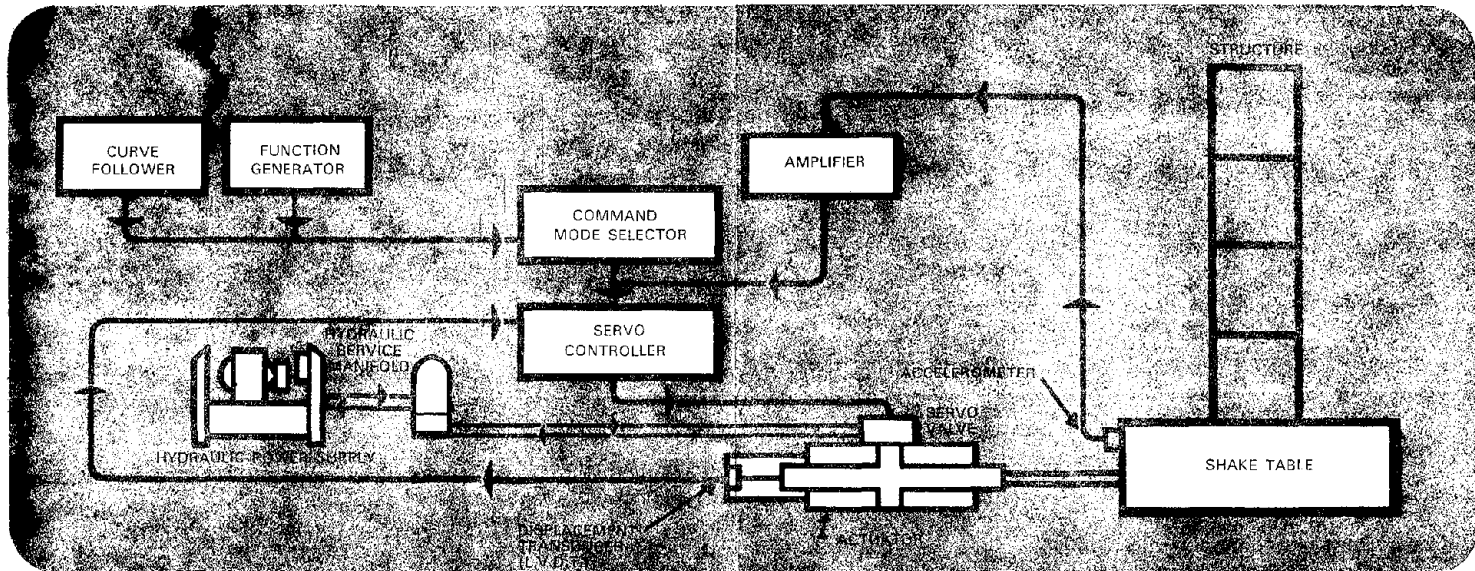


FIGURE 3.3 MODIFICATIONS TO SHAKING TABLE



(MTS Closed Loop Magazine, 1969)

FIGURE 3-4 MTS CLOSED-LOOP SYSTEM

3.4 INSTRUMENTATION

In any laboratory model simulation, the quality of results of the investigation are dependent upon the instrumentation selected to monitor the tests. Such instrumentation must be capable of accurately monitoring those variables thought to be critical to the performance of the test. For the dynamic testing of Reinforced Earth walls the critical variables are

- 1) the wall displacement,
- 2) the wall acceleration, and
- 3) the tensile force in the tie components.

The accurate measurement of these variables precedes an accurate analysis of the model response.

Wall displacements. Because of the high frequency and time dependent nature of the wall motion, it was not possible to use simple mechanical dial displacement indicators to monitor the wall displacements.

Instead the wall displacement was measured using E300 Linear Variable Differential Transformers (LVDT) manufactured by Schalvitz Engineering.

The instruments are electro-mechanical transducers that produce an electrical signal proportional to the displacement of a movable core.

To provide flexibility when the wall failed, ordinary plastic drinking straws were used to connect the core element to the face of the wall.

The physical arrangement of the LVDT is shown in Fig. 3.5.

Wall Acceleration. To measure the input motion of the Shaking Table an accelerometer was mounted on the table. An additional accelerometer was mounted on a vane type appendage and buried in the sand

II-36

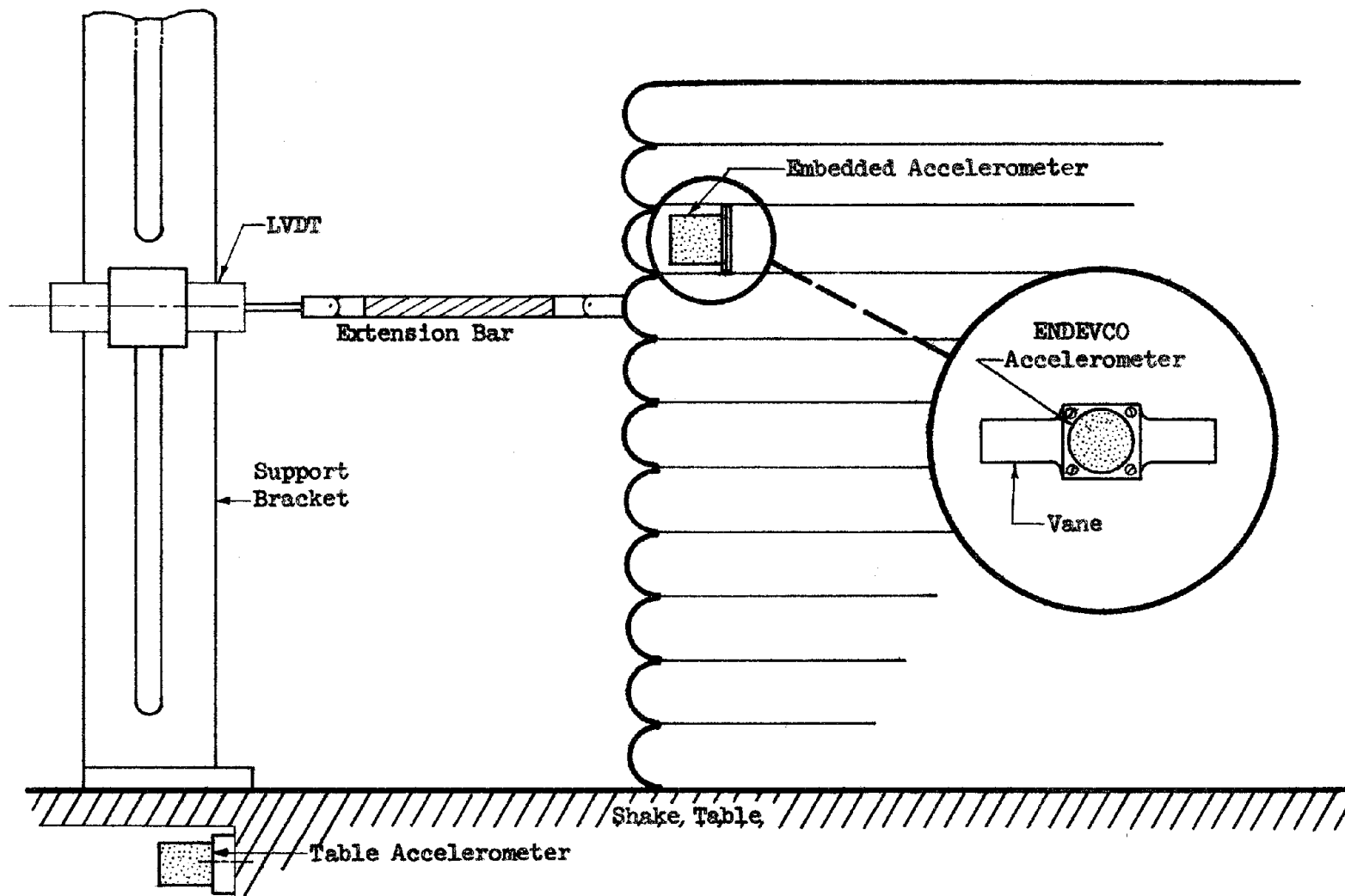


FIGURE 3-5 ACCELERATION & DISPLACEMENT GAUGES

backfield, as shown in Fig. 3.5.

The accelerometer works by measuring the current applied to a torquer coil to prevent the displacement of a proof mass acted upon by an acceleration field. A pickoff unit senses extremely small displacements of the proof mass about its fixed axis and controls the amount of current supplied to the torquer coil, see Fig. 3.6. The proof mass, flexure and flexure support are formed from a single fused quartz blank.

Tie-Tension at the Wall. In the Series A Model tests the tie tensile force was measured using a procedure identical to that used by Lee, et al, (3) for monitoring static forces. This procedure used two strain gauges, Micro-Measurement no. EA-13-125-AD-120, mounted back-to-back on brass shim stock and placed in series with the aluminum ties, Fig. 3.7a. The gauges were attached to the skin components with a short length of aluminum tie, to insure that failure could occur at the wall face.

The tie-tension measuring instruments used in the Series B tests were modified as a result of experience from the Series A tests. It was found that the ties often measured stresses due to slight bending, which overshadowed the tensile stresses which were intended to be measured. To insure that only tensile stresses were measured a new system was developed. The instruments used a simply supported beam mounted in a lucite chamber as shown in Fig. 3.7. The ties were connected to the beams by means of thin extension bars which have brass pads soldered on one end to connect the ties. The tensile

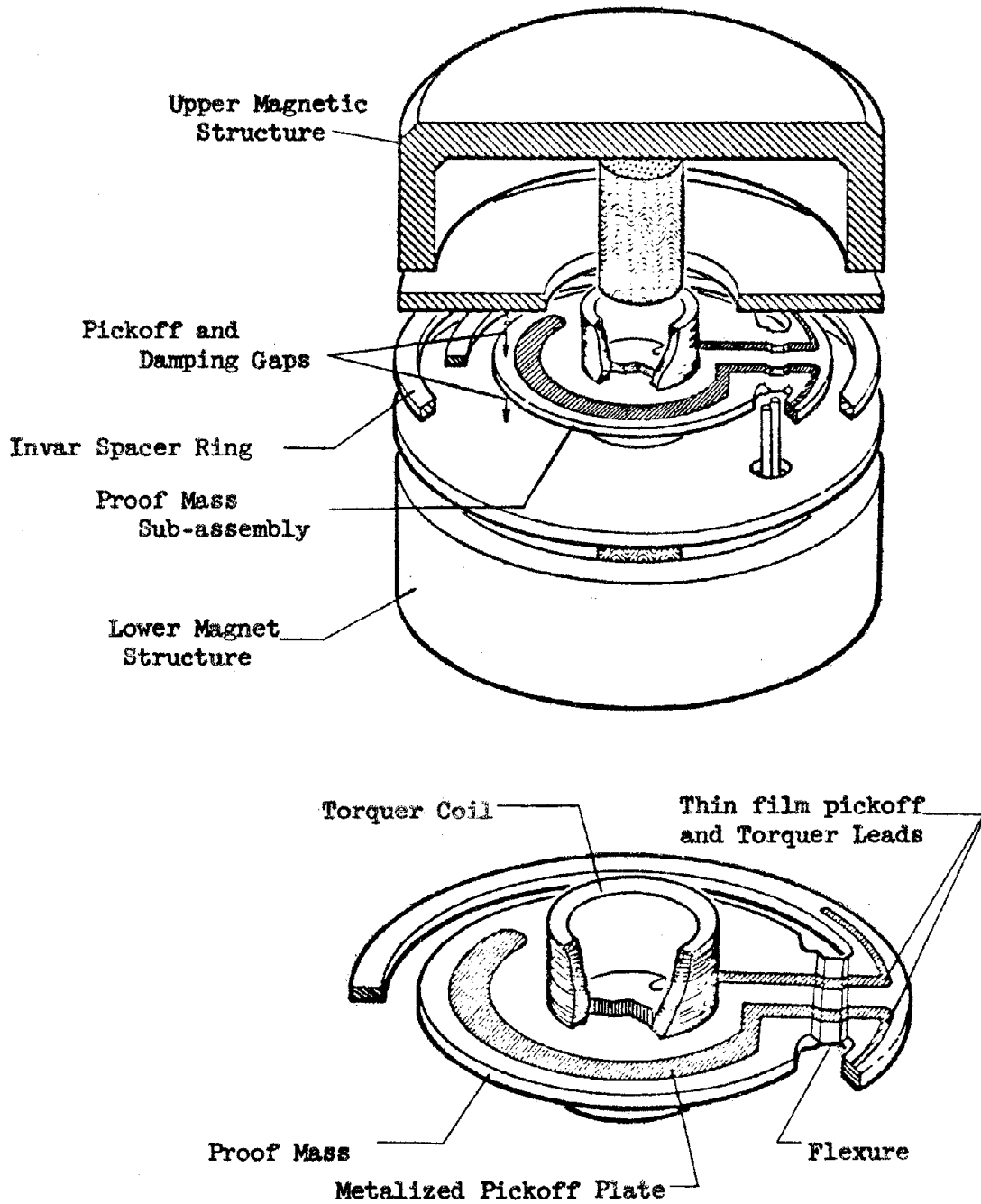


FIGURE 3-6 Q-FLEX ACCELEROMETER

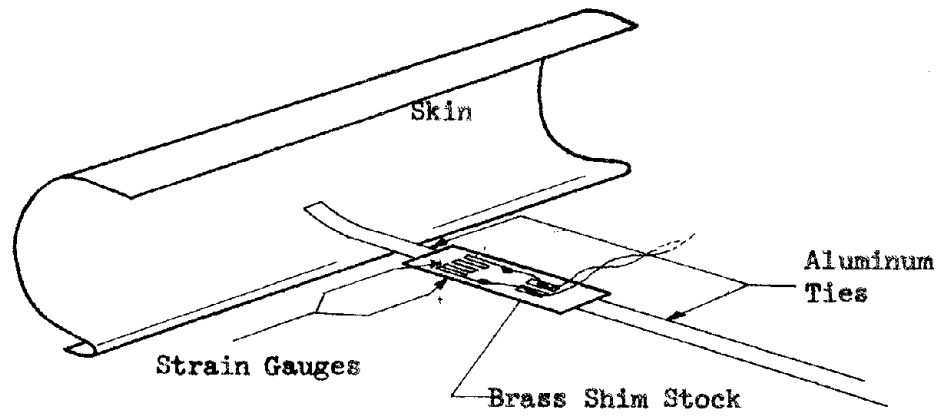


FIGURE 3.7a SERIES A TIE -TENSION GAUGES

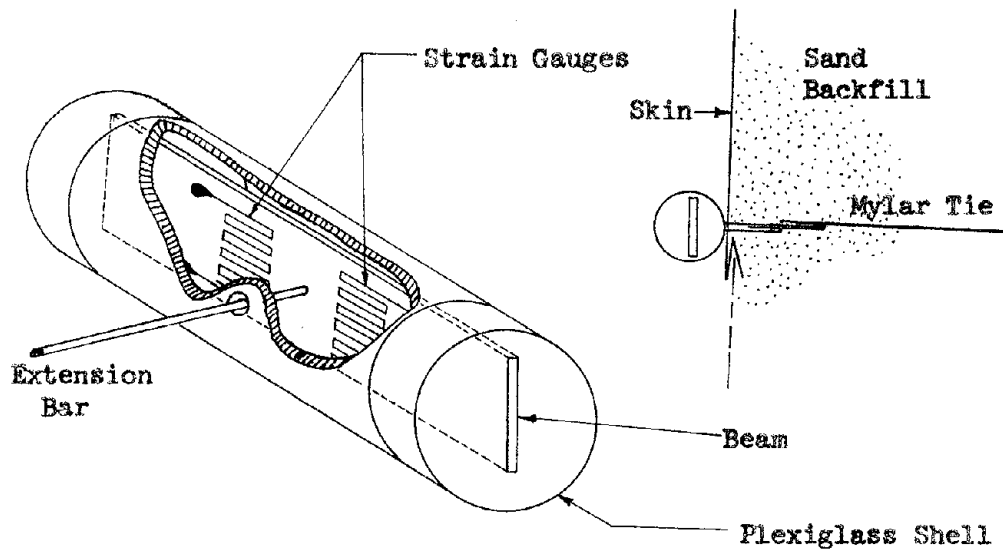


FIGURE 3.7b SERIES B TIE-TENSION GAUGES

FIGURE 3.7 TIE-TENSION GAUGES

force in the tie is transmitted through the rod and acts as a concentrated load acting at the center of the beam. Strain gauges, Micro-Measurement no. EA-06-062AP-120, were mounted on the beam and calibrated to provide a measurement of the tie tensile force.

Because the tie-tension gauge would be acted upon by the acceleration field, it was necessary to insure that the forced vibrations of the beam would not affect the tie-tension measurements. The first fundamental frequency of the clamp-clamped beam is (17)

$$\begin{aligned}
 f &= (4.730)^2 \frac{EI}{ml} \\
 &= (4.730)^2 \frac{432 \times 10^4 \times .00002}{.0071 \times 14} \\
 &= 1.2 \times 10^2 \text{ CPS}
 \end{aligned}$$

where E is Young's modulus, I is the moment of inertia, and l is the length of the beam. Since the forcing frequency, 11.6 cps, is less than the first fundamental frequency the beams will respond in an essentially static manner, unaffected by the accelerations of their mounts.

Tie-Pullout Apparatus. In addition to the instrumentation of the model wall itself, an additional test was performed by measuring the force required to pull-out 'extra' ties placed in the model during construction. These tests were performed to study the frictional resistance between the soil and the ties under various stress and acceleration conditions.

The tie pullout apparatus is shown in Fig. 3.8. It is simply a cantilever beam mounted on a plexiglass slide. The plexiglass slide is mounted with a rail and is driven through a spur gear by means of

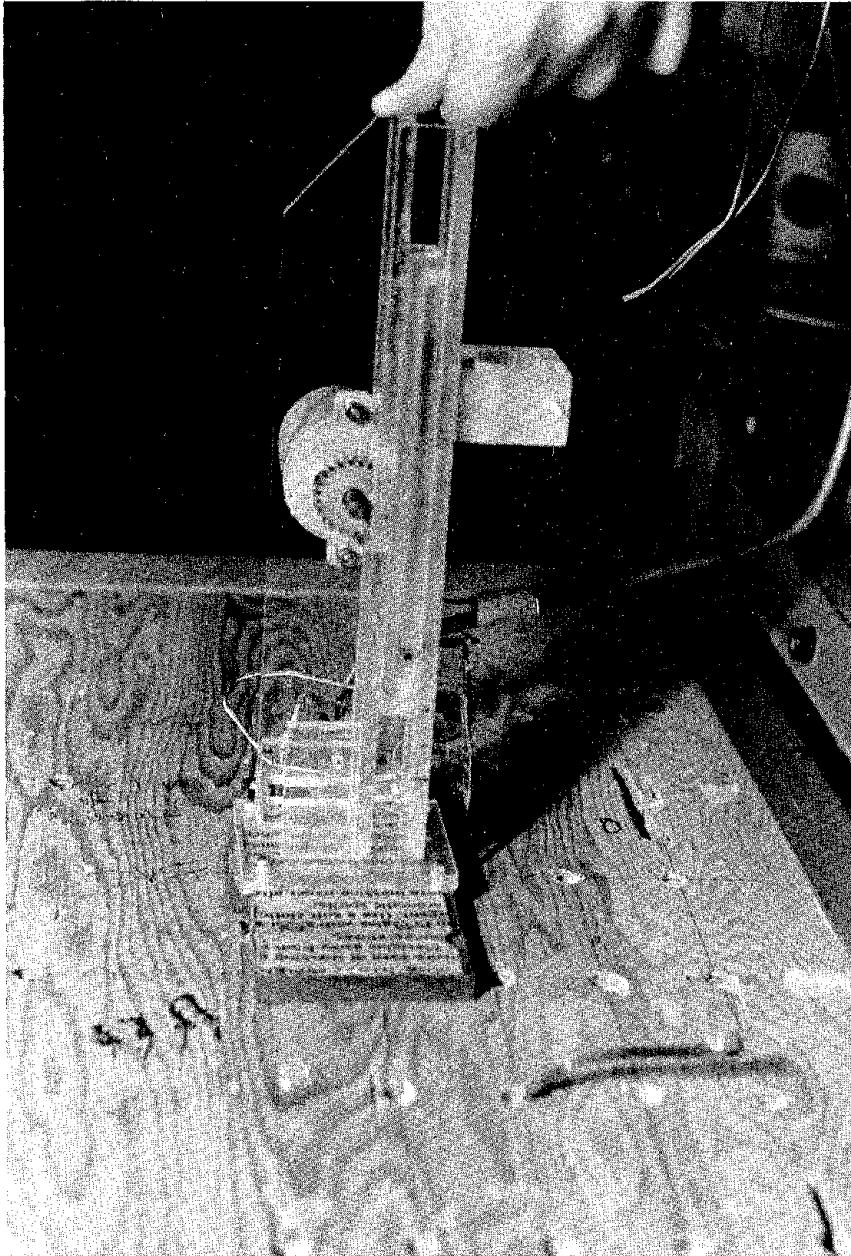


FIGURE 3-8 TIE-PULLOUT DEVICE

a constant speed, 1 rpm, D.C. motor. The slide is mounted in a plexiglass box that in turn mounts on the model test box or a stand. The 'extra' ties placed in the sand were attached to the cantilever beam and 'drawn out' by the slide. Force measurements were obtained by means of a strain gauge mounted on the cantilever beam, and a displacement record is provided by an LVDT attached to the slide or by the time marks on the recording papers, since the motor moves at constant speed.

Recording Instruments. Because of the relatively high frequency of the input motion, it is necessary to continuously monitor the instrumentation measurements. To accomplish this all instruments were connected to a Sanborn, model 7708-A eight-channel recorder. In addition it was frequently necessary to employ additional two-channel recorders of the same type. These recorders were equipped with timers to provide a time scale on the recording paper.

CHAPTER 4 LABORATORY TEST RESULTS

4.1 INTRODUCTION

The laboratory model tests were performed for failure by Tie Breakage, Series A, and Tie Pullout, Series B. Since the experimental emphasis was different for Series A and B tests these will be discussed separately. A complete summary of a laboratory tests performed is given in Appendix A.

Series A Tests. Test Series A model walls were constructed using eleven layers, each 1.0 inch high, curved aluminum skin sections, and aluminum ties. All Series A test models were constructed using one tie arrangement as follows: aluminum foil ties, each 20 inches long and 0.15 inches wide, and a constant horizontal tie spacing of 6 inches. Calculations of the static factor of safety, against tie failure, for each level are shown on Fig. 4.1. For these conditions the minimum static factor of safety of 2.0 occurred at the primary tie level. The studies by Lee, et al, (3) showed that the minimum length of tie required to prevent failure by tie pullout was 9 inches, thus the 20 inch long ties provided a static factor of safety against tie pullout of 2.2.

During the dynamic testing of the Series A wall continuous records were taken of the following data:

- 1) dynamic tie-tensions
- 2) wall displacements, and
- 3) accelerations.

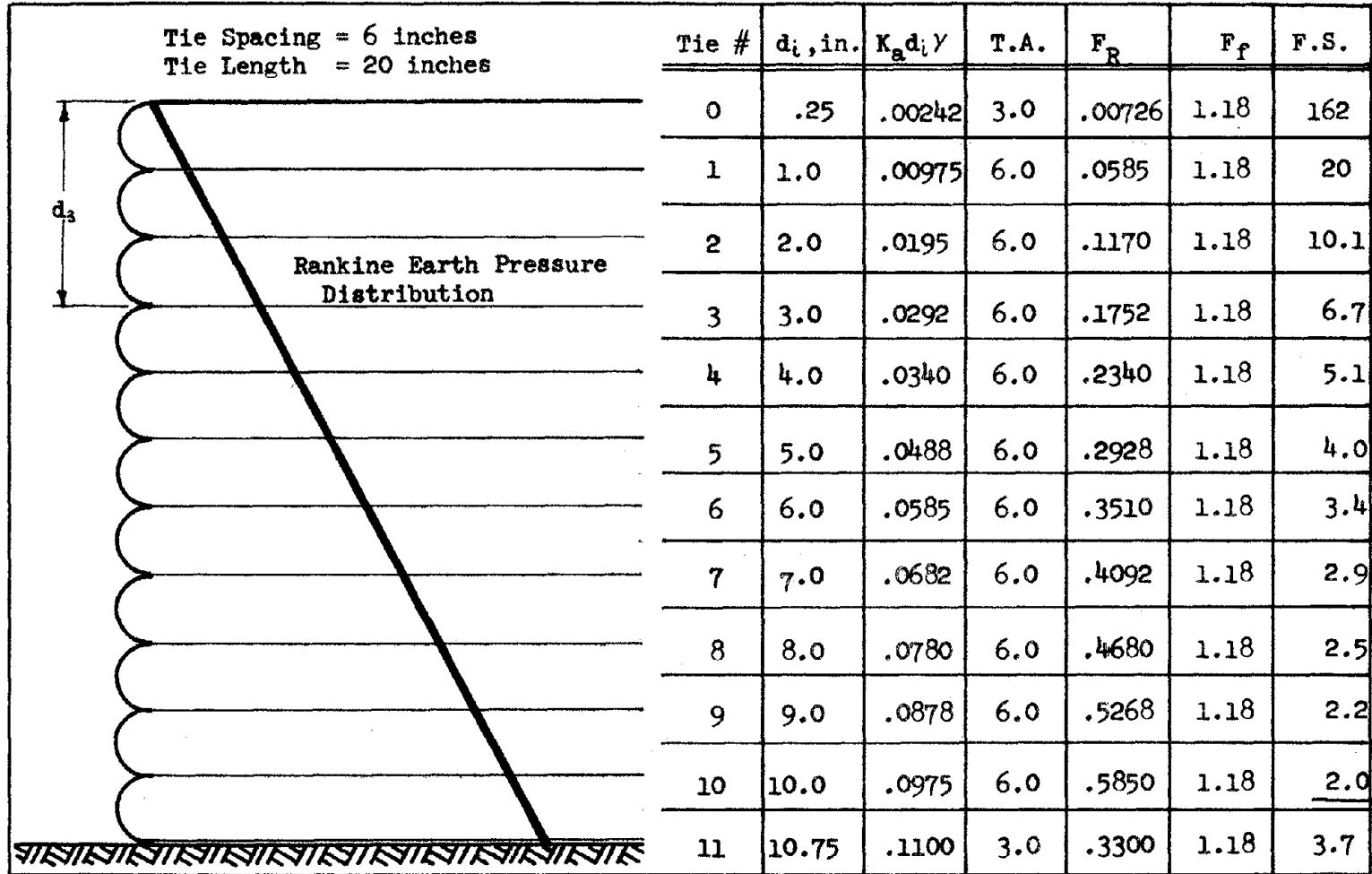


FIGURE 4-1. RANKINE STATIC FACTOR OF SAFETY

These variables are listed in order of the emphasis placed on them during the testing procedure. In addition to these measurements an additional record was maintained of any observed failure surfaces. The failure surfaces were determined by observing discontinuities in colored sand layers placed between the reinforcing layers during construction. Because the viewing window had not been cut in the model box yet, this required careful removal of the sand from the model box after failure of the wall to uncover the layers of colored sand buried within the model. It was hoped that observation of actual failure surfaces would lead to a pseudo-static stability analysis procedure for dynamic loads.

The Series A models were constructed such that failure of the wall would occur by Tie Breakage. The Series A models were primarily intended to provide information concerning:

- 1) the tie forces during dynamic loading, and
- 2) a measure of the displacement time-history during a Tie Breakage failure.

Series B Tests. Test Series B model walls were constructed using eight layers, each 1.5 inches high, flat aluminum skin sections, and mylar ties. Series B differed from Series A in that most of the tie arrangements were designed such that the factor of safety against failure, from Tie Pullout, was constant for all tie levels. Each Series B tie was designed to resist, by tie friction, estimated values of dynamic tie forces acting at each level. These estimated tie forces were based on the value of experimentally measured dynamic tie tensions from preceding Series B tests.

Three different types of tests were performed in Series B using the mylar recording tape so that no tie breaking would occur. These are designated Series B-1, B-2, B-3, and are characterized by an increasingly empirical estimate of dynamic tie forces used in the design of tie arrangements.

During the Series B tests the emphasis was placed on continuous monitoring of the following variables:

- 1) dynamic-tie tension forces, and
- 2) the acceleration amplification in the failure wedge.

In addition, the location of all failure wedges was recorded by observing through the viewing port all discontinuities of the colored sand layers. The use of the viewing port to observe the failure wedges proved to be a significant improvement over the procedure used in Series A tests. Late in Series B tests failure wedges were not forming so the layers of sand were replaced by dots of colored sand to indicate possible shear deformation of the wall.

Series B-1. The Series B-1 mylar tie arrangement consisted of a constant tie length of 20 inches, a constant tie width of 0.25 inches, and a constant horizontal tie spacing of 6 inches. The B-1 tie arrangement was an arbitrary continuation of the tie length and tie spacing of the Series A tie arrangement. This arbitrary selection was based on uncertainty of key variables at that time, primarily dynamic tie-tension forces and the value of the soil-tie friction angle, and a desire to use an initial tie arrangement similar to that previously used in static and dynamic Reinforced Earth wall model

tests. It provided data for tie pullout resistance which was then used for later designs to insure an adequate tie length and spacing to resist the tie forces. In addition Series B-1 provided the first measure of the total tie dynamic tie forces that occur during vibratory loading.

Series B-2. The next group of tests. Series B-2, used a mylar tie arrangement designed by the following assumptions:

- 1) lateral earth pressure coefficient equal to K_0 , where $K_0 = 1 - \sin \phi$
- 2) linear pressure distribution, and
- 3) a soil-tie friction angle of 10° .

The first two assumptions were based on tie-force measurements made in the Series B-1 tests. The third assumption of $\phi_u = 10^\circ$ was based on approximate values determined by a series of monitored tie pullout tests that were being performed concurrently with the Series B tests.

Series B-3. The final group of tests, Series B-3, was designed using dynamic tie forces predicted using a procedure formulated from the results of Series B-1 and B-2 test results. This procedure is based on a calculated Seismic Design Envelope of tie forces for a desired input acceleration. The Series B-3 models were also designed for soil-tie friction angles ranging from 7° to 20° , with a seismic factor of safety against tie pullout of 1.0. This variation reflects a continuing uncertainty as to the true value and nature of ϕ_u . Table 4.1 presents a summary of the basic tie arrangements used in both Series A and B tests.

Table 4.1 Basic Tie Arrangements and Design Assumptions				
Test Series	Tie Arrangement	Tie Length (in)	Tie Spacing (in)	Assumptions Required to Determine Tie Length and Spacing
A	A-1	20	6	Constant Tie Length and Spacing such that the F.S. against Tie Failure was 2.0
B	B-1	20	6	Arbitrary continuation of Series A Tie Spacing and Length
	B-2	Varied	3	1) Lateral Earth Pressure Coefficient equal to K_0 2) Soil-Tie Friction Angle= 10 degrees 3) Rankine Failure Wedge
	B-3	Varied	3**	1) Seismic Design Envelope 2) Constant Soil-Tie Friction Angle 3) Rankine Failure Wedge

** In some cases it was necessary to reduce the tie spacing to 1.5 inches at the upper tie levels.

Additional Tests. Two additional test models were constructed using 10 and 11 layers, each 1.5 inch high, flat aluminum skin sections, and mylar ties. The tie arrangement was designed to resist a Seismic Design Envelope determined in the Series B tests, and discussed in Section 4.3.3. These additional tests were higher than previous dynamic tests and were constructed to determine the influence of the frequency of vibration upon the Seismic Design Envelope.

Terminology. Before presenting the test results it is necessary to introduce some basic terminology that will be used to describe the test results. The following terms are illustrated on Fig. 4.2.

During the Series B tests the emphasis was placed on continuous monitoring the following variables:

- 1) the dynamic-tie tension forces, and
- 2) the acceleration amplification in the failure wedge.

In addition, the location of all failure wedges was recorded by observing through the viewing port all discontinuities of the colored sand layers.

The terminology used to describe the measured tie forces was arbitrarily selected by the author such that there would be a minimum overlap with definitions in related studies (i.e. liquefaction).

Static tie force: Forces monitored in the ties during the construction procedure and in the completed structure prior to dynamic loading.

Minimum dynamic tie force: The minimum force acting on the tie during one cycle of dynamic loading,

Maximum dynamic tie force: The maximum force acting on the tie during one cycle of dynamic loading.

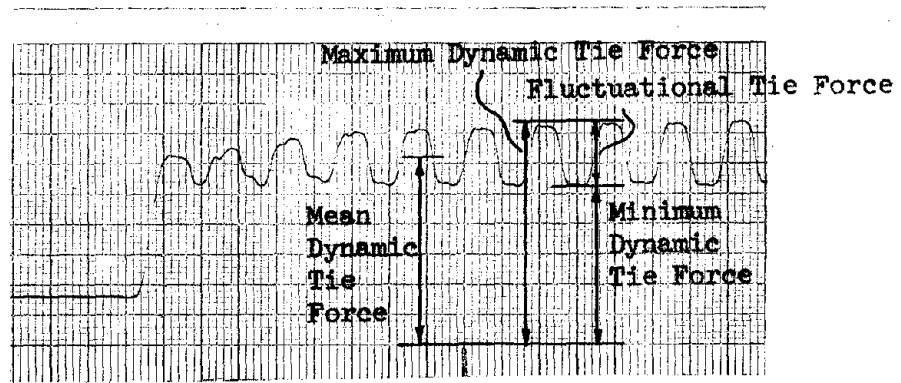


FIGURE 4.2a. TIE FORCE TERMINOLOGY

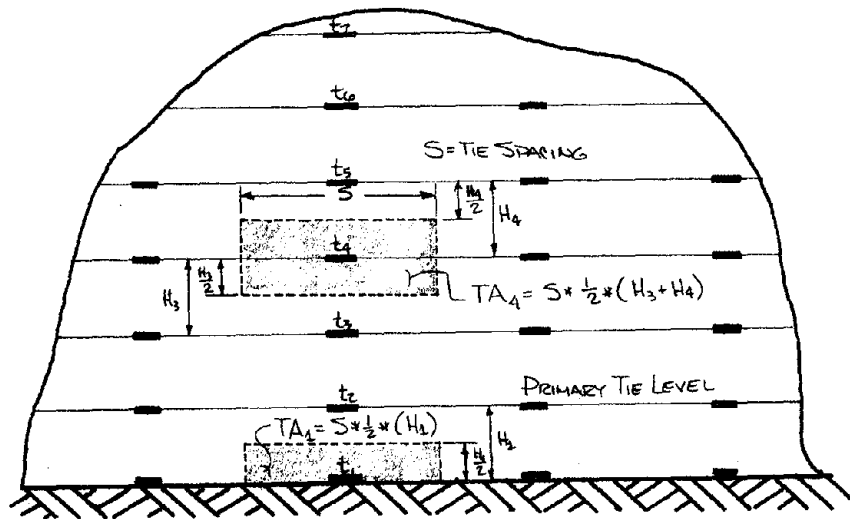


Figure 4.2b TIE TRIBUTARY AREA

FIGURE 4.2 BASIC TERMINOLOGY

Mean dynamic tie force: The average force acting on the tie during a complete cycle of dynamic loading. This is usually taken to equal the average of the minimum and maximum dynamic tie forces.

Fluctuational dynamic tie force: The difference between the minimum and maximum dynamic tie forces.

Primary tie level: The first tie level above ground level.

Tributary area, TA: The area of the wall which must be supported by each single tie. This is illustrated on Fig. 4.2b.

4.2 SERIES A TESTS: TIE BREAKAGE

Series A consisted of seven model tests performed using the same wall configuration subjected to the sinusoidal input motion. A summary of these model tests is presented in Appendix A.

Model Configuration. The Series A Reinforced Earth walls were eleven layers high, each 1.0 inch high, curved aluminum skin sections, and aluminum ties with a uniform length of 20 inches and a constant horizontal spacing of 6 inches. As shown on Fig. 4.1, the minimum static factor of safety against tie failure for these design conditions is 2.0.

Tie Tension Records. As mentioned previously, the tie tension measurement system used for this series of tests did not give good results because slight bending which developed during cyclic loading often affected the absolute readings. However, the gauges did record the cyclic fluctuational dynamic tie forces. One particularly clear record is presented in Fig. 4.3 and shows that as the tension in the instrumented tie was suddenly reduced to near zero the wall displacement dramatically increased, clearly indicating that failure was caused by tie breaking. The basic terminology for the description of dynamic tie tension magnitudes is illustrated in Fig. 4.3 for additional reference.

In general, because of the bending problem, further information from the tie tension monitoring in Series A tests was disappointing and inconclusive. The strain gauges had been mounted back-to-back on opposite sides of the brass strips, Fig. 3.6a, to eliminate bending influence, but this procedure is satisfactory only for very small

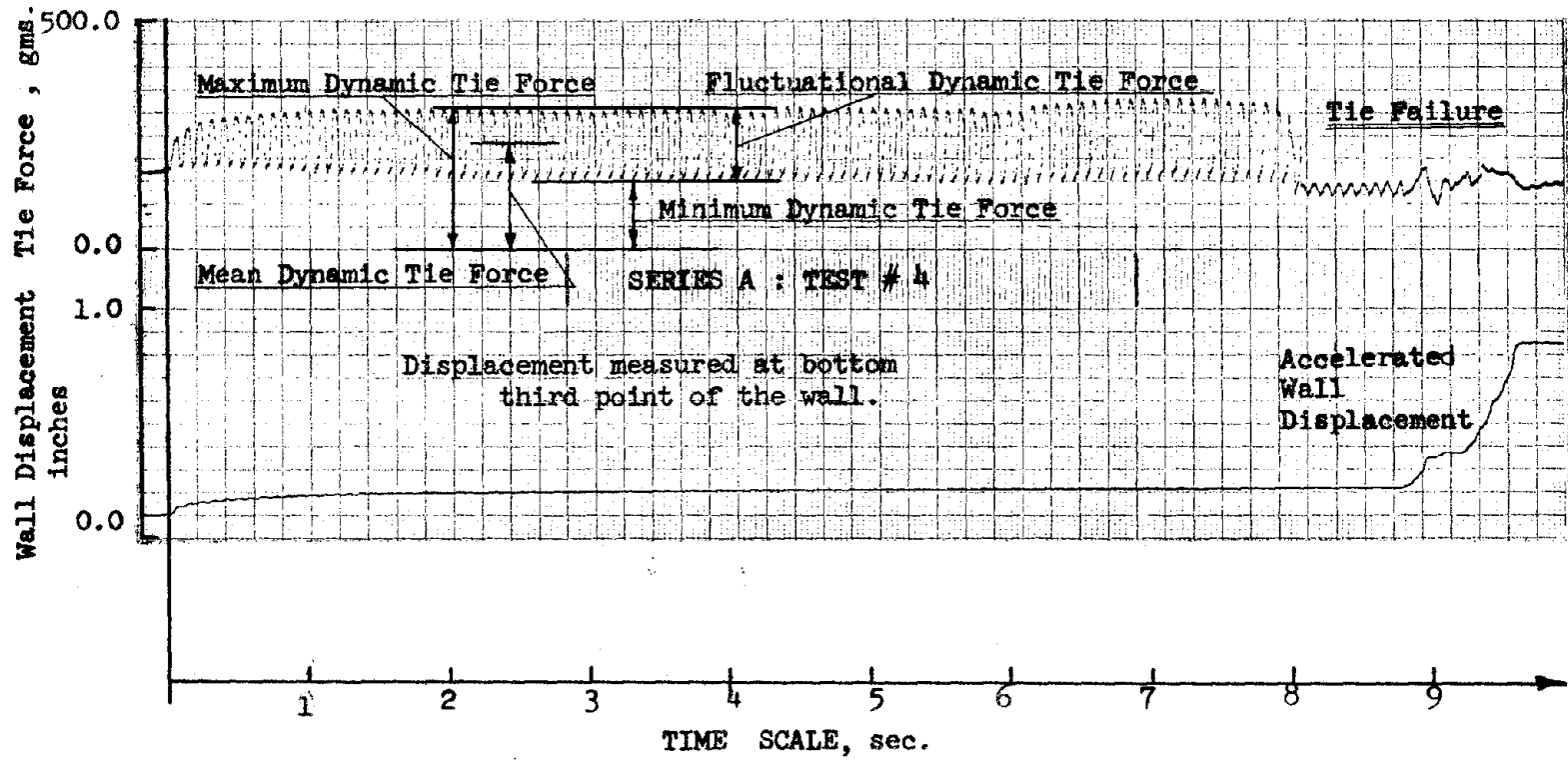


FIGURE 4.3 INSTRUMENTED TIE FAILURE

curvatures. The location of the gauges in the model, Fig. 4.4, subjects the gauges to large bending forces due to the deformation of the failure wedge. The bending of the gauges caused a drifting of the monitored tie stress due to the addition of bending stresses. Thus the mean dynamic tie force measurements included both bending and axial stresses. Because of this the true mean dynamic tie force, due to tension only, could not be determined accurately.

The value of the fluctuational dynamic tie tension measured by the gauges was assumed to be relatively free of bending influences, and a summary of the measured fluctuational dynamic tie tension forces is presented in Fig. 4.5. It should be remembered that the fluctuational dynamic tie tension is relatively useless without an accurate knowledge of the mean dynamic tie force, and this information was not known due to the drifting problem.

Acceleration Records. The embedded accelerometer was mounted in the top layer of sand and approximately 16 inches behind the wall. This was away from the potential failure wedge which extended back about 5 inches behind the wall at the top. The surface accelerations are plotted as a function of the base acceleration in Fig. 4.6. These data indicate that for these test conditions;

- 1) there exists a threshold acceleration below which the wall acts as a rigid body, and
- 2) the amplification increases with acceleration within the limits of test accelerations.

Displacement Records. The time history of displacement of the wall was measured using LVDTs placed at the top and bottom third points of the Reinforced Earth wall, see Fig 3.5. The displacement of the

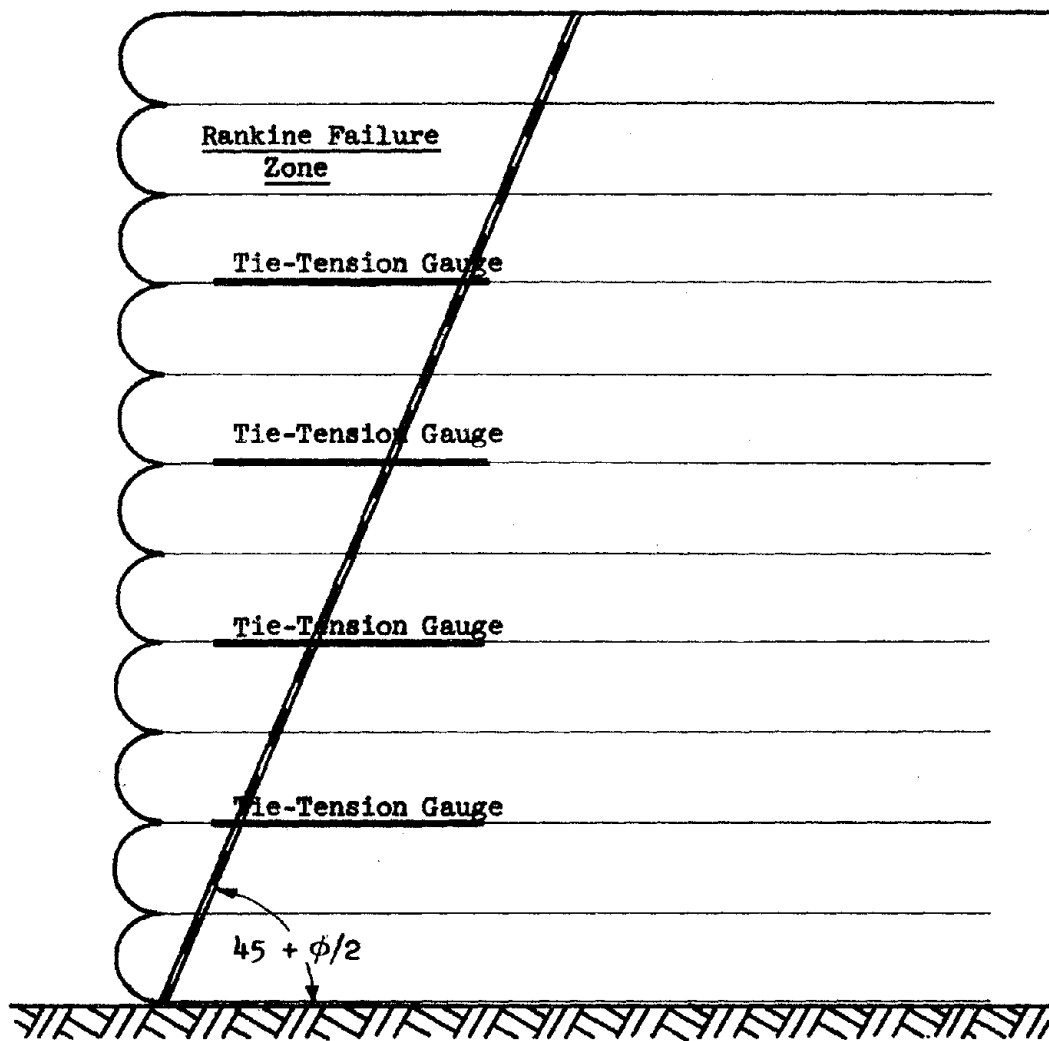


FIGURE 4.4 TIE-TENSION GAUGE LOCATION

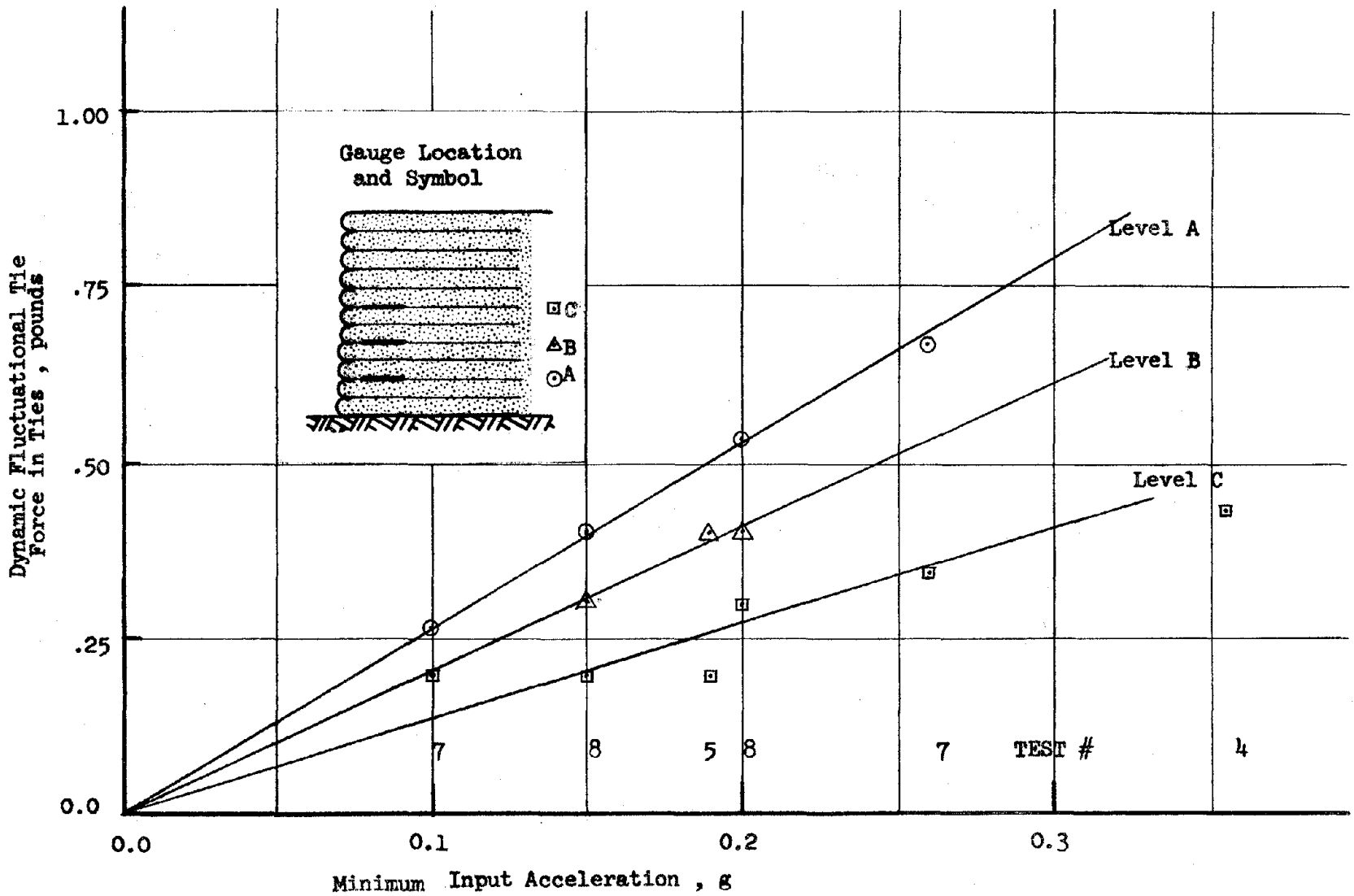


FIGURE 4-5 DYNAMIC TIE FLUCTUATIONAL FORCE

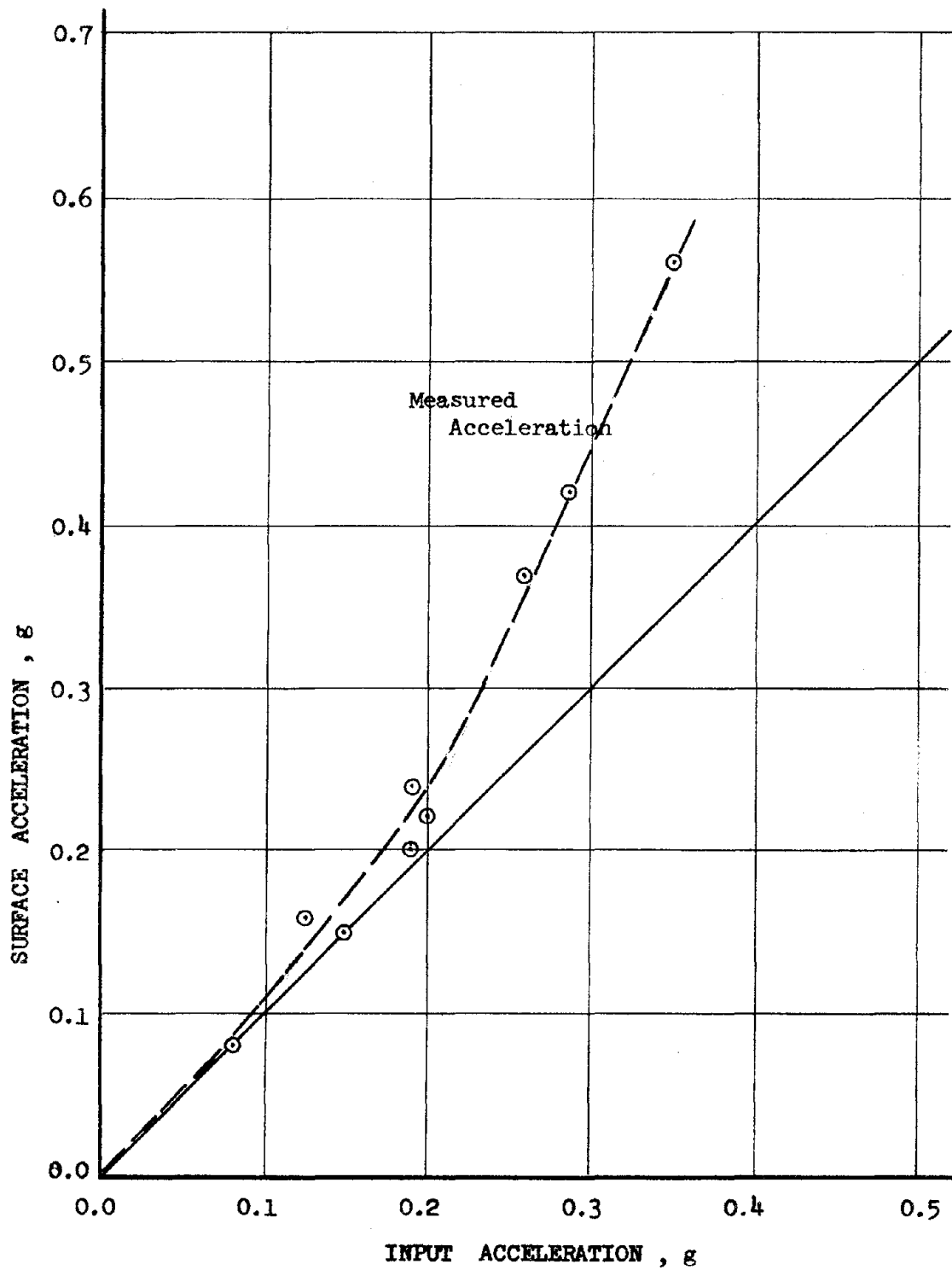


FIGURE 4.6 ACCELERATION AMPLIFICATION

walls in the Series A tests all followed a consistent pattern:

- 1) during vibration of the wall the top of the wall moved out at a rate 2 to 4 times that of the bottom of the wall, and
- 2) after the top had moved out approximately 1 inch relative to the bottom third point, the bottom of the wall would suddenly displace past the top of the wall and failure would occur.

A test record of this series of displacements is shown in Fig. 4.7.

Failure Mechanism. The typical sequence of observed wall displacements described above is shown in Fig. 4.8. The general description, by sequence number, is as follows:

- 1) initial wall configuration, end of construction, static equilibrium,
- 2) shaking begins, the elements begin an outward displacement with the upper level traveling 2 to 4 times faster than the lower,
- 3) the displacement continues as in 2,
- 4) the displacement of the lower wall section suddenly occurs at a rate much greater than the upper section,
- 5) the lower section is now displaced more than the upper (note that the lower skin component shows relatively little displacement), and
- 6) failure of the wall occurs at the second and third levels.

From examination of tie force records it is proposed that tie breakage occurs at levels 2 and 3 during sequence 5. It should be noted that failure sequence 4, 5, and 6 occur so rapidly that it is difficult to view this sequence even by using slow motion photography. Displacement greater than indicated by sequence 6 was prevented by support brackets which were used to reduce the damage to the skin elements that occurs during collapse. When the failure brackets

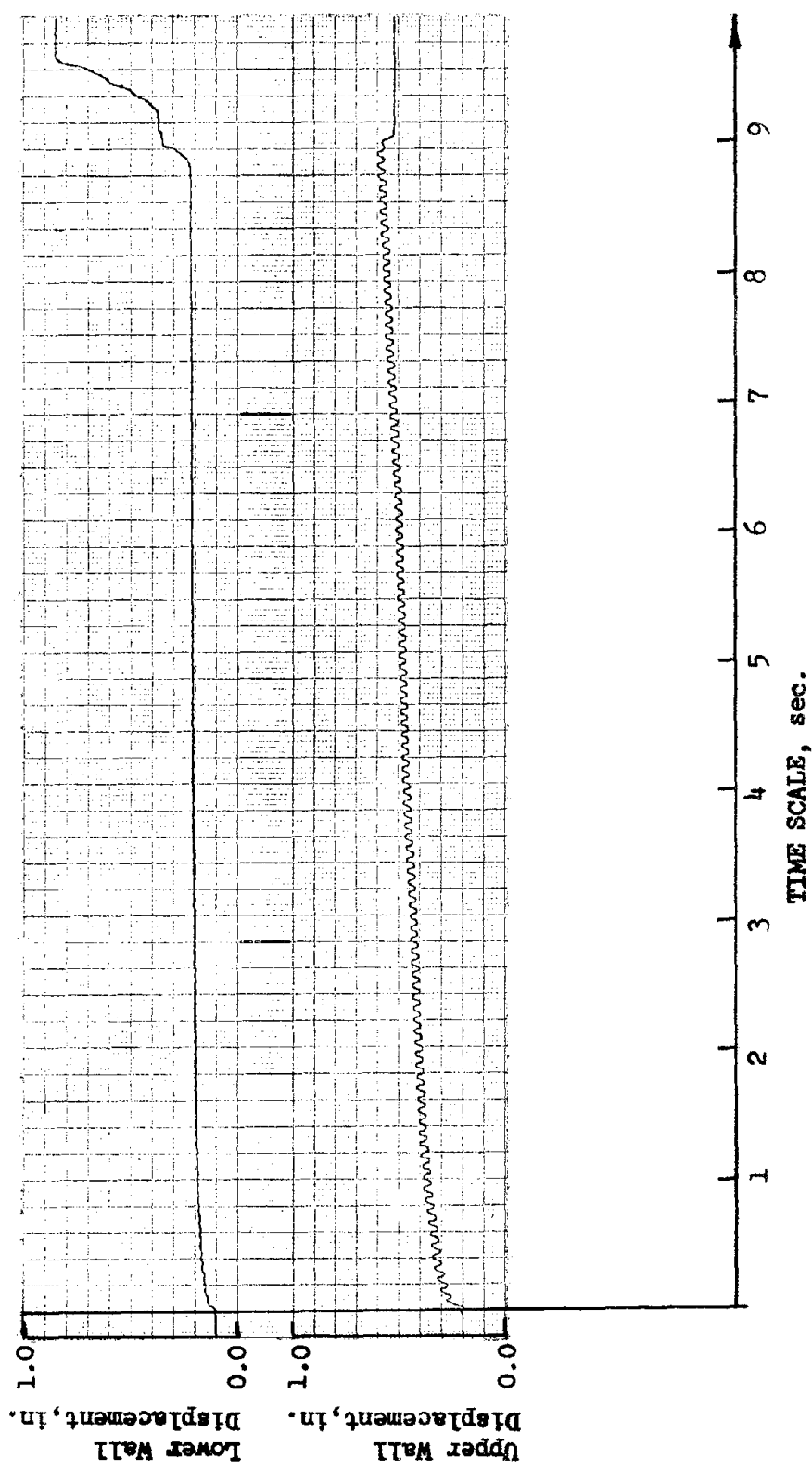


FIGURE 4.7 WALL DISPLACEMENT RECORD

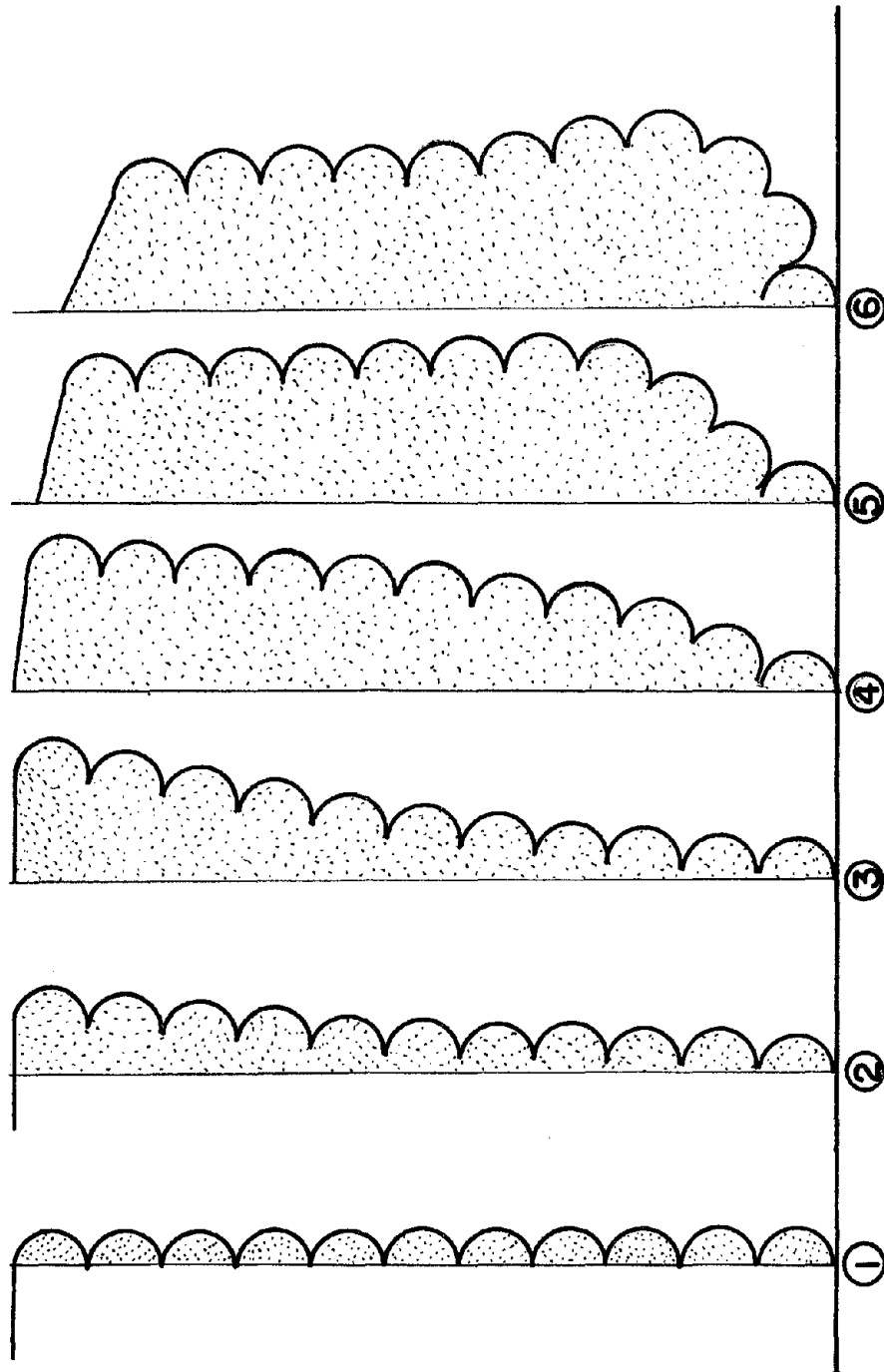


FIGURE 4-8 FAILURE MECHANISM

were omitted there was complete collapse of the wall. The failure occurred suddenly and catastrophically.

Failure Surface. In most Series A tests the failure of the models was so destructive that it was difficult to determine the exact failure surfaces. This was further complicated by the difficult procedure used to measure the failure surface in Series A. The failure surface predicted by the Rankine Earth Pressure Theory is compared in Fig. 4.9 with the only two Series A failure surfaces measured. Notice that the actual failure surfaces do not go through the toe of the wall but actually terminate at the top of the first skin level.

Summary of Series A. The most important knowledge gained from this series of tests is the empirical observation that the dynamic failure of Reinforced Earth walls from Tie Breakage occurs catastrophically. The high rate of displacement of the upper wall sections relative to the remainder of the wall also suggested that an insufficient number, or length of ties were provided to reinforce these sections. This would imply a lateral seismic force distribution other than one that increases linearly with depth, the failure modes suggest a force distribution during dynamic loading that is relatively greater near the top of the wall than the linear assumption. Unfortunately since the tie force gauges did not function properly during the dynamic loading, this conclusion cannot be completely verified by this series of tests alone. However the Series B tests which are described in the next four sections verify this conclusion.

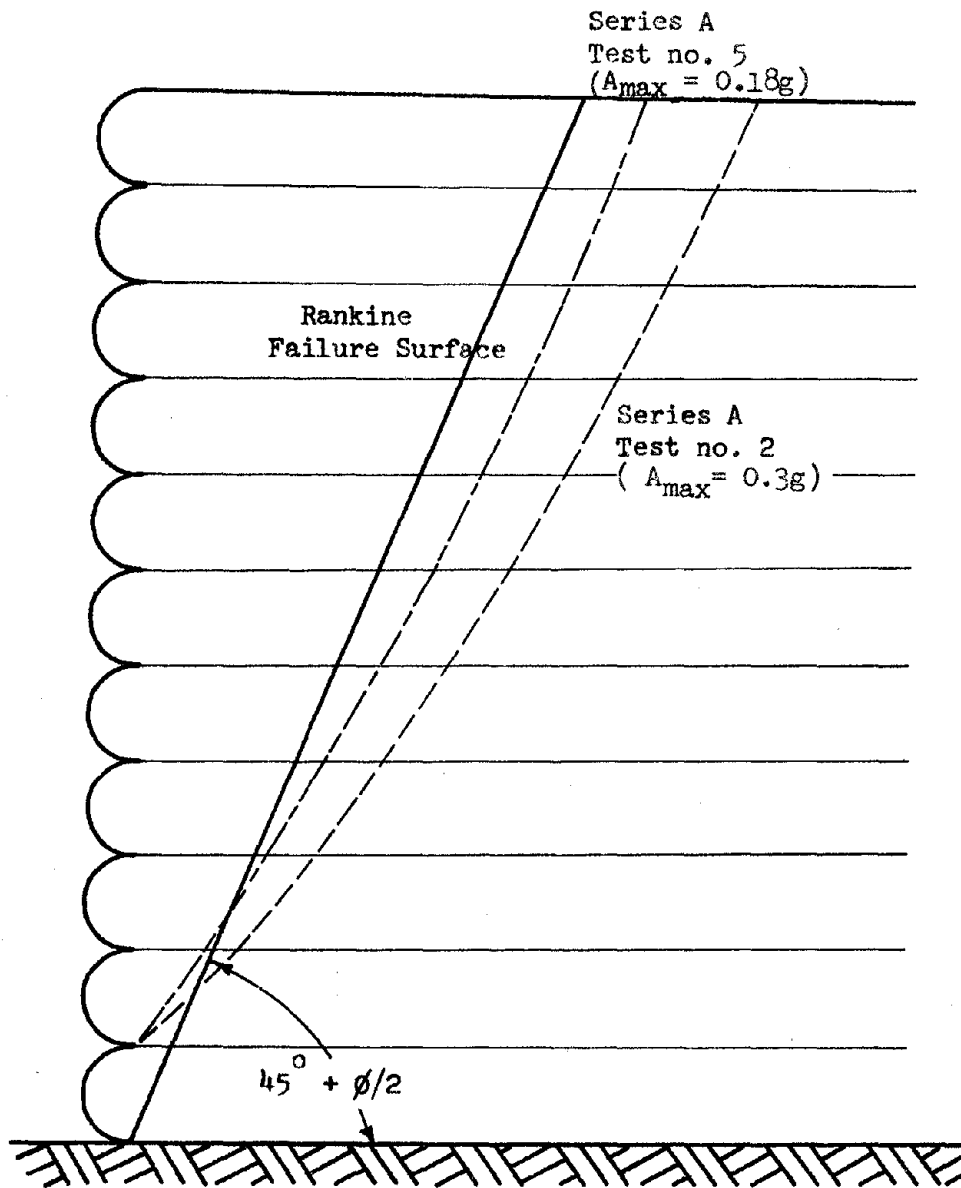


FIGURE 4.9 SERIES A-1 FAILURE SURFACES

4.3 SERIES B TESTS: TIE PULLOUT

The Series B Reinforced Earth walls were intended to provide an empirical knowledge of the failure mechanism due to tie pullout, and to provide a measure of the dynamic tie forces. The Series B models used the flat skin elements and the mylar recording tape. In addition, the Series B models used the improved Tie-Tension gauge that was presented in Fig. 3.7b. The general arrangement of instrumentation is shown in Fig. 4.10. The walls were subjected to a sinusoidal input ground motion with a frequency of 11.6 cps and varying intensities of ground accelerations. A summary of the Series B tests is provided in Appendix A.

As previously discussed, the Series B tests can be broken down into three distinct subseries. These subseries are designated B-1, B-2, B-3, and differ primarily in the assumed dynamic tie forces used in design.

Series B-1. Because the Series A tests did not provide an accurate estimate of dynamic tie forces and because the soil-tie friction angle was not known for mylar, it was necessary to assume an arbitrary design for the Series B-1 models. The Series B-1 tie arrangement consisted of the same uniform tie length and horizontal spacing as used in Series A. The Series B-1 tests provided the first measure of the true dynamic tie forces and an indication of the ductility of the failure mechanism from tie pullout.

Series B-2. The Series B-1 tests had indicated a magnitude of seismic

49 - II

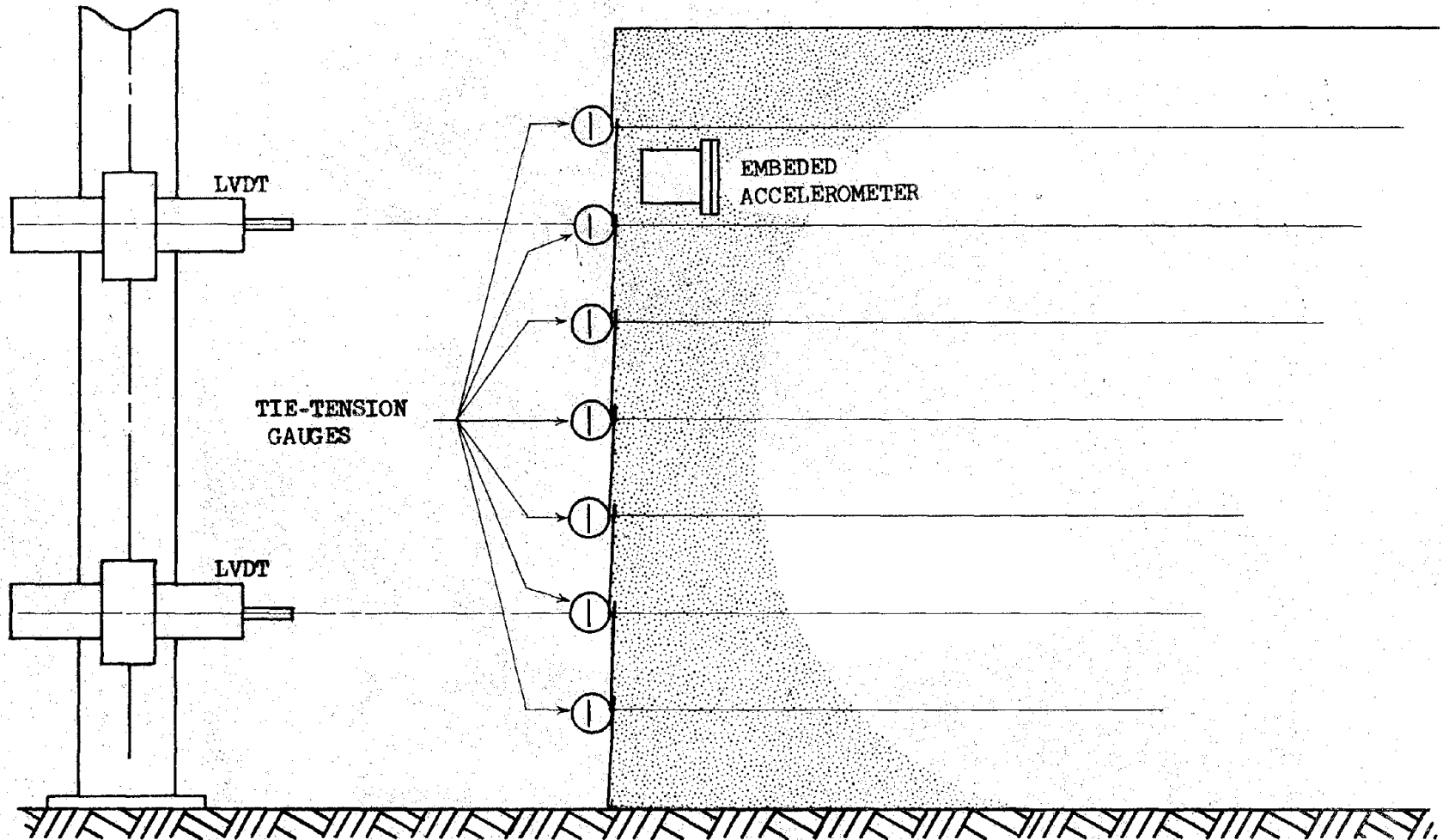


FIGURE 4-10 SERIES B INSTRUMENTATION

lateral forces similiar to those predicted using $K = K_o$. In addition, model tie pullout tests, run concurrently with Series B-1, indicated an approximate soil-tie friction angle of 10° . Based on this empirical data the Series B-2 models were designed using the Rankine Theory with $K = K_o$ and $\phi_u = 10^\circ$. The Series B-2 walls were the first to be designed to resist estimated seismic forces instead of factored static forces. This test series provided additional dynamic tie force measurements and demonstrated the ductility of the failure mechanism from tie pullout.

Series B-3. The Series B-3 models were the first to be designed using a lateral force distribution other than hydrostatic. Based on dynamic tie tension measurements and observations of excessive displacement of the tie levels in Series B-1 and B-2, it became apparent that the seismic forces near the top of the wall exceeded those predicted by a linear force distribution. The Series B-3 walls were designed to resist an empirical Seismic Design Envelope that reflected the larger forces near the top of the wall. The Seismic Design Envelope was a function of the input acceleration.

Because of the continuing uncertainty concerning the true value of ϕ_u , Series B-3 tests models were designed using a range of ϕ_u from 7 to 20 degrees with a dynamic factor of safety of 1.0.

4.3.1 SERIES B-1 TESTS: TIE PULLOUT

The Series B-1 tests consisted of 3 model Reinforced Earth walls subjected to a sinusoidal input ground motion with a frequency of 11.6 cps and varying intensities of acceleration. A summary of the Series B-1 tests is included in Appendix A.

Model Configuration. The three Series B-1 Reinforced Earth walls were eight layers in height, with a total height of 12 inches. It is recalled that Series A tests used 11 layers, at 1.0 inch per layer, making a total wall height of 11 inches.

The Series B-1 mylar tie arrangement, referred to as the B-1 tie arrangement, consists of the following:

- 1) constant tie length of 20 inches, and
- 2) constant horizontal tie spacing of 6 inches.

The B-1 tie arrangement was an arbitrary continuation of the tie length and spacing common to the Series A tests. Because the number of reinforcing layers was reduced from 11 to 8 and the tie spacing was constant, the Series B-1 models had fewer Reinforcing ties than the Series A-1 tests. In addition the overall height of the walls for the Series B tests was one inch more than the Series A test walls.

This arbitrary selection of tie length and spacing reflects the basic uncertainty, at that time, towards key design parameters; primarily the soil-tie friction angle, the seismic design forces, and the desire to use an initial tie arrangement for which previous static and dynamic tests had been performed. This wall had a minimum static factor of safety against tie breakage of 8.1 based on tie forces

calculated using a Rankine active earth pressure distribution. Based on an assumed soil-tie friction angle of 12° the minimum static factor of safety against tie pullout was 2.3.

Tie Tension Records. The tension in the mylar reinforcing ties was measured using the improved design for Tie-Tension instrument, as illustrated on Fig. 3.7b. A typical tie force record is presented in Fig. 4.11 and demonstrates how the static and dynamic force envelopes were selected. By monitoring the tie force gauges during construction and before application of the dynamic loading it was possible to construct static tie force envelopes for the wall at various stages of completion. In general the dynamic tie forces show an initial jump in the first few cycles, and then showed a continual slow rate of increase with time thereafter. For subsequent analysis it was necessary to arbitrarily select tie forces at one specified elapsed time. To be consistent for all tests, the dynamic tie forces were measured, on the tenth cycle after the tie forces had made their initial jump to the dynamic load. When failure occurred before this time, the maximum measured tie force was used.

A summary of the tie tension measurements for the Series B-1 test on wall no. 3, are shown in Fig. 4.12. This data shows the pattern of static tie forces measured during construction and the range of the forces measured at 10 cycles during the subsequent cyclic loading. The data clearly shows an increase of static forces with depth. The irregularities reflect the influence of construction procedures such as failure to tighten or stretch a particular tie, or a slight jar of

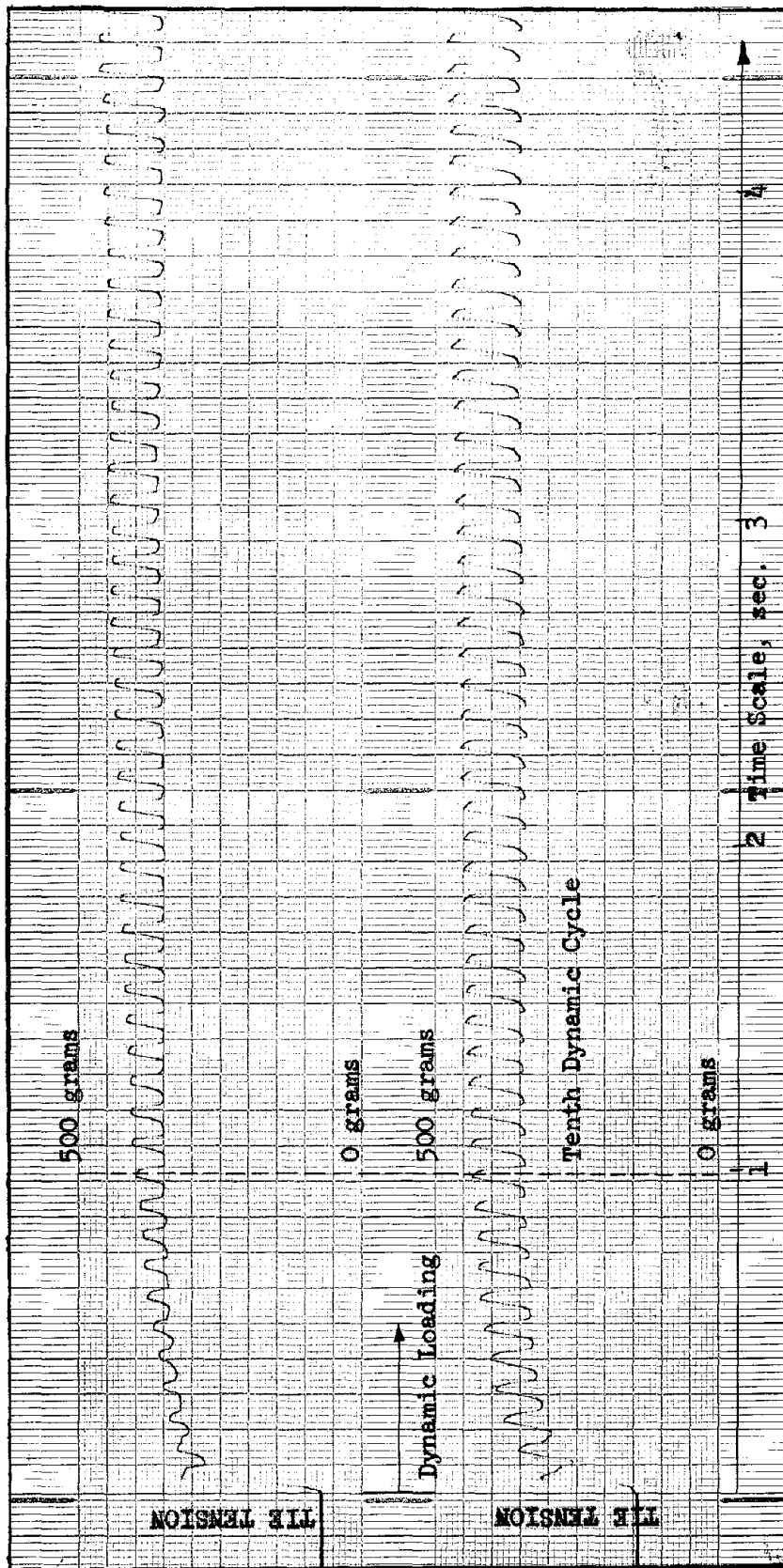


FIGURE 4-11 SERIES B DYNAMIC TIE TENSION

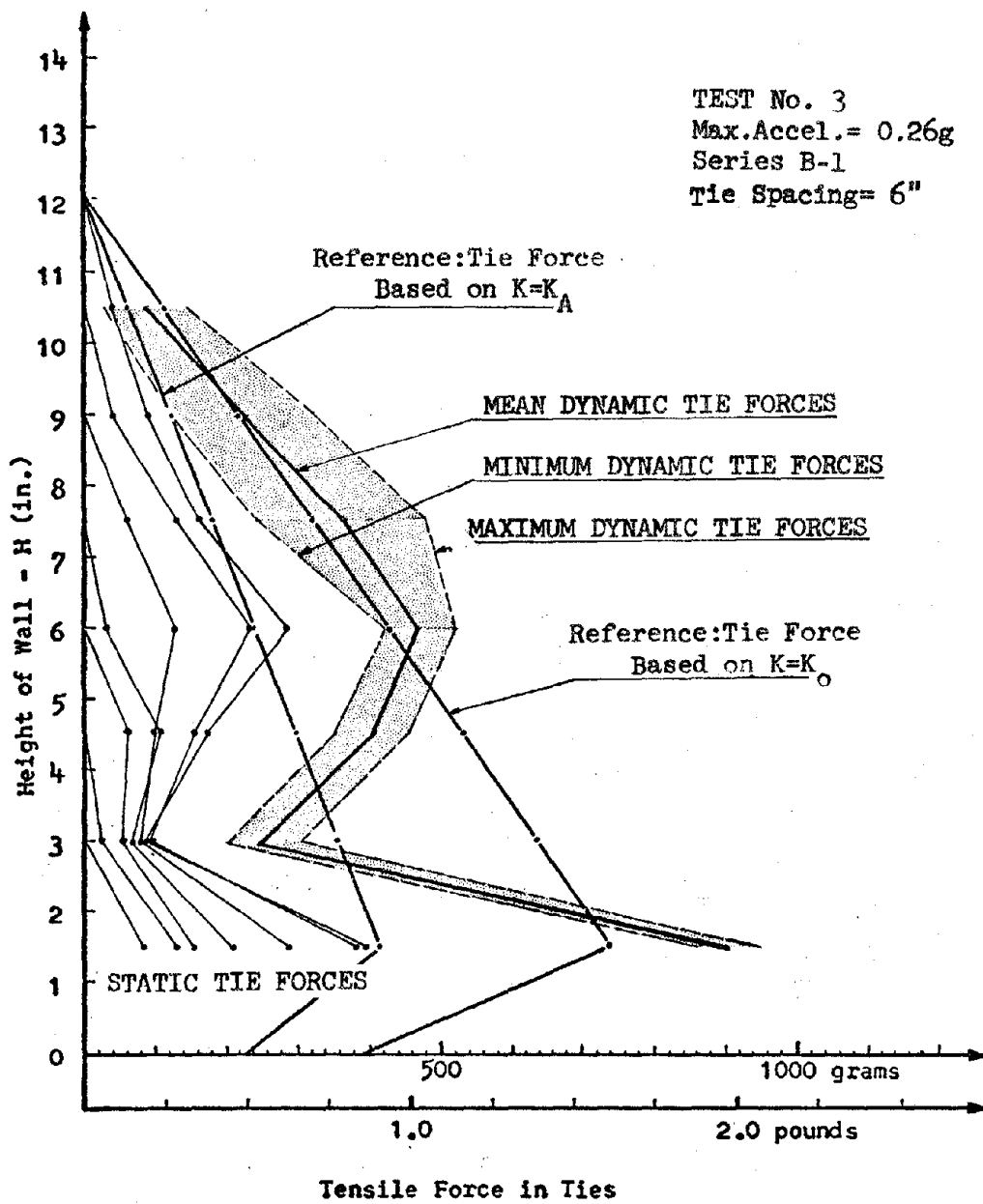


FIGURE 4.12 TIE TENSION MEASUREMENTS

the wall. These irregularities were common for all of the different walls. The reduced tie force at wall heights of 3.0 and 4.5 inches which developed during construction continued to be present even during the dynamic loading. The input acceleration of 0.26g was not sufficient to overcome the localized arching that must have developed during construction and which might have been responsible for the reduction of tie forces at these levels.

Test wall no. 4 was excited by an input acceleration of 0.32g. The tie tension measurements are given on Fig. 4.13. The construction tie tensions again show an increase of force with depth as well as an apparent sensitivity to construction procedures. These tie force irregularities that appear in the static tie force records, namely the reduced tie forces at the 1.5 and 3.0 inch heights, appear to be eliminated in the dynamic tie force envelope.

Regarding the static tie forces it is noted that in both Fig. 4.12 and 4.13 the tie force envelope using active (K_A) earth pressure appears to define an upper bound for the measured static tie forces. This agrees with the data previously reported by Lee, et al, (3) for similar model test walls. It is further noted that the cyclic loading causes the tie force to increase. The median loads measured during cyclic loading are consistently close to those predicted using the at-rest (K_0) earth pressure coefficient.

The third and final test wall using the B-1 tie arrangement was tested at two acceleration values, 0.15g and 0.44g, and the recording tie forces are illustrated on Fig 4.14. To eliminate

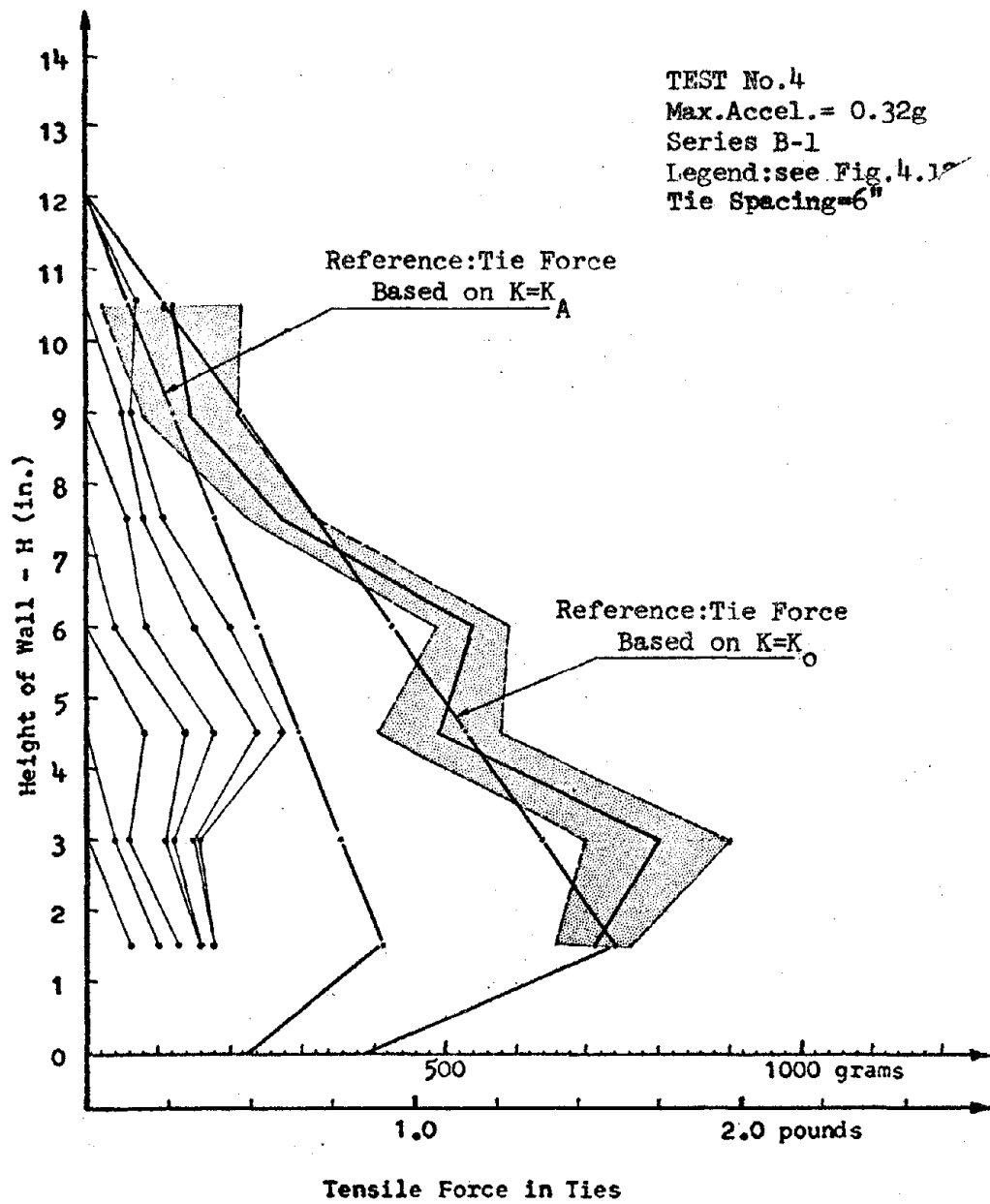


FIGURE 4.13 TIE TENSION MEASUREMENTS

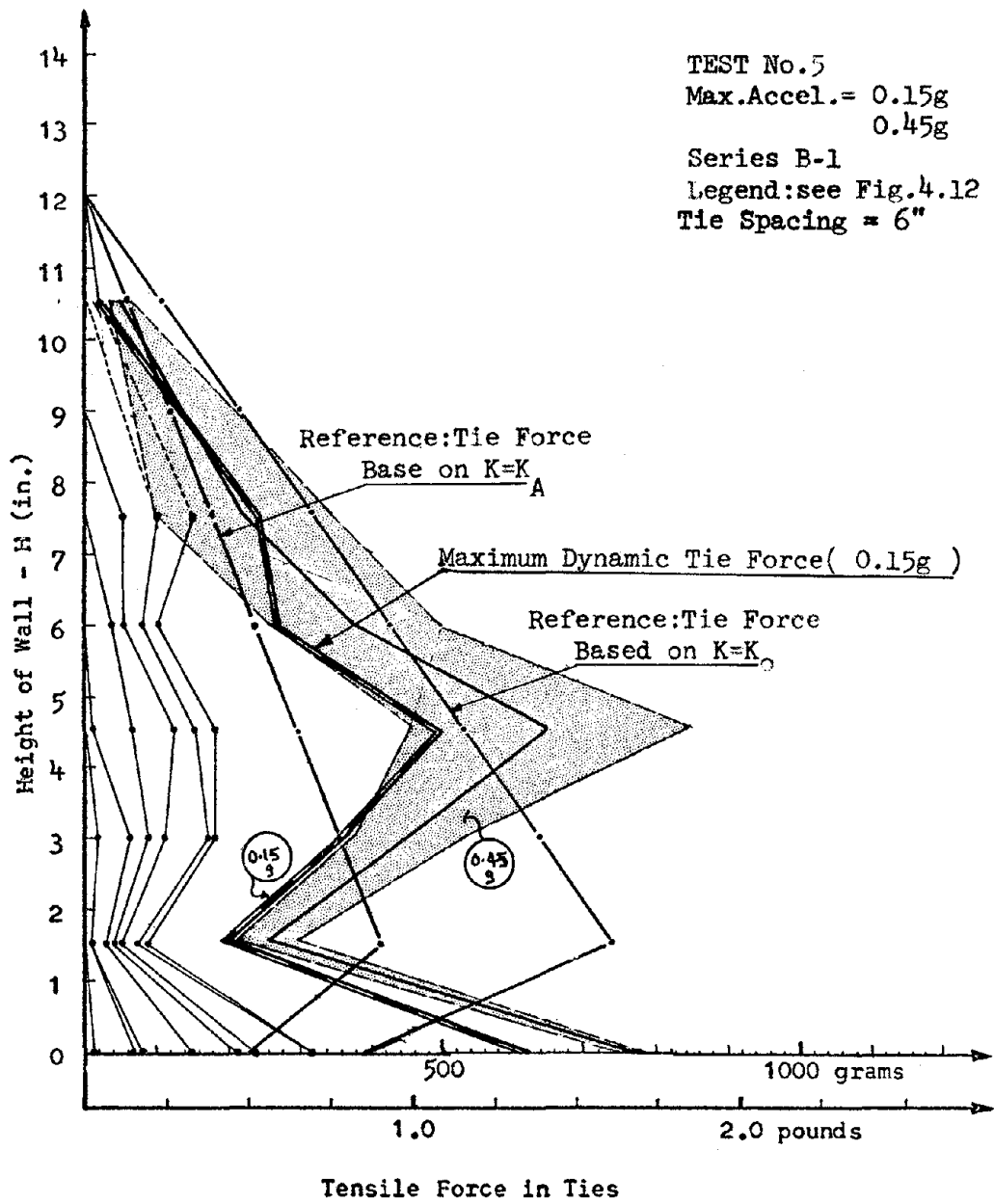


FIGURE 4.14 TIE TENSION MEASUREMENTS

confusion only the maximum dynamic tie force envelopes have been drawn. As with the previous tests the static tie forces increase with the height during construction, exhibit a sensitivity to construction procedures, and the active earth pressure tie force envelope still encloses the static tie forces. The dynamic tie forces also shows the same tie force irregularities found in the static tie forces, and increase with increasing acceleration.

Acceleration Records. Acceleration records were obtained from one accelerometer mounted on the shaking table and from an additional accelerometer embedded in the top layer of the sand. Previously in Series A, the accelerometer embedded in the sand had been located 16 inches from the face of the wall. In the Series B-1 test the embedded accelerometer was placed 5 inches from the face of the wall. This location enabled a measurement of the higher accelerations to be determined within the failure wedge. A summary of these measurements is presented in Fig. 4.20, described in Section 4.3.2.

Displacement Records. Because of the large number of tie tensions to be measured and the limited number of recording channels available it was frequently necessary to eliminate the instrumentation of the wall displacement. Direct visual observation and the limited records which were obtained indicated that the wall displacement pattern for the Series B-1 tests was similiar to the previous observations made during the Series A tests. The lower skin element remained fixed at the base, while excessive displacements developed at the upper layer of the wall.

Failure Mechanism. The sequence of the observed failure progression of Series B-1 tests is presented in Fig. 4.15. The initial wall configuration prior to dynamic loading is shown in sequence 1. Then during the initial application of dynamic loading the upper portion of the wall displaced at a rate exceeding that of the lower portion, sequence 2. After this initial deformation the wall continued to move out at a relatively uniform rate, sequence 3. Notice that the lower skin element exhibits a pivotal motion about its base. The base of the lower skin element acted as though it was hinged to the foundation surface. As the wall moved outward the lower skin rotated to maintain continuity. It is noted that the lower skin element was not fixed to the base of the wooden box except by friction along the length of the skin against the box, and by friction between the lower ties and the box.

The displacements increased as the vibration continued, as shown by sequence 4 and 5, however even though very large displacements developed and the lower skin element rotated by 90° there was no complete failure of the wall. This represents a critical difference from the Series A tests where a sudden and catastrophic failure occurred after some displacements have developed. For the Series B-1 tests, even if the vibration was continued beyond the stage shown on Fig. 4.15, the same failure sequence was repeated with the second skin element pivoting, sequence 6, and so forth.

After the vibration was terminated the Reinforced Earth wall continued to exhibit considerable static strength. This was often

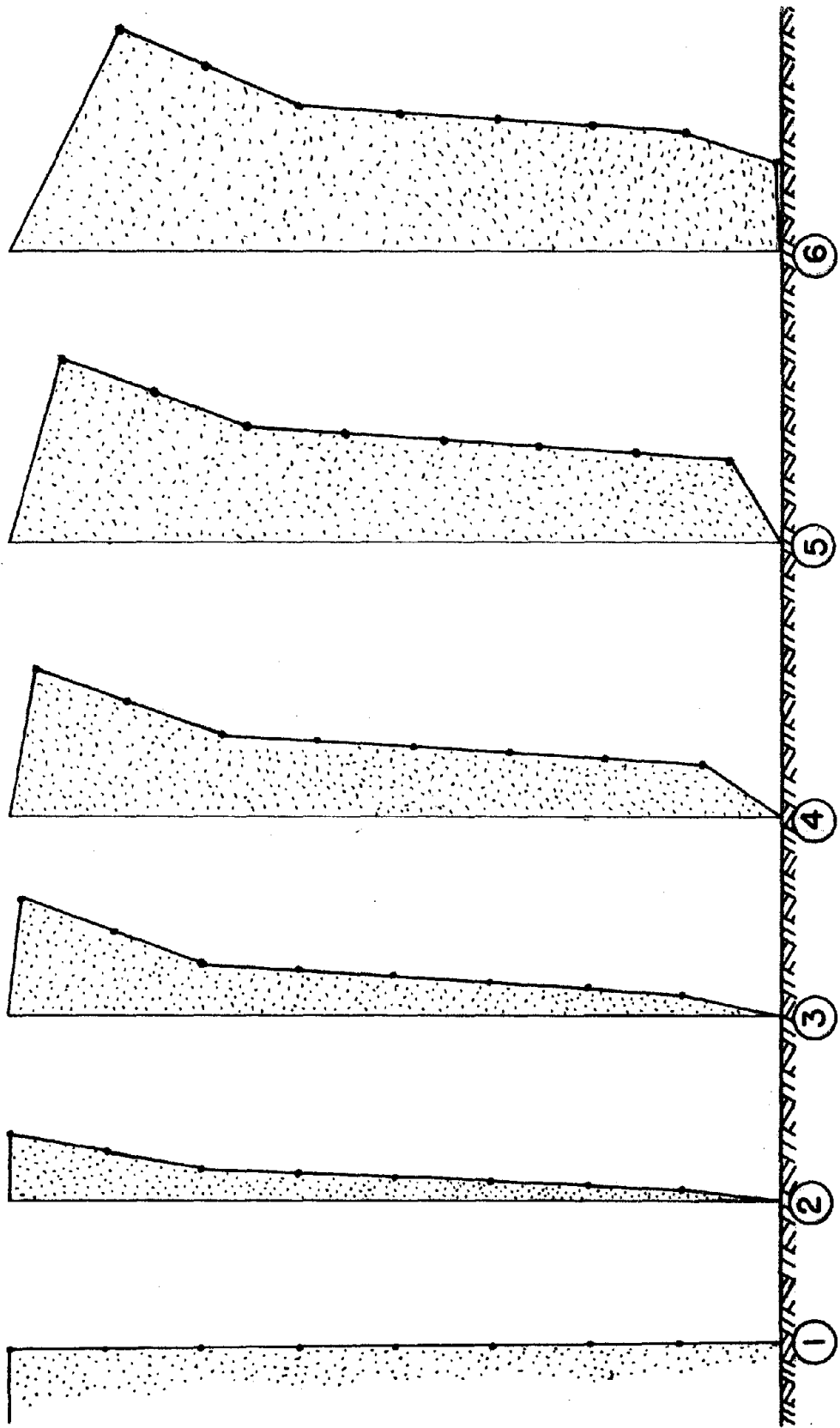


FIGURE 4-15 FAILURE MECHANISM

demonstrated by having a 175 pound student stand on the top edge of the deformed wall. This never caused the wall to fail, and in fact, it did not produce any further excessive deflection.

Failure Surface. The three failure surfaces observed from the sheared layers of colored sand seen through the viewing port in the model box are illustrated in Fig. 4.16. It should be noted that the observed failure surfaces did not extend through the toe of the wall. This is consistent with the previous observation, in both Series A and Series B-1 tests, that the lower boundary along the base of the box did not displace. In general the failure surfaces in the Series B-1 tests were slightly deeper than those previously observed in the Series A tests and that predicted by the Rankine Earth Pressure Theory, see Fig. 4.16.

From the observed failure surfaces it was possible to back calculate the minimum soil-tie friction angle required for stability of the failure wedge. This analysis was performed as a shear-slice slope stability problem, with the addition of tie forces and horizontal forces equal to the lateral acceleration times the soil's mass. The lateral acceleration included an estimate, based on laboratory measurements, of the acceleration amplification due to the flexibility of the wall. It was assumed that the soil-tie friction angle was constant for all depths, and that only the tie lengths behind the failure wedge contribute to the stability of the wall. Such an analysis is shown on Fig. 4.27, described in Section 4.3.3.

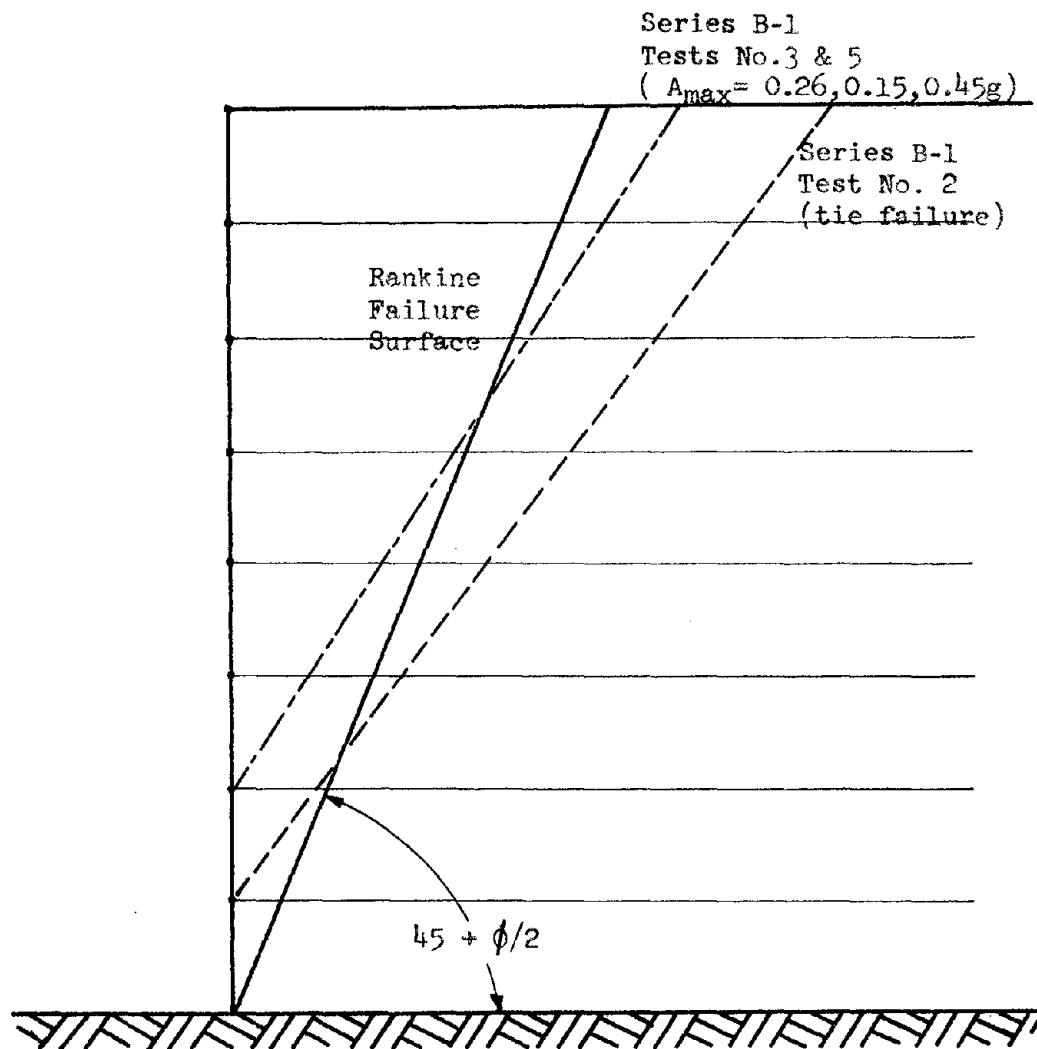


FIGURE 4.16 SERIES B-1 FAILURE SURFACES

Based on the failure wedge of test walls no. 3 and 5, the above pseudo-static analysis gave a minimum soil-tie friction angle, for stability of the failure wedge, of $\phi_u = 14.3^\circ$.

Summary of Series B-1. Tie force measurements for this series confirm earlier observations by Lee, et al, (3) that the static tie forces at the face of the wall are slightly less than those predicted by a linear distribution using an active earth pressure coefficient, K_A .

Test Series B-1 used improved tie force gauges and provided the first reliable measure of the absolute value dynamic tie forces that occur in Reinforced Earth walls under dynamic loading. It was observed that these dynamic tie forces were of about the same magnitude as those predicted using a lateral earth pressure coefficient equal to K_0 . Only 3 tests were performed using base accelerations of 0.15, 0.26, 0.32, and 0.45g. It is recognized that a wider range of input base acceleration would probably have lead to a wider range of peak tie forces.

Probably the most important knowledge gained from this test series was the observation of a Ductile Dynamic Failure Mode, in contrast to the complete collapse type of failure observed in the Series A tests. The dramatic difference in failure modes between the Series A tests and the Series B-1 tests indicate that judicious engineering practice should require that lower factors of safety be used for tie-pullout than for tie-breaking so that in the unfortunate event of a failure during an earthquake, this would occur by a ductile outer yielding of the wall rather than a sudden and complete collapse.

The ductility and strength, after deformation, of the Reinforced Earth wall, reinforced such that failure occurs through tie-pullout, represents the most desirable of seismic structural characteristics.

4.3.2 SERIES B-2 TESTS: TIE PULLOUT

Two tests were performed in Series B-2. The design for the Reinforced Earth walls in the Series B-2 tests was based on observations of the Series B-1 tests and also taking into account the results of a few direct tie pullout tests which had been made at this time. These tests are described in their entirety in Section 4.5. The few tests made at the time of the Series B-2 wall test indicated $\phi_u \cong 10^\circ$ for the mylar tape. It will also be recalled that the Series B-1 tests, completed for a range of accelerations of 0.15 to 0.45g, indicated that the peak dynamic tie tensions during the shaking were approximately equivalent to a K_0 earth pressure condition.

Model Configuration. The Series B-2 Reinforced Earth walls had almost the same configuration and dimensions as the Series B-1 walls: 8 layers each 1.5 inch in height, flat aluminum skin elements, and mylar recording tape ties. The Series B-2 walls differed from the Series B-1 walls only in the length and horizontal spacing of the ties. A comparison of the length, spacing, and total length of ties used in the Series B-1 and B-2 tests is presented in Table 4.2. The general arrangement of instrumentation has been shown on Fig. 4.10.

The Series B-2 mylar tie arrangement was designed using the Rankine Earth Pressure Theory based on the following assumptions:

- 1) the lateral earth pressure coefficient was
$$K = K_0 = 1 - \sin \phi$$
- 2) the soil-tie friction angle was 10° , and
- 3) the tie length embedded between the failure wedge and the wall did not contribute to the support of the wall.

The design was based on a factor of safety of 1.0 against tie pullout during dynamic loading. The static factors of safety calculated on an assumed K_A condition were 8.1 against tie breakage and 1.8 against tie pullout.

Table 4.2 Series B-1 and B-2 Tie Arrangements						
Tie Depth	Series B-1			Series B-2		
	Tie Length	Spacing	Length/6"	Tie Length	Spacing	Length/6"
Top	20"	6"	20"	20.8"	3"	41.6
1.5	20	6	20	20.8	3	41.6
3.0	20	6	20	20.1	3	40.2
4.5	20	6	20	19.5	3	39.0
6.0	20	6	20	18.8	3	37.6
7.5	20	6	20	18.2	3	36.4
9.0	20	6	20	17.6	3	35.2
10.5	20	6	20	16.9	3	33.8
12.0	20	6	20	8.2	3	16.4
Total Tie Length /6" width			180"	321.8"		

The pullout resistance of the ties is a direct function of the horizontal surface area of the tie behind the failure wedge. If the design is based on an assumed constant soil-tie friction angle, and constant tie spacing, then following the suggestion made by Lee, et al, (3) the tie length required to resist pullout, L_E , is given by the following expressions:

$$L_E = \frac{TA * K_o * \gamma * d}{2 * w * \tan \phi_u * \gamma * d} = \frac{TA * K_o}{2 * w * \tan \phi_u} \quad (4.1)$$

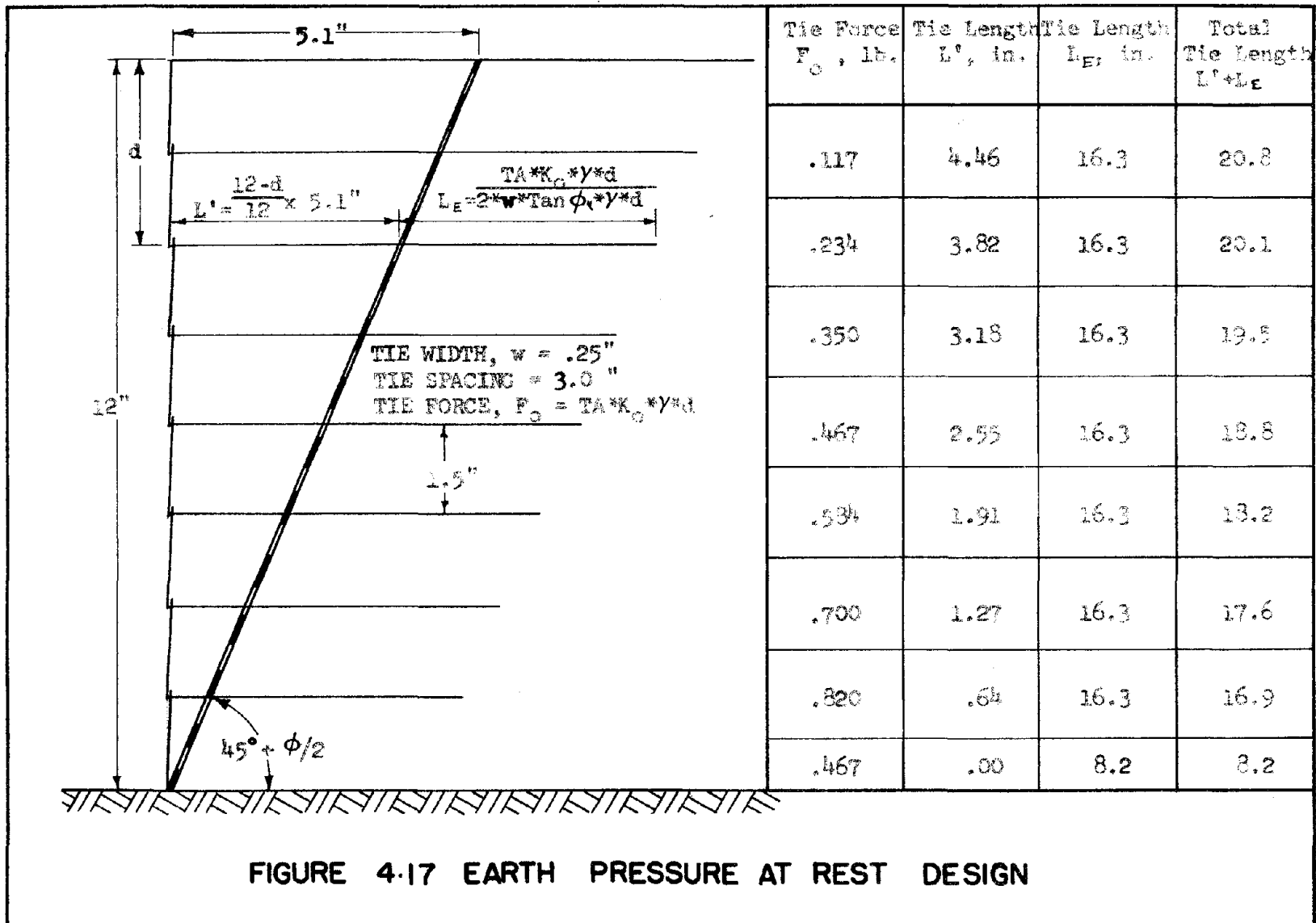
where L_E is shown to be independent of depth. In this expression L_E is the length of tie behind the failure wedge and the total tie length is L_E plus the width of the failure plane at that depth. Thus the distribution of tie lengths is governed by the assumed failure surface. Using the Rankine failure wedge, which slopes at $45 + \phi/2$,

the tie length increases as the height above the base, and for tall walls may be excessively large. In these cases the length L_E can be reduced by decreasing the horizontal tie spacing near the top, thereby maintaining the required tie surface area. This was done for the Series B-3 tests so that the upper ties could fit within the box. Using these assumptions the design of the tie arrangement is presented in Fig. 4.17.

Tie Tension Records. The tension in the mylar reinforcing ties was measured using the improved design for the Tie-Tension instruments, as illustrated on Fig. 3.7b. The recorded dynamic tie forces were determined using a procedure discussed in Section 4.3.1 and illustrated on Fig. 4.11.

The static and dynamic tie force records for the first of the Series B-2 tests, wall no. 6, are presented on Fig. 4.18. Notice that the static tie forces during and at the end of construction (prior to dynamic loading) are generally less than that predicted using the Rankine Earth Pressure Theory with $K_p = K_A$ except near the upper part of the wall.

After all the static data was recorded, the wall was then subjected to four successive dynamic tests with base accelerations of 0.05g, 0.08g, 0.17g, and 0.28g respectively. Each of the input accelerations were applied for a sufficient period of time to insure development of the full dynamic forces. No major permanent displacements were observed for accelerations of 0.05g, 0.08g, and 0.17g. For the two smaller accelerations only the maximum dynamic tie tension envelopes



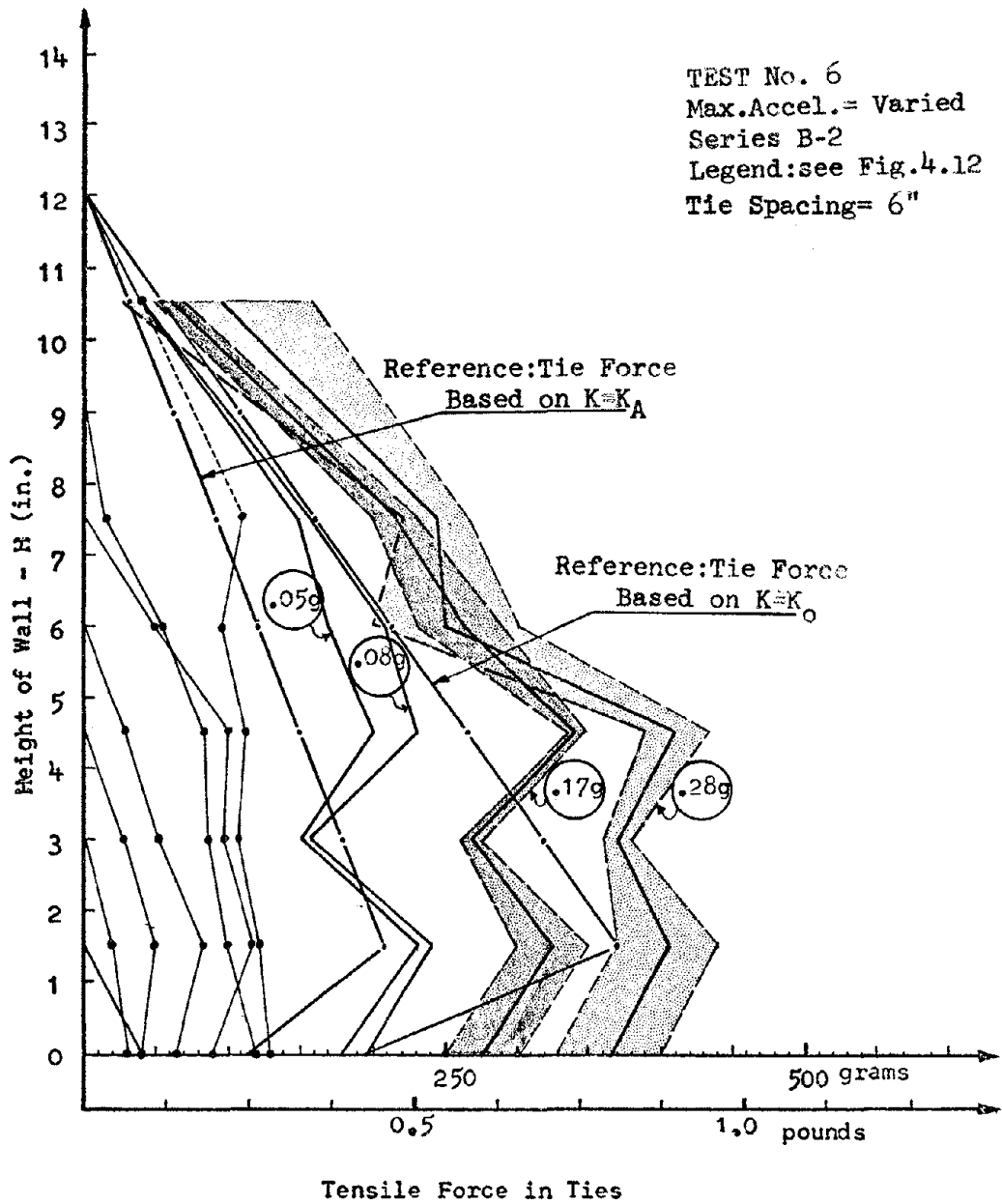


FIGURE 4.18 TIE TENSION MEASUREMENTS

are shown, while for the 0.17g and 0.28g accelerations the complete dynamic envelopes are presented. Notice that the general level of dynamic tie forces increases with increasing acceleration. The dynamic forces for low levels of acceleration are near those predicted using at-rest earth pressures, $K = K_0$, but for higher accelerations the tie forces at the upper wall levels greatly exceeds those predicted using a linear pressure distribution.

The recorded tie tensions for the second test in Series B-2, wall no. 7, are presented in Fig. 4.19. Again the static tie forces are less than those predicted using $K = K_A$, except near the very top of the wall. Only one dynamic test was performed with an input acceleration of 0.32g. In all previous tests the tie tension distributions under both static and dynamic loading showed zones of irregularities which were interpreted to be a result of small disturbances during construction. The dynamic loading was not sufficient to erase these irregularities by breaking up the arching that apparently developed. However, in this test, the base acceleration of 0.32g did destroy the irregularities in the tie tension distribution, and the dynamic stresses increased smoothly with depth. For this reason, the observed shape of the dynamic tie tensions for this test were given preference in developing a seismic design procedure.

Acceleration Records. As in previous tests, acceleration records were obtained from an accelerometer mounted on the shaking table and from an additional accelerometer embedded in the sand. Previously the embedded accelerometer had been located 16 inches from the face

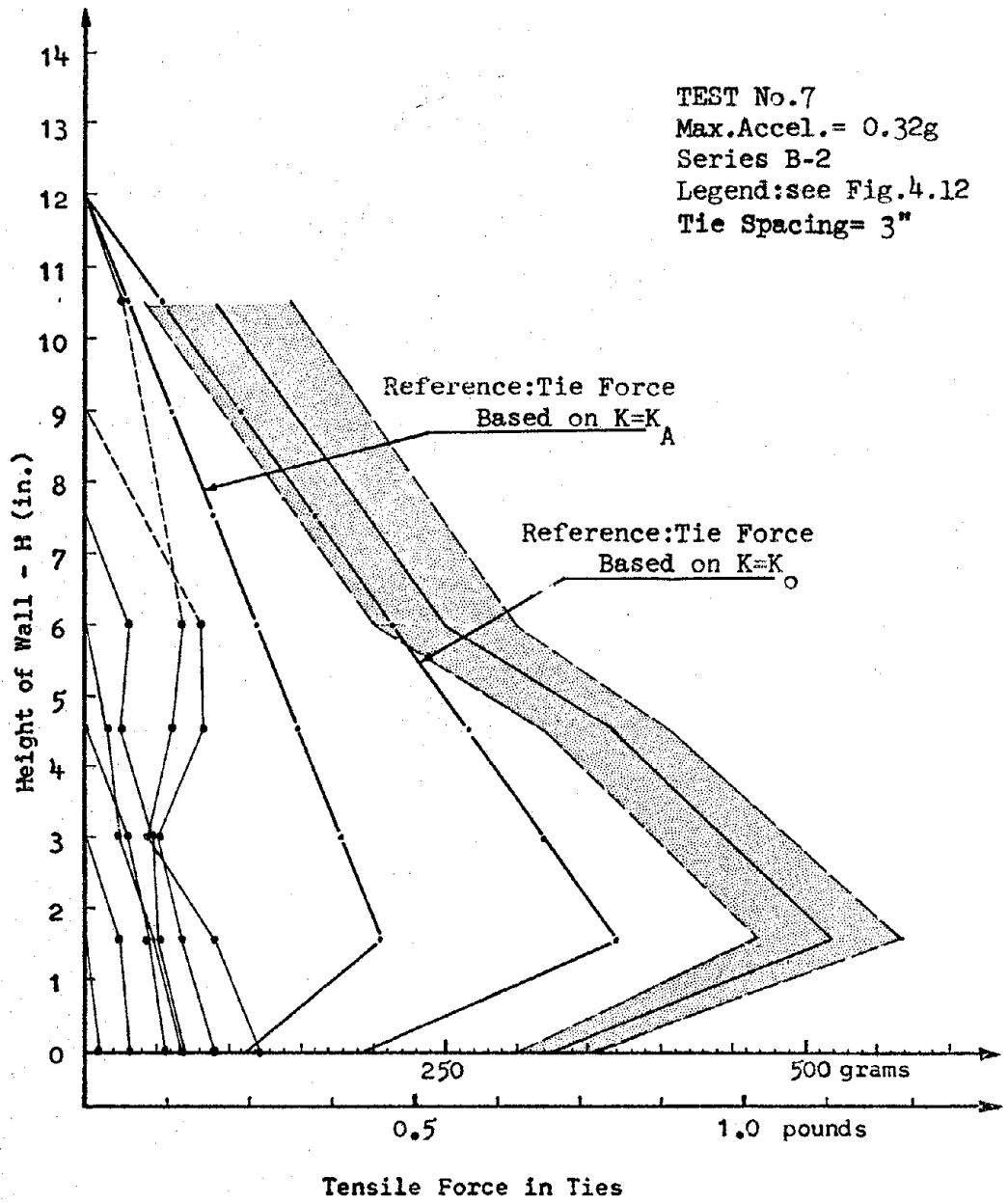


FIGURE 4.19 TIE TENSION MEASUREMENTS

of the wall for Series A tests while in the Series B-1 tests it was located 5 inches from the face of the wall. In the Series B-2 tests the embedded accelerometer was placed immediately behind the face of the wall. A summary of the measured accelerations for Series A, Series B-1, and Series B-2 is presented in Fig. 4.20. Notice that as the accelerometer is placed nearer the face of the wall that the acceleration amplification increases:

$$\text{amplification(A)} < \text{amplification(B-1)} < \text{amplification(B-2)},$$

Displacement Records. As with the Series B-1 tests, the large number of tie tensions to be measured and the limited number of recording channels available frequently made it necessary to eliminate the instrumentation of wall displacements. Neither test walls no. 6 or 7 were instrumented for wall displacement. However, direct visual observation of the Series B-2 tests indicated the following:

- 1) excessive displacement of upper wall layers, and
- 2) the lower wall boundary at the box failed to move a measurable amount.

Failure Mechanism. The failure progression of the Series B-2 tests was the same as described in Section 4.3.1 for Series B-1 tests. This failure progression has been illustrated in Fig. 4.15. The Series B-2 test walls continued to show considerable static strength even after severe deformation.

Failure Surface. Test wall no. 6 did not produce a discernable failure surface, but appeared to deform in shear. Because of this the colored sand layers used to determine failure surfaces were replaced with a line of colored sand dots between each reinforcing layer.

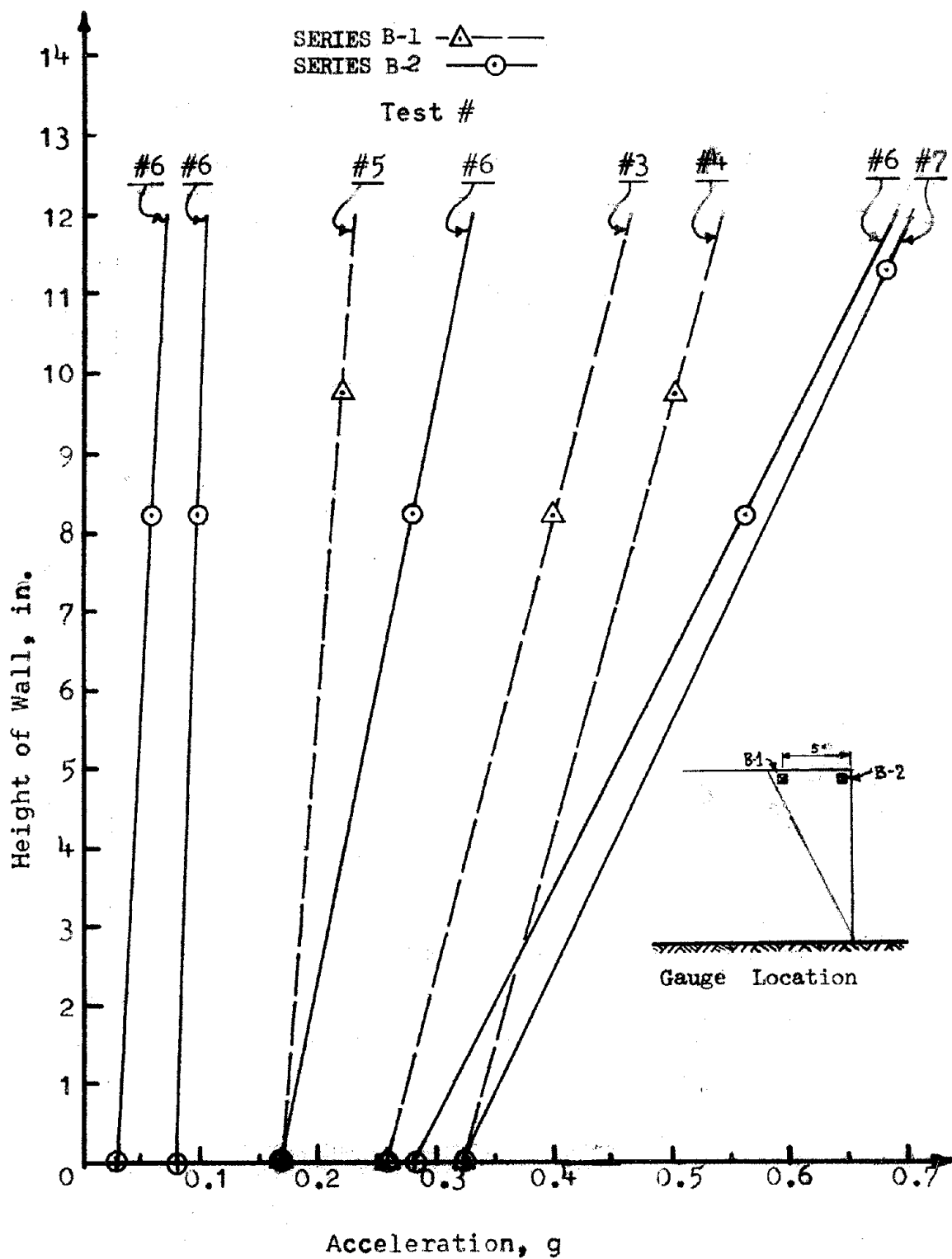


FIGURE 4.20 FAILURE WEDGE AMPLIFICATION

By measuring the deformation between successive dots it is possible to determine where the major deformation occurs. The shear displacement record of wall no. 7 is illustrated on Fig. 4.21. Because a well defined failure surface was not obtained from either Series B-2 test it was not possible to perform the psuedo-static stability analysis, described in Section 3.31, to determine a minimum ϕ_u for these walls.

Summary of Series B-2. The Series B-2 walls were the first test walls where the design was based on estimated values of the soil-tie friction angle and dynamic tie forces. The test walls maintained a constant tie spacing but were the first test walls in this study to use tie lengths that increased with increasing height above the base.

The static tie tension measurements during construction and prior to testing were generally less than the tie forces predicted using Rankine Earth Pressure Theory with an active earth pressure coefficient K_A .

The dynamic tie tensions were found to increase with the increasing base of acceleration, see Fig. 4.18. The magnitude of the maximum dynamic tie forces were near those predicted using $K = K_0$ for small values of accelerations but were greater than this amount for higher accelerations. The upper tie levels were found to exhibit significantly larger tie forces than calculated using a hydrostatic pressure distribution.

Like the Series B-1 tests, the Series B-2 tests walls also demonstrated the Ductile Dynamic Failure Mode and possessed a high static strength even after extreme deformation.

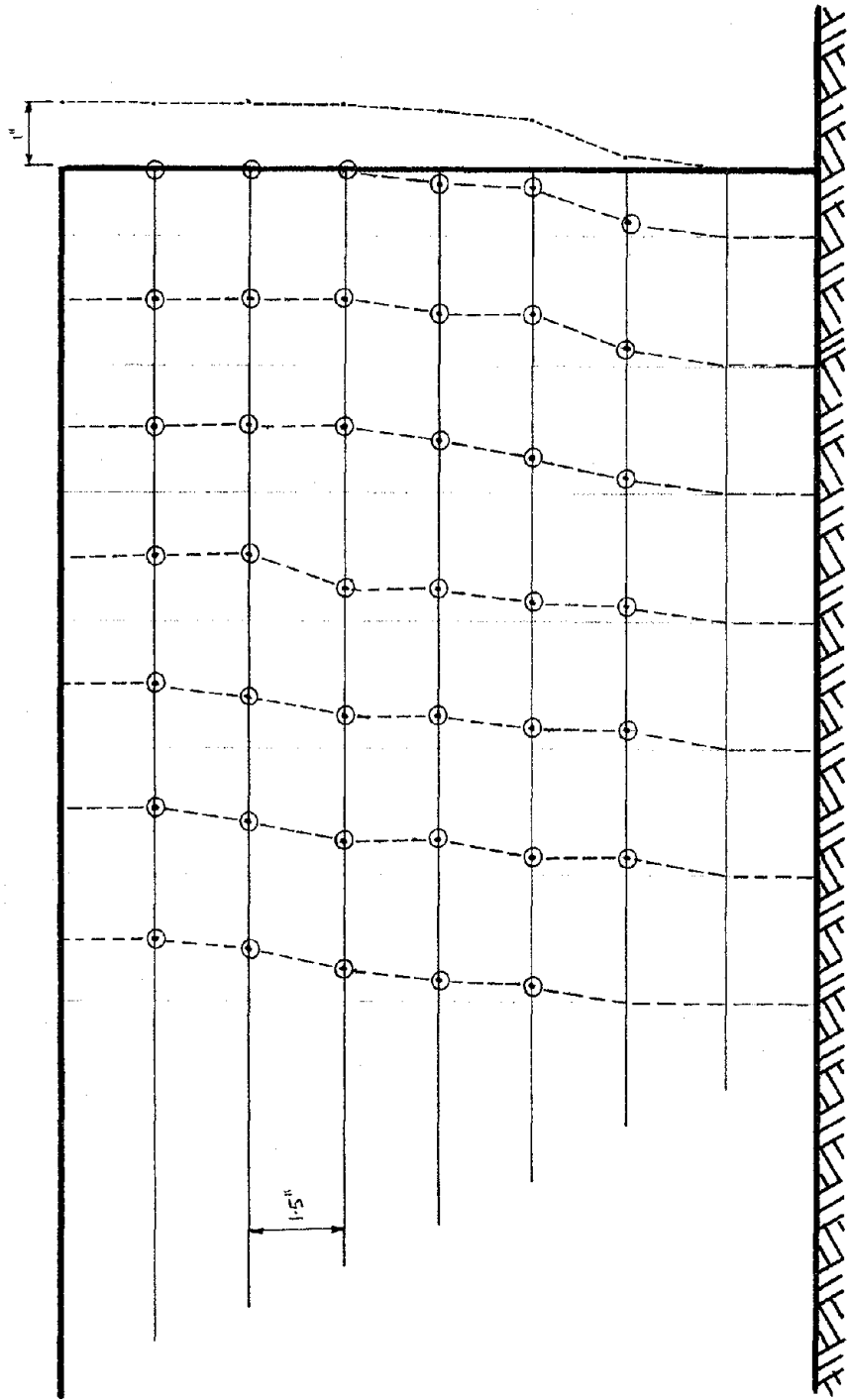


FIGURE 4-21 SHEAR TYPE WALL DEFORMATION

4.3.3 SERIES B-3 TESTS: TIE PULLOUT

Four tests were performed in the Series B-3 tests. Based on Series B-1 and B-2 model tests the following observations were made relating to the measured tie-tension forces:

- 1) initial static forces were usually less than given by $K = K_A$,
- 2) tie forces appear to be sensitive to construction procedures,
- 3) the maximum dynamic tie forces increase with depth, however larger forces are developed in the upper ties than is predicted by a linear variation of the lateral pressure with depth,
- 4) the measured tie forces at low values of acceleration approach those predicted using $K = K_0$, while the tie-tension for higher accelerations exceed these predicted values, and
- 5) dynamic tie-tensions increase with increasing accelerations.

The second of these observations, of the effect of construction procedure, is consistent with past investigations of anchored or braced bulkheads (18,19). The lateral force against these bulkheads has shown a strong dependence on the construction procedures or irregularities. In some cases, especially for low accelerations, the dynamic tie tension force in some cases continue to reflect this dependence on construction whereas other cases did not.

Because of the unpredictable nature of the above occurrence, an attempt was made to estimate envelopes of the Maximum Dynamic Tie Tension Forces that would consistently enclose the measured tie force values. These envelopes were simple and empirical, enclosing

with a few straight lines the maximum observed tie forces for the data recorded in the Series B-1 and B-2 tests. A separate envelope was drawn for each test, using the same general shape of envelope as had been recorded for wall no. 7, Series B-2, but using different actual locations depending on the test data which it was required to represent.

The envelopes enclosing the maximum dynamic tie forces were found to be similar and expressible as a simple function of the input base acceleration as illustrated on Fig. 4.22. The seismic envelopes were developed in the following manner:

- 1) A Seismic Design Coefficient, E, was calculated for each Series B-1 and B-2 tie pullout tests;

$$E = \frac{F_E}{F_R} = \frac{F_E}{K_o * d * \gamma * TA} \quad (4.2)$$

where F_E is the primary tie force for the approximate dynamic envelopes, and F_R is given the Rankine Tie force discussed in Section 2.3.

- 2) The Seismic Design Coefficient was plotted versus the input acceleration on Fig. 4.22a and a straight line relationship found;

$$E = 1.4 A_g \quad (4.3)$$

where A_g is the input acceleration. This enables the peak design force in the primary tie to be calculated directly from the known input acceleration.

- 3) The shape of the design tie force envelope defining the peak tie forces at other depths was selected such that in shape it resembled the tie force envelope of test wall no. 7, Fig. 4.19, and was a consistent upper bound for the remaining tests. This Seismic Design Envelope is a simplified envelope as compared to that measured for wall no. 7, see Fig. 4.22b.

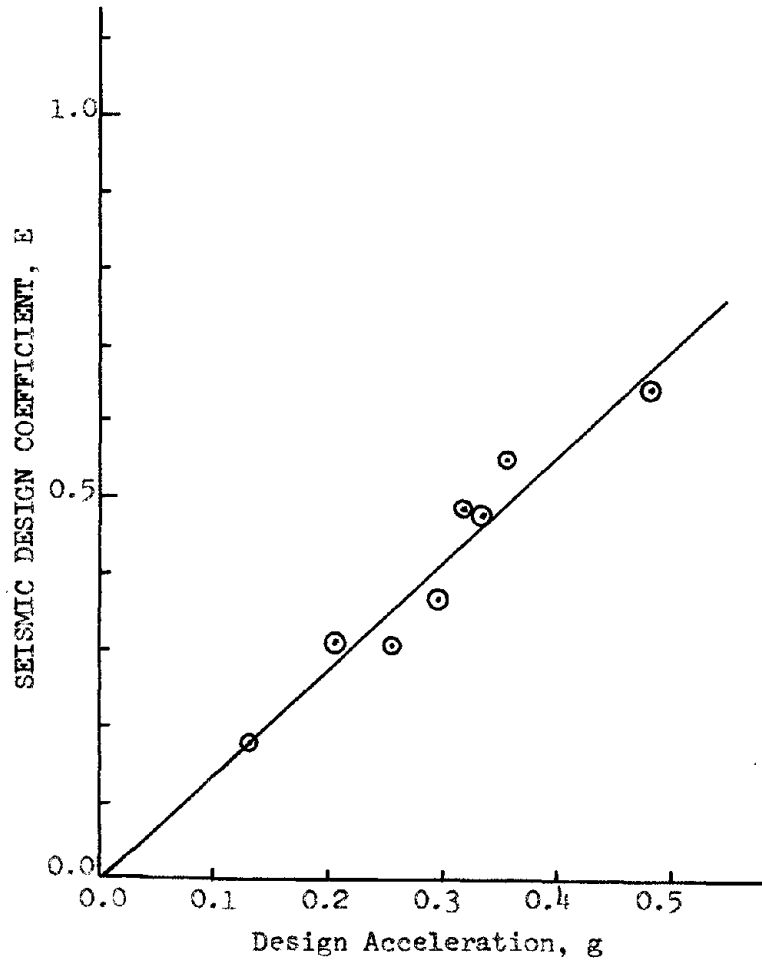
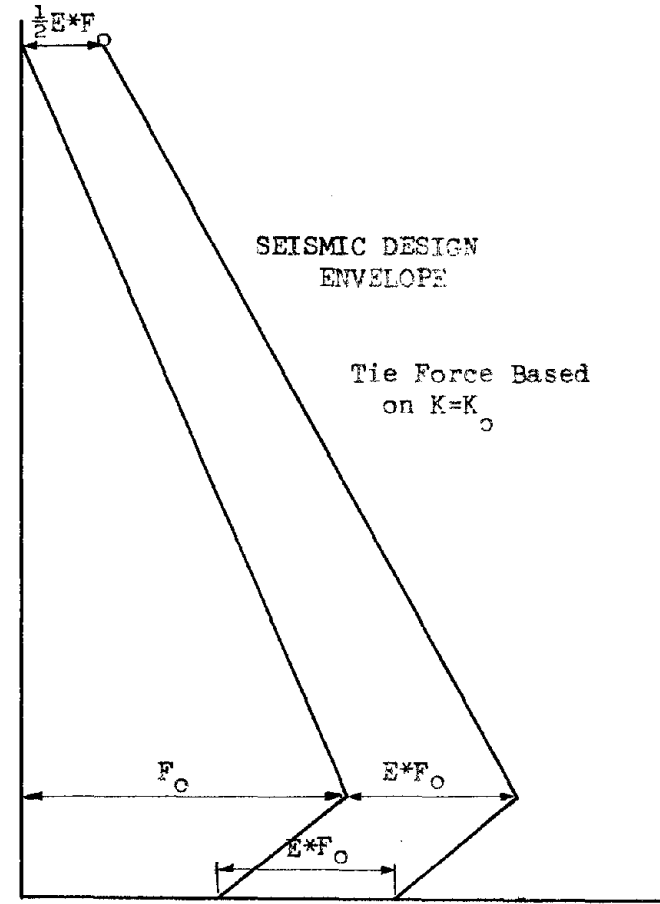


Figure 4.22 SEISMIC DESIGN COEFFICIENT, E



Design Dynamic Tie Force
Figure 4.22 SEISMIC DESIGN ENVELOPE

FIGURE 4-22 SEISMIC DESIGN TIE-FORCE ENVELOPE

To use the Seismic Design Envelope presented in Fig. 4.22 it is necessary to first determine the design level of base acceleration. Next, the Seismic Design Coefficient, E, is obtained using Eq. 4.3. Finally the tie force envelope using at-rest earth pressures is modified using the Seismic Design Coefficient, E, as illustrated in Fig. 4.22b, to obtain the Seismic Design Envelope.

After determining the Seismic Design Envelope, the next step was to design the ties based on tie-pullout criteria. The length of tie required to resist tie pullout due to the design forces is determined from the following expression:

$$L_E = \frac{\text{design force}}{2 * w * d * \text{Tan } \phi u} \quad (4.4)$$

where L_E is the length of tie behind the assumed failure wedge and the total tie length is given by L_E plus the width of the failure wedge at depth d , and w is the tie width.

Model Configuration. The Series B-3 Reinforced Earth walls were similar to the Series B-1 and B-2 walls in that the walls tested were eight layers in height, with each reinforcement layer 1.5 inches thick, making a total wall height of 12 inches. The Series B-3 models used the flat aluminum skin elements and the mylar recording tape ties. The general arrangement of instrumentation has been shown on Fig. 4.10.

The Series B-3 models were designed based on the seismic design force envelopes described above and assuming a Rankine failure wedge sloping at $45 + \phi/2$. Test walls were constructed for a variety of design accelerations and soil-tie friction angles. Table

4.3 presents tie lengths calculated based on an input acceleration of 0.3g assuming soil-tie friction angles of 7, 15, and 20 degrees for a factor of safety against dynamic tie pullout of 1.0. From this table, the economic importance of the soil-tie friction angle, ϕ_u , is evident

The lower ϕ_u , the longer or the closer must be the ties, and hence the greater will be the required amount of material and the overall cost. It should be noted that the proposed seismic design results in greatly increased tie lengths in the upper wall sections as compared to tie lengths designed using conventional static procedures. Because of the excessively long tie lengths calculated it was necessary to reduce the tie spacing such that the tie lengths would physically fit into the model box. For the Series B-3 tests a tie spacing of three inches was used, in addition it was necessary to use a tie spacing of 1.5 inches for the upper tie level when using an assumed value of $\phi_u = 7^\circ$. Table 4.4 compares the actual tie lengths, spacing, and total length of tie material used per 6 inch wall length, for all Series B-1, B-2, and B-3 tests.

At the time the Series B tests were performed a few direct tie-pullout tests had been run to determine the soil-tie friction. The available results at that time were rather variable and inconclusive. Therefore this series of tests was performed for tie lengths and spacing designed to accommodate various soil-tie friction angles within the range of values obtained at that time. A full discussion of the soil-tie friction tests is given later, in Section 4.5.

Table 4.3 Influence of Soil-Tie Friction Angle
on the Required Tie Length

Tie Depth in.	Seismic Force lb.	Total Required Total Length of Ties , in.			
		$\phi_u = 7^\circ$	$\phi_u = 10^\circ$	$\phi_u = 15^\circ$	$\phi_u = 20^\circ$
1.5	.310	66.5	47.9	32.9	25.5
3.0	.455	49.8	35.8	24.8	19.3
4.5	.600	43.7	31.2	21.6	16.8
6.0	.780	41.8	29.8	20.4	15.8
7.5	.880	37.3	26.5	18.0	13.8
9.0	1.02	35.5	25.1	16.9	12.8
10.5	1.16	33.8	23.7	15.8	11.8
12.0	.800	20.0	13.9	9.1	6.7
Total Required Tie Length per 6 inch width		328.4	233.9	159.5	132.5

TABLE 4.4 SERIES B-1, B-2, and B-3 TIE ARRANGEMENTS

Tie Depth	SERIES B-1		SERIES B-2		SERIES B-3					
	Tie Length	Tie Spacing	Tie Length	Tie Length	$\phi_u = 7^\circ$		$\phi_u = 15^\circ$		$\phi_u = 20^\circ$	
					Tie Length	Tie Spacing	Tie Length	Tie Spacing	Tie Length	Tie Spacing
Top	20	6	20.8	3	25	1.5	23	3	18	3
1.5	20	6	20.8	3	25	1.5	23	3	18	3
3.0	20	6	20.1	3	38	3.0	20	3	15	3
4.5	20	6	19.5	3	36	3.0	19	3	15	3
6.0	20	6	18.8	3	34	3.0	17	3	14	3
7.5	20	6	18.2	3	33	3.0	16	3	13	3
9.0	20	6	17.6	3	32	3.0	15	3	11.5	3
10.5	20	6	16.9	3	31	3.0	15	3	11	3
12.0	20	6	8.2	3	21	3.0	10	3	7	3

The design of Series B-3 models for various soil-tie friction angles results in the same tie arrangements as if a varying factor of safety had been applied to the true soil-tie friction angle. If it is assumed that the true soil-tie friction angle was 12° then the design of the wall using ϕ_u equal to 7, 15, and 20 degrees results in dynamic factors of safety ($FS \phi_u$) against tie-pullout equal to 1.75, 0.8, and 0.58, respectively.

Tie Tension Records. The tie tension in the mylar reinforcing ties was measured using the improved design for Tie-Tension instruments, as illustrated in Fig. 3.7b. The recorded dynamic tie forces were determined using a procedure discussed in Section 4.3, and illustrated on Fig. 4.11.

The first two walls of the Series B-3, tests walls no. 8 and 9, were designed using an assumed soil-tie friction angle of 7° ($FS \phi_u = 1.75$) This friction angle was the minimum soil-tie friction angle measured based on peak static pull-out tests. The static and dynamic tie tension records for these tests are given on Fig. 4.23 and 4.24. As for the earlier tests the static tie tensions are generally below the Rankine active pressure tie force envelope. The excessive tie force at the eighth tie level of test no. 9 may be due to excessive compaction or disturbance during placement of this layer. Note that the dynamic tie forces are below the Seismic Design Envelope.

Because of the low soil-tie friction angle used in the above tests, the required tie lengths appeared excessive. To determine whether the dynamic forces were strongly dependent on the lengths

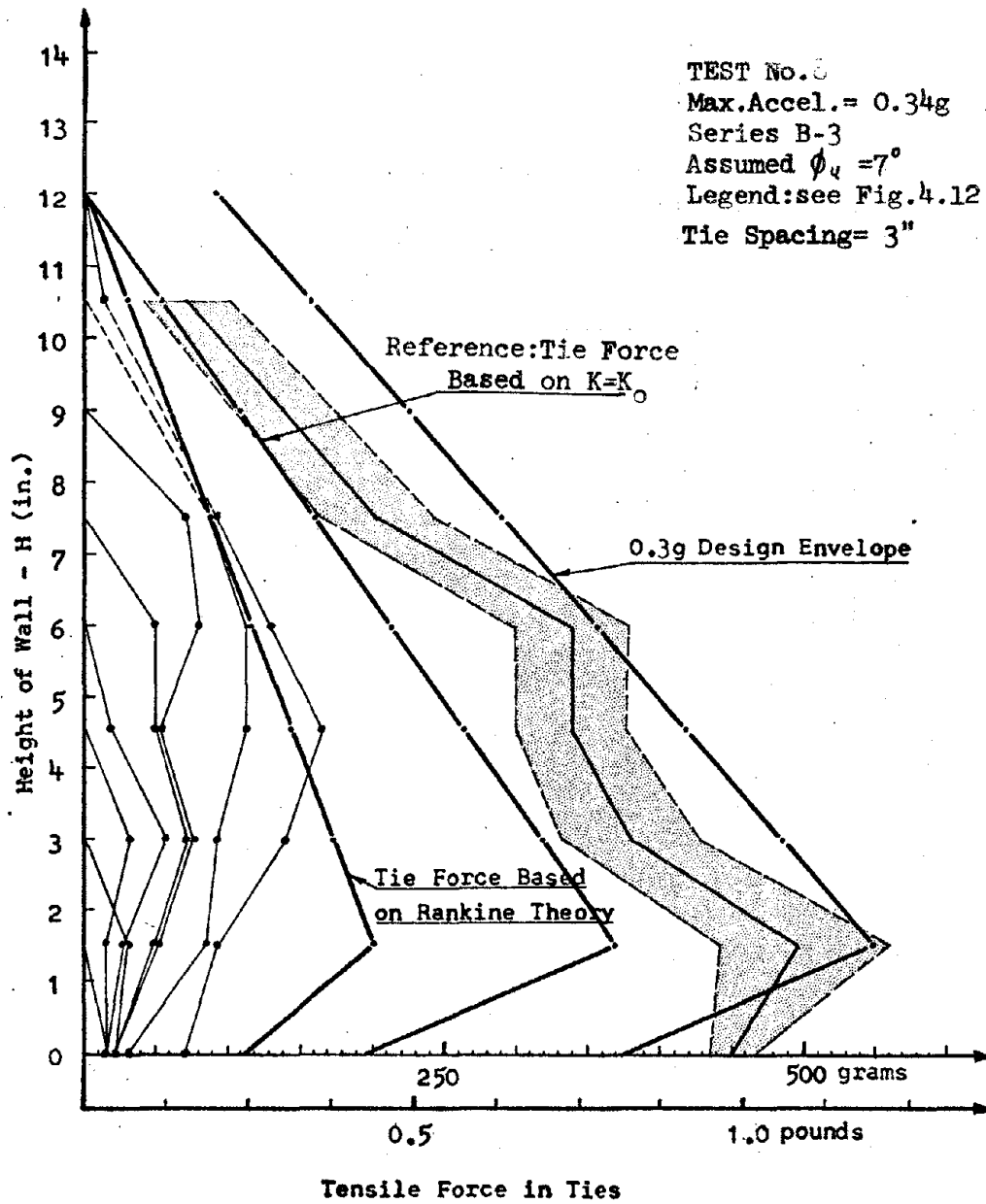


FIGURE 4.23 TIE TENSION MEASUREMENTS

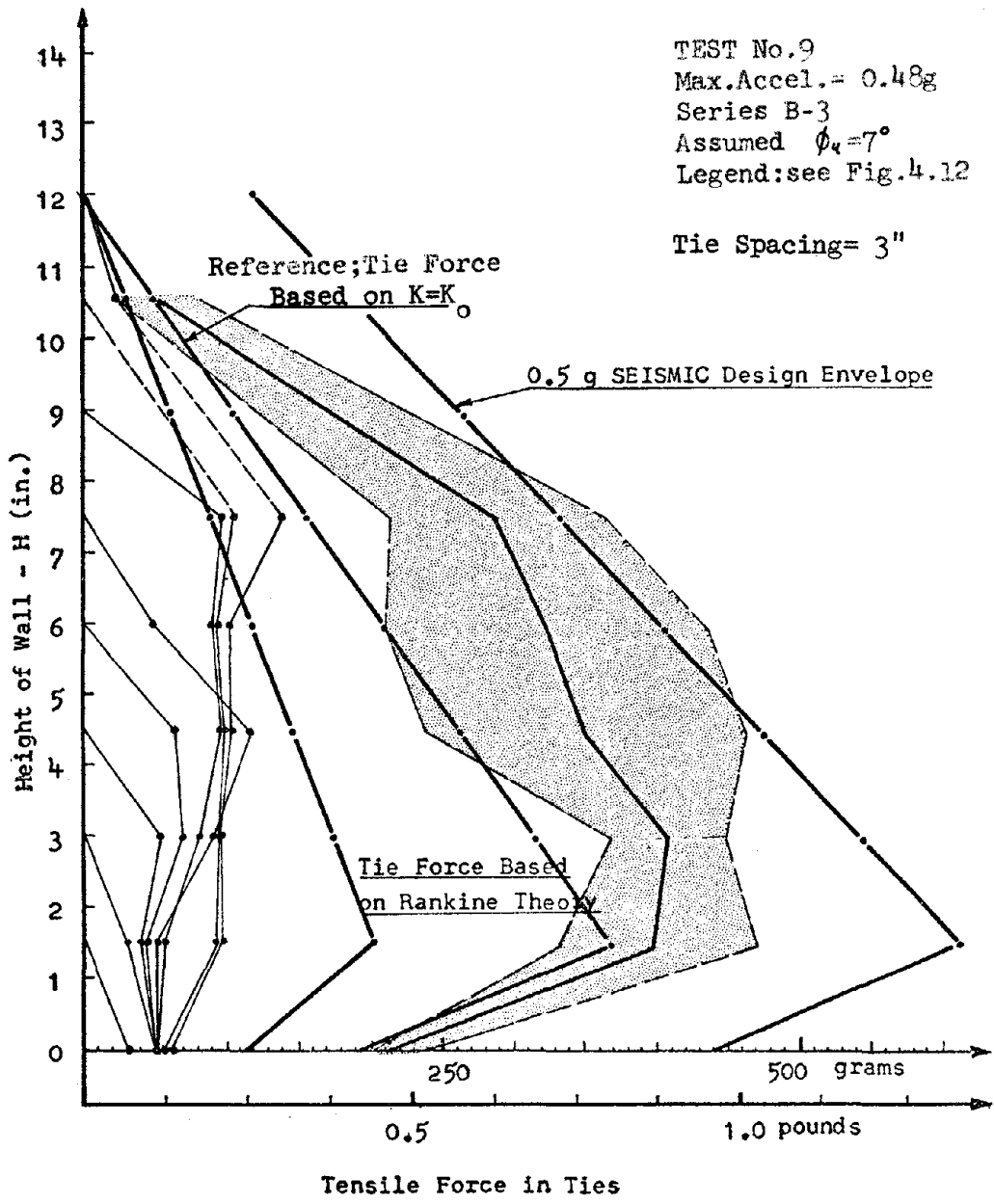


FIGURE 4.24 TIE TENSION MEASUREMENTS

of the ties two additional walls were designed and constructed based on assumed soil-tie friction angles of 20 and 15 degrees (FS dynamic $\phi_u = 0.58$ and 0.8), which resulted in shorter and wider spaced ties. These were test walls no. 10 and 11. The tie tension measurements from these tests are presented on Fig. 4.25 and 4.26, respectively. The measured static forces in test walls no. 10 and 11 were conservatively estimated using $K = K_A$, as in all previous tests. At most locations the maximum dynamic tie force envelopes were also conservatively estimated using the proposed Seismic Design envelopes. Notice that in Fig. 4.23, 4.25, and 4.26 the measured dynamic tie forces at various ties show highly random variations even though the input acceleration was nearly the same (0.3g) for all three tests. As previously mentioned, these random variations appear to be due, in part, to the irregular tie forces developed during the construction stage, demonstrating the probabilistic nature of the actual dynamic tie forces and justifying the use of conservative empirical design envelopes.

Acceleration Records. As in previous tests, acceleration records were obtained from an accelerometer mounted on the shaking table and from an additional accelerometer embedded in the sand. In the Series B-3 tests the embedded accelerometer was placed directly behind the face of the wall. The acceleration records of Series B-3 are in agreement with those of Series B-2, as shown on Fig. 4.20.

Displacement Records. As in Series B-2, the increased number of tie tensions measured and the limited number of recording channels available

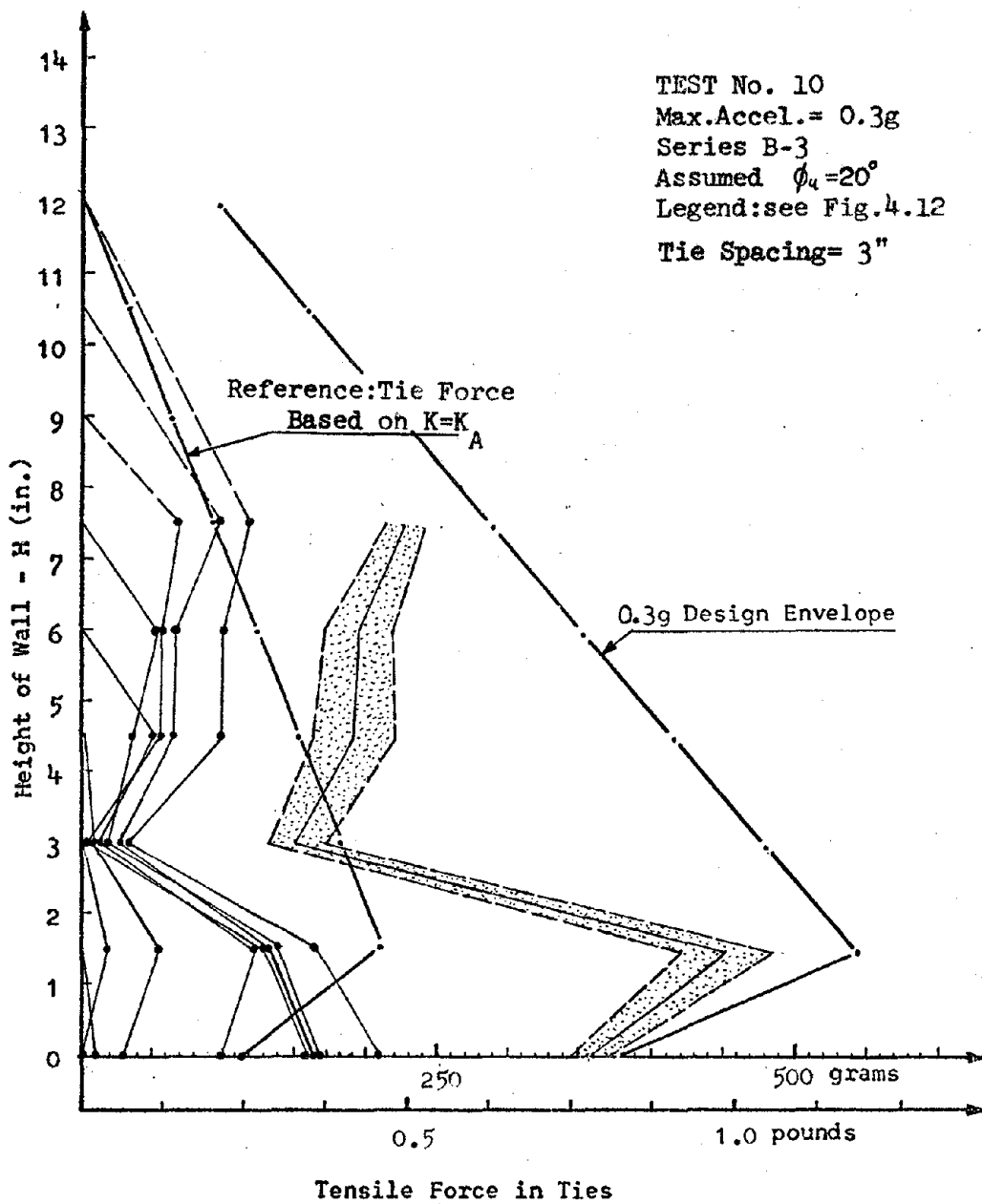


FIGURE 4.25 TIE TENSION MEASUREMENTS

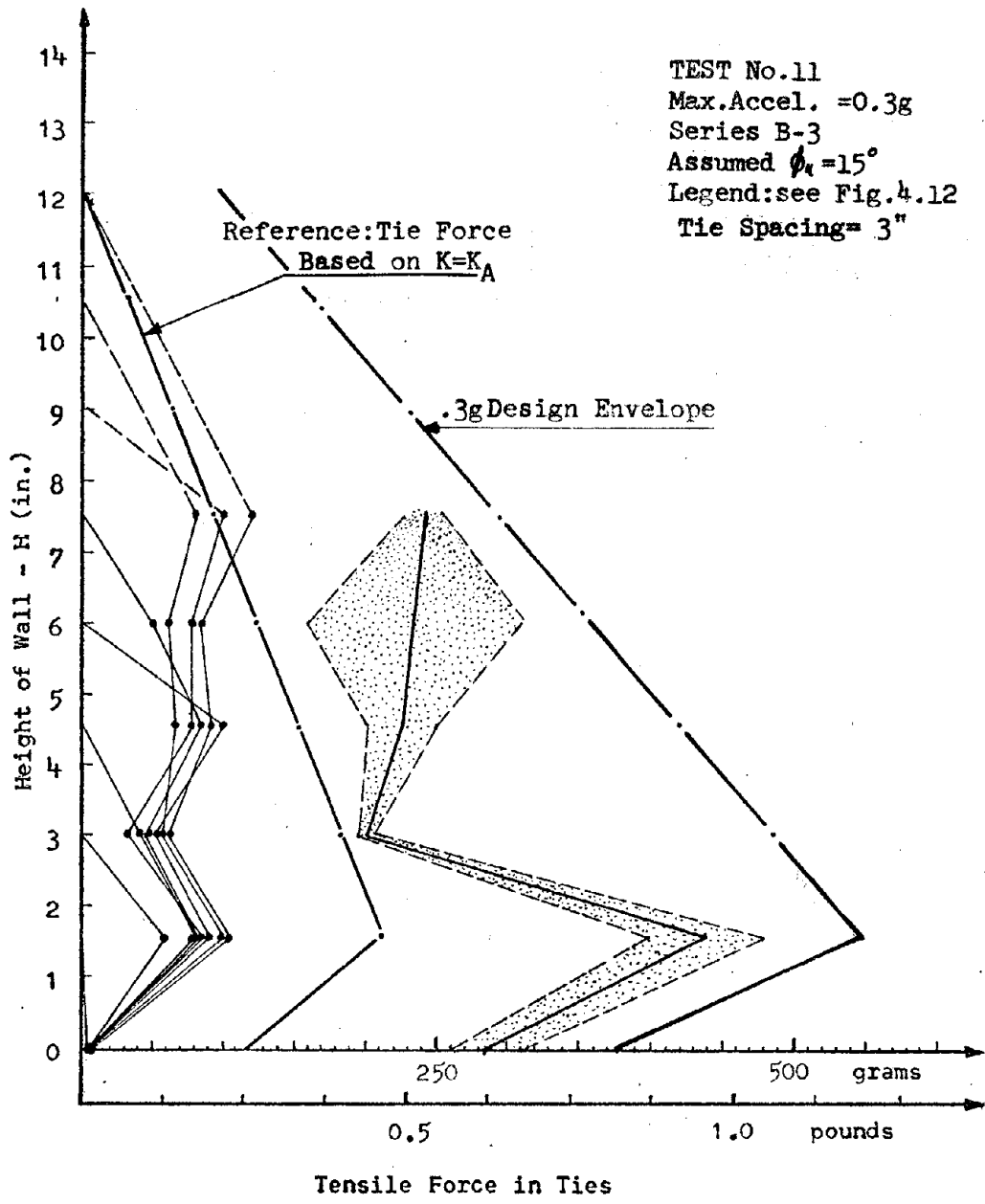


FIGURE 4.26 TIE TENSION MEASUREMENTS

prevented the instrumentation of any Series B-3 models for wall displacement.

Model walls no. 8 and 9, designed for $\phi_u = 7$ (FS $\phi_u = 1.75$), did not exhibit noticeable permanent displacements when acted upon by the design accelerations. On the other hand, model walls no. 10 and 11, using assumed $\phi_u = 20^\circ$ and 15° (FS $\phi_u = 0.58$ and 0.8) respectively, were not able to survive the design acceleration without extreme deformation. This occurrence leads to the observation that the soil-tie friction angle of 7° for the mylar tape, as indicated by tie-pullout tests, may not be overly conservative. In addition it was observed that the rate of displacement of a wall decreases with increasing tie lengths. Unfortunately, since no records were taken, this is only a visual observation and there is no data available to compare actual displacement rates.

Failure Mechanism. The Series B-3 failure mechanism was markedly different from the failure mechanisms observed in all of the previous tests in that the walls displaced essentially as a rigid body about the first skin element. In previous tests the upper portion of the test walls always deformed much more rapidly than the remaining portions of the wall. As the lower skin element approached full collapse there was a steady increase in the tie tension forces. Once the lower skin element had completely collapsed the tie tensions reduced to those predicted by the Seismic Design Envelope.

Failure Surface. A well defined failure surface was obtained only for test no. 10. Calculations for a pseudo-static dynamic analysis

for this model are presented in Fig. 4.27 and indicated a minimum soil-tie friction angle of 18 degrees required for minimum stability of the failure wedge.

Summary of Series B-3. The Series B-3 model walls were based on designs using the proposed Seismic Design Envelopes. These design envelopes were based on tie force measurements from Series B-1 and B-2 tests. The Series B-3 models designed using the Seismic Design Envelope shown on Fig. 4.22 had longer tie lengths in the upper wall levels than Series B-1 or B-2 models, as previously shown in Table 4.4. The empirical nature of these envelopes and their ability to conservatively estimate Seismic tie forces is demonstrated by the composite summary of measured peak tie forces and Seismic Design Envelopes shown in Fig. 4.28. The measured data represents the envelopes of maximum tie forces observed in all Series B tests as follows:

a max = 0.16g = Test no. 5, 6
a max = 0.28g = Test no. 3, 6, 10, 11
a max = 0.35g = Test no. 4, 7, 8
a max = 0.42g = Test no. 5, 9.

While there appears to be considerable scatter or randomness in the recorded data, the deformation of the test wall built using the Seismic Design Envelope would appear to substantiate the general shape of the design envelope. The deforming walls, designed according to the Seismic Design Envelope, moved outward as rigid bodies about the lowest skin element. The Series B-3 walls did not have the excessive displacement of the upper reinforcement layers that was

TEST No. 10

LAYER THICKNESS = 1.5"

SOIL PROPERTIES: FRICTION ANGLE, $\phi = 44^\circ$

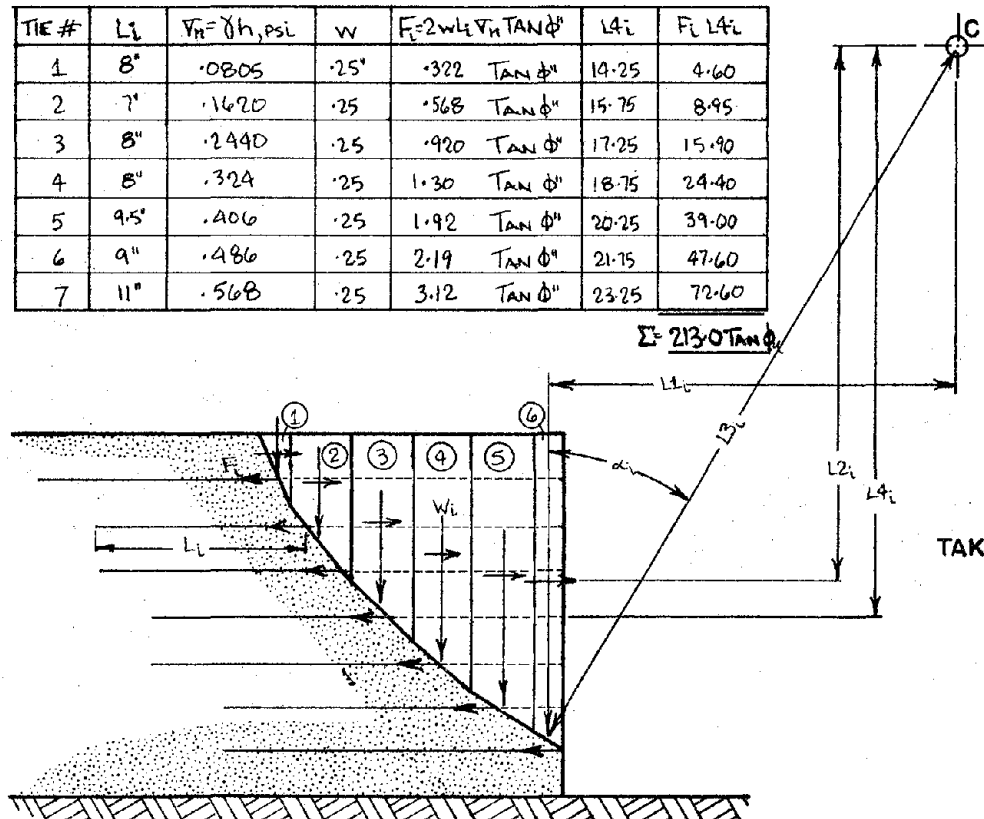
DENSITY, $\gamma = 93.5$ PCF = .054 PCI

TIE SPACING = 3.0"

TIE #	L_i	$V_R = \gamma h$, PSI	W	$F_i = 2wL_i V_R \tan \phi'$	L_{1i}	$F_i L_{1i}$
1	8"	.0805	.25'	.322 $\tan \phi'$	14.25	4.60
2	7"	.1620	.25	.568 $\tan \phi'$	15.75	8.95
3	8"	.2440	.25	.920 $\tan \phi'$	17.25	15.90
4	8"	.324	.25	1.30 $\tan \phi'$	18.75	24.40
5	9.5'	.406	.25	1.92 $\tan \phi'$	20.25	39.00
6	9"	.486	.25	2.19 $\tan \phi'$	21.75	47.60
7	11"	.568	.25	3.12 $\tan \phi'$	23.25	72.60

SEISMIC SHEAR SLICE INFORMATION							
SLICE #	b_i	h_i	$W_i = b_i h_i$	α_i	L_{1i}	L_{2i}	L_{3i}
1	1"	1"	.162	57°	22.0	13.5	26.25
2	2	3.5	1.135	52	20.75	14.4	26.25
3	2	5.75	1.87	45	18.75	15.6	26.5
4	2	7.5	2.44	40	17.0	16.5	26.5
5	2	9.0	2.92	35	15.0	17.25	26.5
6	1	10.0	1.62	30	13.5	17.5	26.5

$W_i \times L_{1i}$	AVG. ACCEL.	$Acc \times W_i \times L_{2i}$	$W_i \times \cos \alpha_i \times \tan \phi \times L_{3i}$
3.56	.58	1.27	2.24
23.55	.59	9.64	17.71
35.06	.58	16.92	33.52
41.48	.59	23.75	47.83
43.80	.59	29.72	61.21
21.87	.40	17.01	35.90



$\Sigma = 169.3 \quad \Sigma = 98.3 \quad \Sigma = 198.4$

TAKING MOMENTS ABOUT POINT 'C'

$169.3 + 98.3 - 198.4 - 213.0 \tan \phi_c = 0.0$

OR

$\tan \phi_c = \frac{69.2}{213.0} = .325$

$\phi_c = 18^\circ$

FIGURE 4-27 FAILURE WEDGE ANALYSIS

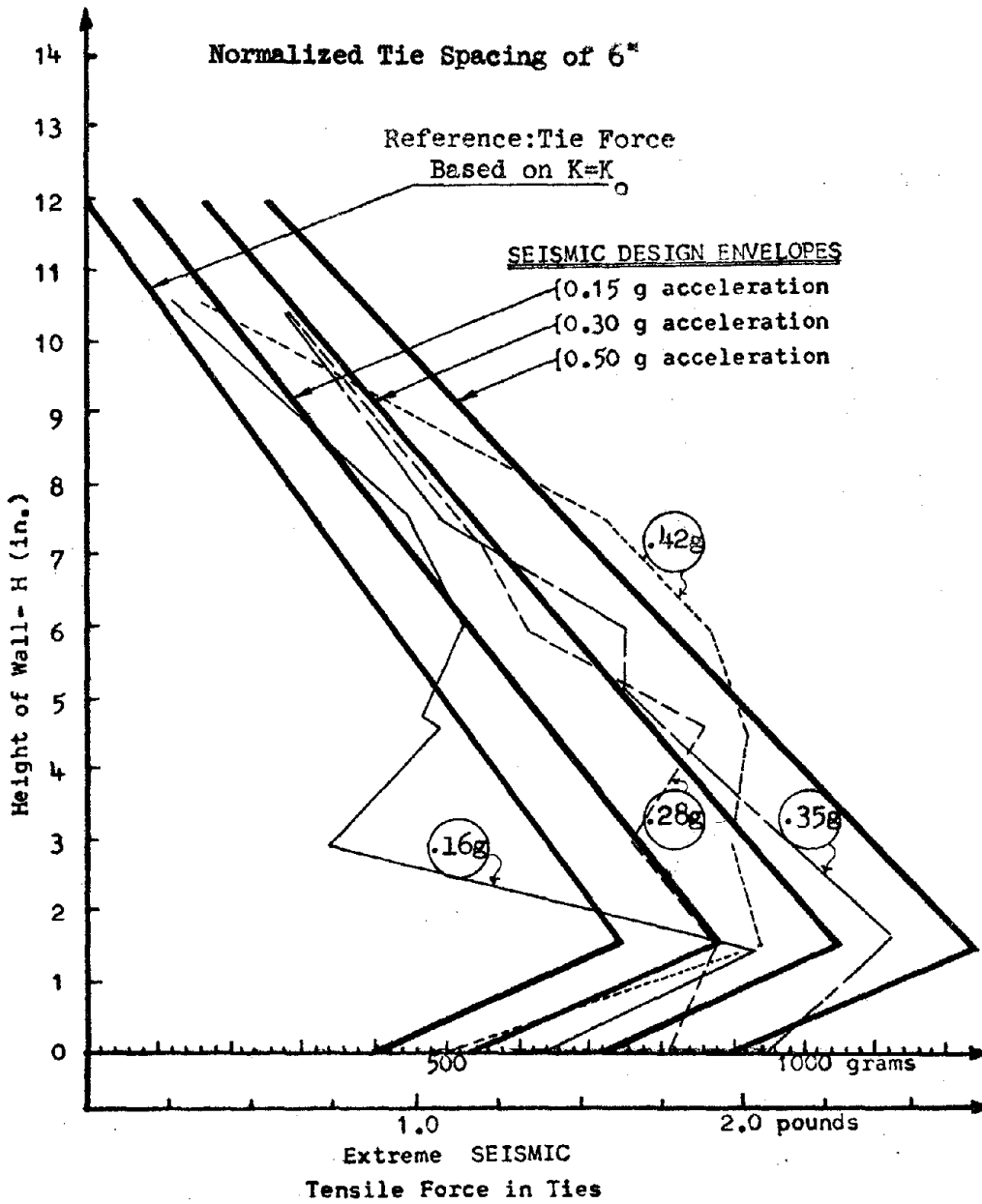


FIGURE 4.28 EXTREME DYNAMIC TIE FORCES verses
SEISMIC DESIGN ENVELOPES

common to Series A, B-1, and B-2 tests.

The very long ties used in the Series B-3 tests were required because of the remarkably low soil-tie friction angle of the mylar tie material. As described in the following Section 4.5, this low soil-tie friction angle was measured to be about 7° to 12° . It is peculiar to the smooth mylar tape used for the model ties, and does not necessarily reflect the nature of fullscale structures, using steel ties, where the soil-tie friction angle may be in the order of 20 to 30 degrees.

4.4 ADDITIONAL TESTING

Because all Series B tests were performed using the same model height and input frequency, two additional model tests were performed to determine the influence of model height and the frequency of the input motion. Both model tests used the flat aluminum skins and mylar ties common to the Series B models. The tie lengths and spacing used in the two tests are presented in Table 4.5.

The first additional test, test no. 12 was built 16.5 inches high, vs 12 inches for Series B, and was intended to provide a measure of the influence of wall height on the lateral forces. The input motion was maintained at a constant 11.6 cps, same as Series A and B. The data of primary concern from this test was the dynamic tie forces.

The second additional test, test no. 13, was built 15.0 inches high and was intended to provide a measure of the influence of the frequency of the input motion upon the dynamic tie forces. The acceleration of the input motion was maintained at 0.1g while the frequency was increased from 10 to 40 cps, sinusoidal motion.

The laboratory results from these tests are discussed in Section 6.3 of this report. This section deals with the influence of frequency on the dynamic lateral earth pressures.

Table 4.5 Additional Model Tests
Tie Arrangement

Tie Depth	Test Model no. 12			Test Model no. 13		
	Force	Length	Spacing	Force	Length	Spacing
1.5	.36 lb	28 ⁴	1.5"	.6	33"	1.5"
3.0	.50	35	3	.85	24"	1.5"
4.5	.64	23	3	1.10	21	1.5
6.0	.80	21	3	1.40	20	1.5
7.5	.94	20	3	1.65	33	3
9.0	1.06	18	3	1.90	32	3
10.5	1.22	18	3	2.15	30	3
12.0	1.36	16	3	2.40	28	3
13.5	1.50	15	3	2.65	28	3
15.0	1.64	15	3	1.66	15	3
16.5	1.12	10	3	—	—	—

4.5 TIE PULLOUT-TESTS

As indicated by Eq. 2.7 and the example design calculations illustrated on Table 4.2, it is apparent that the developed soil-tie friction angle, ϕ_u , is a decisive factor in calculating tie lengths. Since the soil-tie friction angle is critical for wall stability and for economic reasons, an attempt was made to determine the nature of this property for the sand and mylar tape ties used in the Series B tests which investigated failure by tie-pullout.

For this purpose, additional ties were placed in some of the walls during construction. The physical location of these 'extra' ties is indicated in Fig. 4.29. In general the pullout tests were performed to determine the effect of

- 1) the distance from the face of the wall, and
- 2) vibration

on the soil-tie friction angle.

To determine the effects of vibration on ϕ_u some embedded ties were pulled out at various stages such as:

- 1) initially after construction of the wall,
- 2) during 0.05g acceleration, and
- 3) statically after the acceleration was removed.

The result of the first few tests indicated some very low friction angles, suggesting that there was some arching developed to reduce the normal stress on the ties. The 0.05g acceleration was used to create a minimal amount of vibration found necessary to break up this arching tendency. As a result, this amount of acceleration caused

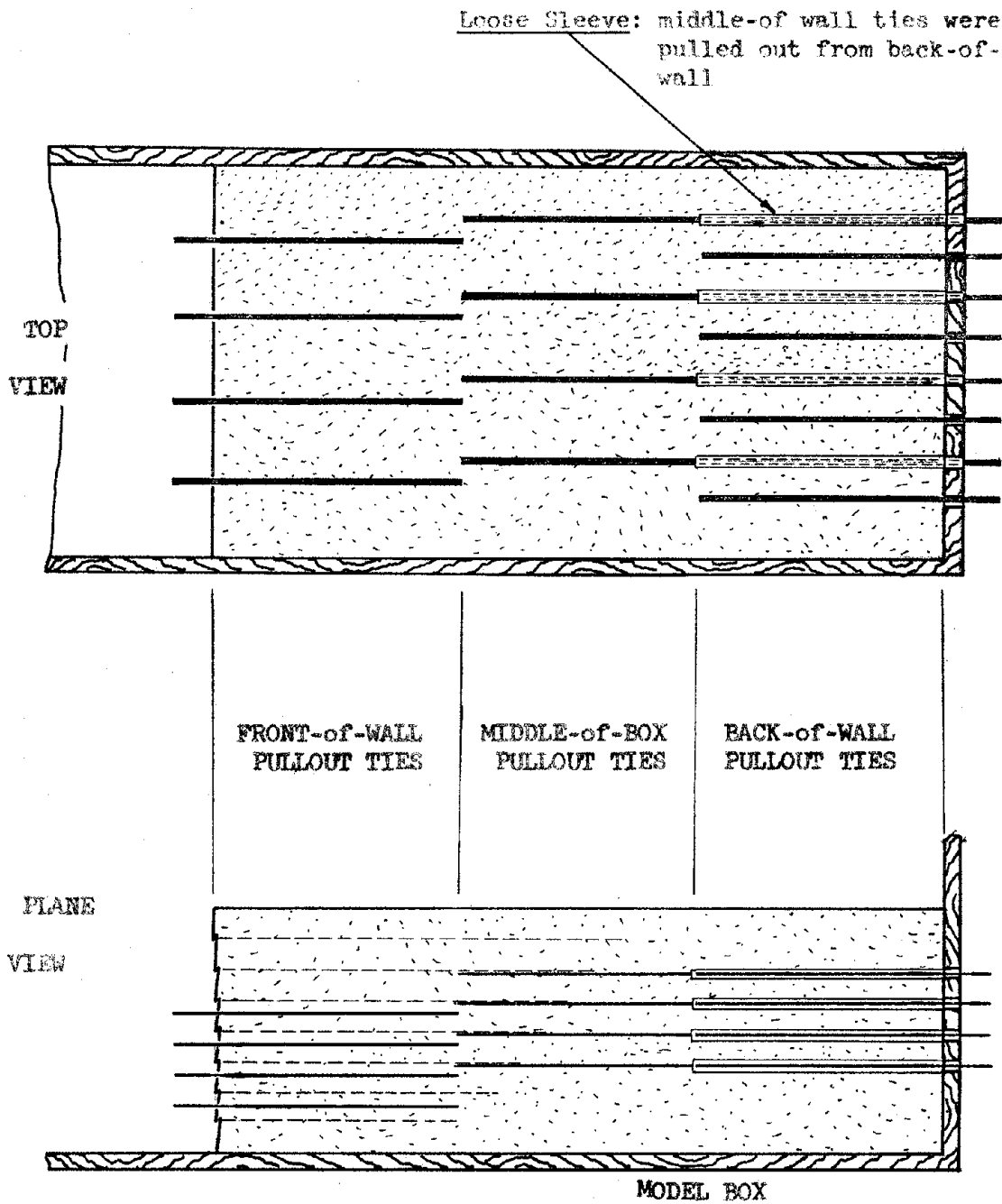


FIGURE 4.29 'PULLOUT' TIES

an increase in the monitored forces which held up the wall from the initial static tie forces approximated by a K_A condition to forces predicted by $K = K_0$ lateral earth pressure. However, these small "seating" accelerations did not cause a noticeable deformation of the wall, Fig. 4.18.

To perform the actual tests the pullout device illustrated in Fig. 3.8, was used to measure force-displacement as the tie was drawn out at a constant velocity. A typical tie force verses displacement record, is given in Fig. 4.30.

The force-displacement records were used to calculate the values of ϕ_u for varying embedment lengths of the tie. This was done using the expression

$$\text{TAN } \phi_u = \frac{\text{friction force}}{2 * \gamma * h * \text{width} * L_E} \quad (4.5)$$

where L_E is the length of tie still embedded in the sand during the instant the tie force was measured. Soil-tie friction angles calculated from the results of these test's are presented in Fig. 4.31, 4.32, and 4.33 for backwall, middle of model, and wall face pullout tests, respectively.

The most significant observation to be drawn from these tests is that the soil-tie friction angle is not constant. In nearly all tests the withdrawal of the tie only $\frac{1}{2}$ inch, 8.33% of the total tie length, was sufficient to develop a peak resistance, and then a reduction in tie force of nearly 50%.

The most surprising observation was that the soil-tie friction

h11-11

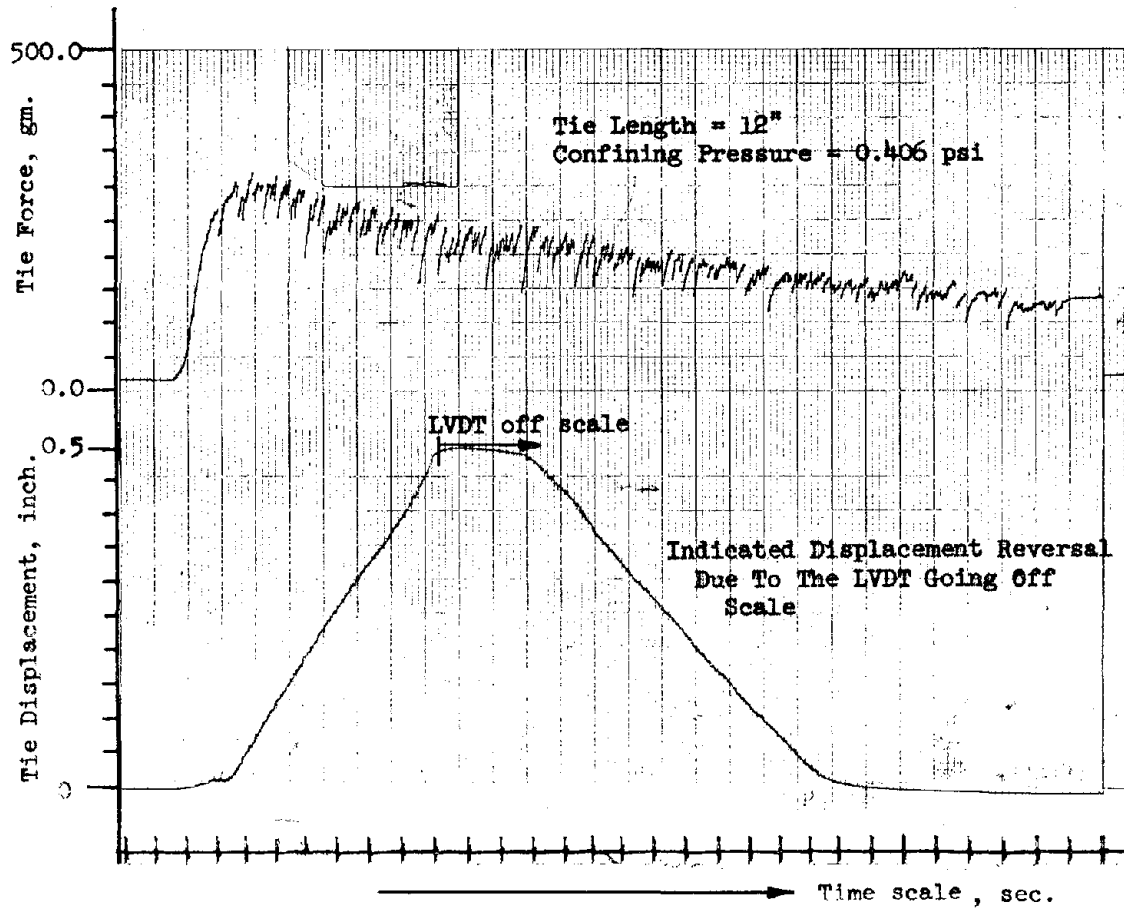


FIGURE 4.30 TIE PULLOUT RECORD

Dynamic vibration was 0.05g sinusoidal with a frequency of 11.6 cps. Total Tie Length = 12 inches.

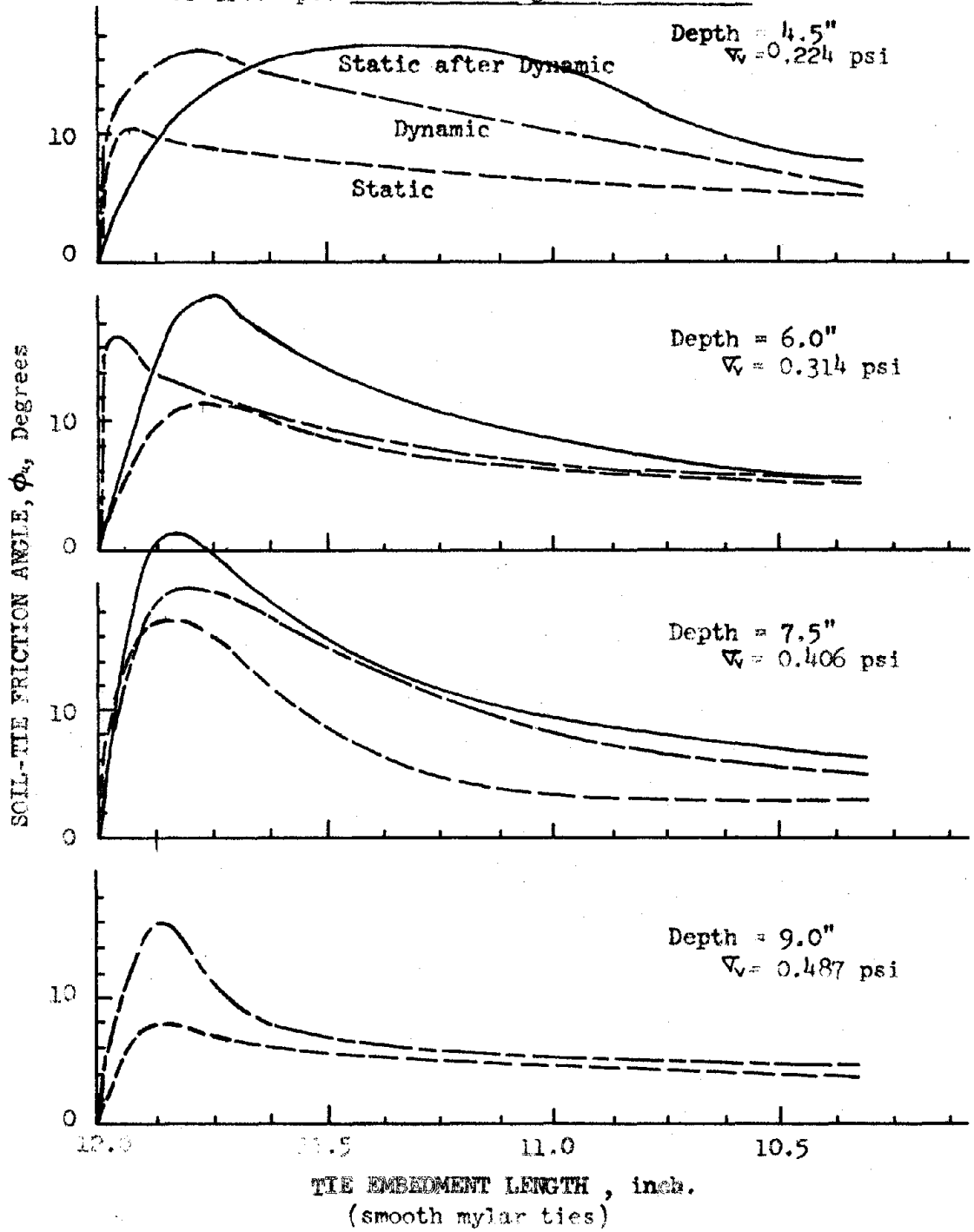


FIGURE 4.31 BACKWALL PULLOUT

Dynamic vibration was 0.05g sinusoidal with a frequency of 11.6 cps. Total Tie Length = 12 inches.

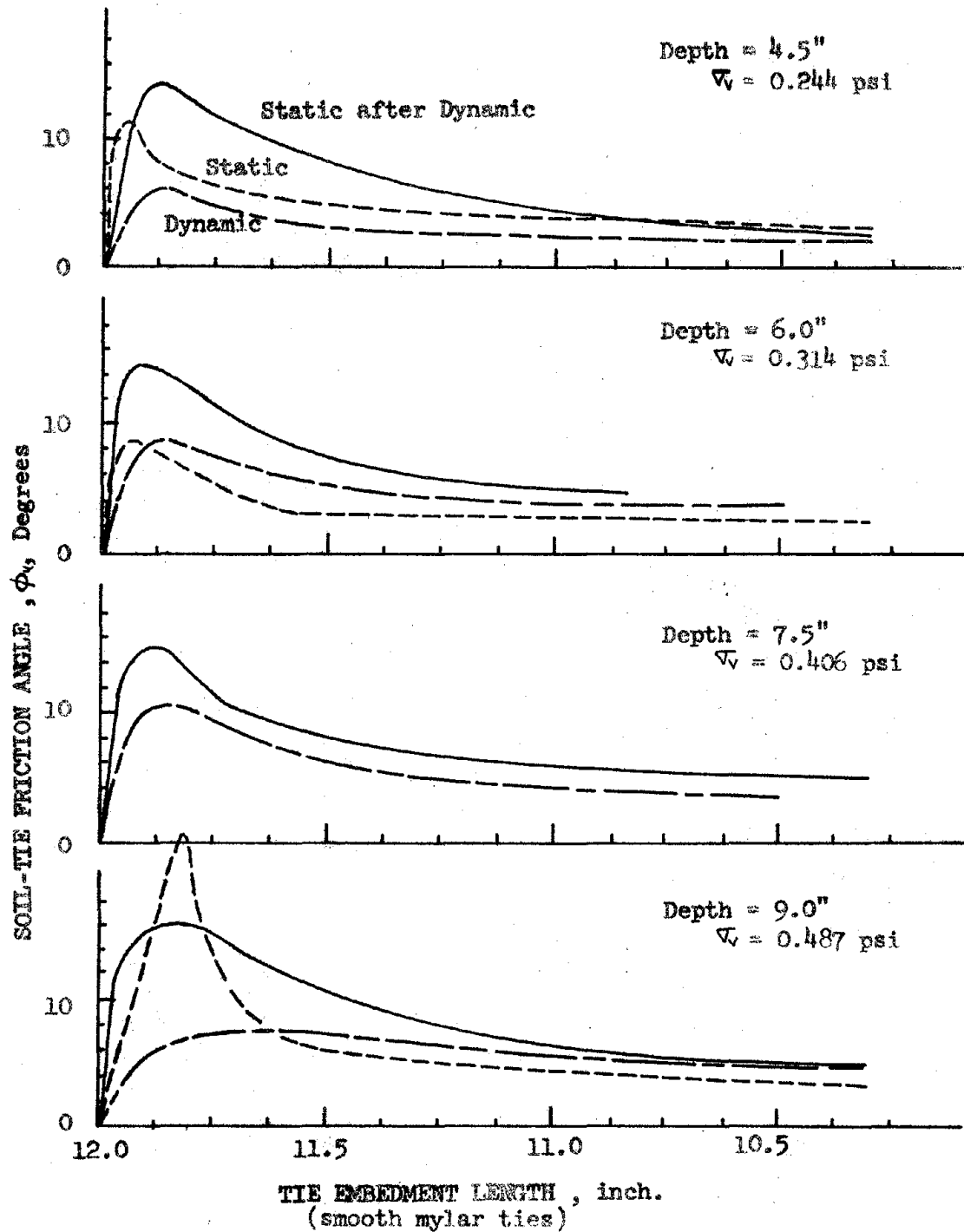


FIGURE 4-32 MIDDLE-OF-BOX PULLOUT

Dynamic vibration was 0.05g. sinusoidal with a frequency of 11.6 cps. Total Tie Length = 12 inches.

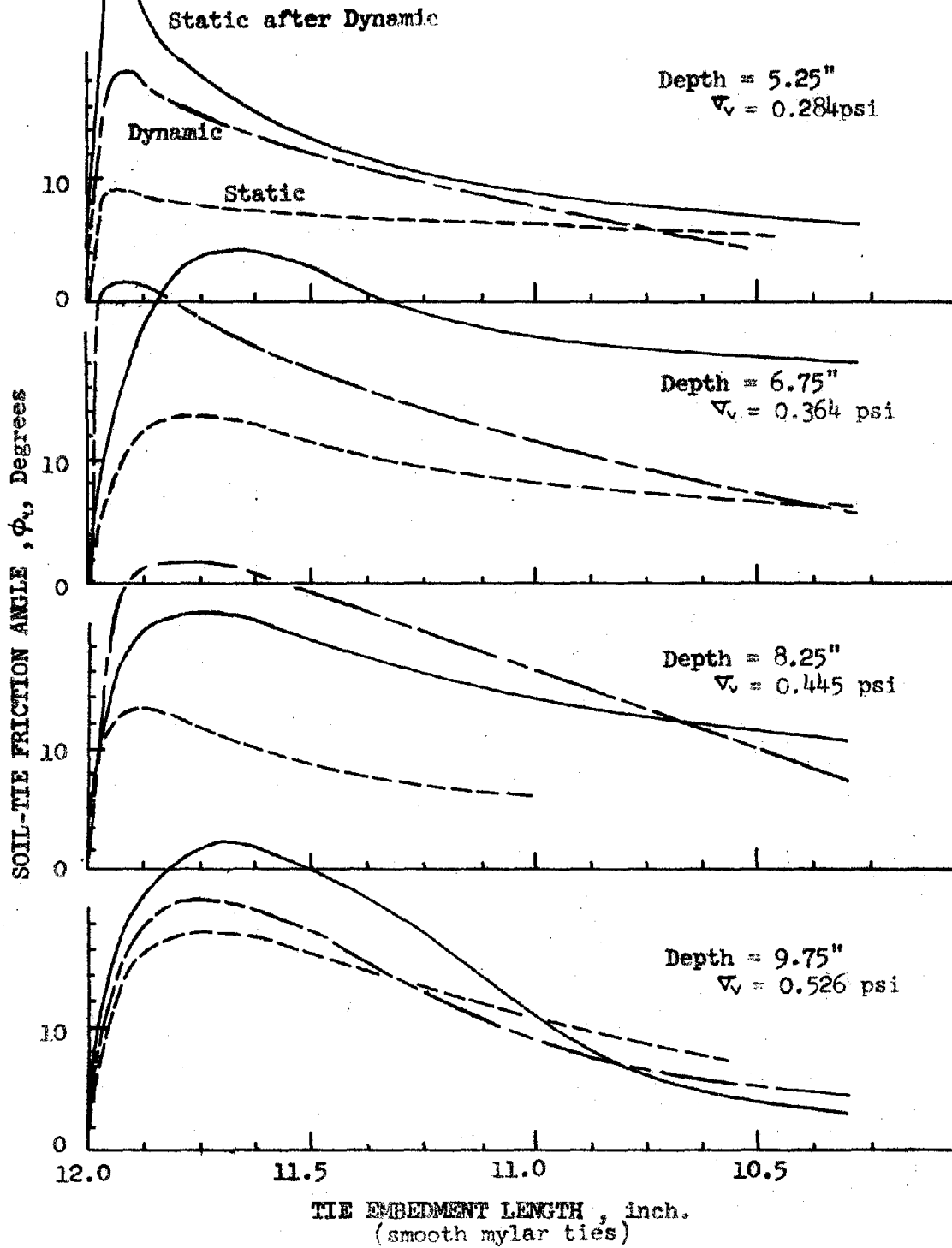


FIGURE 4-33 FRONT-OF-WALL PULLOUT

angle was larger during vibration than under previbration static conditions. It was also larger during static loading after the vibrations had ceased than for initial static conditions.

An alternative way of looking at the tie-pullout data was to plot the tie-pullout force per unit surface area vs the overburden pressure. Since the pullout tests were performed for ties embedded at 3 to 4 different depths, this enabled an average value of ϕ_u to be defined by the best fit straight line through the origin and through these 3 to 4 data points. Data for peak and for residual conditions are shown on Fig. 4.34 to 4.36 for all of the pullout tests. Although in general the peak data show more scatter than the residual data, the points do show a reasonable trend of linearly increasing pullout resistance vs. confining pressure compatible with a constant ϕ_u .

Because the data was scattered, especially for the peak resistance several additional check tests were also performed. The results of many of these tests were not reduced and plotted, but examination of the raw data shows that the scatter was random, not related to any known construction detail, or defect in the test strip of tape.

It is significant to point out that for the materials tested, the residual friction angle was only 1/3 to 1/4 of the peak friction angles. Small movements of the wall could conceivably push the skin beyond the peak, and lead to a failure by tie-pullout.

It is believed that both the low residual values, and to some extent, the randomness in the peak values is due to a tendency for

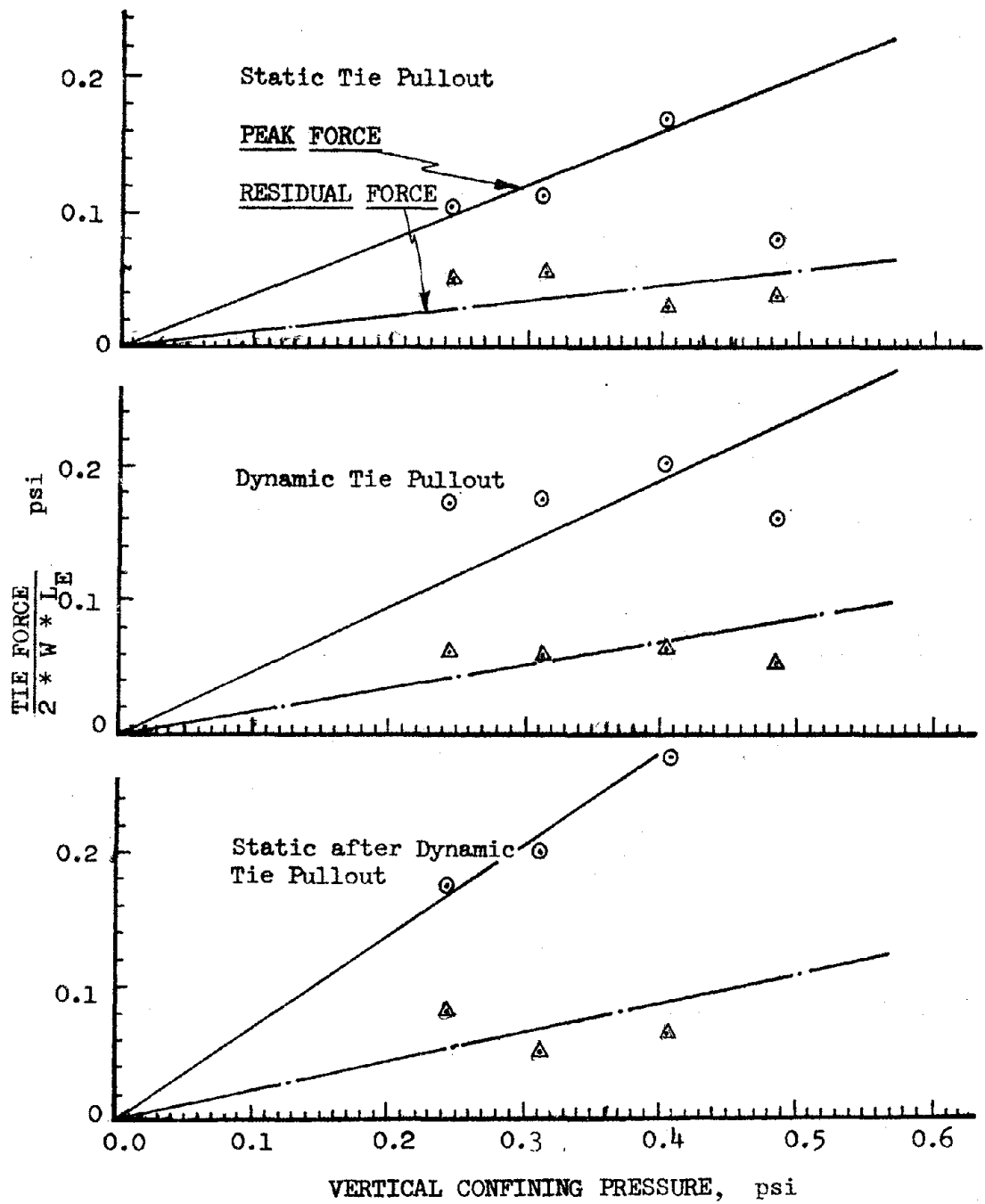


FIGURE 4.34 BACKWALL PULLOUT TEST

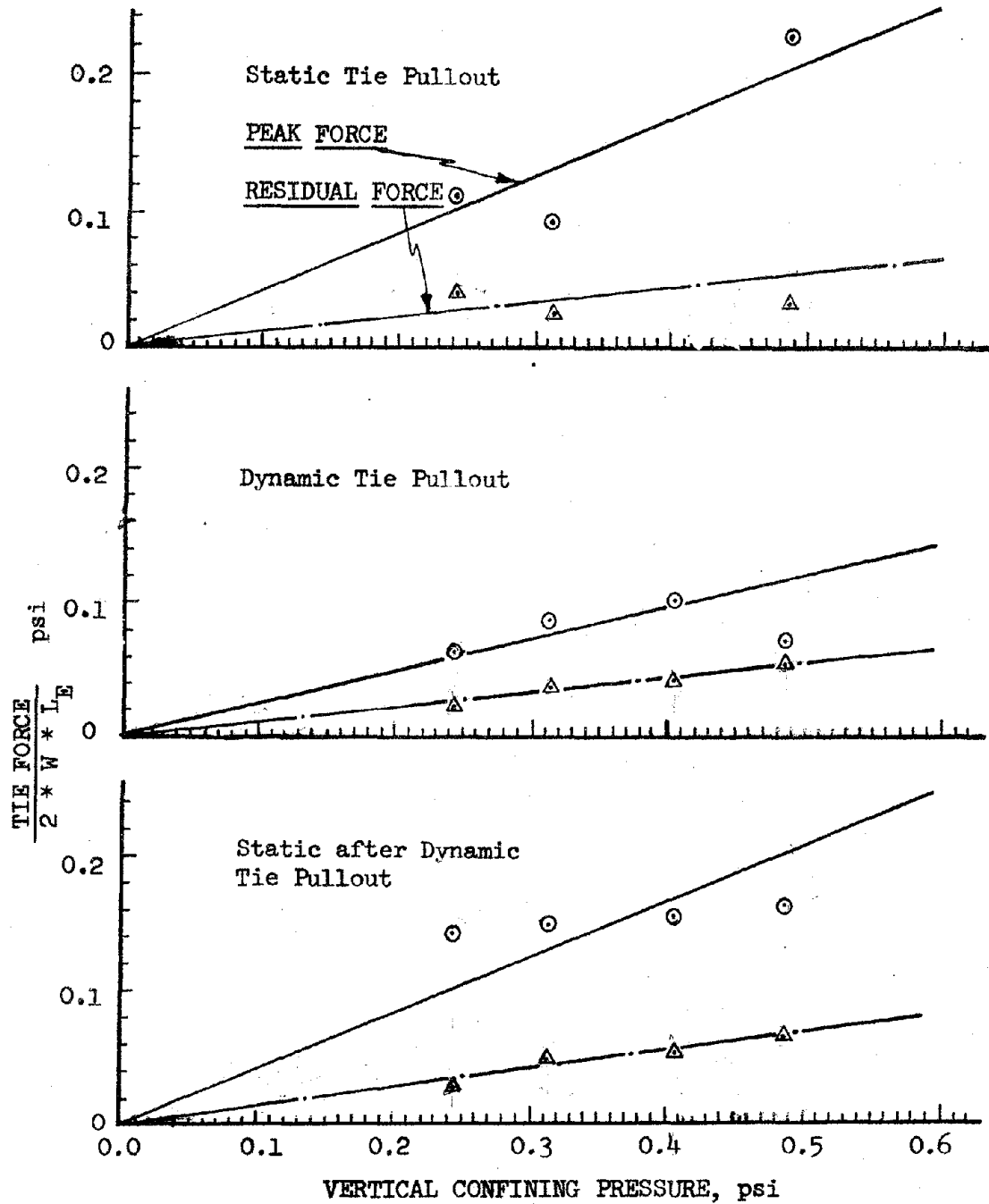


FIGURE 4.35 MIDDLE-OF-BOX PULLOUT TEST

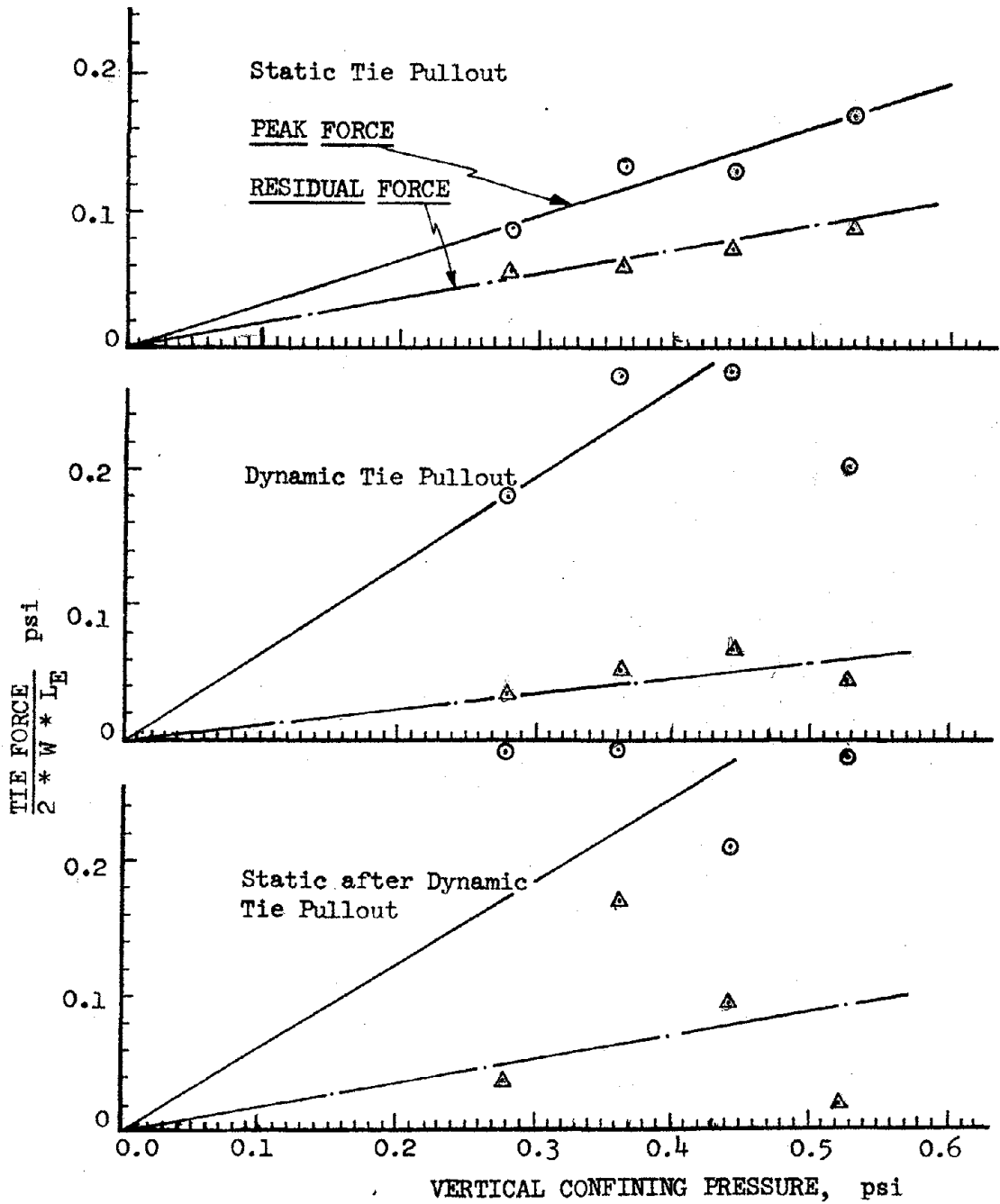


FIGURE 4.36 FRONT-OF-WALL PULLOUT TEST

the soil to arch over the tie, and once the peak has been reached the tie can pull out easily, almost as if the hole remained open without the tie to support it. However, relative deformations within the soil will tend to break up this arching, and allow more of the overburden to act on the tie.

Under static loading, the small wall movements which develop during construction lead to sufficient deformations in the sand behind the wall to break up the arch. Hence ties pulled out immediately after construction from the front of the wall had higher peak ϕ_u values than ties pulled from the middle or the back of the box, where construction deformations would have been less. Further, vibration also tends to break up the arch, so that pullout resistance was greater during vibration and only about 0.05g was sufficient to increase the tie-pullout resistance significantly. Thus, although in the controlled pullout tests very low values of residual ϕ_u were measured, it would appear that small vibrations or even wall deformations under static loading would be sufficient to keep ϕ_u well above the low measured residual values. This explains why catastrophic failures were never observed for the shaking tests on the walls where the ties pulled out but did not break.

It must be pointed out that all these data were obtained using very smooth and surface hardened mylar tape. These data indicate that the property ϕ_u is difficult to define, and is likely to depend on many factors such as amount of movement, disturbance, and shaking etc. as well as on the tie and soil materials. Much more study is required using more realistic soils and tie materials

associated with real field installations.

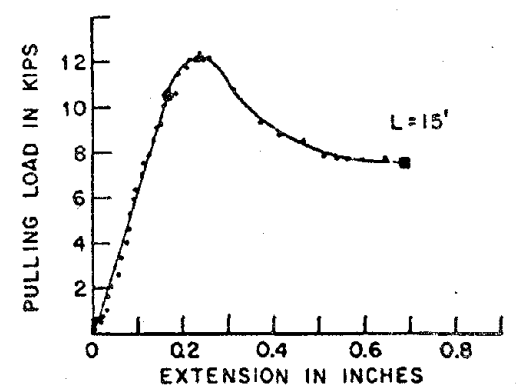
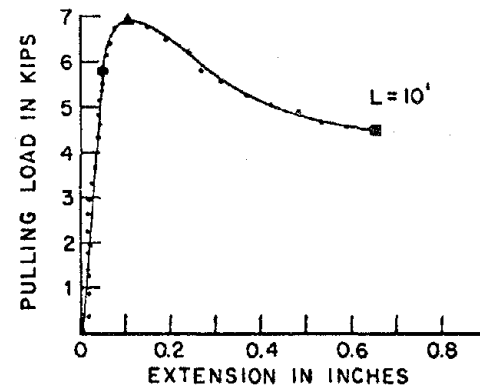
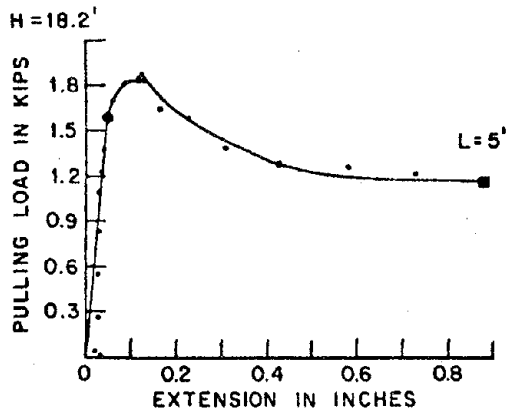
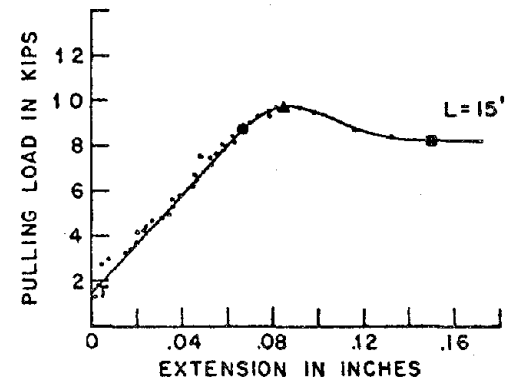
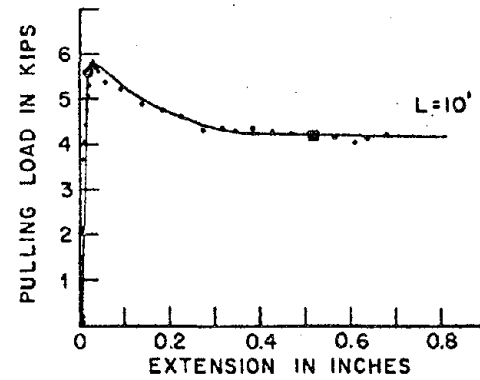
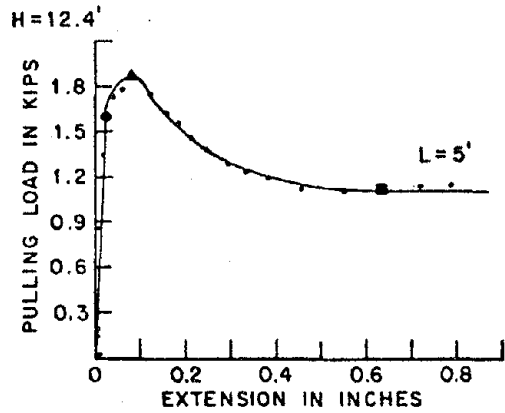
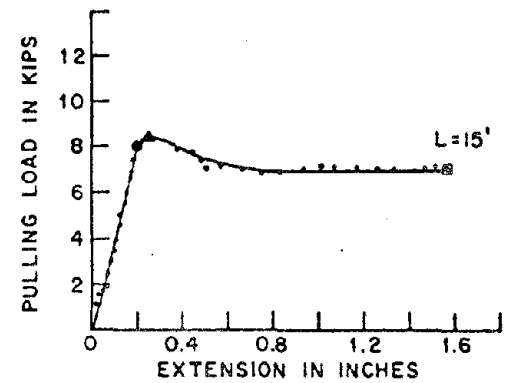
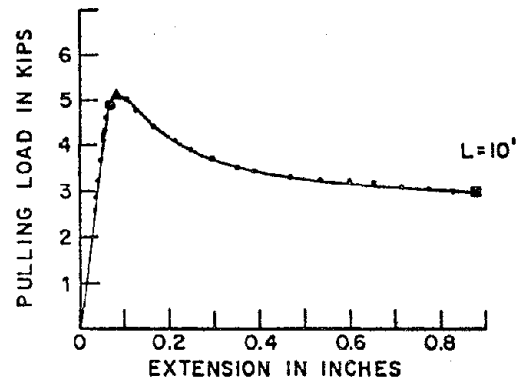
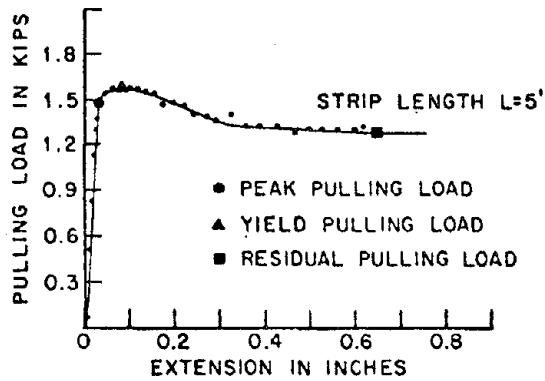
The field data obtained by Beaton et al. (12) from full scale static tests is a big step toward the better understanding of the pullout resistance in reinforced earth walls. Extra ties were buried in the fill at various locations during construction of the Highway 39 wall. These were later pulled out and force deformation measurements were taken. These data as presented by Beaton et al. (12) are reproduced in Fig. 4.37 and 4.38. It is noted that two types of failure developed: tie pullout and tie breaking. As would be expected, the tie breaking failures occurred for the longer ties at the greater depths where the total frictional resistance was large.

It is especially noted that for all ties which did not break, the pullout force-deformation curves were very similar to those shown in Figs. 4.30 to 4.33. A peak force rapidly developed, followed by a significant reduction in pullout resistance to a residual force which was considerably lower than the peak.

The average shear stress along the tie face is plotted vs. the vertical overburden pressure in Fig. 4.39 to show the soil-tie friction as measured by field tests. The data show a fairly wide scatter, not at all unlike the scatter observed in the laboratory test data presented in Figs. 4.35 and 4.36.

In addition to the field pullout tests, Beaton et al. report the results of some small scale laboratory sliding friction tests in which ties were pulled through a small box of soil which carried a known vertical load. The load-deformation curves for these tests are not presented, but the soil-tie friction angle measured from

OVERBURDEN
HEIGHT $H=7.5'$



(from Beaton et al)

FIGURE 4-37 LOAD DEFORMATION CURVE FROM FIELD PULLING TESTS

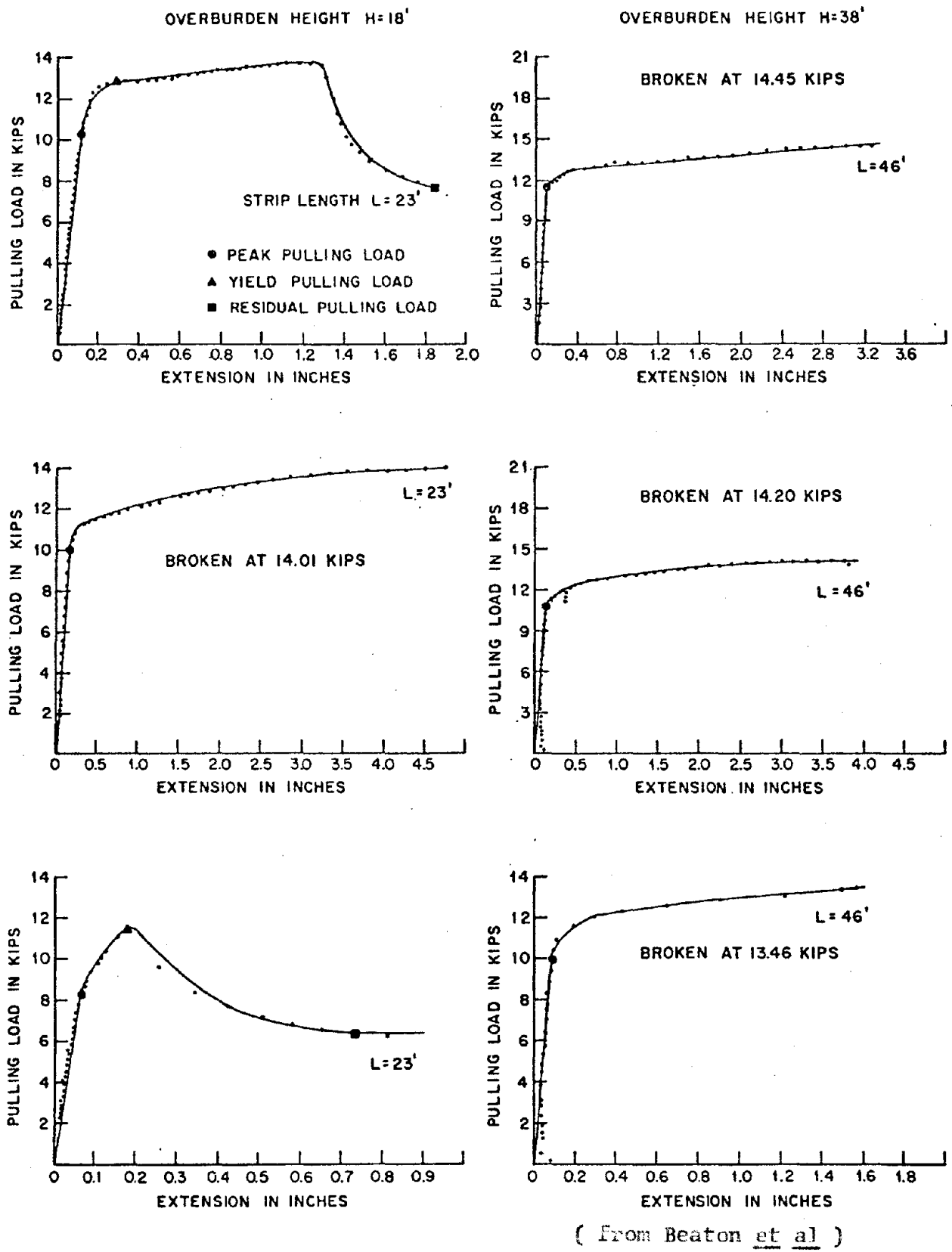


FIGURE 4.38 LOAD DEFORMATION CURVE FROM FIELD PULLING TESTS

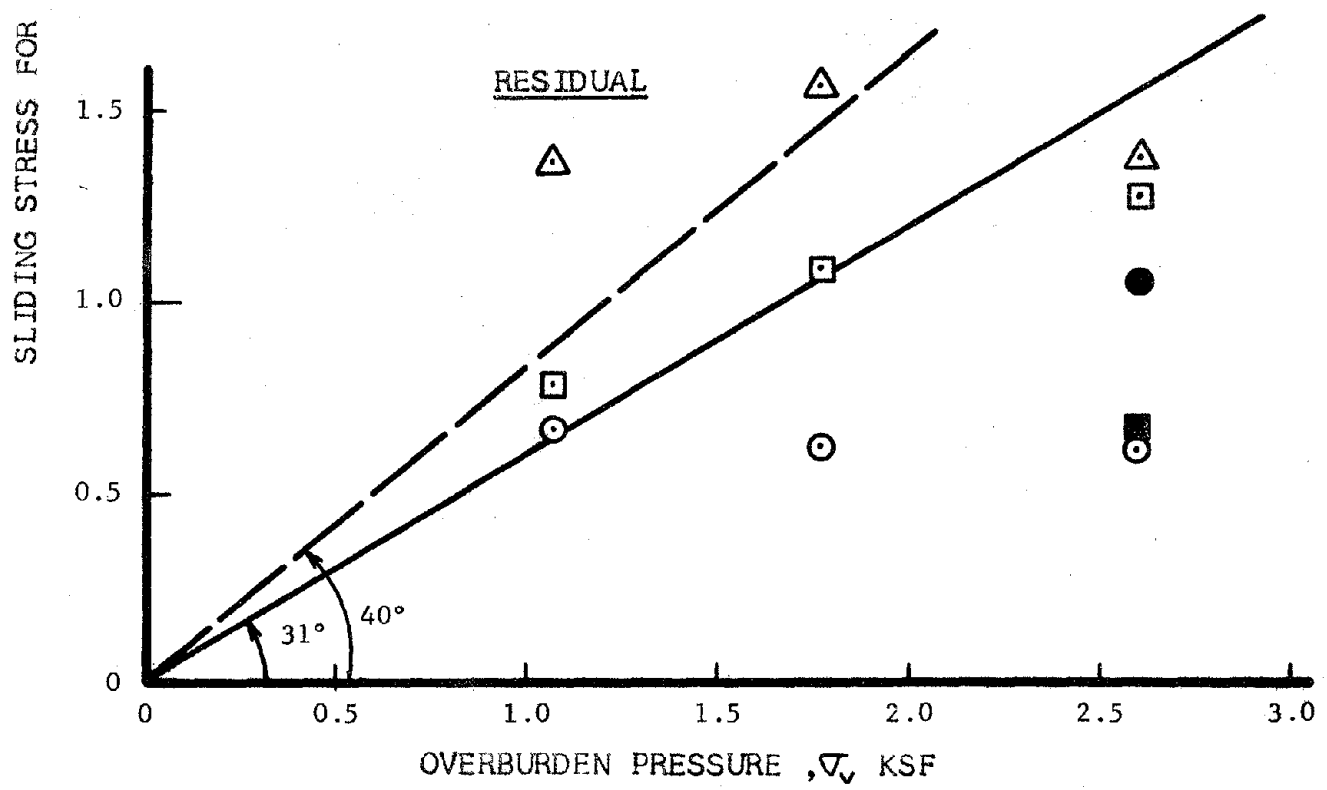
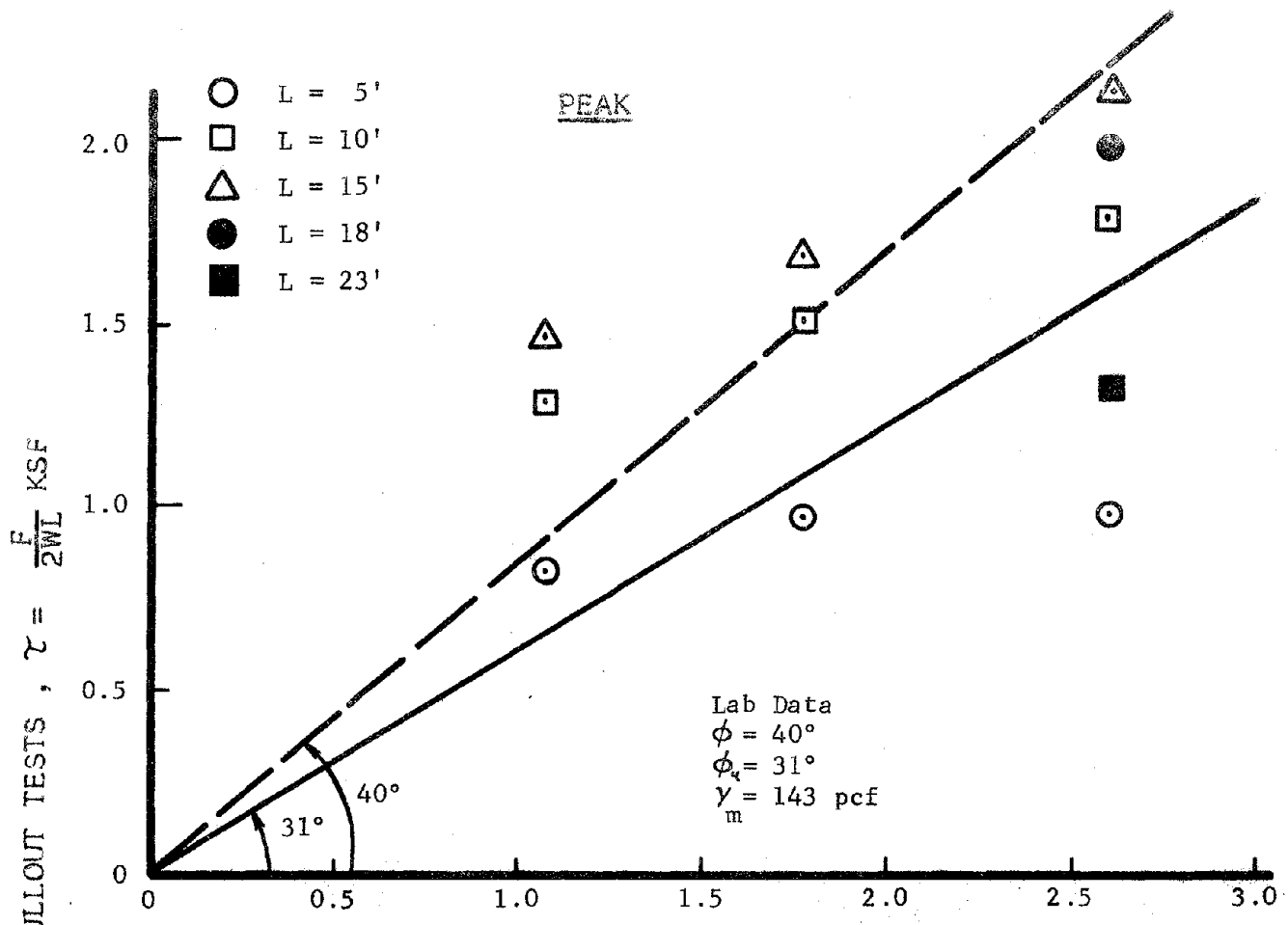


FIGURE 4.39 SUMMARY OF FIELD PULLOUT DATA FROM HIGHWAY 39
 IT-126

these laboratory tests is given as $\phi_u = 31^\circ$. The ordinary angle of internal friction of the soil was given as $\phi = 40$ degrees, and the total unit weight in the field was given as 143 lb/ft³. Straight lines sloping at ϕ_u and ϕ from the laboratory test data are also shown in Fig. 4.39 for comparison.

Following the field and laboratory studies of soil-tie friction, Beaton et al. recommend using for design a factor of safety of 4.0 on the residual value of $\tan \phi_u$ measured in field pullout tests.

CHAPTER 5 ANALYTICAL PROCEDURES AND RESULTS

5.1 PROGRAM LEVSFC

The computer program LEVSFC developed by Idriss at Berkeley (19) determines the seismic response of a soil layer with horizontal boundaries, using lumped mass analysis procedures to a given input base motion. The program uses non-linear, strain dependent modulus and damping properties in the soil. It was used to provide an initial estimate of

- 1) acceleration amplification,
- 2) the fundamental period of motion,
- 3) the displacement due to horizontal shearing and,
- 4) initial values of the strain-dependent damping and moduli for future analysis work.

This program was first presented by Seed and Idriss (20) using linear elastic procedures. At this time it was shown that this linear analysis procedure could be used on non-linear systems through the use of equivalent linear properties. This procedure involves the determination of an equivalent linear modulus, G_{EQ} , and an equivalent damping ratio, λ_{EQ} , for use in the linear elastic solution. Procedures used in determining these equivalent properties are shown in Fig. 5.1. Additional reference to this procedure was later presented by Silver and Seed (21). In this later work the equivalent moduli and damping were also presented as strain dependent properties. This procedure equated the equivalent modulus to the

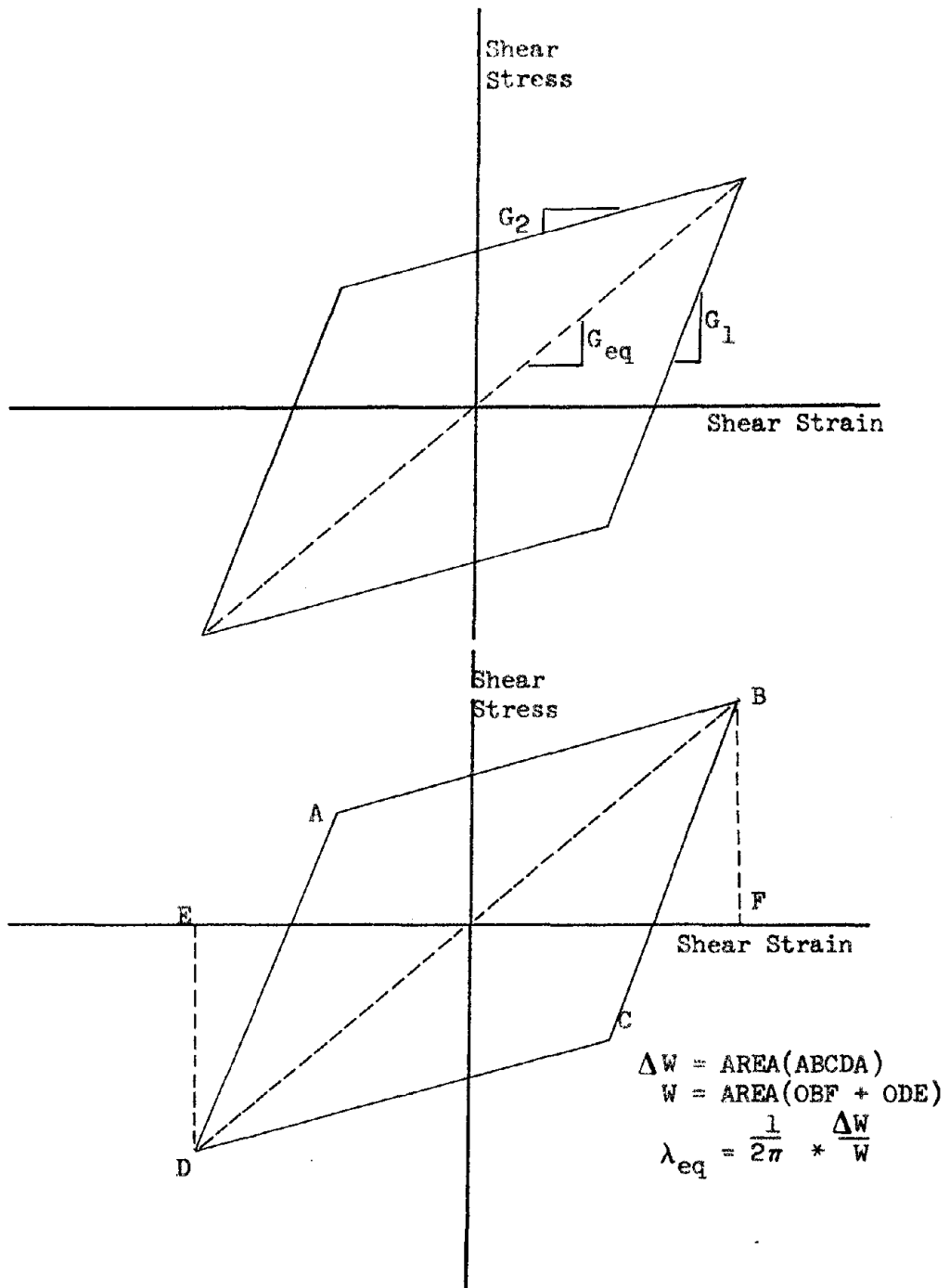


FIGURE 5-1 EQUIVALENT DAMPING AND SHEAR MODULI

secant modulus and equivalent damping to the area enclosed by the stress-strain hysteresis loop. The strain-dependent relationship of the equivalent moduli and damping for sands are presented in Fig. 5.2 and 5.3.

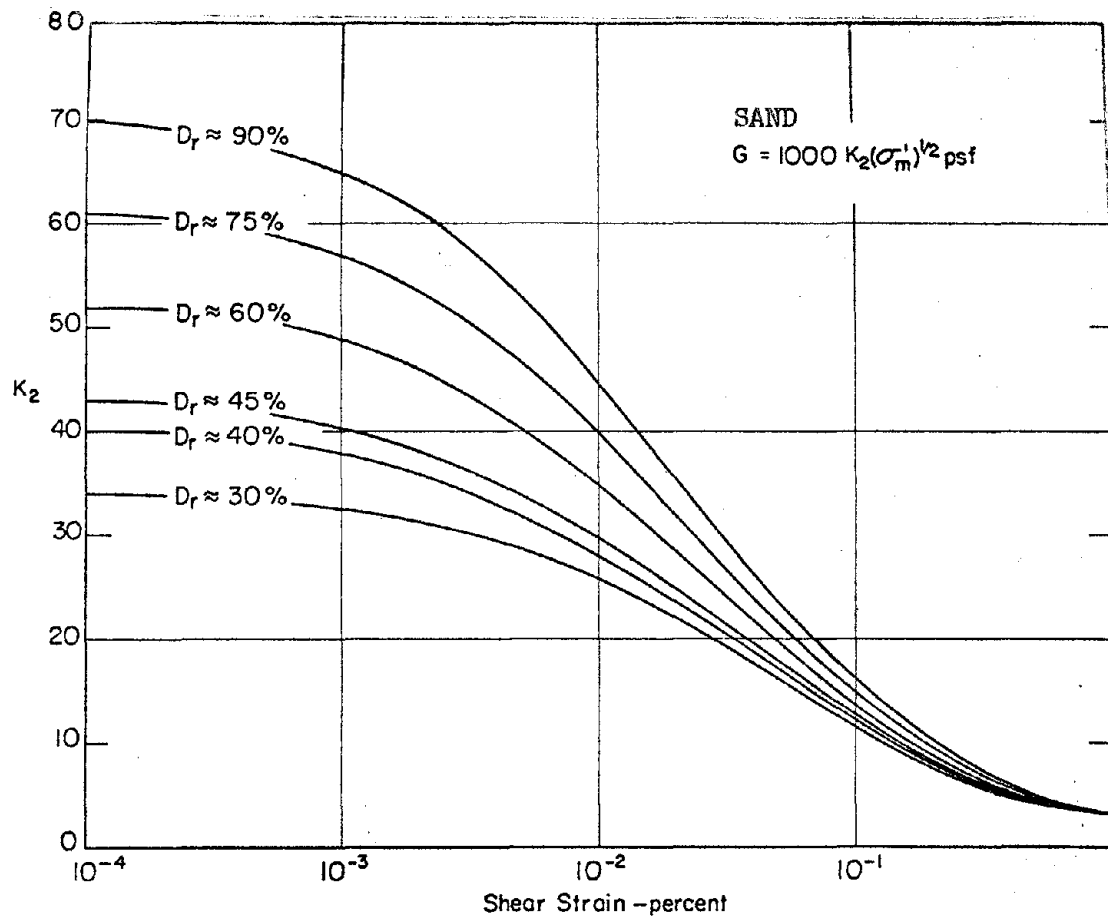
The program, in its present form, was presented by Idriss, Dezfulian, and Seed (22) and incorporates strain dependent moduli and damping ratios.

Program Theory. To use the lumped mass procedure for evaluating the seismic response of a soil layer, it must be possible to represent the deposit as a series of horizontal layers. Since all boundaries are horizontal, a unit vertical slice may be considered for analysis purposes and analyzed as a plane strain, $\epsilon_z = 0$ problem. The layered system is modeled as a lumped mass system by 'lumping' the mass of each layer at the top and bottom of each layer and by using equivalent shear springs to connect the lumped masses, see Fig. 5.4. This system of N soil masses results in N simultaneous equations of motion which may be represented in matrix form:

$$[M] \{\ddot{u}\} + [C] \{\dot{u}\} + [K] \{u\} = \{P(t)\} \quad (5.1)$$

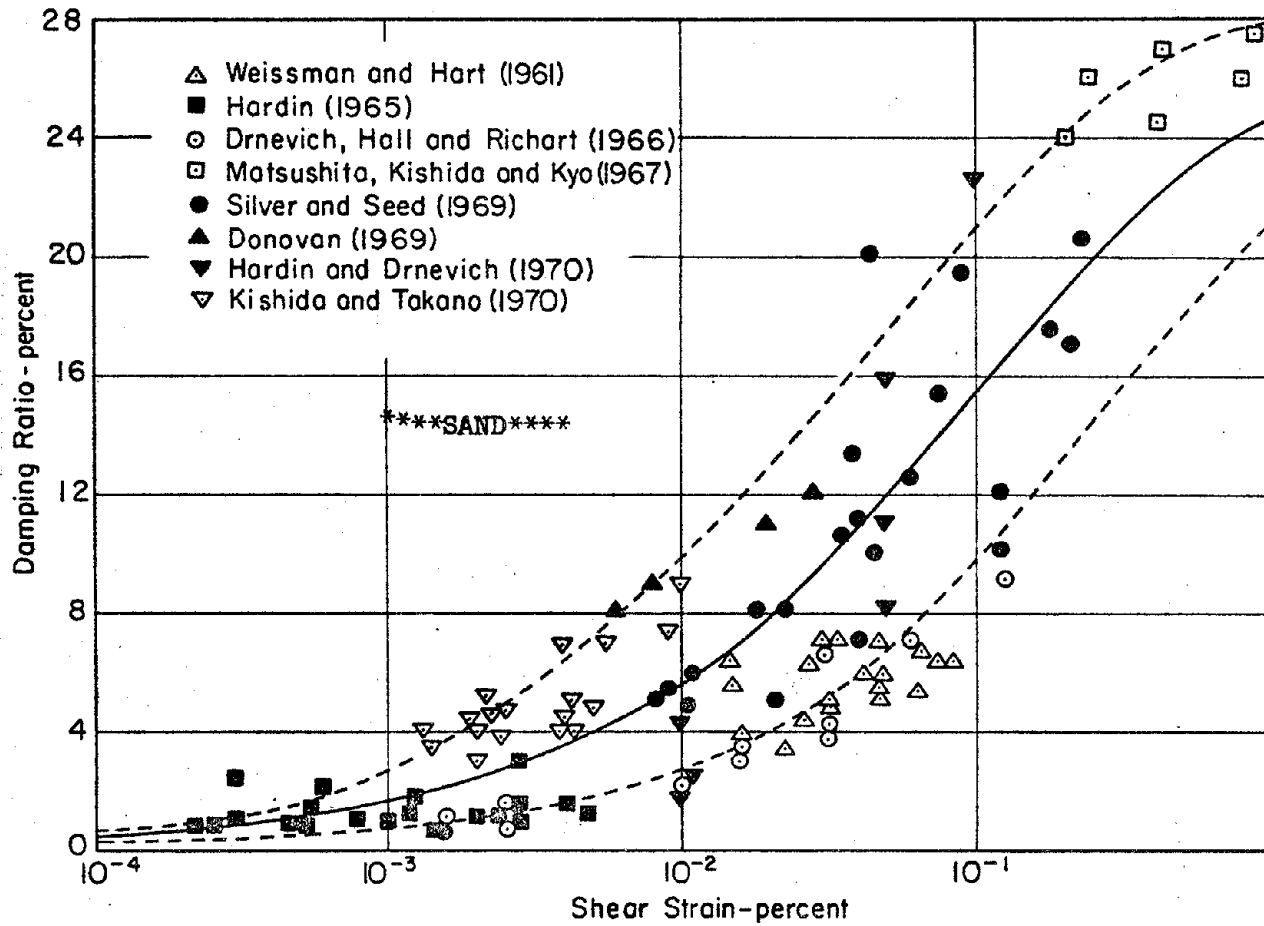
where

- $\{u\}$ = vector of lumped mass displacements,
- $\{\dot{u}\}$ = vector of lumped mass velocities,
- $\{\ddot{u}\}$ = vector of lumped mass acceleration,
- $[M]$ = mass matrix,
- $[C]$ = damping matrix,
- $[K]$ = stiffness matrix, and
- $\{P(t)\}$ = vector of inertial forces due to lumped mass and applied ground acceleration.



(From Seed & Idriss, 1971)

FIGURE 5-2 STRAIN DEPENDENT MODULI



(From Seed & Idriss 1971)

FIGURE 5.3 STRAIN DEPENDENT DAMPING

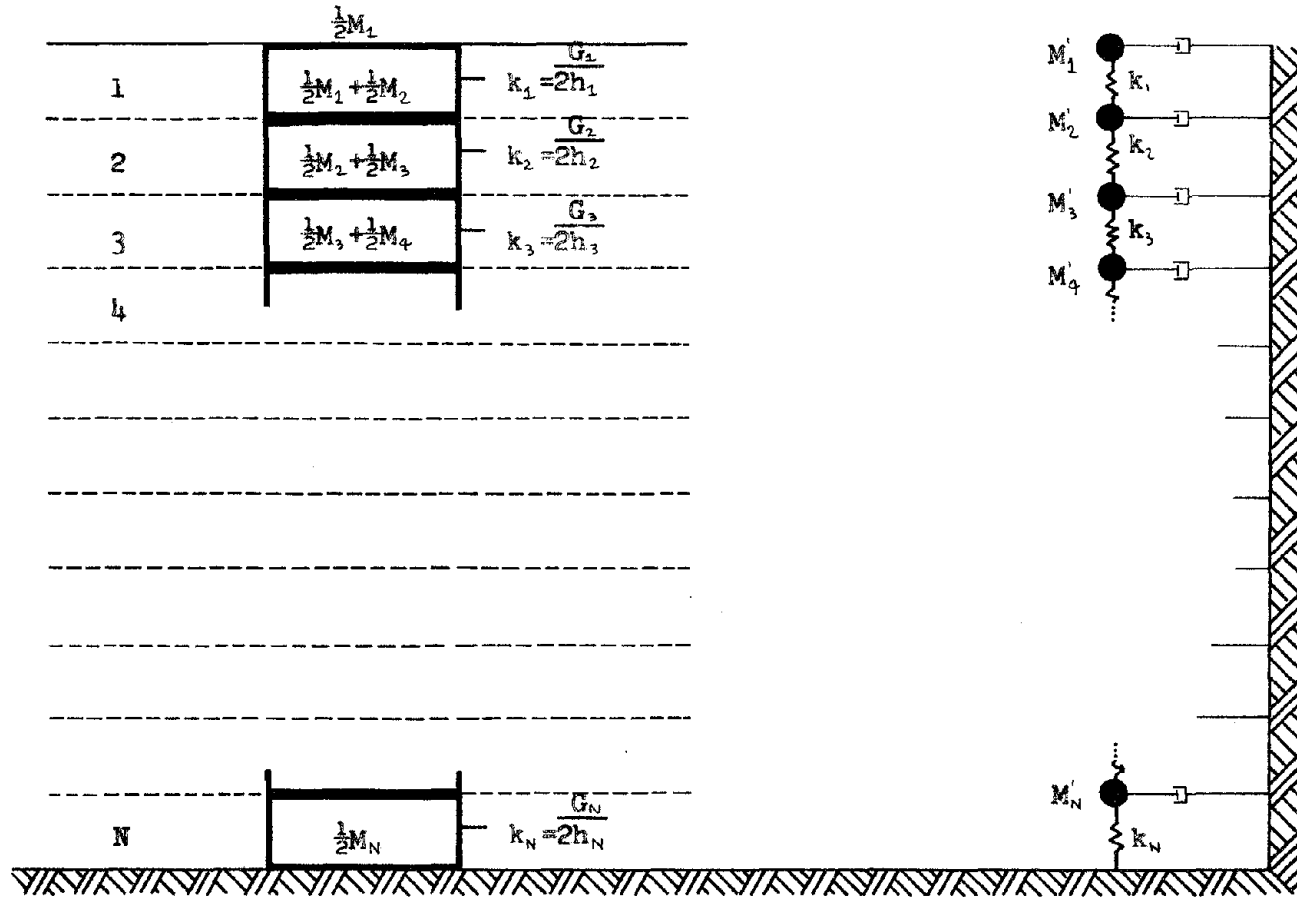


FIGURE 5-4 LUMPED-MASS MODEL

Program Results. In applying this program to the Reinforced Earth wall, it is realized that only a horizontal layer is modeled. Stress concentrations near the wall, and the possible effect of the ties are ignored. The ties should have little effect since they are horizontal, and the actual response is largely horizontal shearing. The response near the wall may be influenced by the vertical discontinuity, but back from the wall the actual and the analytical model should agree rather well. The program LEVSFC was used to analyze a Series A model Reinforced Earth wall. This wall was eleven inches tall and consisted of eleven layers of reinforcement. Each of the layers was subdivided into sublayers according to criteria previously outlined by Seed and Idriss. This procedure involves the following steps:

- 1) calculate the period of each segment using

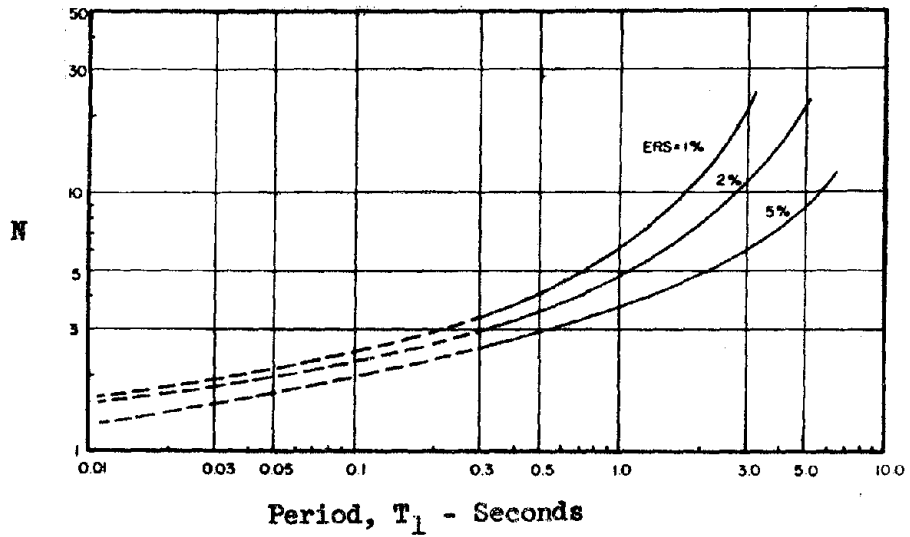
$$(T_1)_i = \frac{4 H_i}{\sqrt{G_i g / \gamma_i}}, \text{ and} \quad (5.5)$$

- 2) determine the number of sublayers using Fig. 5.5.

For the wall analyzed, two sublayers per layer proved to be adequate.

The initial shear modulus of each layer was calculated using Fig. 5.2. It must be pointed out that the extremely small confining pressures in the wall were well outside the experimental range that served as the basis for the soil moduli and damping relationships of Fig. 5.2 and 5.3.

The results of the LEVSFC analysis for shear deformation and acceleration amplification are presented in Fig. 5.6. From these two conclusions maybe reached;



where ERS = percent error in the lumped mass representation

(After Seed,Idriss)

**FIGURE 5.5 REQUIRED NUMBER
OF SUBLAYERS**

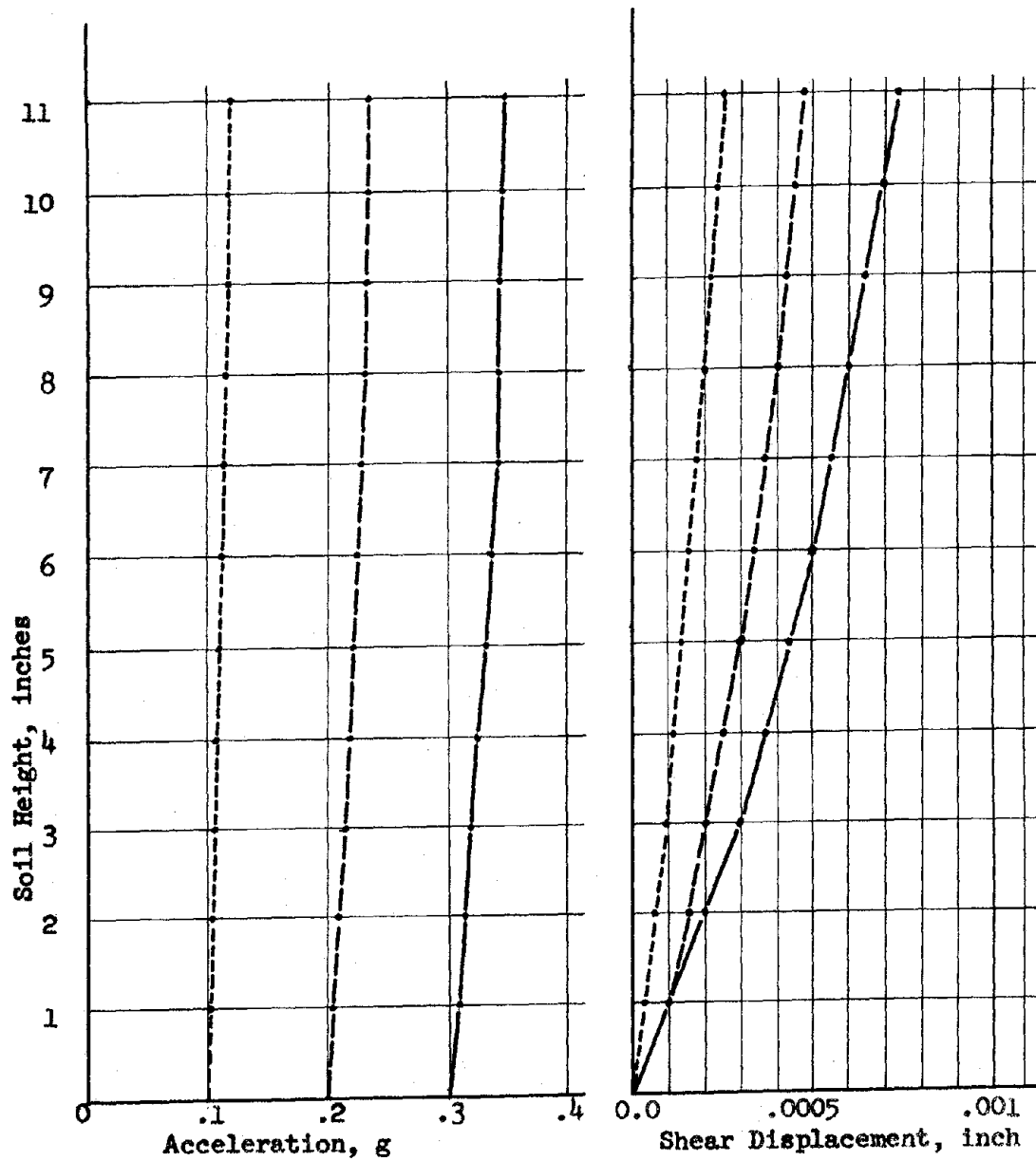


FIGURE 5-6 ACCELERATION AMPLIFICATION AND SHEAR DEFORMATION

- 1) the shear deformation of the wall is small, and almost linear with depth,
- 2) the motion of the wall is primarily rigid body and first mode motion.

The second conclusion naturally follows from the type of damping used in the analysis and from the relationship of the fundamental period of the wall with the period of excitation. The fundamental period of the wall, as calculated by LEVSFC for various input accelerations, is presented in Table 5.1 and compared to the input frequency. This shows that the frequency of the input motion is below that of the first mode, thereby ruling out any major contributions of higher modes.

Input Accel., g	LEVSFC Wall Period, sec.	Input Period, sec.
0.1	.0121	.086
0.2	.0124	.086
0.3	.0127	.086

The measured and computed ground surface accelerations in Series A and B for different input accelerations are shown on Fig. 5.7. Recall that the surface accelerometer was placed a distance behind the wall of 16 inches for Series A, 5 inches for Series B-1, and 1 inch for Series B-2 and B-3. Thus, from Fig. 5.7, it is apparent that calculated accelerations from the LEVSC program increase in accuracy as the distance from the wall increases. This observation is in agreement with the previously discussed assumptions that the stress concentrations near the wall, and the effect of ties can be ignored.

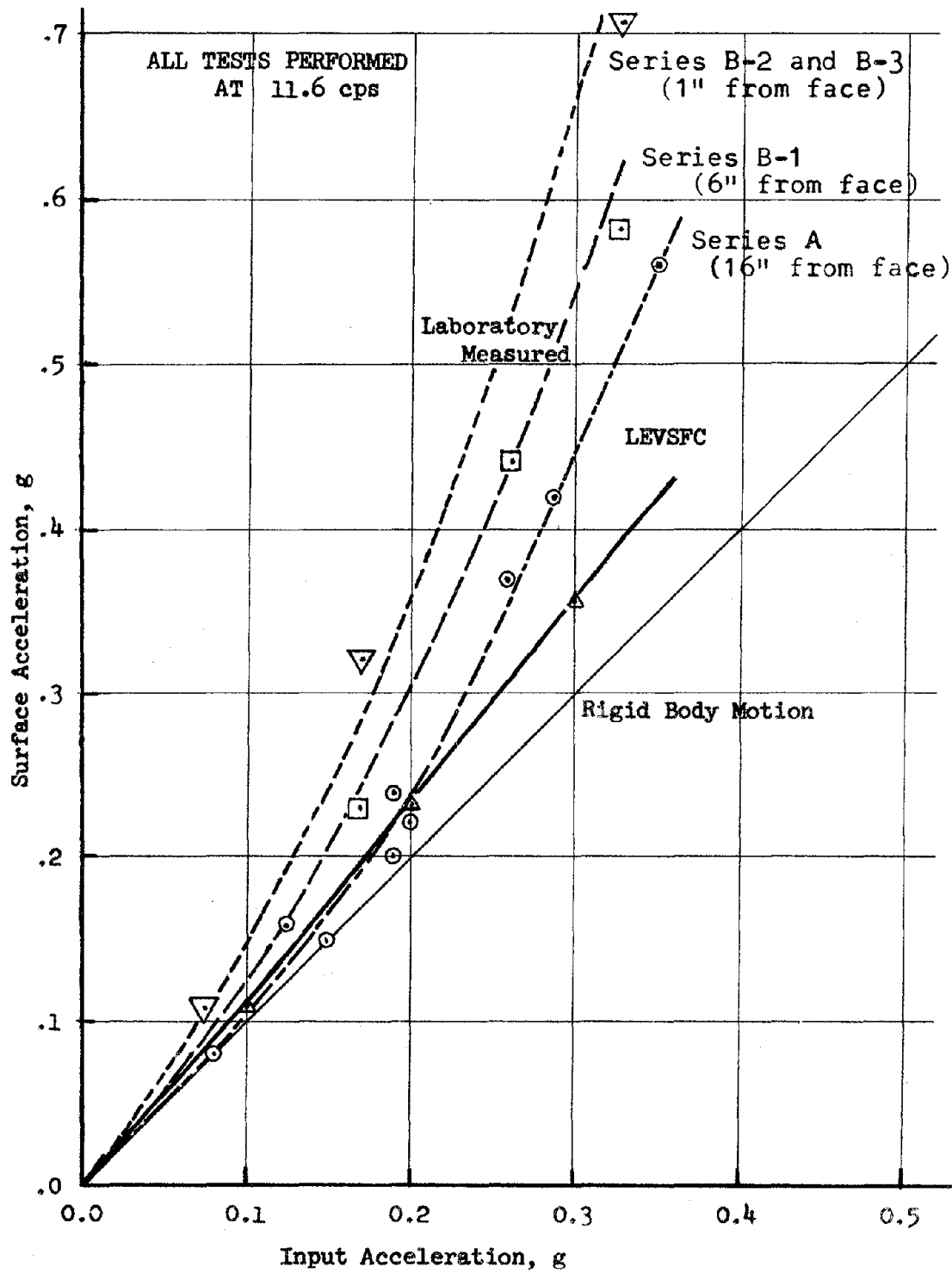


FIGURE 5-7 SURFACE ACCELERATION AMPLIFICATION

5.2 FINITE ELEMENT ANALYSIS

The analysis previously presented in Section 5.1 modeled the Reinforced Earth wall as consisting of infinite horizontal layers. To include the influence of the embedded ties and the wall geometry, an analysis was performed using dynamic finite element program.

The finite element program QUAD⁴B was used in this analysis. It is based on an earlier program by I.M. Idriss. The program in its current form incorporates modifications to the earlier program by John Lysmer and Tak Udaka (23) of the University of California, Berkely. The primary modifications made by Lysmer and Udaka are the

- 1) inclusion of 1-dimensional shear bar elements and
- 2) use of quadrilateral elements rather than the triangular elements used by Idriss.

The program QUAD⁴B provided a dynamic analysis of a structure using the equivalent linear method to account for non-linear behavior. The program incorporates plane strain quadrilateral elements with 8 degrees of freedom and shear-bar elements with 4 degrees of freedom. Program Theory. The equations of motion for a cross-section of a soil deposit idealized by a finite element system are the same as presented for a semi-infinite lumped mass solution:

$$[M] \{\ddot{u}\} + [c] \{\dot{u}\} + [k] \{u\} = \{P(t)\} \quad (5.6)$$

where the matrices and vectors have previously been defined.

The mass matrix is formed by lumping the mass of the elements at their modal points. For the quadrilateral elements one fourth of the total mass of the element is "lumped" at each modal point defining

that element, while for the bar element one half the total mass of the element is lumped at its nodal points. This procedure produces a diagonal mass matrix with only masses associated with the horizontal translational degrees of freedom. This mass matrix form is preferred over the "consistent mass" matrix because of its savings in computational time.

The system stiffness matrix is obtained by appropriate addition of the stiffnesses of all the elements in the assemblage. The quadrilateral element stiffness matrix is 8×8 while the shear-bar element stiffness matrix is 4×4 . The system mass, stiffness, and damping matrices are $N \times N$, where N is the total number of nodal translations allowed.

The type of damping matrix employed is governed by the solution method used to solve the system of simultaneous solutions. In the previously discussed program, LEVSFC, the simultaneous equations were solved using the mode-superposition method. The mode-superposition method involves the solution of the eigenvalue problem representing the free vibration response of the system, followed by a transformation to the normal coordinates by means of the eigenvectors of the system. This procedure uncouples the equations and produces N independent first-order equations that are readily solved. To use this solution procedure the damping matrix must also be of a form that will be diagonalized by the coordinate transform. Because of this the damping associated with the mode-superposition method is a 'smeared' or system damping. With this method it is not possible to account

for major differences in element dampings. As a result the overall damping factor used may be appreciably higher than the damping developed in some zones.

The alternative solution method for the set of simultaneous equations is called the step-by-step method. It involves the direct integration of the equations of motion in their original form, without transformation to the principle coordinates of the system. Utilizing this solution technique it is possible to account for the damping in each element. Because of the greater accuracy in assigning element damping, the step-by-step procedure is used by the program QUAD4B.

In the variable damping solution, a damping submatrix must be formulated for each individual element and then added to obtain the damping matrix for the entire systems. The damping submatrices are added in a manner similiar to that use in the formation of the system stiffness matrix. The damping submatrix utilizes the Rayleigh damping expression of the form

$$[c]_q = \alpha [m]_q + \beta_q [k]_q \quad (5.7)$$

in which $[c]_q$, $[m]_q$, and $[k]_q$ are the damping, mass and stiffness submatrices respectively for element q , and α_q and β_q are given by

$$\alpha_q = \lambda_q * \omega_1 \quad (5.8)$$

$$\beta_q = \lambda_q / \omega_1. \quad (5.9)$$

The value of λ_q , which represents the damping ratio for element q , is chosen based on the strain developed in the element. The parameter ω_1 is equal to the fundamental frequency of the system.

Program Results. The program QUAD4B was used to analyze three Reinforced Earth wall configurations.

The first Reinforced Earth wall analysis was of a typical test wall used in the Series B test. This wall was modeled by using actual laboratory dimensions and material properties. The wall was subjected to two cycles of a 0.1g sinusoidal acceleration at 11.6 cps. Thus both the model configuration and the type of input motion were identical to that used in the laboratory.

The second Reinforced Earth wall analyzed was a 12 foot tall wall designed to resist the tie forces predicted by the Seismic Design Envelope previously presented in Fig. 4.22. The sinusoidal input motion frequency was scaled up from the model using the dimensional similitude relationships discussed in Section 3.1; resulting in a frequency of 3.3 cps. The acceleration magnitude remains constant with scale but the acceleration was arbitrarily increased from 0.1g to 0.2g.

A final QUAD4B analysis was performed on a 21 foot high Reinforced Earth wall. This analysis differed from the previous two in that an earthquake accelerogram was used for the input motion instead of a sinusoidal motion. Since Chapter 6 deals with the treatment of random vibrations, discussion of the finite element analysis using an actual earthquake input is delayed until Section 6.7.

In modeling the above walls no attempt was made to include the skin elements or the effect of overall skin rigidity. For Reinforced Earth walls constructed in a fashion similar to the Series B walls

This assumption should cause negligible error.

Series B. The finite element model and the material properties used in the QUAD4B analysis of the Series B Reinforced Earth model walls are shown in Fig. 5.8. The calculations are based on a uniform horizontal tie spacing of 3 inches. The strain dependent soil properties automatically built into the QUAD4B program, were those recommended by Seed and Idriss (20). The shear modulus is expressed as:

$$G = 1000 K_2 (\bar{\sigma}_m)^{\frac{1}{2}} \text{ psf} \quad (5.10)$$

where $\bar{\sigma}_m$ is the mean principle stress and K_2 depends on relative density and shear strain as shown in Fig. 5.7.

Since the relative density, D_R , of the sand backfill was 63%, Fig. 5.7 indicates that $K_{2\text{max}}$ should equal approximately 54. Thus the expression for the shear modulus may be stated as follows:

$$G = 54000 (\bar{\sigma}_m)^{\frac{1}{2}}. \quad (5.11)$$

Solving this expression for each reinforcement layer resulted in a value for the low strain shear modulus (G_{max}). The program automatically iterates to other values depending on the average shear strain during the seismic excitation.

An initial analysis was performed using initial shear modulus values given by Eq. 5.11. The surface accelerations calculated from QUAD4B using these values for the maximum shear moduli are shown in Fig. 5.9. Comparing these calculated surface accelerations to the measured surface accelerations indicates that the wall, as modeled, is overly rigid; indicating that the shear moduli values

9471-II

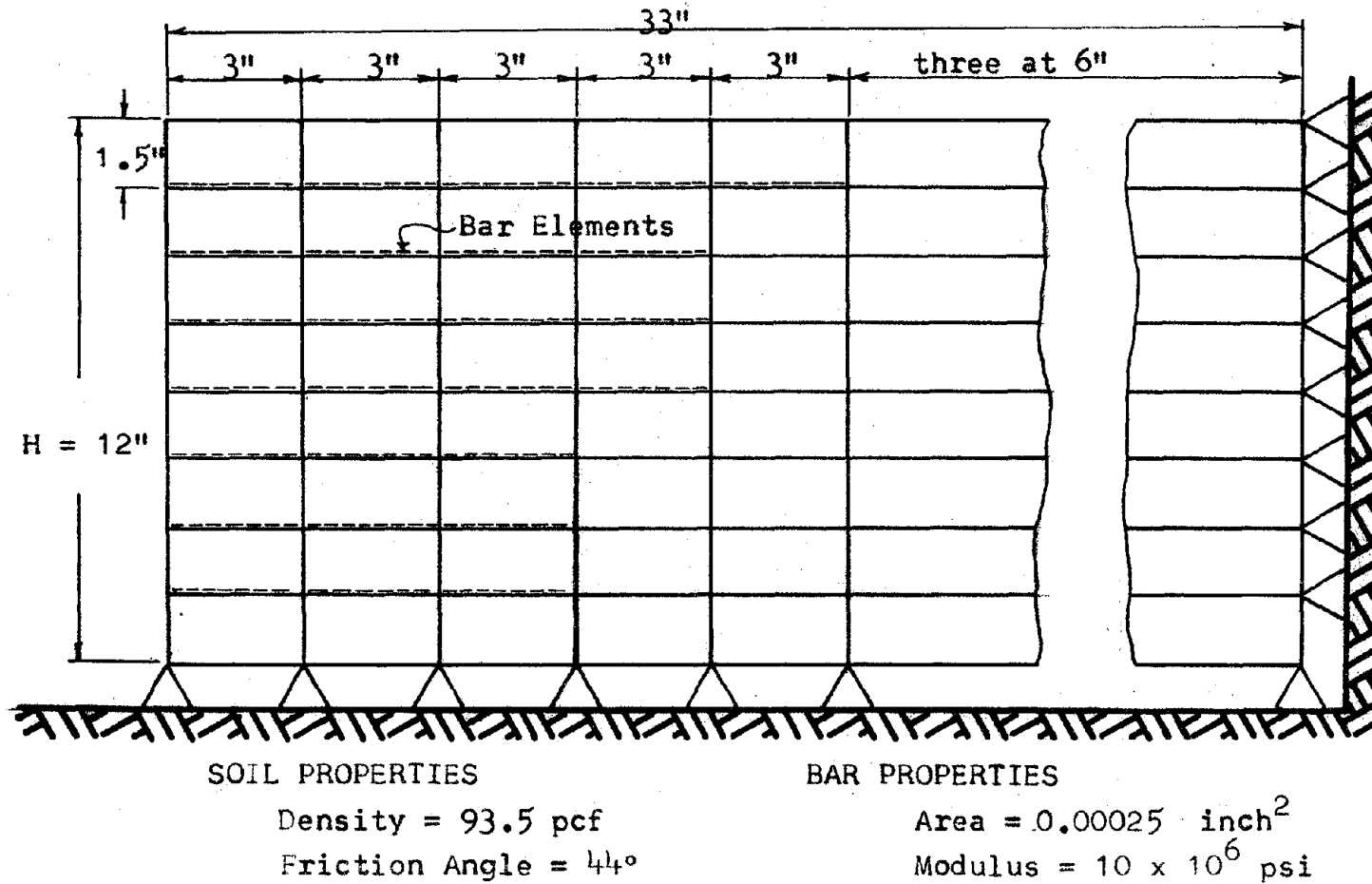
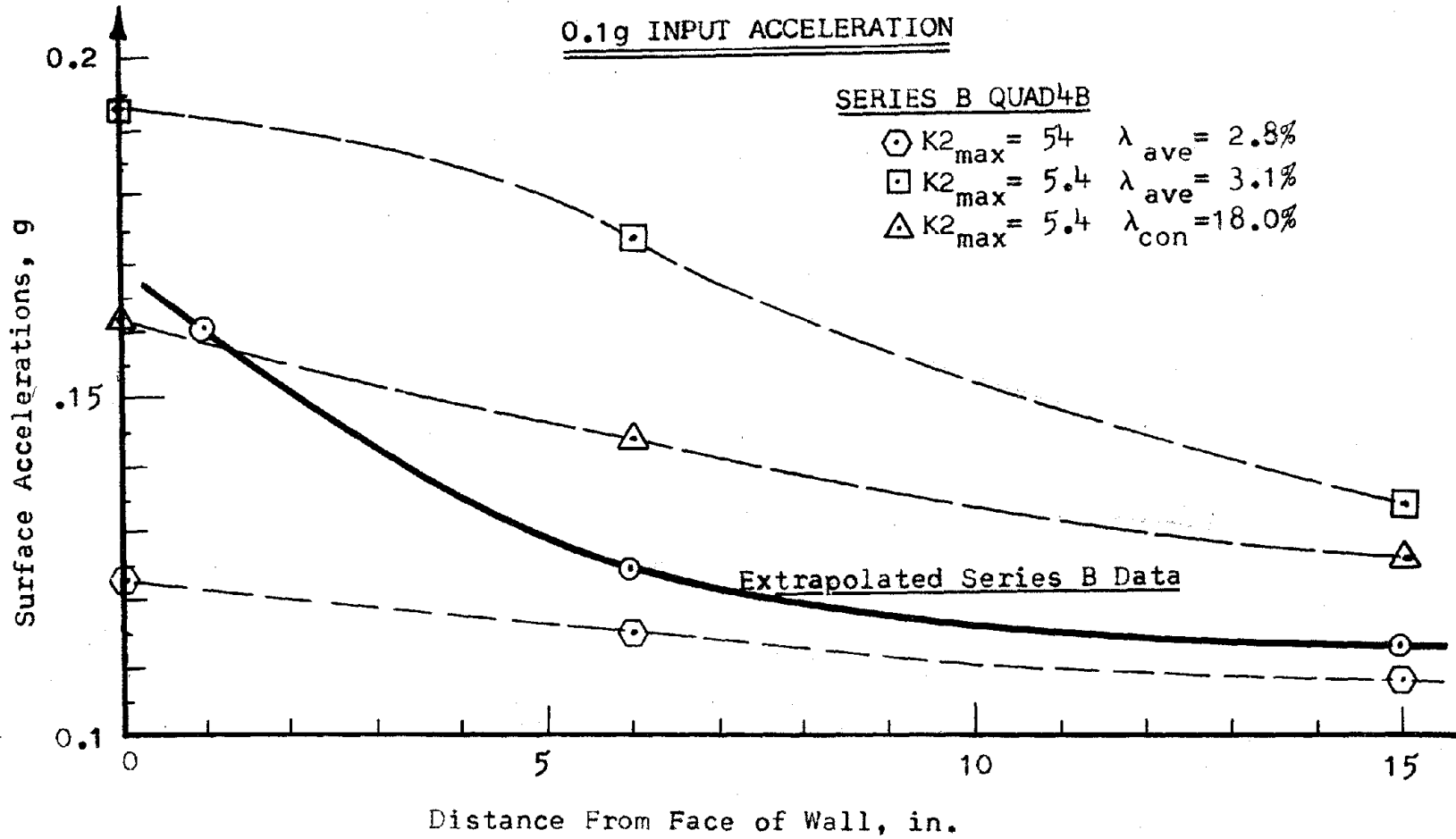


FIGURE 5-8 FINITE ELEMENT MODEL - SERIES B

0.1g INPUT ACCELERATION



II-147

FIGURE 5-9 SURFACE ACCELERATIONS

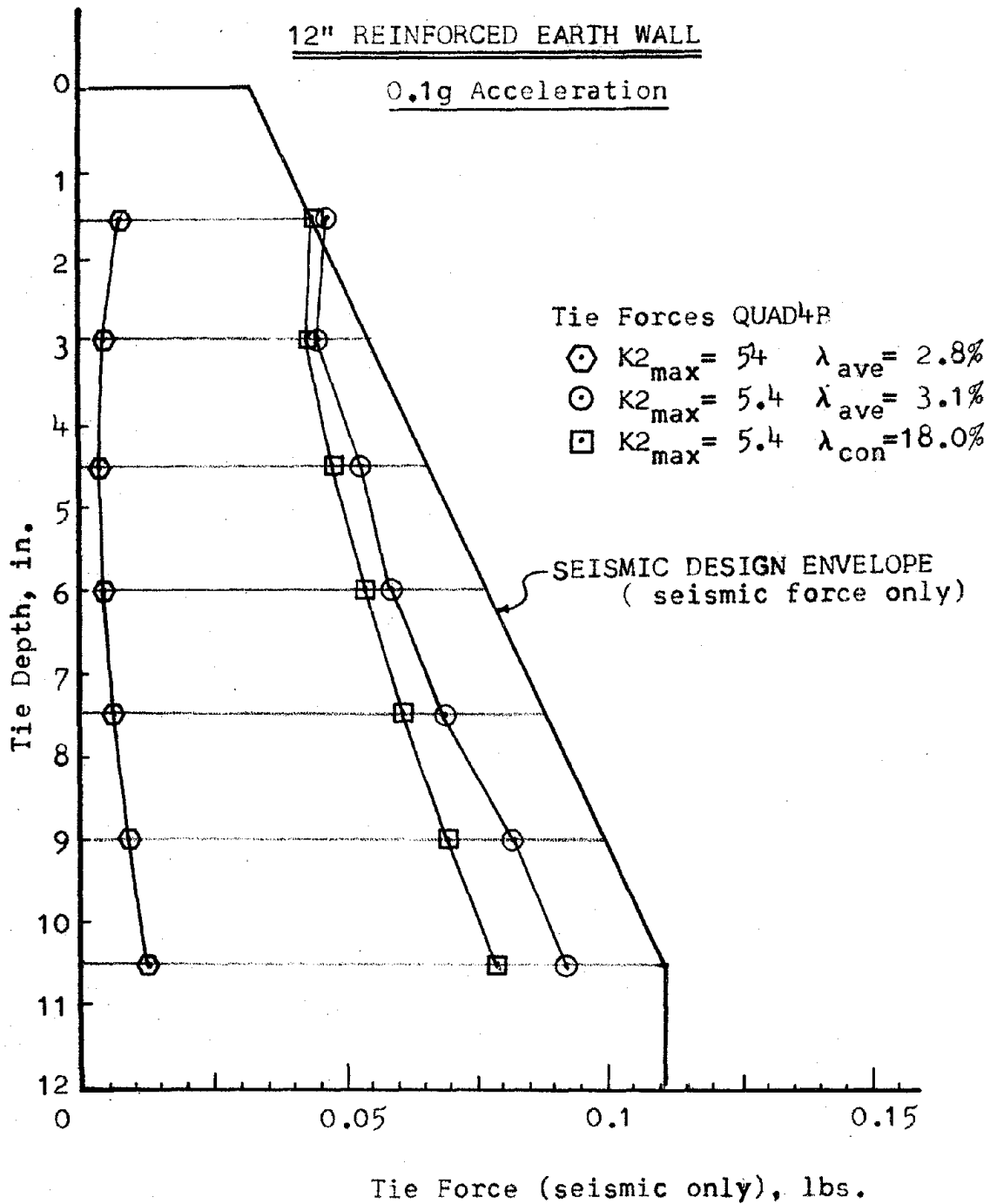


FIGURE 5-10 SEISMIC TIE FORCES

calculated with Eq. 5.11 are too large. The tie forces calculated at the wall are shown on Fig. 5.10 and compared to the seismic force portion (that force exceeding the K. condition) of the Seismic Design Envelope. This comparison also indicates that the soil elements are overly rigid and are not allowing the tie elements to take an appropriate portion of the seismic forces. In addition, the damping which was computed from QUAD4B was only 2.8%, which was much too low for soil.

Because the equation for the soil moduli given by Eq. 5.10 is built into the QUAD4B program, the only way to reduce the soil moduli values was to reduce the value of K_{2max} .

As discussed in Section 6.3, laboratory measurement of the influence of the input frequency indicated a fundamental period of 0.047 seconds for the Series B walls. The fundamental period of a layered soil system may be given by the following expression (see Eq. 6.7):

$$T_1 = \frac{4H}{V_s} \quad (5.12)$$

where V_s is the average shear wave velocity and H is the wall height.

From basic wave propagation theory, the shear wave velocity is given by

$$V_s = \sqrt{\frac{G}{\rho}} \quad (5.13)$$

where G is the shear modulus and ρ is the mass density. Substituting

Eq. 5.13 into Eq. 5.12 yields a solution for the average shear

modulus based on known laboratory values.

$$G = \frac{16 \rho H^2}{T_1^2} = \frac{16 * 2.9 * 12^2}{(0.047)^2} = 21,000 \text{ psf} \quad (5.14)$$

By substituting this into Eq. (5.10), it is possible to solve for the value of K_2 that yields this average shear modulus;

$$K_2 = \frac{21,000}{1000 (\bar{V}_m)^{\frac{1}{2}}} = 2.8 \quad (5.14)$$

Based on the above calculation, tempered by judgment, an additional analysis was performed using QUAD4B with $K_2 = 5.4$. This represented a ten fold reduction in the shear moduli used for the soil elements. The surface accelerations calculated in this analysis are shown on Fig. 5.9 and indicate much higher accelerations than were measured in the laboratory. The seismic tie forces are shown on Fig. 5.10 and appear to be in very close agreement with the tie forces estimated using the seismic design procedure. However the calculated damping was still a low value of only 3.1%.

As previously stated, the laboratory tests indicated 18% critical damping, λ , in the Series B model tests. The QUAD4B analyses described so far resulted in a calculated level of damping of only 3%. Because of the large discrepancy in the measured vs. calculated surface accelerations, an additional QUAD4B analysis was performed using $K_{2max} = 5.4$ and a constant damping value of 18% in all elements. This value was set to override the computer program, so that it was constant at all elements and not strain dependent. Based on this assumption, the calculated surface accelerations are shown on Fig. 5.9. While the calculated surface accelerations are still somewhat larger than the measured values, the magnitude of the difference has been greatly reduced. In addition, the measured tie forces, Fig. 5.10, are still in close agreement with

the values predicted by the Seismic Design Envelope.

This series of analysis has shown that the laboratory measured tie forces and accelerations can be reasonably duplicated using the dynamic finite element program QUAD4B when the program moduli and damping values are modified to reflect actual laboratory measured values. Thus the limit to an accurate calculation of dynamic accelerations and forces in a small laboratory model is the limited knowledge of moduli and damping values at low confining pressures. Fig. 5.11 shows the calculated fundamental period vs. the assumed values of K_2 . This indicates a high sensitivity of fundamental period with low values of K_2 . Note the extreme sensitivity of the fundamental period for very low values of K_2 , which would be associated with small scale laboratory models. On the other hand, note that for K_2 greater than about 30, (appropriate for actual condition), the period is not nearly so sensitive to K_2 . A more accurate determination of the strain dependent damping and moduli values for low confining pressures is beyond the scope of this report, and is probably of very limited practical interest.

As discussed in Section 6.5, full scale field tests (12) have indicated that the maximum static tie forces occur at the center of the tie length and not near the face. The calculated dynamic tie forces along the tie, from the QUAD4B analysis using $K_2 = 5.4$ and $\lambda = 18\%$, are plotted in Fig. 5.12. This would indicate that the actual dynamic tie forces resisted by the upper ties may be greater than given by the Seismic Design Envelope. The calculations performed

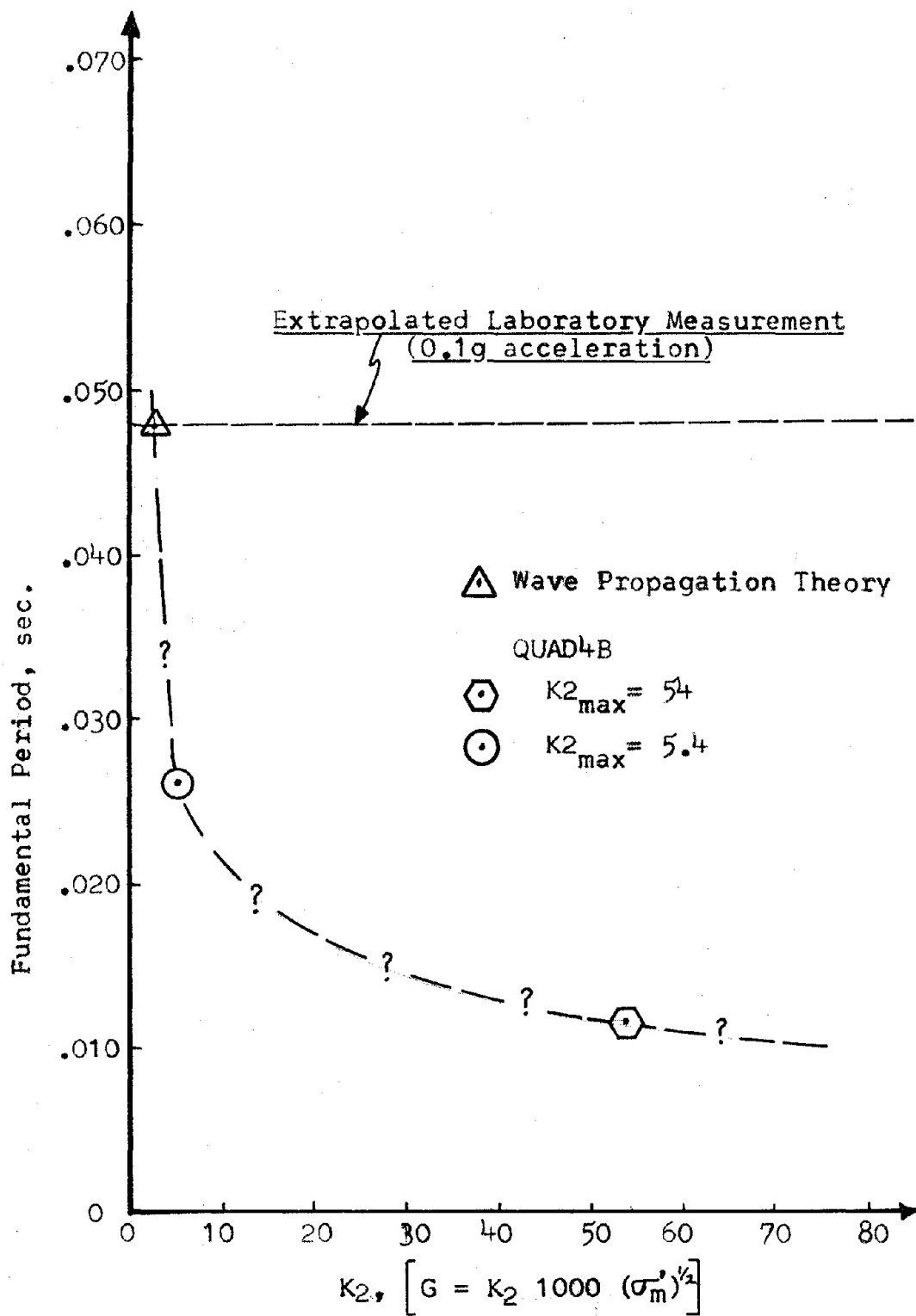


FIGURE 5-II FUNDAMENTAL PERIODS

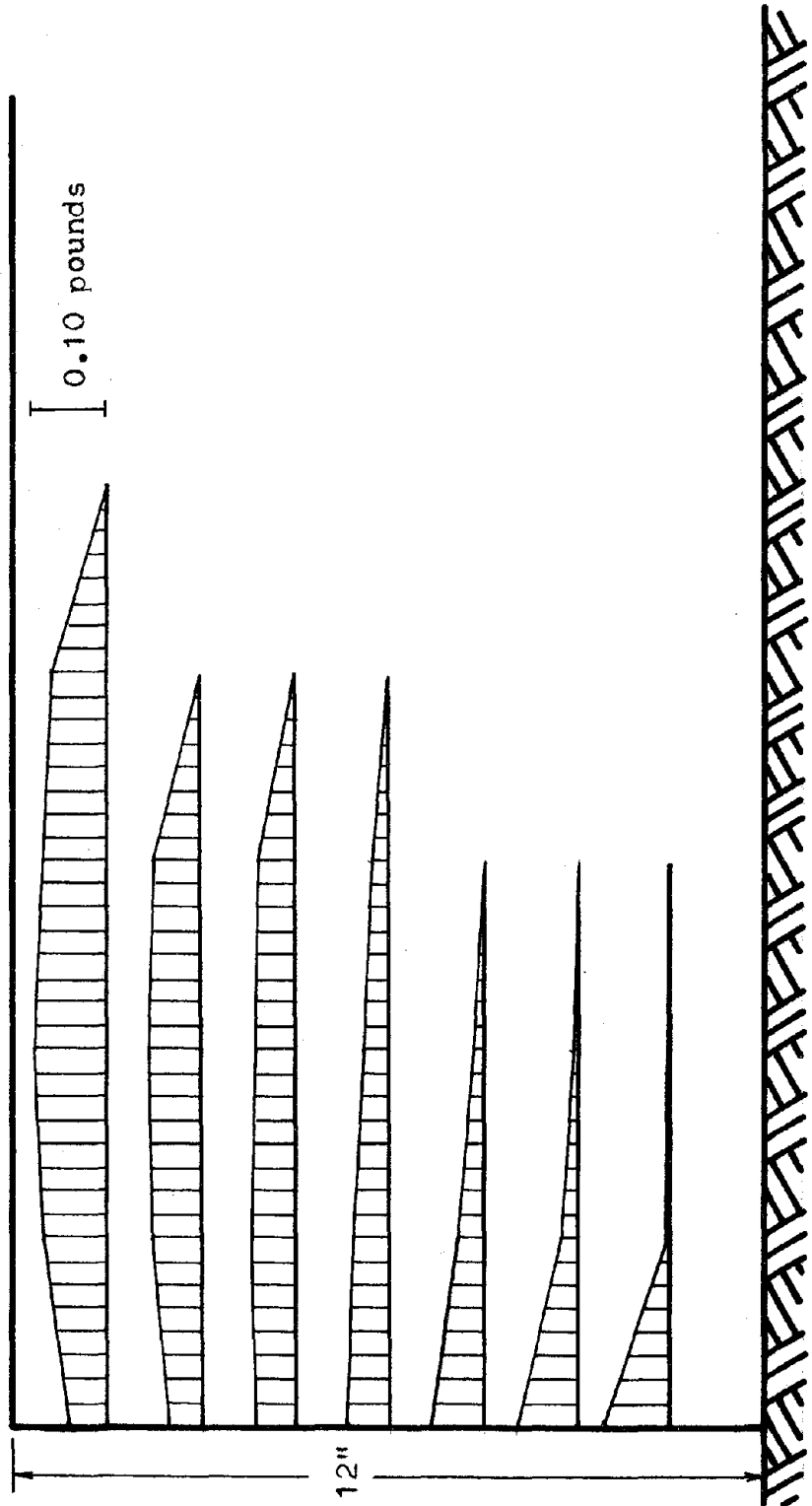
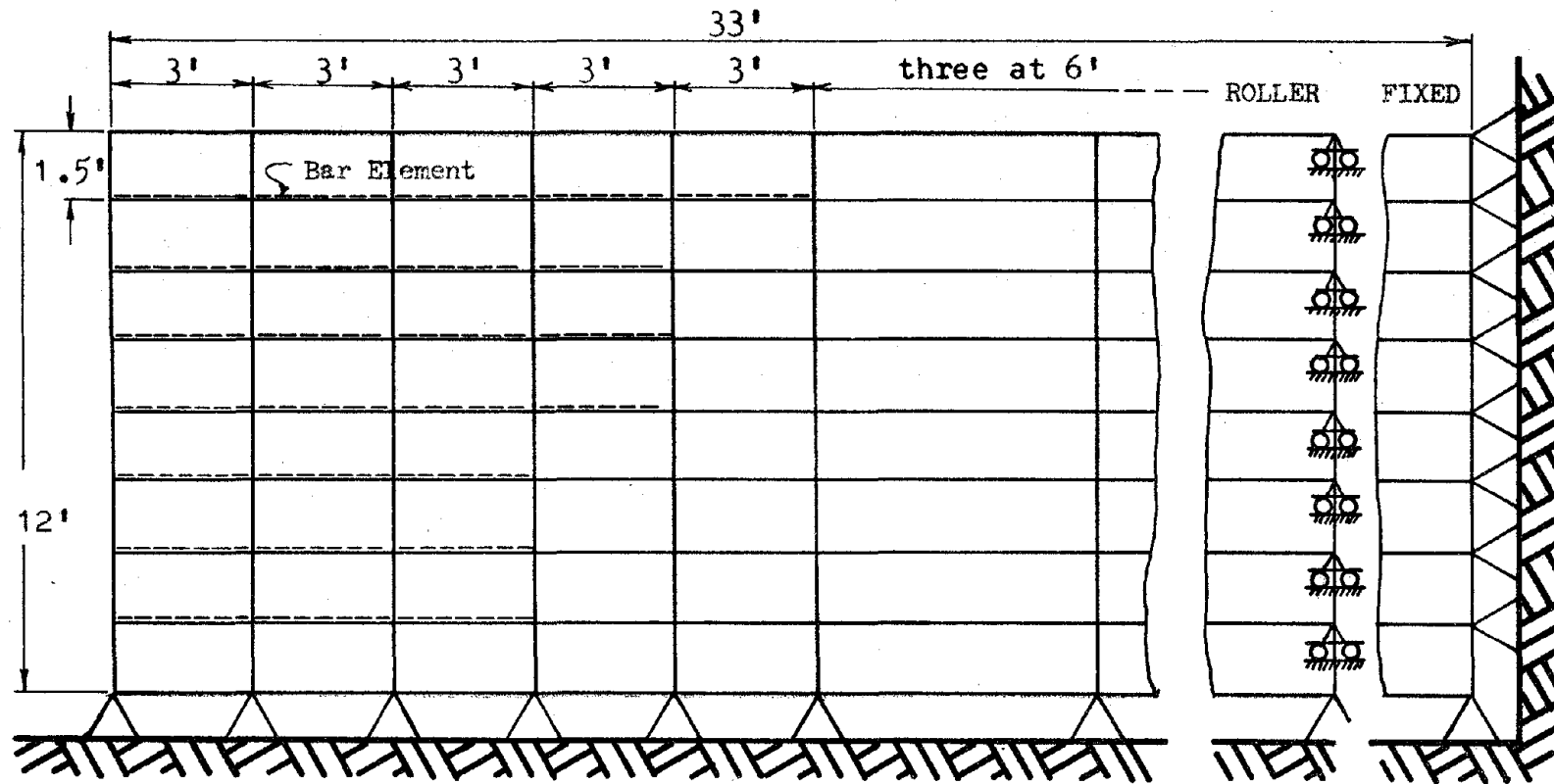


FIGURE 5-12 TIE FORCE ALONG THE TIES

II-154



SOIL PROPERTIES

Density = 93.5 pcf
Friction Angle = 44°

BAR PROPERTIES

Area = 0.375 inch²
Modulus = 30 x 10⁶ psi

FIGURE 5-13 FINITE ELEMENT MODEL - 12' WALL

here indicated that in the upper tie, the tie forces toward the back of the tie could be 1.5 to 2 times the force at the face of the wall. This is discussed further in Section 6.5 where a factor of safety is included in the design procedure to account for this.

Full Scale Wall. The material properties and finite element model used to analyze a 12 foot high Reinforced Earth wall are shown in Fig. 5.13. Additionally, the wall was assumed to have a uniform horizontal tie spacing of 1.5 feet and soil moduli given by Eq. 5.11. This analysis was performed using two types of boundary conditions for the end boundary of the soil backfill; initially the boundary was assumed fixed, as in the Series B calculations, and then the analysis was repeated assuming these boundary nodes were on rollers.

A fuller discussion of this comparison is presented in Section 6.7, but in brief the use of a roller boundary was intended to prevent the soil elements from being placed in tension. The calculated tie forces using both boundary conditions are shown in Fig. 5.14. Comparing these forces with those predicted by the Seismic Design Envelope shows close agreement between the predicted values and those calculated using a fixed boundary.

The tie forces calculated using the roller boundary conditions appear to be in contradiction with what was observed in the model dynamic tests and it is concluded that the use of a fixed back boundary provides the best conditions for the finite element method.

An additional analysis was performed to determine the influence of the additional ties in the top reinforcement layer, that are included to provide stability of the top skin section, see Fig. 2.1.

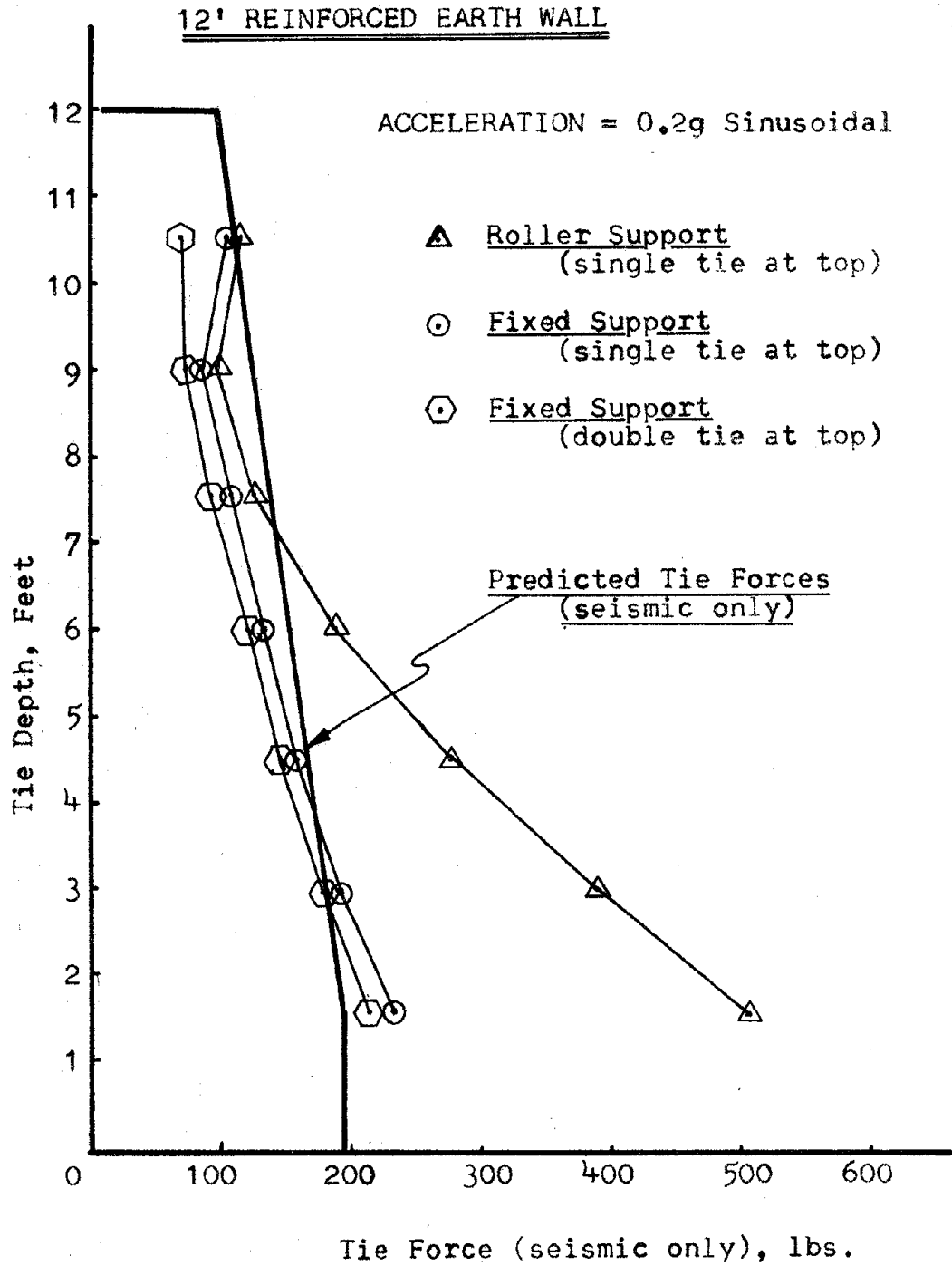


FIGURE 5-14 SEISMIC TIE FORCES

A QUAD4B analysis was performed using twice the bar area in the upper tie. The tie forces calculated are shown in Fig. 5.14 and indicate no major changes in the tie forces as compared to those calculated using only one bar area in the upper tie.

CHAPTER 6 PROPOSED SEISMIC DESIGN PROCEDURE

6.1 INTRODUCTION

In Section 4.3.3 of this report a procedure was developed to predict an envelope of maximum dynamic tie forces to be expected in a Reinforced Earth wall subjected to a uniform sinusoidal acceleration. This empirical procedure was based on tie forces measured in laboratory model tests. In addition a finite element analysis of a full scale Reinforced Earth wall was found to yield tie forces in substantial agreement with those predicted by the Seismic Design Envelope.

The above research was performed using a dynamic input motion with the following characteristics:

- 1) the period of the input motion was larger than the fundamental period of the structure, and
- 2) the input motion was sinusoidal.

This chapter will discuss the effect of the input motion (including random motions) upon the structural response of Reinforced Earth walls and suggest a simple seismic design method that takes the input motion characteristics into account. The suggested procedure is based on the spectral modal response method.

The final section in this chapter presents, as a design example, the design of a 21 foot high Reinforced Earth wall for a random seismic input motion. The design is based on the proposed seismic design procedure and is compared to conventional static designs.

6.2 SEISMIC EQUIVALENT LATERAL EARTH PRESSURE

In Fig. 4.22 a procedure was presented to determine a Seismic Design Envelope. This design envelope represented the maximum probable tie forces occurring during sinusoidal seismic loading. The Seismic Design Envelope was in terms of tie forces because the laboratory emphasis in Series A and B tests was the measurement of tie forces. This tie force diagram can be converted into an equivalent seismic lateral earth pressure diagram, by dividing the tie forces by their tributary areas. This yields a design average seismic plus static earth pressure at each tie level. The resulting diagram is shown on Fig. 6.1a. It inherently assumes that the lateral earth pressure varies linearly with depth, as assumed when making the tie force diagram. Since the equivalent lateral earth pressure was solved for directly from the Seismic Design Envelope there is no change in the Seismic Design Coefficient, E , and the curve of the E versus input acceleration shown in Fig. 6.1b is the same as that presented earlier on Fig. 4.22b and given by Eq. 4.3.

Thus the maximum lateral earth pressure which acts at any level on a Reinforced Earth wall due to a given input acceleration can be readily calculated using the design envelope on Fig. 6.1. Having determined the lateral earth pressure the size and spacing of the ties can be selected to resist these forces both from possible tie breaking and from tie pullout, with an appropriate allowance for safety factors.

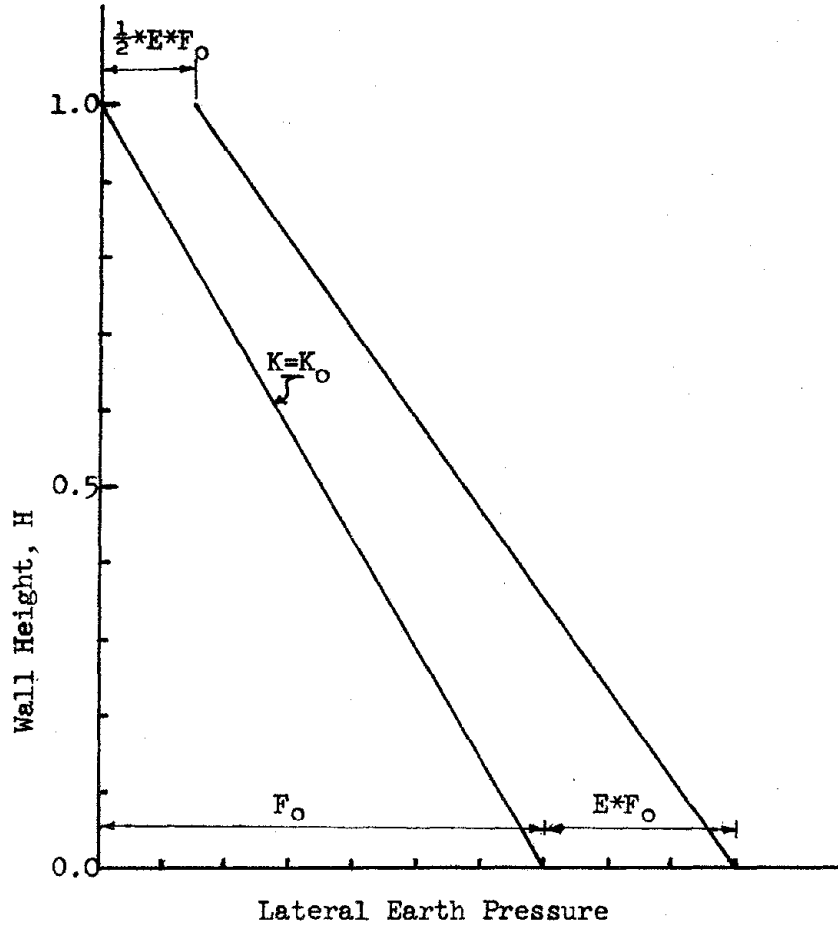


Fig. 6.1a Seismic Design Envelope

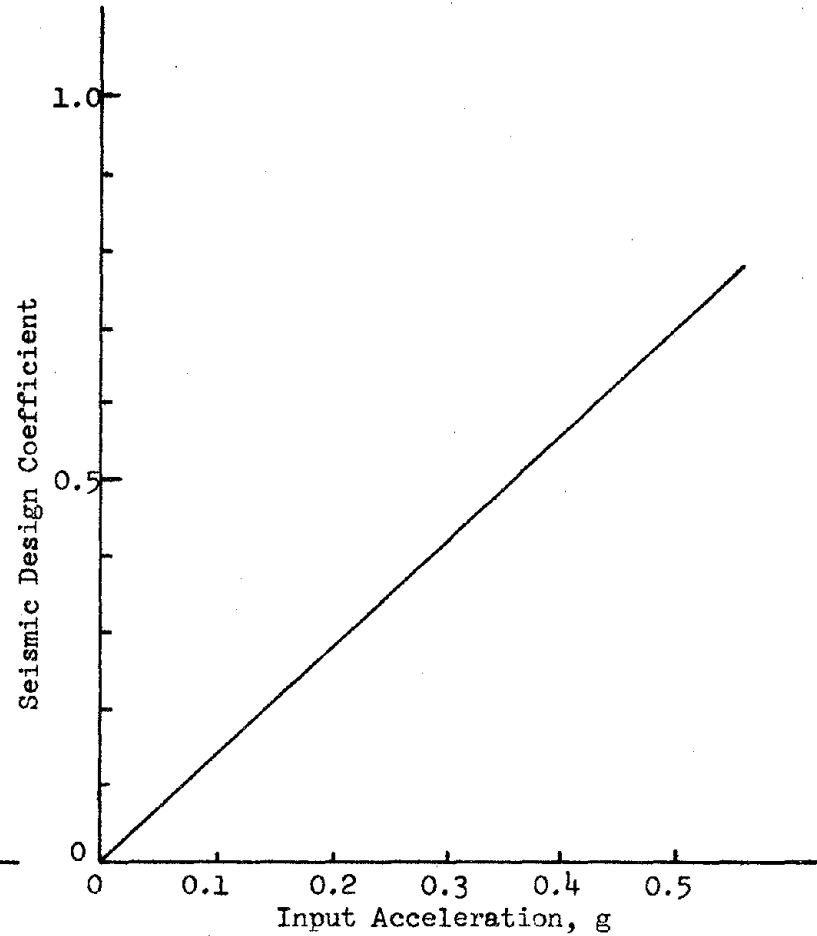


Fig. 6.1b Seismic Design Coefficient

FIGURE 6.1 EQUIVALENT LATERAL EARTH PRESSURE SEISMIC DESIGN ENVELOPE

In addition to the data measured on the model Reinforced Earth walls described herein, data is shown on Fig. 6.2 of seismic earth pressures measured by Ishii, Arai, and Tsuchida (24) against a 70 cm high rigid wall in a shaking table test as compared to the Seismic Design Envelope predicted for Reinforced Earth walls. The experimental data was obtained by means of pressure transducers embedded in a rigid concrete wall. While it should not necessarily be assumed that the lateral earth pressure against a rigid wall will correspond to that in a Reinforced Earth wall, it is encouraging that the magnitudes of forces predicted and measured are similar.

Probably the earliest research related to seismic lateral earth pressures was presented by Okabe (25), and Mononobe and Natsuo (26). Their research has recently been summarized in English by Seed and Whitman (27). It is a pseudo-static design approach known widely as the Mononobe-Okabe method. At present a seismic analysis using the Mononobe-Okabe method is required for all earth retaining structures in Portugal, Turkey, Greece, and Japan.

The Mononobe-Okabe method is based on the Coulomb method of calculating earth pressures on walls, with the addition of a single lateral force to account for the effect of the earthquake. This pseudo static earthquake force can have any direction, but considering only horizontal seismic input the total lateral force developed during an earthquake for the active case is given by the following:

$$P_{AE} = \frac{1}{2} \gamma H^2 K_{AE} \quad (6.1)$$

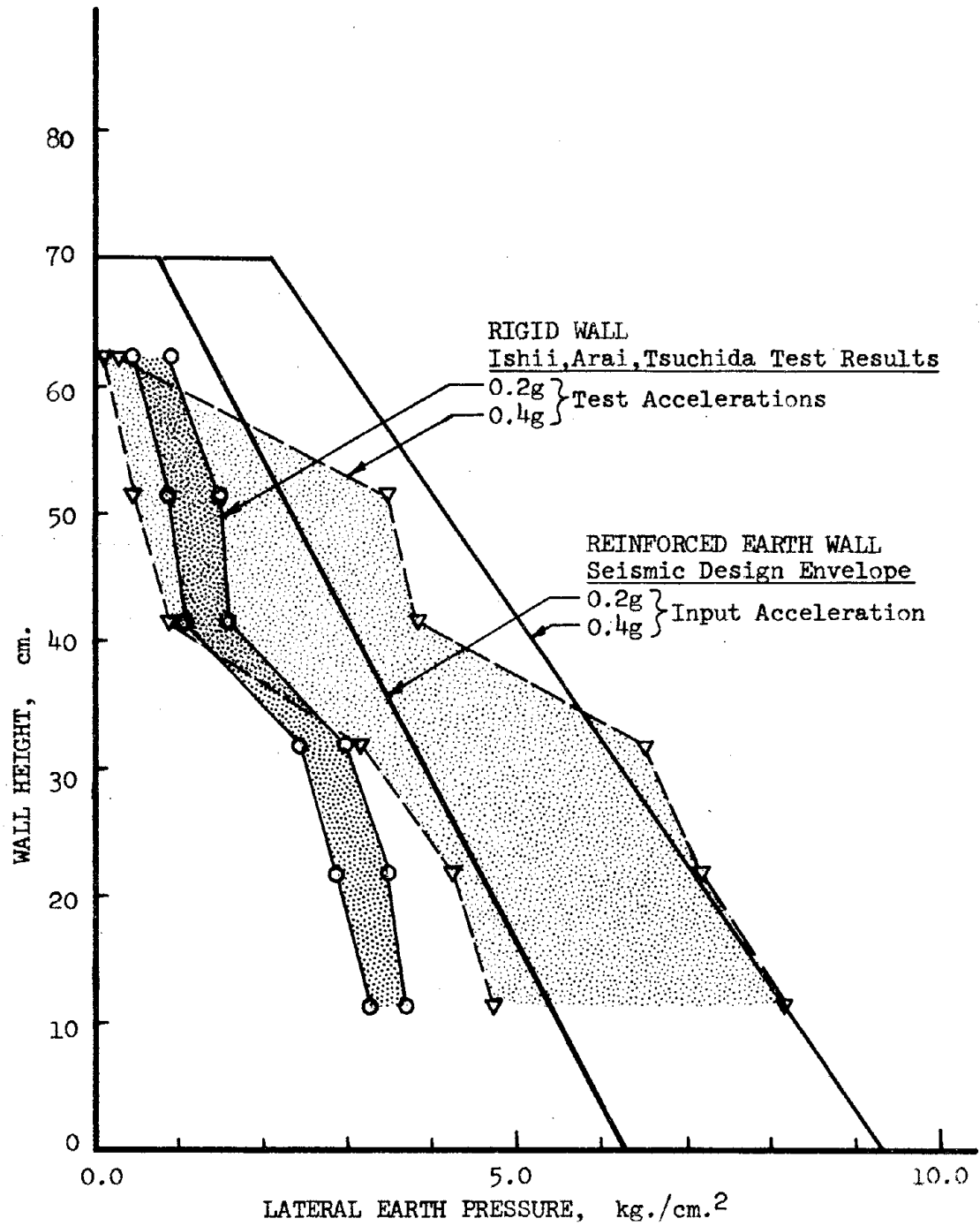


FIGURE 6-2 COMPARISON OF
LATERAL EARTH PRESSURES

where

$$K_{AE} = \frac{\cos^2(\phi + \psi - \theta)}{\cos\theta \cos^2\psi \cos(\delta + \psi + \theta) \left[1 + \sqrt{\frac{\sin(\phi + \delta) \sin(\phi - \theta)}{\cos(\delta + \psi + \theta) \cos(\psi)}} \right]^2} \quad (6.2)$$

ϕ = angle of internal friction
 ψ = angle between wall surface and vertical
 δ = angle of friction between soil and wall
 θ = $\text{TAN}^{-1} K_h$

and K_h is called the pseudo static horizontal seismic coefficient. It defines the pseudo static horizontal earthquake force $F_E = K_h W$, where W is the weight of the soil within the active failure wedge.

Fig. 6.3 compares the coefficient of lateral pressure, K_{AE} , predicted by the Mononobe-Okabe method to an equivalent coefficient of lateral pressure calculated from the Seismic Design Envelope of Fig. 6.1a. The total lateral force predicted by the Seismic Design Envelope is greater than that predicted by the Mononobe-Okabe method. Seed and Whitman have reported that the total lateral force in tie-back walls, based on model measurements of tie rod forces, also exceeds that predicted by Mononobe-Okabe.

Returning again to the proposed seismic design method illustrated by Fig. 6.1 it is noted that as the design acceleration approaches zero the Seismic Design Envelope approaches lateral earth pressures for $K = K_o$ and not the $K = K_A$ condition found by Lee et al (3) and in these studies for static conditions. Therefore the K_o minimum design earth pressure requires an explanation. In constructing the test walls extreme care was always taken not to vibrate or jar the walls during construction. Then in performing many of the tests,

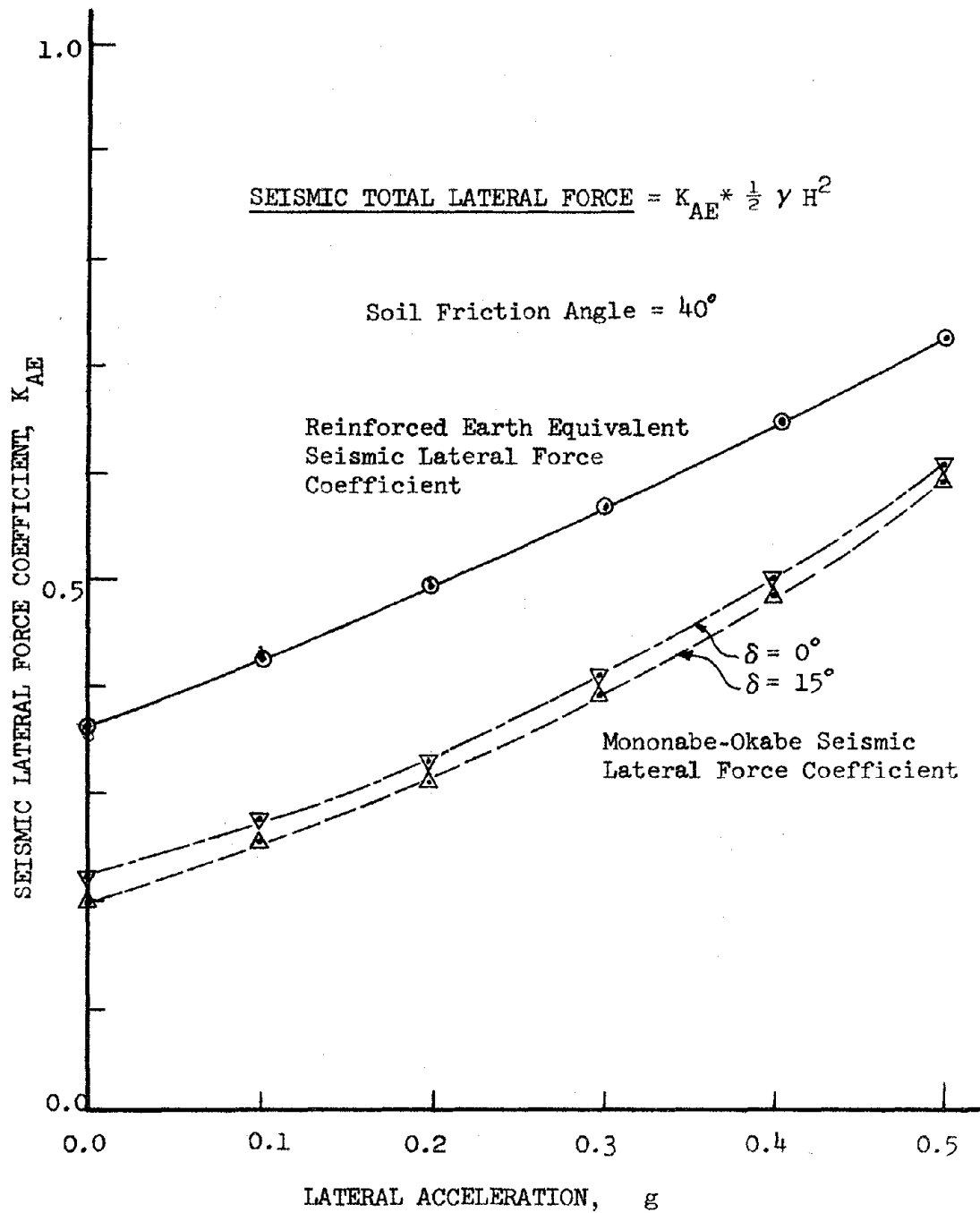


FIGURE 6.3 SEISMIC COEFFICIENTS

especially when using small accelerations to study the arching effect in the tie pullout tests, it became apparent that accelerations as small as 0.02 to 0.05g would increase the tie forces from the initial K_A pressures to the higher K_O condition. For actual field conditions these low levels of acceleration are likely to be achieved during construction due to hauling and compaction equipment. Thus it would appear to be realistic to use K_O rather than K_A as the lower limit for field static conditions. An additional justification for this lower bound is based on the results from instrumentation of a 50 foot high Reinforced Earth wall, as reported by Beaton, Forsyth, and Chang (12). Tie force measurements on this wall showed that tie forces were largest in the middle portion of the strap and the authors recommended that the K_O pressures be used for design for static loading.

To add some perspective to the recommended seismic design procedure, it is of interest to compare the proposed seismic design pressure envelope with the static stress envelope, and with envelopes defined by various multiplying factors greater than the static envelope. These multiplying factors may be thought of as factors of safety based on a static $K = K_O$ lateral earth pressure. This comparison is shown on Fig. 6.4.

The purpose of this comparison is to demonstrate the effect of simply using an increased static factor of safety to develop a seismic design. It is apparent from the relative positions of the factored envelopes and the proposed Seismic Design Envelope that by this approach

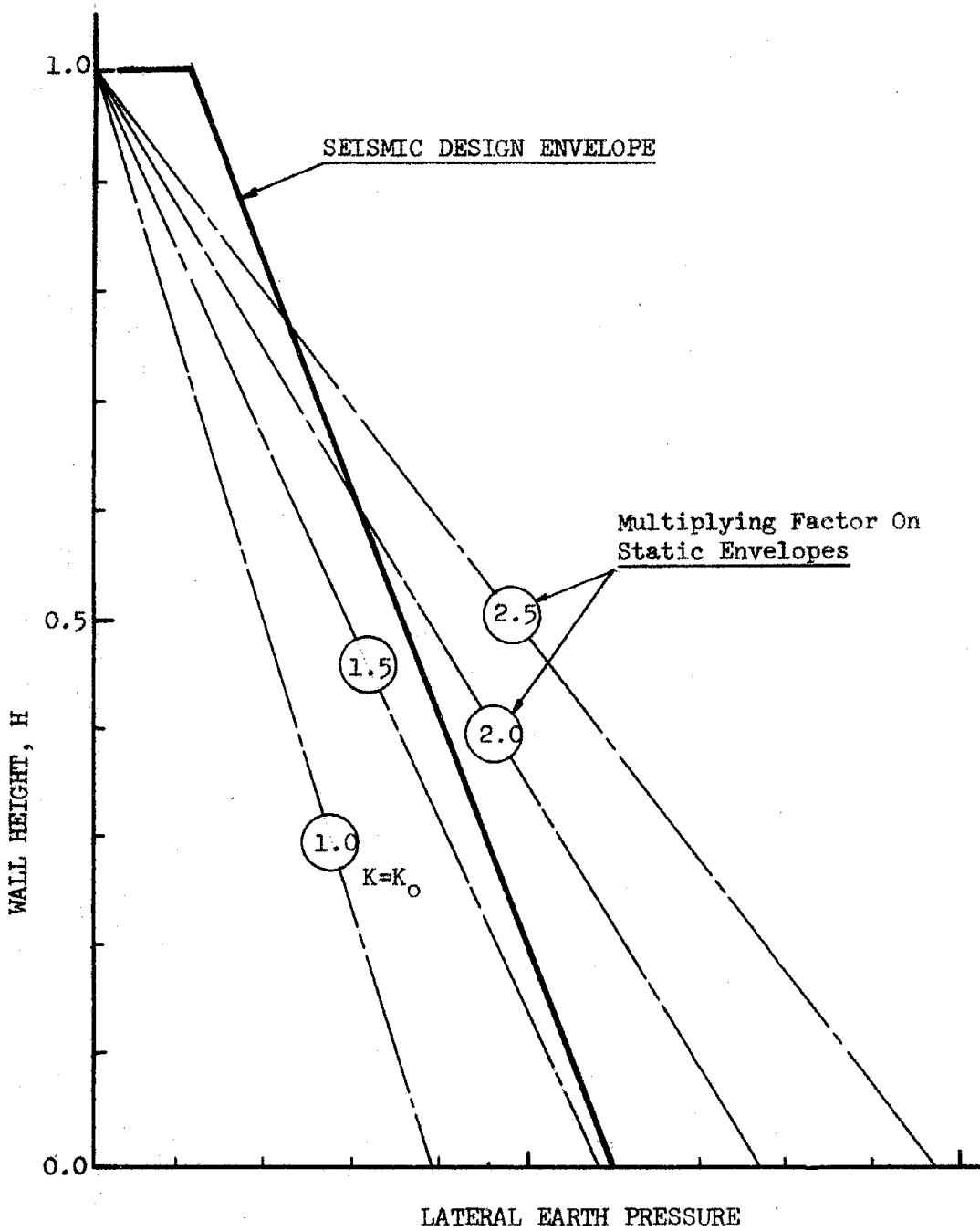


FIGURE 6.4 FACTORED STATIC DESIGN ENVELOPE

the static envelopes will always be highly over conservative at the lower wall sections and nonconservative at the upper wall sections. Therefore this possible short cut method of seismic design is not recommended.

6.3 INFLUENCE OF FREQUENCY OF VIBRATION

An additional test (test No. 13) was performed to determine the influence of the frequency of vibration on the response of a Reinforced Earth wall. This test was conducted mainly to observe the surface accelerations due to different input base motions. The input frequencies varied from 10 cps to 30 cps, each using a constant input acceleration of 0.10 g. To enable a larger range of frequency ratios to be used, the height of the wall was increased from the 12 inches common to Series B to 15 inches. The magnification of the input motion was determined by placing an accelerometer in the top layer of the wall, approximately 8 inches from the face of the wall. This was away from the possible influence of the skin elements, but within the active failure wedge.

The Magnification Factor, MF, is defined as the ratio of surface acceleration to base acceleration. Values of MF for various input frequencies for this test are shown in Fig. 6.5. In addition, the magnification factors for 1 degree-of-freedom oscillators with 15 and 25% critical damping are included for comparison. The observed data are in excellent agreement with the form of the theoretical curves. The data showed that the fundamental period of test No. 13 was 0.059 seconds. For damping less than 20% the critical damping may be computed from the MF at resonance as follows:

$$\lambda = \frac{1}{2MF} \quad (6.3)$$

For this case the fraction of critical damping was about 0.18, for the Reinforced Earth wall.

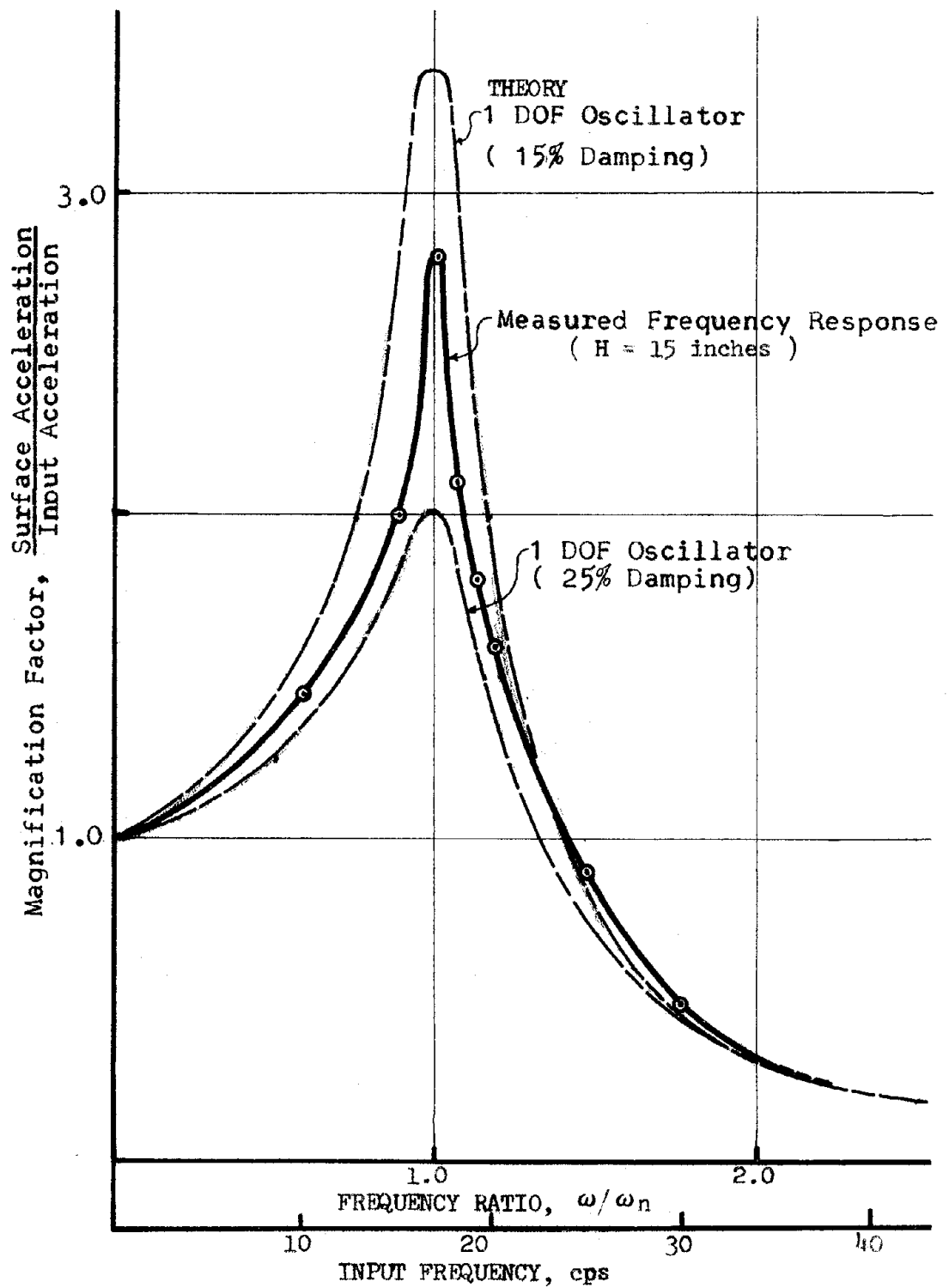


FIGURE 6.5 FREQUENCY RESPONSE

If it is assumed that the fundamental period varies linearly with the height of wall, see Eq. 6.8 and 6.9, the fundamental period of Series B walls, 12 inches high, is given by the following expression:

$$P_B = \frac{H}{15} * 0.059 = \frac{12}{15} * 0.059 = 0.047 \text{ sec.} \quad (6.4)$$

where P is the fundamental period of a wall H inches in height.

Recall that the Series B tests used an input frequency of 11.6 cps (period = 0.086 sec). Thus the frequency ratio for the Series B tests would be

$$\text{Freq. Ratio} = \frac{\text{input freq}}{F_B} = \frac{F_B}{P} = \frac{0.047}{0.086} = 0.55 \quad (6.5)$$

where F_B is the natural frequency of the Series B walls and P is the period of the input motion. Reference to the measured frequency response on Fig. 6.5 indicates that the magnification factor for this frequency ratio is about 1.3.

Since the lateral forces vary directly as the magnification, it should be possible to determine the Seismic Design Envelope of a Reinforced Earth wall with a known frequency ratio by multiplying the seismic portion of the previous Seismic Design Envelope by a frequency factor defined by the following:

$$FF = \frac{MF}{MF_B} = \frac{MF}{1.3} \quad (6.6)$$

where MF is the magnification factor based on the frequency ratio of any particular model, and MF_B is the magnification factor of the Series B (12 inch) walls.

To illustrate the significance of different magnifications for different wall heights, it is of interest to develop a seismic design envelope for a 16.5 inch tall wall. This height was chosen because an earlier test (Test No. 12) had been performed on a 16.5 inch tall wall excited by a 0.3g sinusoidal acceleration at 11.6 cps. The details of test No. 12 have previously been discussed in Section 4.4. The measured tie forces for this test are shown in Fig. 6.6. In addition, for comparison the Seismic Design Envelope, based on Series B tests (12inch) with no allowance for different magnification due to the different fundamental period for the 16.5 inch wall, is also shown on Fig. 6.6 as line (A). This design envelope is obviously much lower than the observed tie forces.

The results of test No. 13 clearly show that the magnification varies with the natural period of the wall. From Eq. 6.4, the fundamental period of this 16.5 inch wall is calculated to be 0.065 seconds and the frequency ratio is $0.065/0.085$ or 0.765. From Fig. 6.5, the magnification factor corresponding to this frequency ratio is 1.72. Therefore, in comparison to the Series B walls, the frequency factor, FF, is calculated from Eq. 6.5 to $1.72/1.30 = 1.32$. This means that the acceleration in the 16.5 inch tall wall should be 1.32 times the acceleration in the 12 inch wall. Since the dynamic forces are proportional to acceleration, it follows that the dynamic forces in the 16.5 inch wall will be 1.32 times the dynamic forces in the 12 inch wall from which the design envelope concept on Fig. 6.1 is based.

The frequency corrected Seismic Design Envelope shown as line (B)

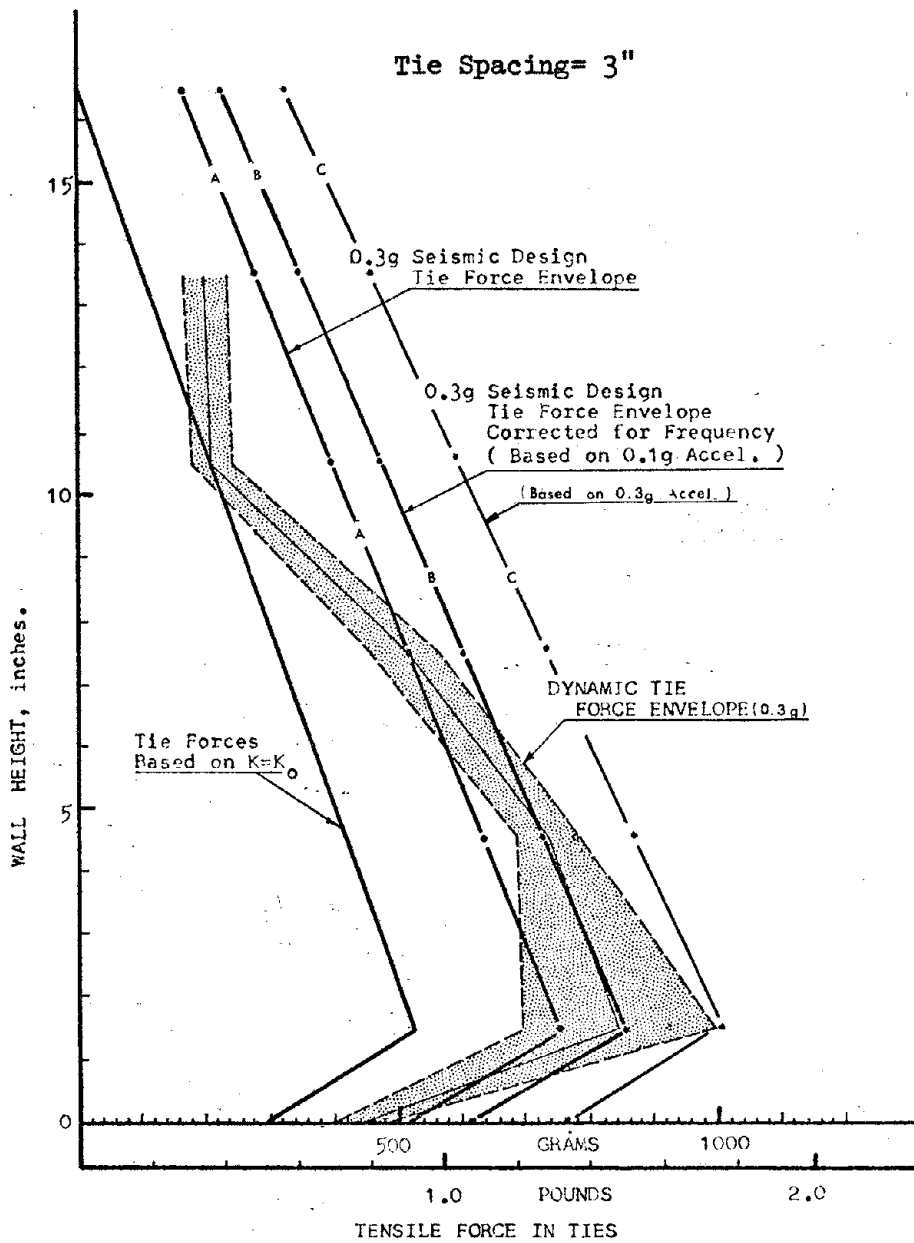


FIGURE 6.6 FREQUENCY CORRECTED SEISMIC DESIGN ENVELOPE

on Fig. 6.6 was obtained by multiplying the dynamic portion of the standard Seismic Design Envelope by 1.32. The dynamic tie forces at the base of the wall also exceed those predicted by this seismic design envelope.

Recall that all of the magnification factors were developed for an input acceleration of 0.1g. However, as shown on Fig. 4.6 and Fig. 5.7 the magnification does not increase linearly with acceleration, especially for input accelerations approximately above 0.1g. Thus the magnification factors used to determine the frequency factor should be based on a level of acceleration comparable to what the structure is being designed for.

The 16.5 inch wall was tested at an input base acceleration of 0.3g, and thus according to the previous data on Fig. 4.6 and Fig. 5.7, the response should be relatively greater than for tests at an acceleration of 0.1g.

Unfortunately a complete set of response data at various frequencies was only obtained for 0.1g acceleration. However an indication of the influence of the level of acceleration on the magnification factor can be determined by examining the acceleration amplification curves for the Series A and B tests shown on Fig. 5.7. All Series B tests were performed on 12 inch walls at 11.6 cps and thus all had a frequency ratio of 0.55. Interpolating between the data points the MF values for 0.1, 0.2, and 0.3g accelerations are 1.3, 1.85, and 3.2 respectively. It then becomes of interest to plot these three sets of data on the frequency response curve, as shown on Fig. 6.7.

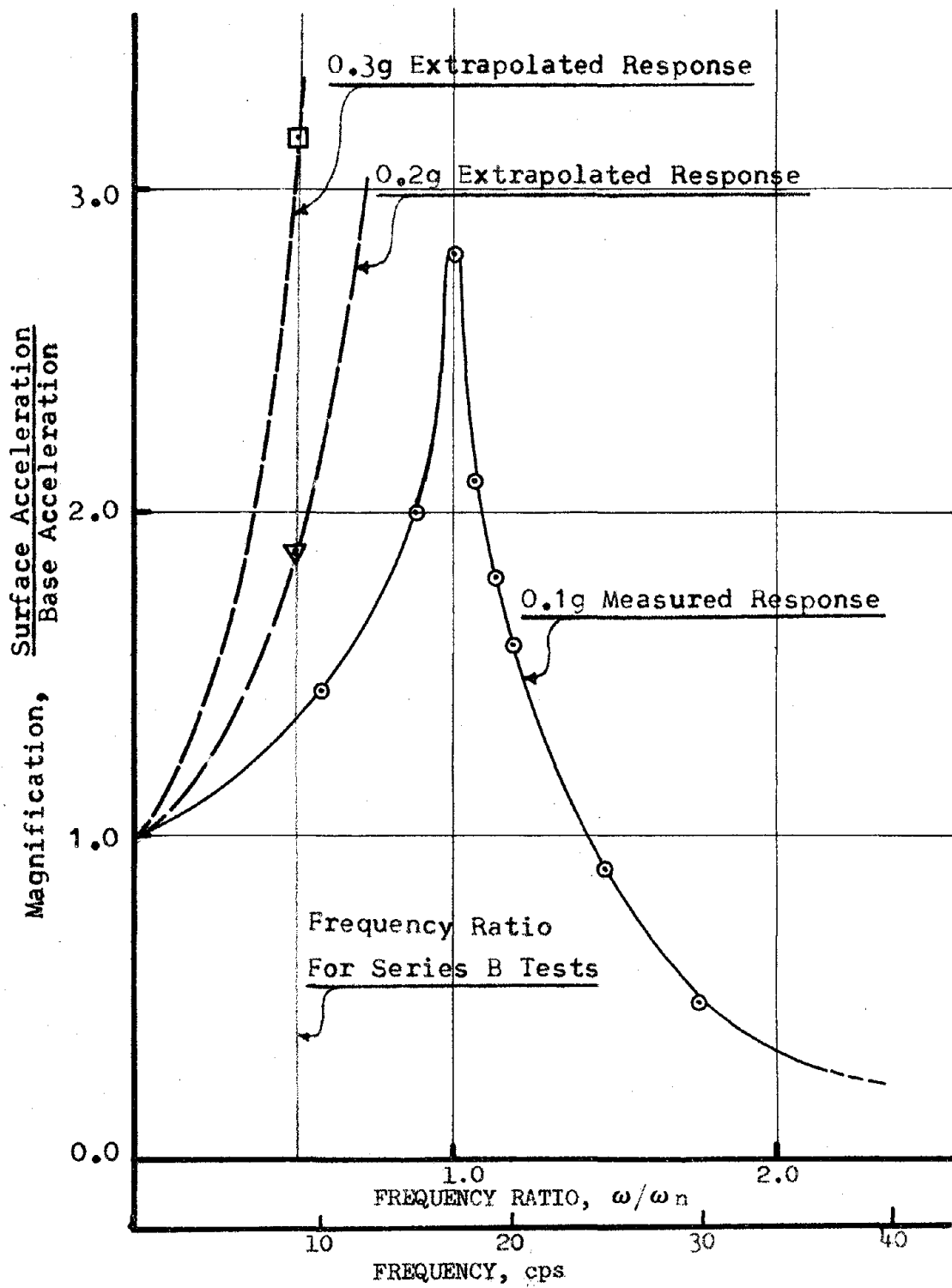


FIGURE 6-7 EXTRAPOLATED FREQUENCY RESPONSE

These data points show the MF for a frequency ratio is a function of the input acceleration. Because other data are not available the MF for the 0.3g acceleration must be estimated by extrapolating along the dashed curve shown on Fig. 6.7. Recognizing that there is considerable uncertainty involved, it seems very reasonable that for 0.3g acceleration the frequency factor, FF, is about 2.0.

A seismic design envelope based on $FF = 2.0$ is also shown on Fig. 6.6 as line (C). Thus by accounting for the observed acceleration factors, the proposed seismic design envelope method predicts maximum tie forces which are in reasonable agreement with actual measured data.

6.4 RANDOM VIBRATION

A procedure is outlined in this section for the determination of a design acceleration from a random acceleration input. This procedure uses the concepts of response spectra, normal modes, and modal participation factors. The theoretical basis for this procedure is the normal mode method of dynamic analysis as generalized in the spectral modal response method (28, 29). The experimental basis is the previously described data which clearly demonstrates that Reinforced Earth walls behave as damped flexible structures. The model surperposition method models the response of a multi-degree-of freedom system as if it were a system of simple single-degree-of freedom elements. Each of these elements is considered to have its particular frequency, and to be excited seperately by the ground motion in a manner determined by a "participation" coefficient and the spectrum response. The response spectrum gives the maximum response for each of the modes and neglects the fact that these modal maximums do not occur concurrently in time. The Relative participation of each mode to the overall response of the entire structure is accounted for by including a "participation factor." Thus overall response is taken as the sum of the response of each mode multiplied by their respective participation factors. For most cases only the response from the lower 1 to 3 modes need be included since the higher modes usually have a minor contribution to the overall response.

The spectral modal response method is commonly used for the determination of seismic lateral loads in buildings and, because of

its conservative nature, is accepted by all regulatory agencies in this country. The use of this procedure will be illustrated in Section 6.7 for the design of a full scale Reinforced Earth wall subjected to a simulated earthquake acceleration.

Acceleration Response Spectra. Each one-degree-of-freedom element used to model the complete dynamic system will be excited by that portion of the excitation motion that has a frequency near that of the elements fundamental frequency. The acceleration response spectra is a plot of the maximum acceleration of a damped one-degree-of-freedom oscillator, responding to the prescribed base input dynamic loading, vs. the undamped frequency of the oscillator. Thus it is possible to determine the acceleration in each single-degree-of-freedom element used to model the system by simply computing the acceleration response spectra and by knowing the natural frequencies of each of the one-degree-of-freedom elements or modes.

The design example of Section 6.7 uses a modified artificial earthquake originally developed by Chopra (30) for the magnitude 6.5 San Fernando Earthquake ground motion at the Olive View Hospital, Fig. 6.8. It represents a reasonable approximation to a typical ground motion accelerogram. As used here the accelerations have been reduced so that the maximum acceleration is 0.2g. The acceleration response spectra for the reduced earthquake motion is shown on Fig. 6.9 for 12% critical damping.

Natural Frequencies. As previously explained the determination of each modal response of a multi-degree-of-freedom system is dependent

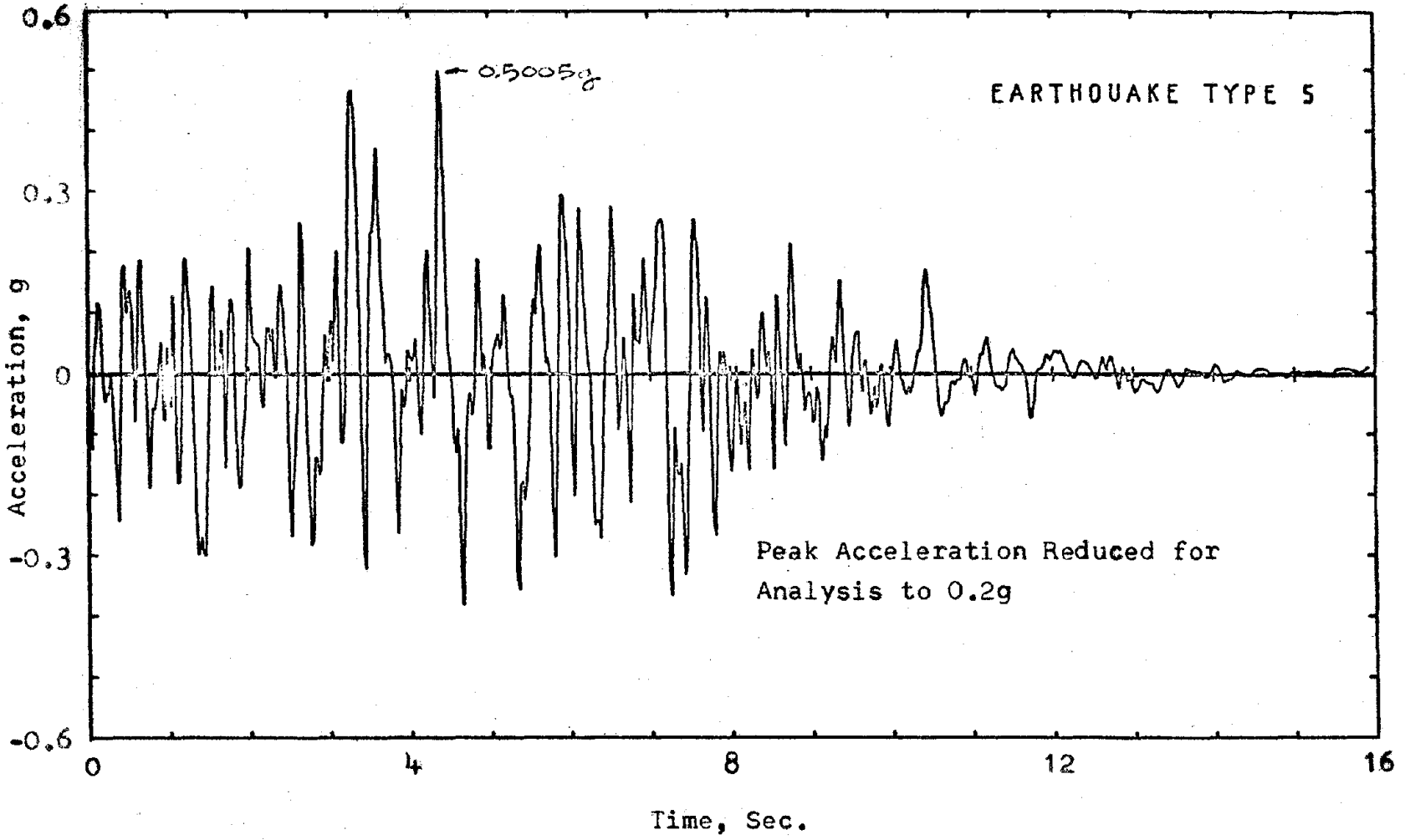
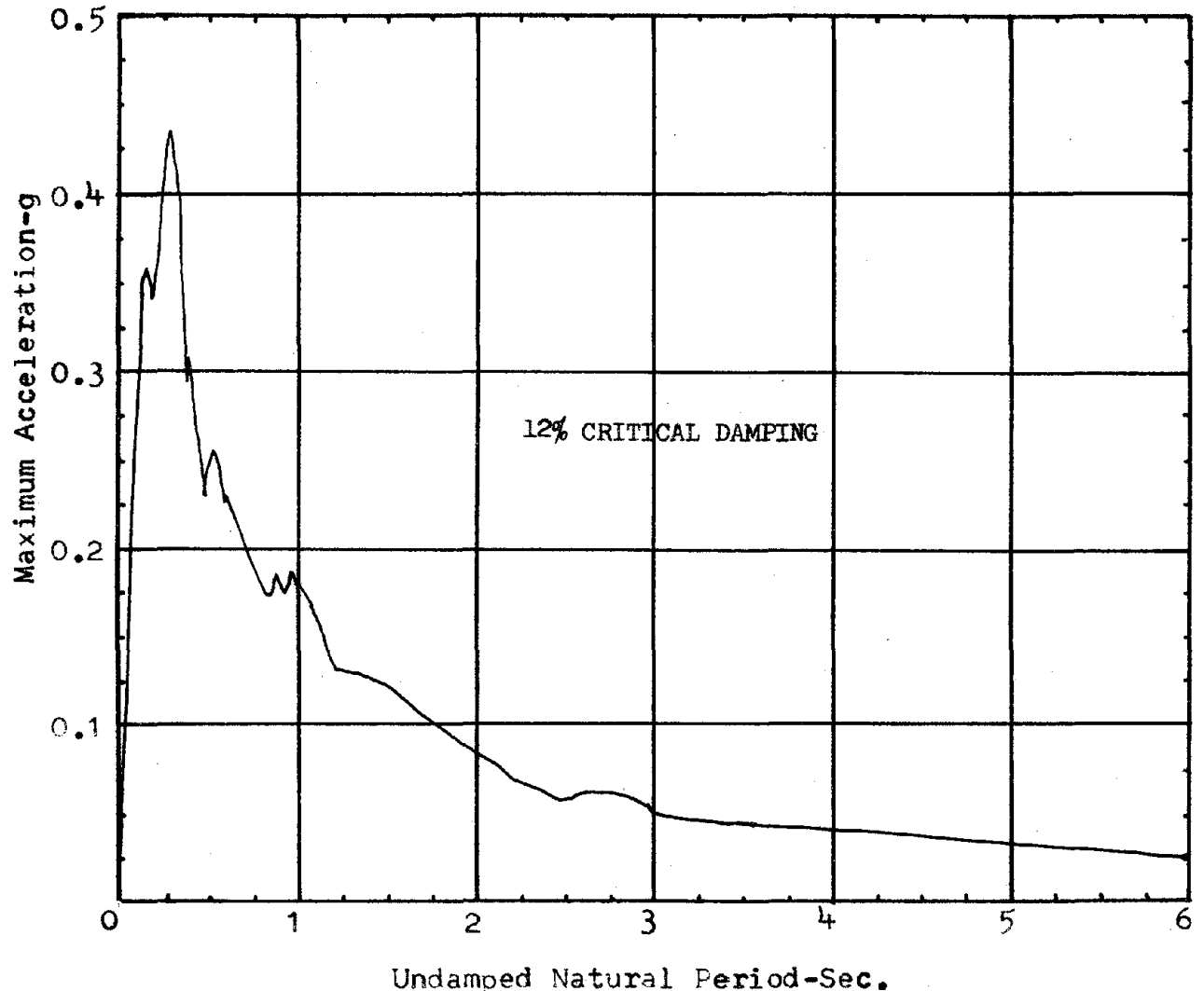


FIGURE 6-8 CHOPRA-SAN FERNANDO EARTHQUAKE



Undamped Natural Period-Sec.
FIGURE 6-9 PSEUDO ACCELERATION SPECTRA

upon knowing the natural frequencies or periods of each mode. The fundamental periods of a layered soil system can be approximated using the following expression based on wave propagation theory and presented by Idriss and Seed (31):

$$T_i = \frac{4H}{2i - 1} * \sqrt{\frac{\rho}{G}} \quad (6.7)$$

where i is the mode number, H is the layer thickness, ρ is the mass density, and G is the average shear modulus of the layer. The shear modulus G should be evaluated at various depths taking into account the effect of overburden pressure and shear strain likely to develop during the earthquake. As a guide, strain dependent shear modulus values presented by Seed and Idriss are reproduced on Fig. 5.2 for sand. Since Eq. 6.6 is for infinitely horizontal soil layers there were differences in the fundamental periods predicted using finite element models (QUAD4B). These fundamental periods are given on Table 6.1 and suggest that T_1 for design may be taken as follows:

$$T_1 = (0.006 \text{ to } 0.010) H \quad (6.8)$$

where H is the height of the wall in ft. and T_1 is in seconds/cycle. The period within this range that gives the maximum spectral acceleration should be used for design.

Table 6.1 Fundamental Periods		
Wall Height	$T_1 = 4 H \sqrt{\rho/G}$	$T_1 = \text{QUAD4B}$
12	0.08	0.124
21	0.121	0.190
30	0.160	—

In addition it will be assumed for design purposes that the second natural period is one third the fundamental frequency selected.

This assumption follows directly from Eq. 6.7.

Participation Factors. The total dynamic design force of a multi-degree-of-freedom system using the spectral response method is equal to the sum of lateral forces due to each mode times its respective participation factor. The modal participation factors reflect the influence of the distribution of the structure's mass on the response of a particular mode. It has been shown (32) that, for lumped mass systems, the i^{th} mode participation factor can be expressed by the following:

$$\Gamma_i = \frac{\sum M_n \Theta_{ni}}{\sum M_n \Theta_{ni}^2} \quad (6.9)$$

where M_n is the mass on the n^{th} level (in buildings this corresponds to the n^{th} floor mass, for Reinforced Earth walls this corresponds to the weight of the soil in the n^{th} layer) and Θ_{ni} is the relative displacement of the i^{th} mode at the n^{th} level. The approximate calculation of the first two modal participation factors for a Reinforced Earth wall idealized as a lumped-mass system is shown on Fig. 6.10. The use of only two modes in calculating the spectral response of a Reinforced Earth wall is similar to what occurs in the computer analysis where Rayleigh damping is used (ie $\lambda \propto \omega^2$); as the modal frequency increases the damping increases and the higher modes are effectively filtered out. In an actual design care should be taken to insure that significant spectral accelerations do not occur at the natural frequencies of higher modes not considered.

Design Acceleration. The Seismic Design Envelope, Fig. 6.1, requires that a single input acceleration be used. The total seismic design force at the i^{th} level from the spectral modal response method is

$$F_i = M_i \sum \Gamma_j A_j \Theta_{ij} \quad j = 1, 2 \quad (6.10)$$

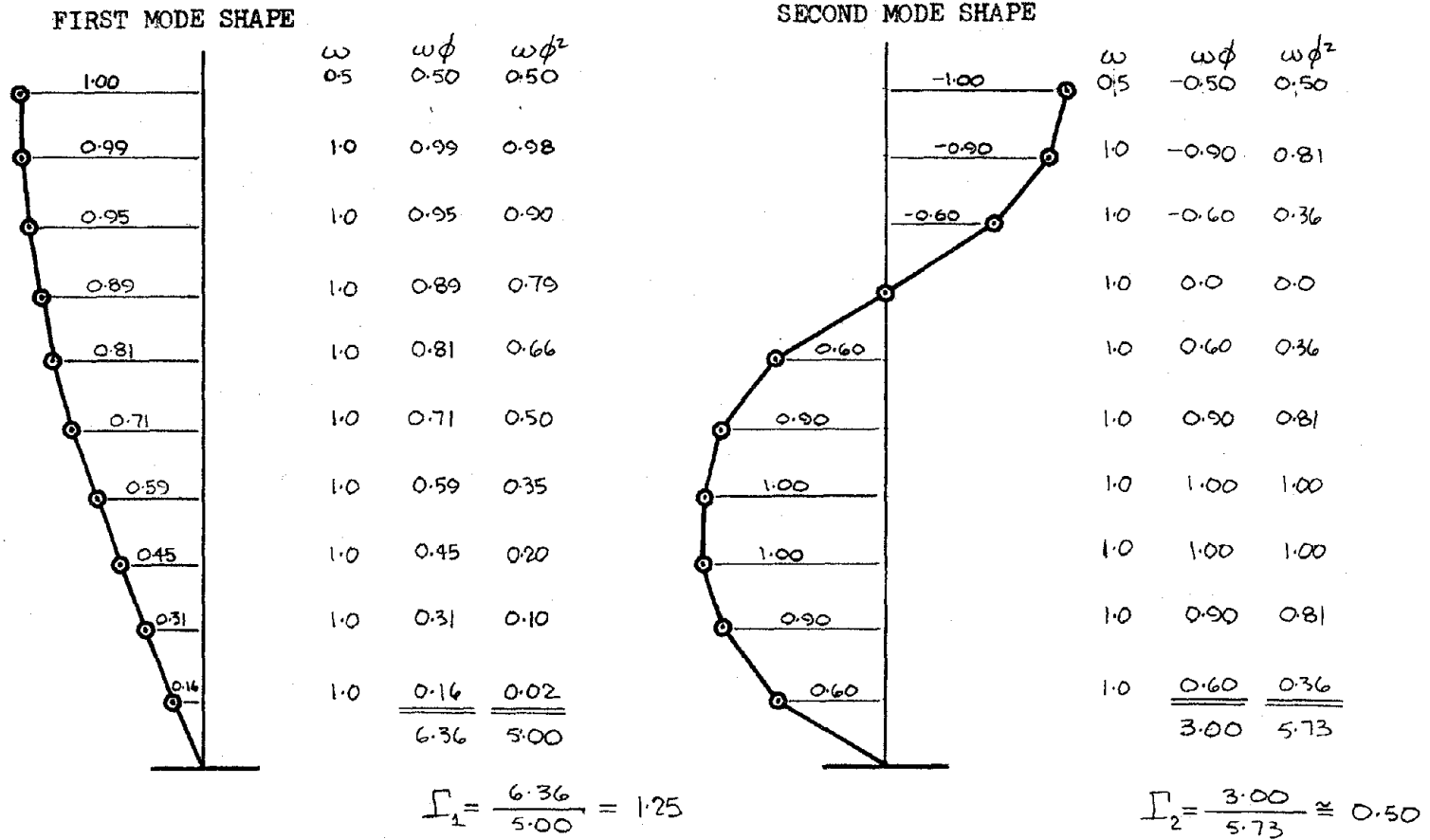


FIGURE 6.10 MODAL PARTICIPATION FACTORS

where Θ_{iJ} is the absolute value of the J^{th} modal displacement at the i^{th} level, M_i is the mass at the i^{th} level, A_J is the J^{th} mode spectral acceleration, and n is the total number of modes considered.

The Seismic Design Envelope is based on empirical measurements of the lateral earth pressures occurring in Reinforced Earth walls vibrating in their fundamental mode. Because the lateral earth pressure distribution is not known for higher modes of vibration, it will be assumed that the distribution of lateral forces in the second mode is the same as occurs for the first mode. Examination of Fig. 6.10 indicates that this assumption will lead to underestimating the second mode lateral forces in the lower half of the wall.

Based on the above assumption it is possible to write Eq. 6.10 as follows:

$$F_i = M_i \Theta_i \sum \Gamma_J A_J \quad (6.11)$$

where $M_i \Theta_i$ represents the distribution of seismic lateral forces and $\sum \Gamma_J A_J$ represents the design acceleration. But it is recalled that the distribution of seismic lateral earth pressures has previously been defined by the Seismic Design Envelope procedure shown on Fig. 6.1a as a function of a design acceleration. Thus the seismic lateral earth pressures can be calculated using Fig. 6.1 with a design acceleration equal to

$$A_{\text{des}} = \sum_{J=1, 2} \Gamma_J A_J \quad (6.12)$$

substituting the participation factors calculated in Fig. 6.10 yields the following expression:

$$A_{\text{des}} = 1.25 * A_1 + 0.5 * A_2 \quad (6.13)$$

6.5 DESIGN FACTORS of SAFETY

The design factors of safety used for the seismic design of a Reinforced Earth wall should insure that the wall performs as follows:

- 1) failure should occur in a ductile dynamic manner such that the wall should be able to tolerate small amplitude displacements at each cycle,
- 2) ties must not be allowed to fail in tension, and
- 3) the average dynamic tie force must not exceed the peak pullout force of the tie, thus precluding excessive deformation of the wall.

The performance of the skin components and the foundation have not been covered by this report and it will be assumed that these elements can be satisfactorily designed using conventional procedures.

Because the residual strength of the ties against pullout may be much lower than the peak strength, the factor of safety to insure that the design tie force will not exceed the peak pullout force must be substantial. Beaton, Forsyth, and Chang (12) found that the residual pullout resistance of full scale ties was only about $\frac{1}{4}$ of the peak resistance to cause sliding. Based on this finding they stated that "a conservative factor of safety of 4 is recommended for design purposes to select the minimum length of strip at different overburden heights." This factor of safety was defined as follows:

$$F.S. = \frac{\tan \phi_u}{\tan \phi'_u} \quad (6.14)$$

where ϕ_u is the measured soil-tie friction angle and ϕ'_u is the design soil-tie friction angle. Similarly it was shown in Section 4.5 of this report that for model tie pullout tests the residual soil-tie

friction angle was consistently only $\frac{1}{4}$ to $\frac{1}{2}$ the peak soil-tie friction angle. Thus the full scale and model tie pullout tests are in agreement on this point.

To insure a Ductile Dynamic Failure Mode it is necessary to insure that the ties do not fail in tension. Because the distribution of tie forces along the length of the tie is not known, a factor of safety must be introduced to cover this uncertainty. It is noted that Beaton, et al, (12) and the few finite element analyses performed in this study both found that the maximum tie force occurred some distance back from the wall. The maximum values within the length of tie were about 150% of the value at the face. Assuming that this is generally applicable, a design factor of safety of 2.0 on the yield strength is recommended against the higher tie forces possible along the length of the tie. Since the ultimate strength on structural steel is approximately twice the yield strength, there is an additional hidden factor of safety against tie breaking if the ties are made of mild steel. Finally additional steel must be included to allow for corrosion. In normal circumstances the allowance for corrosion over the design life of the wall may have a greater influence on the size of ties selected than the factors of safety against breaking.

6.6 TIE ARRANGEMENT CRITERIA

After the design lateral earth pressure envelope has been calculated, a suitable tie arrangement must be designed. In general, the design of the tie arrangement is independent of the method used to calculate the design lateral earth pressures. Thus the following tie design criteria are applicable to designs based on Rankine theory and the proposed seismic theory.

The design of a suitable tie arrangements involves calculation of values for the following variables:

- 1) vertical tie spacing,
- 2) horizontal tie spacing,
- 3) tie width,
- 4) tie thickness,
- 5) tie length,
- 6) tie-skin connection, and
- 7) strength characteristics of the skin.

It is reasonable to assume that the vertical tie spacing (variable 1) will be constant for the wall and within the range of 10.0 to 16.0 inches. The remaining variables are mutually dependent.

The ties must be designed to resist failure from the following mechanisms:

- 1) tie pullout,
- 2) tie breakage,
- 3) connection failure, and
- 4) skin failure.

Due to the limitations of this report the skin failure criteria has not been considered. This leaves 5 design variables to be evaluated using only three failure criteria. Therefore it is necessary to make arbitrary assumptions for two of the design variables. This section presents expressions for the horizontal tie spacing governed

by the above failure mechanisms and expressed in terms of the remaining 5 variables.

Tie Pullout. The maximum tie spacing at any level, based on tie pullout criteria can be solved by equating the tie pullout force to the tie pullout resistance. The lateral force acting on the tie is equal to the following:

$$F_i = x * S_i * (\nabla_{hi}) \quad (6.15)$$

where $\nabla_{hi} = K (\gamma d + q)$ for Rankine Theory, or

$$\nabla_{hi} = \nabla_{AE_i} + K_0 q \quad \text{for proposed Seismic Theory and}$$

S_i is the horizontal tie spacing at the i th tie level. Equating the lateral force with the frictional force resisting pullout, Eq. 2.7, results in the following expression:

$$S_i = \frac{2 * w * L_{E_i} * (\gamma d_i + q) * \tan' \phi_u}{X * (\nabla_{hi})} \quad (6.16)$$

Tie Breakage. The tie must resist, in tension, the lateral force given by Eq. 6.13. The tensile strength of the tie can be expressed as follows:

$$F_t = w * t * \frac{F_y}{2.0} \quad (6.17)$$

where w is the net effective width of the tie, and t is the thickness. Thus the horizontal tie spacing from tie failure criteria is as follows:

$$S_i = \frac{w * t * F_y}{X * (\nabla_{hi}) * 2.0} \quad (6.18)$$

Unless the ends of the ties are built up, the net effective width of the tie will be equal to the total width minus the width of bolt holes.

Connection Failure. The connection between the tie and the skin can fail in the following ways:

- 1) shear failure of the bolts,
- 2) bearing failure of the ties,
- 3) tearing failure of the tie, and
- 4) bearing failure of the skin.

The fourth failure mode will not be investigated in this report. In addition, it should be recalled that the wall must fail by tie pullout and not a breaking to insure a Ductile Failure Mode. Thus the connection must reflect conservative design.

The tearing failure mode is eliminated by using minimum edge distances from the bolt holes. These minimum edge distances are given in Table 6.2 (33).

Table 6.2 Minimum Edge Distance	
Bolt Diameter	Edge Distance (inch)
0.50	0.875
0.625	1.125
0.750	1.250

The bearing failure in the ties is eliminated if the plate is thick enough to develop the allowable bearing stress, $1.35 F_y$. If the tie is designed to develop the capacity of the connector bolts, the ties must resist the shear strength of the bolts in bearing. The minimum thickness required by this criteria is given by the following:

$$t_1 = \frac{F_B}{d * 1.35 * F_y} \quad (6.19)$$

where F_B^1 is the single shear capacity of a bolt, and d is the bolt diameter. In many instances it is necessary to build up the thickness

of the ties to develop bearing resistance. For example, this was done on the Reinforced Earth wall built on Highway 39, California, (11,12).

Based on the above criteria the tie spacing can then be designed for the connectivity, using for the maximum stress the shear strength of the bolts. The maximum tie spacing based on shear failure of the connection bolts is given by the following:

$$S_i = \frac{n * F_B}{X * (\nabla h_i)} \quad (6.20)$$

where n is the number of bolts in the connection.

- 1 Based on AISC code for standard steel:
F_B = 2.12 for 1/2 inch bolt
F_B = 3.07 for 5/8 inch bolt

6.7 SEISMIC DESIGN EXAMPLE

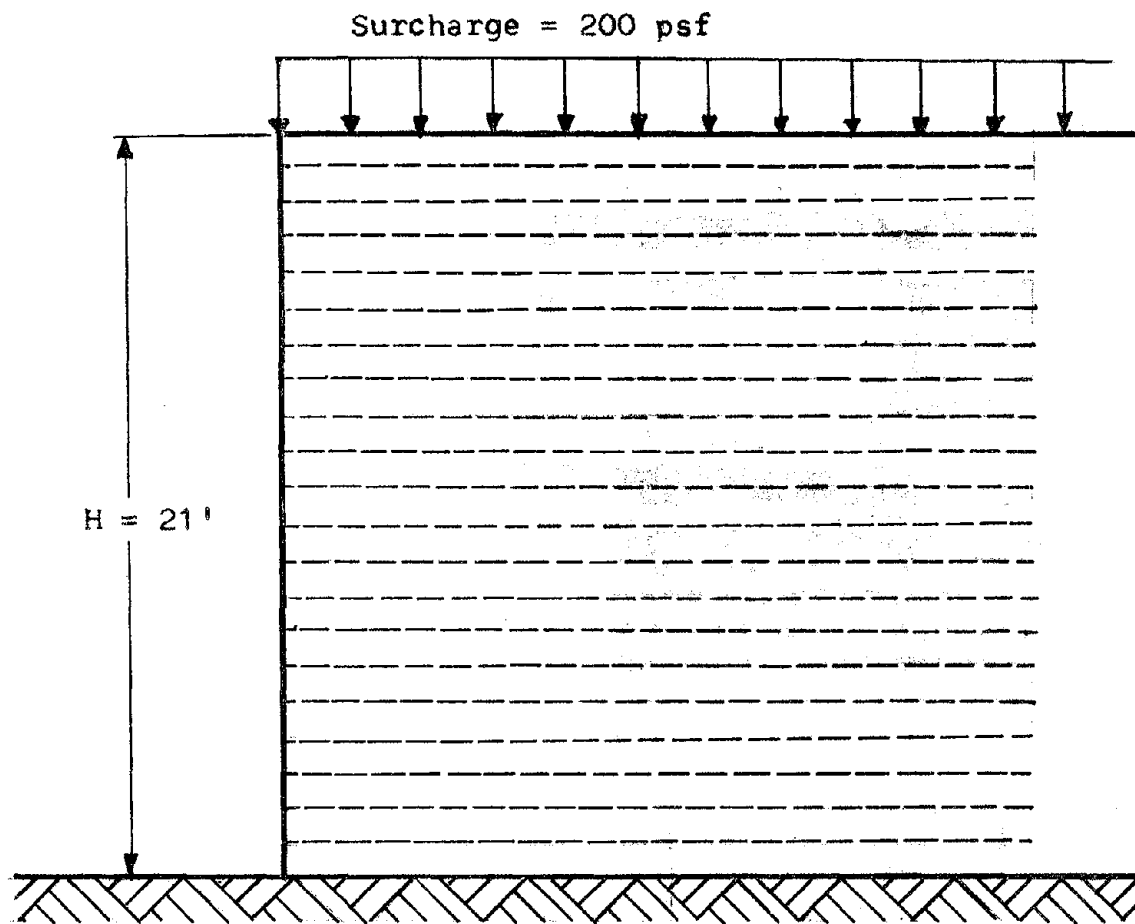
As an example, the previous sections of this chapter are incorporated in the design of a 21 foot Reinforced Earth wall to resist the simulated earthquake motion shown on Fig. 6.7. This accelerogram was developed by Chopra (30) to simulate a typical ground motion for the San Fernando 1971 earthquake. The original accelerogram had a maximum acceleration of 0.5g. This was reduced to 0.2g for this problem. The choice of this earthquake was one of convenience and does not imply any extrapolation to the actual San Fernando earthquake.

The design lateral earth pressures were calculated using the procedure outlined in Section 6.4. In addition, these seismic design lateral earth pressures are compared to those predicted using the finite element solution discussed in Section 5.2.

The Tie arrangement was designed for both seismic and static Rankine lateral earth pressures based on the failure criteria presented in Section 6.6. A final comparison of static and dynamic designs was made by arbitrarily assuming equal tie and connection properties for each loading case.

As shown on Fig. 6.11, the design was based on the following given data:

- 1) soil friction angle = 40°
- 2) soil-tie friction angle = 32° (typical design value)
- 3) soil density = 93.5 pcf,
- 4) wall height = 21.0 feet, and
- 5) surcharge = 200 psf (roughly corresponding to two feet of unreinforced soil placed atop the wall)



SOIL PROPERTIES

Density = 93.5 pcf

Soil Friction Angle = 40°

Soil-Tie Friction Angle = 32°

FIGURE 6.11 REINFORCED EARTH WALL DESIGN EXAMPLE

As stated earlier it is necessary to begin a design with some arbitrary but reasonable assumptions. The first assumption was to select a tie width, $w = 3$ inches, which is about the size used in current designs. The second assumption was to use $\frac{1}{2}$ inch bolts to connect the ties to the wall. The use of a bolt larger than this would require reinforcing the skin and ties against bearing failure which would probably be more costly. By using $\frac{1}{2}$ inch bolts with 3 inch wide ties it was also possible to use either one or two bolts to secure the ties to the skin without inducing tearing failure in the ties. An additional constraint was placed on the design by designing the tie-skin connection such that failure would occur in the bolts. Thus the minimum tie thickness is given by Eq. 6.17 as follows:

$$t_1 = \frac{F_B}{d * 1.35 * F_y} \quad (6.17)$$

$$t_1 = \frac{2.12}{.625 * 1.35 * 36} = 0.08 \approx 0.10" \quad (6.21)$$

Seismic Lateral Earth Pressures. The psuedo-acceleration response spectra for the design input motion with 12% critical damping was calculated for the design earthquake and is shown on Fig. 6.9.

The probable range of the fundamental period, T , of the 21 foot high wall is given by Eq. 6.5;

$$T_1 = (0.006 \text{ to } 0.10) * H \quad (6.5)$$

$$T_1 = (0.006 \text{ to } 0.010) * 21 = 0.126 \text{ to } 0.210 \text{ sec.} \quad (6.22)$$

Referring to the acceleration response spectra, within this range of periods, the maximum acceleration occurs for $T_1 = 0.210$ sec. Thus the design fundamental and second periods are

$$\begin{aligned} T_1 &= 0.210 \text{ sec} \\ \text{and } T_2 &= T_1 / 3 = 0.210 / 3 = 0.070 \end{aligned} \quad (6.23)$$

The spectral accelerations for the first two modes at these two periods are 0.38g and 0.22g, respectively. The seismic design acceleration can be calculated from Eq. 6.11 as follows:

$$A_{des} = 1.5 A_1 + .5A_2 \quad (6.11)$$

$$A_{des} = 1.5 (0.38) + .5 (0.22) = 0.59 \quad (6.24)$$

Substituting this design acceleration into Eq. 4.3 yields the following value for the Seismic Design Coefficient:

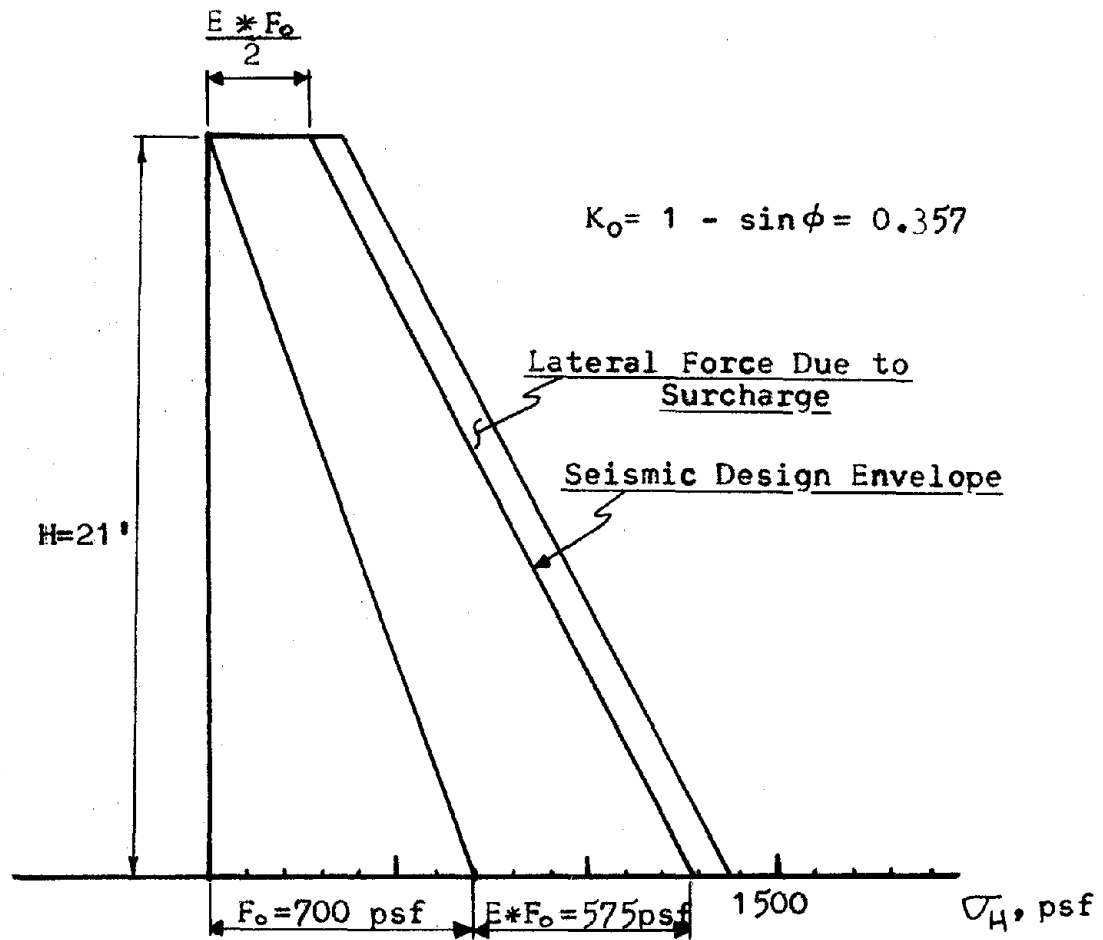
$$E = 1.4 (A_{des}) \quad (4.3)$$

$$E = 1.4 (0.59) = 0.82 \quad (6.25)$$

Based on Fig. 6.1a the Seismic Design Envelope was calculated as shown on Fig. 6.12. The total design lateral earth pressure was assumed to be the Seismic Design Envelope plus the static lateral pressure due to the surcharge.

Finite Element Solution for Lateral Earth Pressures. The 21 foot Reinforced Earth wall was idealized for finite element analysis as shown on Fig. 6.13 and subjected to the modified Chopra earthquake using 0.2g maximum acceleration.

As discussed in Section 5.2, the dynamic finite element program considers only the Seismic components, and therefore the calculated tie forces do not include static forces. As in Section 5.2, the



Spectral Acceleration = $0.59g$

$\therefore E = 0.82$

FIGURE 6-12 DESIGN LATERAL EARTH PRESSURES

66T-II

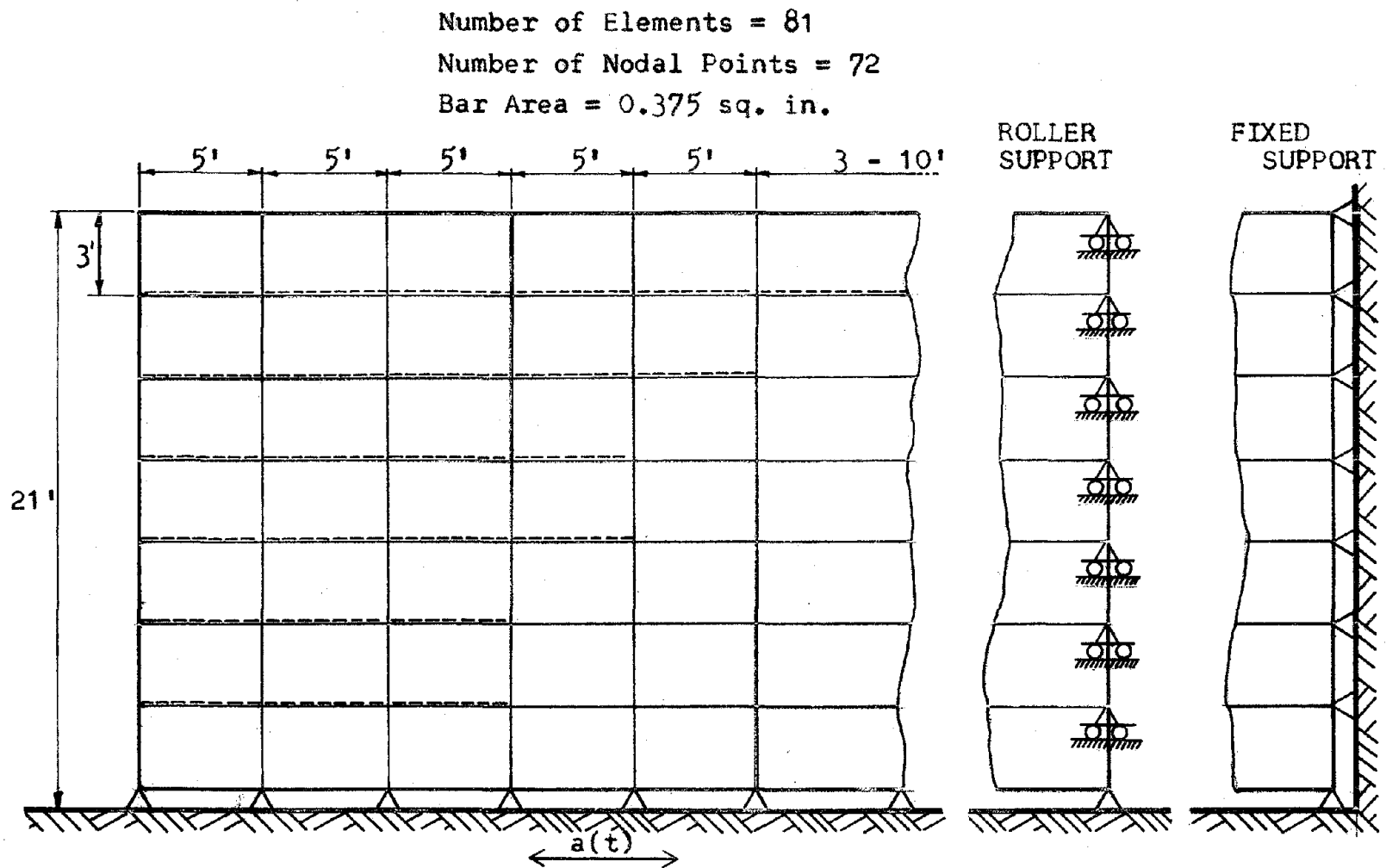


FIGURE 6-13 FINITE ELEMENT MODEL—
21 FOOT REINFORCED EARTH WALL

finite element seismic lateral earth pressure at each tie level were assumed to equal the Rankine at-rest earth pressure plus the seismic pressure given by dividing the tie force by the tie tributary area. Based on this assumption the seismic lateral earth pressures predicted by finite element analyses are compared to the Seismic Design Envelope in Fig. 6.14. Notice that the analysis was performed using two different boundary constraints for the backside of the soil backfill.

The actual back boundary condition in a field case is probably somewhere between these two limits, perhaps closer to the fixed than to the roller idealization. For example, as the wall moves out from the back boundary, an analysis based on a fixed boundary for the backfill will assume that a portion of the lateral force near the back boundary is taken by tension in the soil elements. This will reduce the amount of force taken by the ties, especially those which extend near to the back boundary. The real tie forces due to seismic loading would therefore be somewhat greater than that predicted by this finite element analysis.

On the other hand, as the wall moves toward the back boundary an analysis based on a roller boundary for the fill will ignore the compressive resistance of the soil and this will lead to larger forces into the lower ties. The wall will essentially act as a shear beam and the upper ties will not be heavily loaded.

Thus an analysis based on a roller boundary will result in tie forces which are too small at the top of the wall and too large

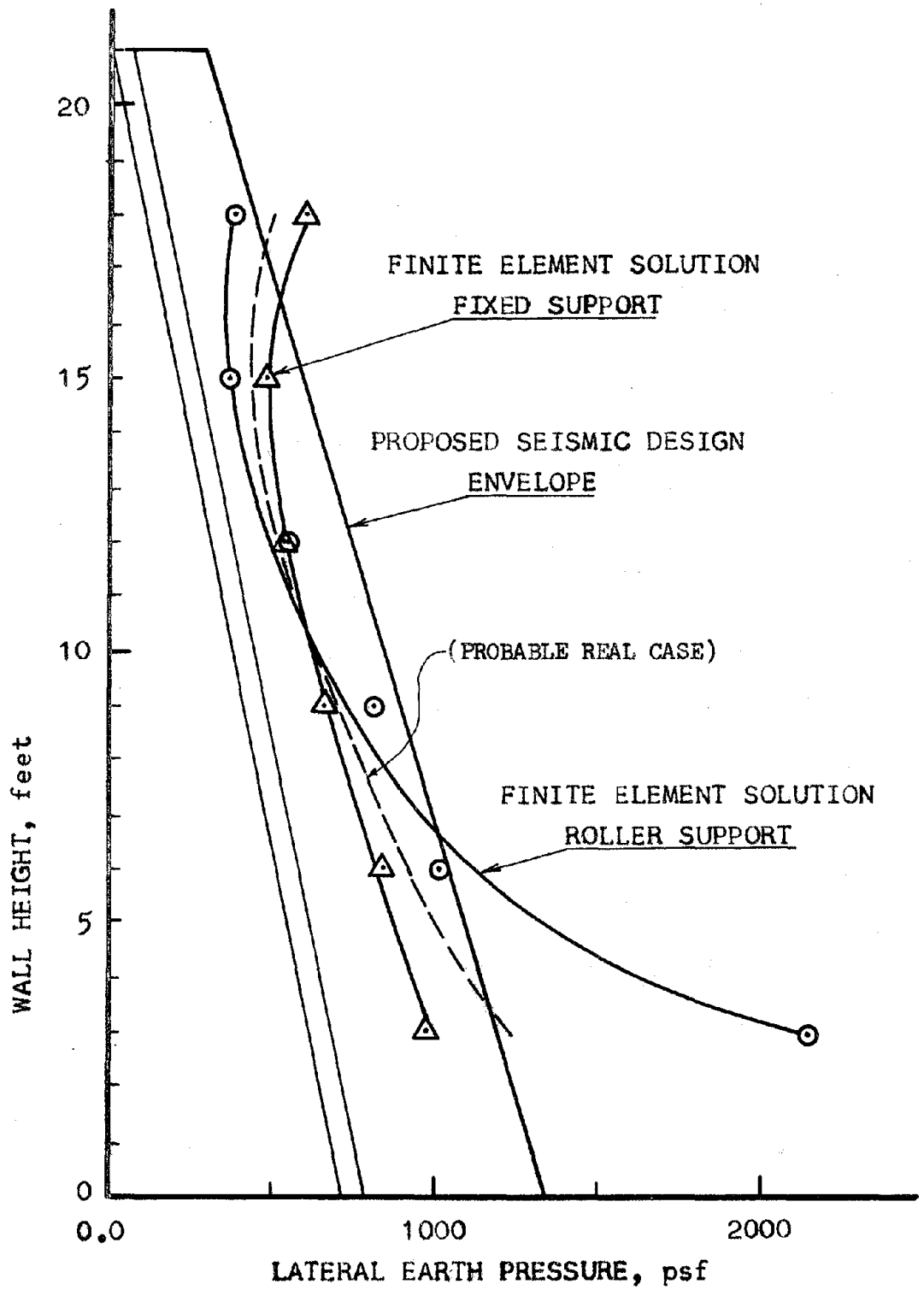


**FIGURE 6-14 FINITE ELEMENT
LATERAL EARTH PRESSURE**

at the base of the wall. Conversely, an analysis based on a fixed back boundary will probably result in tie forces which are too large at the top and too small at the bottom of the wall. But since a natural boundary is probably more fixed than free, the error should be less for the fixed boundary than for the free boundary solution.

Based on the above criteria the best theoretical solution should be somewhere between the free and fixed support case, but closer to the fixed back boundary solution, as shown on Fig 6.14. Thus the results of this finite element analysis is in good agreement with the semi empirical design criteria developed earlier.

Tie Arrangement Criteria-Seismic Design. The maximum tie spacing, S_i , for any level of ties i was calculated for the three different failure criteria, previously discussed in Section 6.6, as follows:

1) Tie Pullout,

$$S_i = \frac{2 * w * L_{Ei} * (\gamma_{di} + q) * \tan' \phi_u}{X * (\sqrt{AE_1} + K_o q)} \quad (6.26)$$

for $L = 21, 25, \text{ and } 30$ feet

2) Tie Breakage,

$$S_i = \frac{w * t * F_y}{X * (\sqrt{AE_1} + K_o q) * 2} \quad (6.27)$$

3) Connection Failure,

$$S_i = \frac{n * F_B}{X * (\sqrt{AE_1} + K_o q)} \quad n = 1, 2 \quad (6.28)$$

The results of the above calculations are given in Table 6.3 and are plotted in Fig. 6.15. The curves represent the maximum allowable tie spacing for each of the three failure criteria for

Table 6.3 MAXIMUM TIE SPACING for SEISMIC LOADING

EARTH PRESSURES					TIE PULLOUT CRITERIA (w = 3.0")						TIE BREAK CRITERIA (t=1")				CONNECTOR		
TIE DEPTH, d _t	Y _d	Y _d +q	V _{AEI}	V _{AEI} +K _o q	$\frac{2w_w(1+q)T_w}{x \cdot (V_{AEI} + K_o q)}$	L=21'		L=25'		L=30'		$\frac{t \cdot F_u}{x \cdot (V_{AEI} + K_o q)}$	S _{i,FE} (W=30")	S _{i,FE} (W=237)	S _{i,FE} (W=175)	S _{i,FE} ONE BOLT	S _{i,FE} TWO BOLT
						L _{FE}	S _{i,FE}	L _{FE}	S _{i,FE}	L _{FE}	S _{i,FE}						
1	93.5	293.5	345	416	.055	11.7	.64	15.7	.86	20.7	1.14	4.31	13.0	10.2	7.60	5.10	10.2
2	187	387	400	471	.064	12.1	.78	16.1	1.04	21.1	1.35	3.82	11.5	9.09	6.68	4.50	9.0
3	280	480	450	521	.072	12.6	.91	16.6	1.20	21.6	1.55	3.46	10.4	8.20	6.05	4.30	8.6
4	374	574	490	561	.080	13.1	1.04	17.1	1.36	22.1	1.77	3.20	9.61	7.61	5.61	3.80	7.6
5	468	668	540	611	.085	13.5	1.15	17.5	1.49	22.5	1.91	2.95	8.84	7.00	5.15	3.47	7.0
6	561	761	590	661	.090	14.0	1.26	18.0	1.62	23.0	2.07	2.72	8.16	6.46	4.76	3.20	6.4
7	655	855	640	711	.095	14.5	1.37	18.5	1.75	23.5	2.23	2.53	7.60	6.00	4.42	2.98	6.0
8	748	948	690	761	.098	14.9	1.46	18.9	1.85	23.9	2.34	2.36	7.10	5.61	4.13	2.79	5.6
9	841	1041	740	811	.101	15.4	1.56	19.4	1.97	24.4	2.46	2.22	6.65	5.27	3.88	2.61	5.2
10	935	1135	790	861	.104	15.8	1.65	19.8	2.07	24.8	2.58	2.09	6.27	4.96	3.65	2.46	4.9
11	1030	1230	840	911	.106	16.3	1.75	20.3	2.18	25.3	2.68	1.98	5.93	4.69	3.46	2.32	4.6
12	1120	1320	890	961	.108	16.8	1.82	20.8	2.24	25.8	2.78	1.87	5.61	4.44	3.28	2.20	4.4
13	1215	1415	940	1011	.109	17.3	1.89	21.3	2.33	26.3	2.86	1.78	5.34	4.23	3.12	2.10	4.2
14	1310	1510	990	1061	.110	17.7	1.96	21.7	2.40	26.7	2.94	1.70	5.09	4.03	2.97	2.00	4.0
15	1400	1600	1040	1111	.112	18.2	2.04	22.2	2.49	27.2	3.04	1.62	4.86	3.85	2.83	1.90	3.8
16	1495	1695	1090	1161	.113	18.7	2.12	22.7	2.58	27.7	3.13	1.55	4.65	3.68	2.71	1.82	3.6
17	1590	1790	1140	1211	.115	19.1	2.20	23.1	2.66	28.1	3.23	1.49	4.46	3.48	2.60	1.75	3.5
18	1680	1880	1190	1261	.116	19.6	2.28	23.6	2.75	28.6	3.32	1.43	4.28	3.39	2.50	1.68	3.4
19	1780	1980	1240	1311	.118	20.0	2.35	24.0	2.82	29.0	3.42	1.37	4.11	3.26	2.40	1.61	3.2
20	1870	2070	1290	1361	.119	20.5	2.43	24.5	2.90	29.4	3.50	1.32	3.96	3.14	2.31	1.56	3.1
21	1965	2165	1335	1406	.120	21.0	2.52	25.0	3.00	29.0	3.60	1.28	3.84	3.04	2.24	1.51	3.0

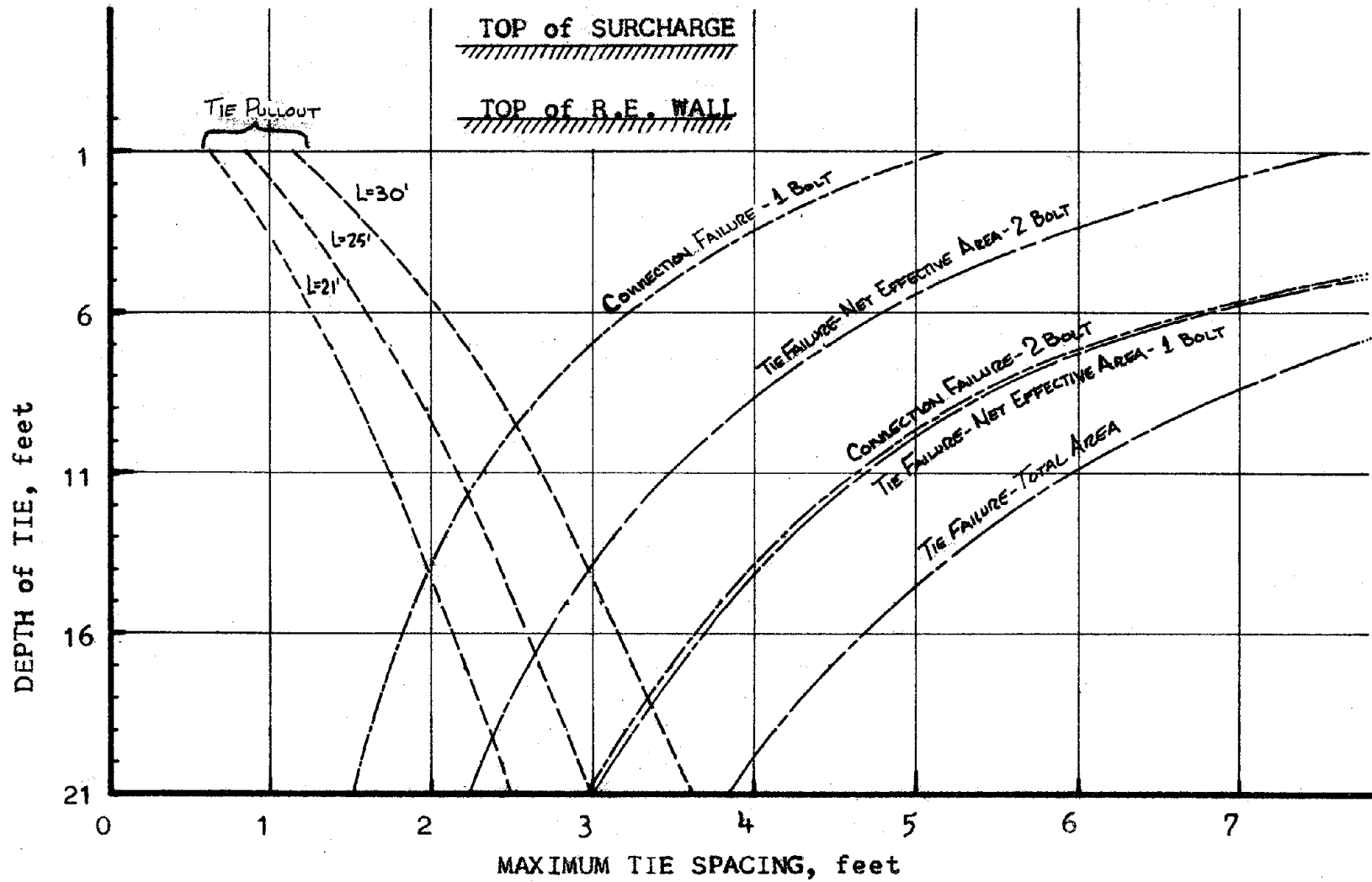


FIGURE 6-15 SEISMIC TIE SPACING CRITERIA

the assumed values of the variables. Note that there is a considerable difference in maximum tie spacing at any depth depending on the particular mode of failure and the failure criteria. The longer the ties the greater the tie spacing. Near the top, the ties must be closely spaced to prevent pullout. Near the base, the pullout criterion is over shadowed by the need for close tie spacing to prevent tie breakage or a connection failure.

To define the maximum allowable tie spacing at any level it is necessary to select a tie length and a bolt pattern for the skin-tie connection and then, from Fig. 6.15, the maximum tie spacing that will satisfy the minimum value of all three failure criteria.

In practice an additional constraint would be placed on the allowable tie spacing based on skin failure criteria. This extra constraint has been neglected in this report, but it is noted that in practice the maximum tie spacing is of the order of 2 or 3 feet depending upon the height of the wall.

Tie Arrangement Criteria-Static Design. The tie arrangement criteria presented in Section 6.6 and previously used for seismic loading may also be applied to static lateral earth pressures. The maximum tie spacing for the 21 foot Reinforced Earth wall acted upon by Rankine active or at-rest pressures were calculated based on the three following failure criteria:

1) Tie Pullout

$$S_i = \frac{2 * w * L_{Ei} * (\gamma d + q) * \tan' \phi_u}{X * K * (\gamma d + q)} = \frac{2 * w * L_{Ei} * \tan' \phi_u}{X * K}$$

for L = 16, 21 feet (6.29)
K = K_A, K_O

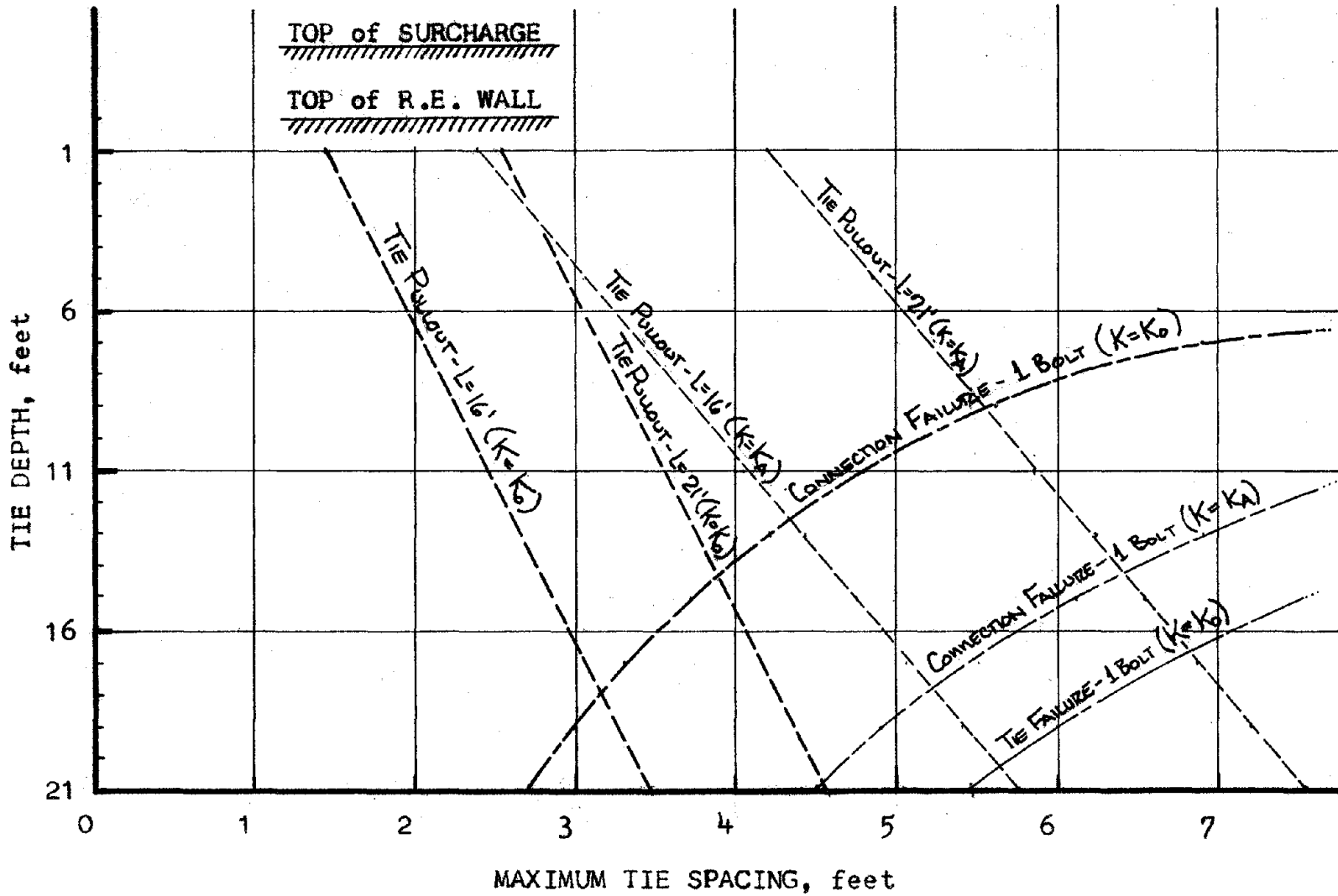


FIGURE 6-16 STATIC TIE SPACING CRITERIA

objective function. Because this is beyond the scope of this report, a comparison will be made between the seismic and static designs based on an 'all-things-equal' criterion.

The comparison between the seismic and static designs will be based on the arbitrary assumption of the following:

- 1) Tie length = 21 feet, and
- 2) Connection = one - $\frac{1}{2}$ " bolt per tie.

This is in addition to the earlier assumptions of 3 inch tie width and 0.1 inch tie thickness.

Based on this arbitrary criteria, the maximum tie spacing for the static and seismic designs is shown on Fig. 6.17. For the particular value of the design variables used in this comparison, the tie spacing above the eighth tie is governed by tie pullout and below the eighth tie is governed by shear failure of the connection.

In examining Fig. 6.17 it should be recalled that the smaller the tie spacing the larger the quantity of required steel and therefore the larger the cost. In estimating the increase in cost due to seismic design it should be recalled that, though Lee, et al, (3) recommended using $K = K_A$ and static factor of safety of 1.5 for static design, later full scale testing by Beaton, et al, (12) indicated that $K = K_o$ and a factor of safety of four on the soil-tie friction angle should be used for static design. In either case the tie spacing calculated using $K = K_A$ will result in tie spacing greater than the practical minimum tie spacing.

If the static design proposed by Beaton is compared to the

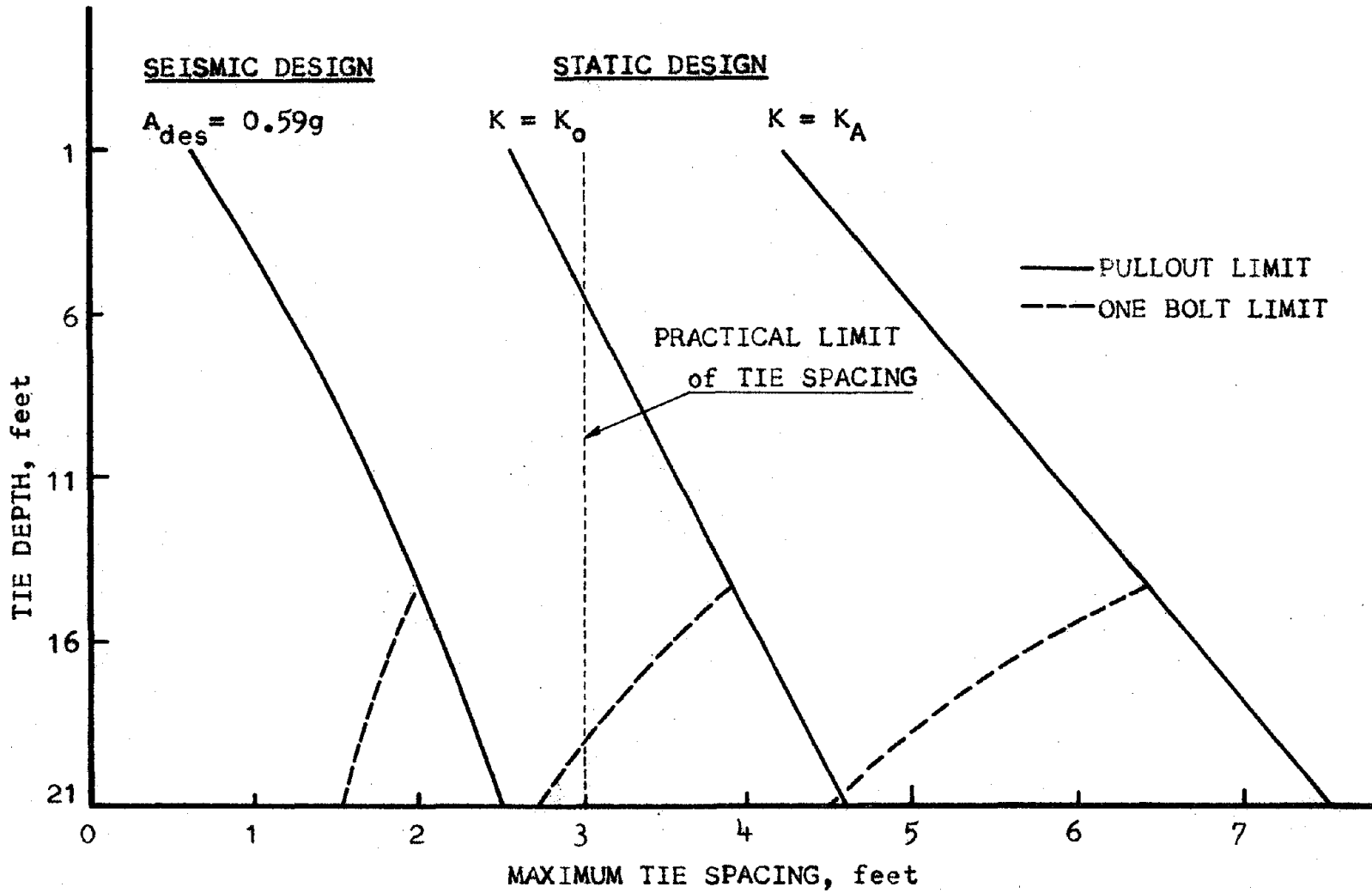


FIGURE 6-17 SEISMIC VS STATIC DESIGN

seismic design proposed by this report it is apparent that the tie spacing required for seismic loads is about half that required for static loads. Thus the seismic design, based on the assumed criteria, will double the amount of tie steel in the wall and most of the steel is in the ties. Lee, et al, (3) reported that the cost of steel fabrication and assembly was approximately 30 to 40% of the total job cost for a wall of this size. If it is assumed that cost is directly proportional to quantity of the tie steel, this would indicate that seismic design considerations would add about 15% to 20% to the total cost of the job as compared to static design only.

CHAPTER 7 SUMMARY

This report describes an investigation into the response of Reinforced Earth walls to vibratory loading. Data were obtained from the response of laboratory models subjected to sinusoidal accelerations on a shaking table. In addition a numerical study was performed using a dynamic finite element program with nonlinear strain dependent soil modulus and damping. Finite element analyses were performed for the small models, and for some full scale structures. These experimental and analytical studies have defined the significant structural characteristics of Reinforced Earth walls that are required for a safe and economical seismic design.

The first model studies performed for this report, Series A, used models designed to fail by tie-breakage. Dynamic failures which occurred in these models were sudden, catastrophic, and complete. The second series of model tests, Series B, were designed to fail by tie-pullout. The dynamic failures that occurred in these models were typified by a gradual outward movement of the wall. Even though large displacements developed with time, there was no collapse. The walls in the second series of tests also had significant static strength after the completion of dynamic loading in spite of the sometimes severe deformations. Based on the difference in failure modes between the tie-failure and tie-pullout

tests, it was concluded that to insure a ductile structure the Reinforced Earth wall must be designed such that if the wall becomes overstressed, failure will occur from tie-pullout and not by tie-breaking.

Tie forces measured during the Series B tests were used to formulate a procedure for calculating the envelope of maximum probable tie forces that would occur during dynamic loading, and this was then incorporated into a seismic design procedure. This envelope defines the maximum probable tie forces. Because the test models showed that localized, and unpredictable, soil arching could influence the individual tie force magnitudes, the design curve was drawn as an envelope or upper bound to encompass these variations. The Seismic Design Envelope was determined by modifying the envelope of predicted tie forces based on static Rankine at-rest pressures by use of a seismic coefficient multiplying factor E , which depended on the input spectral acceleration.

Use of the Seismic Design Envelope results in higher lateral pressures and tie forces near the top of the wall than would be obtained by using a hydrostatic pressure distribution. As the magnitude of the input acceleration decreases, the Seismic Design Envelope of lateral earth pressures approaches the Rankine at-rest earth pressures. Thus for static designs it is recommended that the Rankine at-rest earth pressures be used for design. This is a departure from an earlier UCLA study which showed that static designs could be based on the Rankine Active pressure. However, it

was found that even very small vibrations less than 0.05g, as might be caused by heavy traffic or compaction equipment under normal construction conditions, would lead to at-rest earth pressures.

Additional model testing has shown that the lateral earth pressures during dynamic loading are not only a function of base accelerations, but are also a function of the frequency of the input motion. Based on these tests a procedure was developed using the spectral modal response method to predict the lateral earth pressures that occur during random dynamic vibration. This procedure calculates the spectral accelerations for the first two modes of the Reinforced Earth wall based on empirical formulas for the first and second fundamental periods. Using approximate modal participation factors these spectral accelerations are combined into one design acceleration. This design acceleration is used to calculate the Seismic Design Coefficient E, and the Seismic Design Envelope.

The predicted seismic lateral earth pressures occurring from sinusoidal input motions were compared with those calculated using a dynamic finite element analysis. By adjusting the values of damping and modulus to the values measured in the actual laboratory model tests, it was possible to achieve a close correlation between laboratory and calculated values of tie forces and accelerations. The modulus and damping values used in these correlations were slightly different from the values suggested by Seed and Idriss (22), but the difference is reconcilable by recognizing that the Seed-

Idriss values are for prototype conditions, and not for small models with only a few inches of overburden pressure.

Because of this success in duplicating, in a finite element analysis, the Seismic Design Envelope for the laboratory models, the finite element program was then used to calculate the tie forces for two full scale prototype structures, and compare with the tie forces predicted by the Seismic Design Envelope. The unmodified Seed-Idriss modulus and damping relations were used in these prototype studies. For both sinusoidal and random vibrations the calculated tie forces, and therefore the lateral earth pressures, were in close agreement with the finite element results for walls 12 and 21 feet in height.

During the design of Reinforced Earth walls to resist seismic lateral earth pressures, it became apparent that the value of the friction angle between the soil and the ties strongly influenced the amount of reinforcing required. To investigate the soil-tie friction angle, a series of monitored tie pullout tests were performed on the ties used with the model walls. Additional or 'extra' ties were embedded at different locations in the sand fill during construction and then pulled out at a constant rate while recording the force required to move the tie. Based on these tests, it was possible to calculate an average soil-tie friction angle for each instant of time during the pullout test. These tests indicated a large initial friction angle that reduced to some residual value after the pullout force had exceeded the maximum pullout resistance of the tie. This residual friction angle was

usually $\frac{1}{2}$ to $\frac{1}{4}$ of the peak friction angle. This is in agreement with earlier tests performed on full scale structures under static conditions (12). In addition the peak soil-tie friction angle was shown to be a function of the location in the wall and the stress history of the wall. The peak friction angle in the model tests was higher during vibration and after vibration than it was before any vibratory loading had occurred. It decreased with distance away from the face of the reinforced earth wall. Thus it appeared that a stress arch tended to develop around the tie, preventing the full overburden pressure from acting. This arch could be broken by soil movements from vibration or outward yielding of the wall. Largely because of these observations, it is recommended that a factor of safety of four be used on the tangent of the measured peak soil-tie friction angle to determine the tangent of the soil-tie friction angle to be used for design.

Using the Seismic Design Envelope procedure and the limited tie pullout information, a 21 foot high Reinforced Earth wall was designed to resist a seismic event which would produce a 15 second accelerogram at the site. The design evaluated the maximum allowable tie spacing for each of the possible failure modes: tie-pullout, tie-breakage, tie-skin connection failure. (For this report the skin failure mode was neglected.) The design tie spacing was the maximum tie spacing that would satisfy all failure criteria. Based on this design procedure, it was observed that the design tie spacing in the upper reinforcing layers was governed by tie-pullout, while the design tie spacing of the lower

layers was governed by either tie strength or connection detail requirements. While the design of the 21 foot wall was simplified and not optimized to minimize the amount of reinforcing, it indicated that the extra material required for seismic considerations led to an approximate increase in cost of only about 20% in the total cost of the job.

Additionally, the design example showed that the minimum, and therefore the most costly design tie spacing occurs in the upper reinforcing layers where tie pullout is the governing criterion. This was due to the increased seismic lateral force and the minimal amount of overburden at these upper layers. Because the tie pullout resistance is a direct function of the overburden pressure, it may be possible to improve the design in the upper zone, and hence the overall cost of a project by using a fairly thick upper layer of unreinforced surcharge above the main reinforced earth backfill. If this surcharge had a sloping face and/or was kept behind the potential failure zone, it would increase the overburden pressure over the effective portion of the reinforcing which resists the pullout, but would not significantly increase the lateral earth pressures.

In summary, it has been shown that Reinforced Earth walls can be designed to resist seismic loads in a ductile manner by insuring that if failure occurs it will be from tie pullout. To insure failure by tie pullout this report recommends designing based on the following factors of safety:

- 1) tie failure- the design tie force shall be twice that predicted using the Seismic Design Envelope, and
- 2) tie pullout- the tangant of the design soil-tie friction angle shall be $\frac{1}{4}$ the tangant of the peak measured soil-tie friction angle.

While this would seem to imply a larger factor of safety against tie pullout than tie breakage, it should be recalled that there was a high degree of uncertainty in the measured peak soil-tie friction angle and that only a small amount of displacement was required to reduce the soil-tie friction angle to its residual value. The Seismic Design Envelope on the other hand represents an envelope of maximum possible tie forces and is already conservative in nature. In addition, the Seismic Design Envelope did not appear to be as sensitive to small displacements as the soil-tie friction angle. Based on these observations it is felt that the factors of safety used in this report will lead to a failure by tie pullout and thus insure a ductile failure mode.

REFERENCES

1. Vidal, H. " 'Reinforced Earth," (in French), Annales de l'Institut Technique du Batiment et des Travaux Publics, July-Aug, 1966, mos. 223-229, pp. 888-938.
2. Vidal, H. "The Principal of Reinforced Earth," Highway Research Record, no. 282, 1969, pp. 1-16.
3. Lee, Kenneth L. and B.D. Adams and J.J. Vagneron "Reinforced Earth walls," Report to NSF, UCLA-ENG-7233, April 1972.
4. Vidal, H. " 'Reinforced Earth' Steel Retaining Wall," Civil Engineering, February 1970, pp. 70-73.
5. Vidal, H. "La Terre Armee (realisations re centes)," Annales de l' I.T.B.T.P., 22e anne, juillet-aout, No. 259-260, pp 110-1157.
6. Vidal, H. "La Terre Armee," (in French) diffusion restreinte, 1963.
7. Uesawa, H., et al 'A large Scale Experiment on Reinforced Earth,' (in Japanese) Publication of the Japanese National Railways Research Institute, April 1969, pp. 223-226.
8. Uesawa, H. "A Conception and Basic Experiment on Reinforced Earth Method," (in Japanese) Publication of the Japanese National Railways Research Institute, April 1968, pp. 206-212.
9. Sanglerat, G. "Massifs de Terre Armee (in French)," Revue Technica, July-September 1971.
10. Vidal, H.C., United States Patent No. 3, 421, 326, January 14, 1969.
11. Chang, J, R. Forsyth, and T. Smith "Reinforced Earth Highway Embankment-Road 39," Highway Focus, vol. 4, No. 1, January 1972, Federal Highway Administration, U.S. Department of Transportation
12. Beaton, J.L., R.A. Forsyth, and J.C. Chang "Design and Field Behavior of the Reinforced Earth Embankment-Road 39" Unpublished report, California Department of Transportation, Sacramento, California, 1973.
13. Lee, Kenneth L., Research Proposal to NSF for Reinforced Earth Structures, UCLA, Eng.-P-2378-N, 1972.

14. H. Uezawa, and M. Nasu "Anti-earthquake Measures for Embankment on a Weak Ground, "Proceedings, 5th World Conference on Earthquake Engineering, Paper 40, Rome, 1973.
15. Jaky, J. "Pressure in Silos, "Proceedings, 2nd International Conference on Soil Mechanics, v.1, 1948, pp. 103-107.
16. Clough, R.W. and Pirtz, D. "Earthquake Resistance of Rockfill Dams," Trans. American Society of Civil Engineers, Vol. 123, 1958, pp. 792-816.
17. Hurty, Walter C. and Moche F. Rubinstein Dynamics of Structures, Prentice-Hall, 1969, pp 203.
18. Tschebotarioff, Gregory D. Foundations, Retaining and Earth Structures. Mc Graw-Hill, 2nd edition.
19. Casagrande, L. "Comments on the Conventional Design of Retaining Structures," Journal, Soil Mech. Found. Div., ASCE, Vol.99, No. SM2, Feb 1973, pp 181-198.
20. Seed, H.B. and I.M. Idriss "Influence of Soil Conditions on Ground Motions During Earthquakes," Journal, Soil Mech. Found. Div., ASCE, Vol. 95, No. SMI, January, 1969.
21. Silver, M.L. and H.B. Seed "The Behavior of Sands Under Seismic Loading Conditions," Report to U.S. Army Corps of Engineers, EERC 69-16 , December 1969.
22. Idriss. I.M. and H. Dezfulian and H. Boulton Seed "Computer Programs for Evaluating the Seismic Response of Soil Deposits With Non-Linear Characteristics Using Equivalent Linear Procedures," Department of Civil Engineering Institute of Transportation and Traffic Engineering, Berkeley, 1969.
23. Idriss, I.M., Lysmer, J., Wang, R., and H.B. Seed "QUAD-4 A Computer Program for Evaluating the Seismic Response of Soil Structures by Variable Damping," Report No. EERI 73-16, July, 1973.
24. Ishii, Yasumaru, Hideo Arai, and Hajime Tsuchida "Lateral Earth Pressure In An Earthquake," Proceedings, Second World Conference on Earthquake Engineering, Vol 1, 1960, pp 211-230.
25. Okabe, S. "Bearing Capacity of Sandy Soils and Lateral Earth Pressures During Earthquakes, "Proceedings, Earthquake Engineering Conference, 1956, Berkeley.
26. Mononobe, N. and H. Matsuo "On the Determination of Earth Pressures During Earthquakes," Proceedings, World Engineering Conference, 1929, Vol. 9, pp. 176.

27. Seed, H. Bolton and Robert V. Whitman "Design of Earth Retaining Structures for Dynamic Loads," ASCE, Specialty Conference, Lateral Stresses in the Ground and the design of Earth Retaining Structures, Cornell University, 1970.
28. Blume, John A, N.M. Newmark, and L.H. Corning Design of Multistory Reinforced Concrete Buildings for Earthquake Motions, Portland Cement Association, 1961.
29. Przemieniecki, J.S. Theory of Matrix Structural Analysis McGraw Hill, 1968.
30. Chopra, A.K. "Artificial Accelerogram for San Fernando Earthquake of February 9, 1971 at Olive View Hospital." Private communication to K.L. Lee.
31. Idriss, I.M. and H.B. Seed "Seismic Response of Soil Layers," Journal, Soil Mech. Found. Div., ASCE, Sm2, March 1970, pp 631-637.
32. Housner, G.W. "Behavior of Structures During Earthquakes," Journal, Engineering Mechanics Division, ASCE, Vol. 85, No. EM 4, October 1959, pp. 109-129.

APPENDIX A

II-219

TYPE OF TEST	DISCRIPTION OF TEST		TEST No.	WALL HEIGHT (in)	DESIGN ϕ_u	INPUT ACCEL. (g)	FAILURE SURFACE	CHIEF CONCLUSIONS	
SERIES A	TIE BREAKAGE FAILURE MODE ALUMINUM TIES TIE LENGTH = 20 INCHES HORIZONTAL TIE SPACING = 6 INCHES VERTICAL TIE SPACING = 1.0 INCHES STATIC FACTOR OF SAFETY (FS) TIE BREAKAGE = 2.0 CYLINDRICAL SKIN ELEMENTS		2	11	-	0.15	YES	TIE BREAKAGE LEVELS 2,3,4 RESTRAINED AGAINST COMPLETE FAILURE	
			3	11	-	0.30	NO	TIE BREAKAGE LEVELS 2,3,4,5,6 RESTRAINED AGAINST COMPLETE FAILURE	
			4	11	-	0.36	YES	NO RESTRAINT - CATASTROPIC FAILURE	
			5	11	-	0.18	YES	TIE BREAKAGE LEVELS 2,3,4 RESTRAINED AGAINST COMPLETE FAILURE	
			6	11	-	0.20	NO	NO RESTRAINT - CATASTROPIC FAILURE	
			7	11	-	0.15 0.26	YES	RESTRAINED AGAINST COMPLETE FAILURE	
			8	11	-	0.10	NO	NO RESTRAINT - CATASTROPIC FAILURE	
			SERIES B	TIE PULLOUT FAILURE MYLAR TIES	SERIES B-1 TIE LENGTH = 20 IN. HORIZONTAL TIE SPACING = 6 IN. STATIC FS- 8.1 TIE BREAKAGE 2.3 TIE PULLOUT	2	12	-	0.10
3	12	-				0.26	NO	LARGE DISPLACEMENT OF UPPER WALL DUCTILE FAILURE	
4	12	-				0.32	NO	LARGE DISPLACEMENT OF UPPER WALL DUCTILE FAILURE	
5	12	-				0.15 0.45	YES	LARGE DISPLACEMENT OF UPPER WALL DUCTILE FAILURE	
6	12	10				0.05-0.08 0.17-0.28	NO	LARGE DISPLACEMENT OF UPPER WALL DUCTILE FAILURE	
VERTICAL TIE SPACING = 1.5" FLAT SKIN ELEMENTS	SERIES B-2 K = K ₀ STATIC FS- 8.1 BREAK 2.3 PULLO	7		12	10	0.32	NO	LARGE DISPLACEMENT OF UPPER WALL DUCTILE FAILURE	
		SERIES B-3 LATERAL DESIGN FORCES PER SEISMIC DESIGN ENVELOPE		8	12	7	0.34	NO	UNIFORM DISPLACEMENT DUCTILE FAILURE
				9	12	7	0.48	NO	UNIFORM DISPLACEMENT DUCTILE FAILURE
				10	12	20	0.30	YES	UNIFORM DISPLACEMENT DUCTILE FAILURE
				11	12	15	0.30	YES	UNIFORM DISPLACEMENT DUCTILE FAILURE
		ADDITIONAL TESTS		TIE PULLOUT FAILURE MYLAR TIES VERTICAL TIE SPACING = 1.5 INCH LATERAL DESIGN FORCES PER SEISMIC DESIGN ENVELOPE		12	16.5	12	0.30
13	15.0		12			0.30	YES	UNIFORM DISPLACEMENTS NOTE: FREQUENCY OF INPUT ACCELERATION WAS VARIED FROM 5 TO 40 CPS	

Part III

Summary Paper

Pseudo Static and Vibration Studies

Seismic Design of Reinforced Earth Walls

by

Gregory N. Richardson and Kenneth L. Lee

A paper prepared for presentation

at the ASCE National Meeting

Los Angeles, California

January 21 - 25, 1973



SEISMIC DESIGN OF REINFORCED EARTH WALLS

by Gregory N. Richardson¹, Associate Member ASCE, and
Kenneth L. Lee², Member ASCE

SYNOPSIS

This paper is a summary progress report of ongoing studies at UCLA toward developing a rational design method for reinforced earth retaining walls. The method described herein is based largely on the results obtained from small laboratory scale walls subjected to horizontal sinusoidal seismic loading with a shaking table. The tests showed that the walls responded like a non-linear damped elastic system to the input vibrations. From measurements of the peak tie forces, an empirical design force envelope was developed which is a function only of input acceleration. It is suggested that the design earth pressures for an actual wall subjected to earthquake loading be based on this design force envelope using a base acceleration determined by response spectra modal participation factor techniques. Data are also presented of soil-tie friction under static and vibratory loading. Recommendations are given for calculating the size and spacing of the ties including appropriate factors of safety. The recommendations presented herein are tentative, and must await verification from additional analytical, laboratory and field studies.

INTRODUCTION

Reinforced earth is a construction material composed of frictional soil and strong bars or fibers embedded to resist the tensile stresses. Applied to retaining wall construction, a thin outer skin is also required to retain the soil at the outer face. The skin may be very light weight and relatively weak. It is supported by numerous connecting ties which are anchored through friction into the backfill. Thus the skin acts only as an outer membrane. The membrane design has not been considered in these studies. The ties must be strong enough at all points, including the connections, to resist the tensile forces induced from the lateral earth pressure. They must also be long and wide enough to develop sufficient friction with the soil to resist the lateral earth pressure.

Previous studies by Lee et al. (7,8) indicated that for carefully placed backfill under static loading, the lateral earth pressures closely

¹Graduate Student, School of Engineering and Applied Science, University of California at Los Angeles.

²Associate Professor, School of Engineering and Applied Science, University of California at Los Angeles.

approximated the active Rankin pressure, and the tie lengths effective in resisting this pressure were those portions extending beyond the outer zone of an active failure wedge. Tie force measurements on a 50 ft. high wall recently constructed in Southern California (the first in the United States) suggest that an at rest K_0 , earth pressure distribution may be more appropriate for static loading, and because of low measured residual soil-tie friction angles, a factor of safety of 4.0 was recommended for designs to resist a pull out failure (1).

Very little data exists on the behavior of reinforced earth under seismic loading. The Japanese National Railway have conducted some shaking table tests on model structures (14, 15, 16). A 10 ft. high wall designed for a theoretical static factor of safety of 8 was subjected to a dynamic loading from a vibrator mounted at the top of the wall. Peak accelerations up to 1.0g carried only a few millimeters permanent deformation. In another seismic model study, various types of reinforcing in a railway embankment or its loose saturated sandy foundation were tried in the hope of developing a liquefaction resistant design (16). These studies appeared to have met with only limited success.

In the absence of other available work on the seismic behavior of reinforced earth, the studies described herein were initiated with the objective of developing a rational seismic design procedure. The first step was to observe the behavior of reinforced earth walls under vibratory loading conditions and this was followed by more detailed measurements and calculations.

PSEUDO STATIC CONSIDERATIONS

Seed and Whitman have recently summarized the classical early work by Mononobe and Okabe and other supplementary studies on the seismic earth pressures behind conventional retaining walls (11). The analytical approach introduces the seismic effect by a constant seismic force kW acting in the direction of the vibratory loadings where W is the weight of the soil contained within an assumed failure wedge. The seismic coefficient k , is largely an empirical representation of the effect of the input base acceleration. For constant amplitude sinusoidal loading k is set equal to the maximum base acceleration a_{max} . For erratic earthquake loading Seed and Whitman suggest using $k = 0.65 a_{max}$. Introduction of the pseudo static force component into a Coulomb equilibrium wedge analysis leads to a unique expression for the slope θ_{AE} of the most probably failure wedge, and the total earth force P_{AE} acting on the wall. Apparently Mononobe and Okabe assumed that the earth pressure under seismic loading would increase proportionally with depth, as for the static case. Thus the lateral force

could be expressed as:

$$P_{AE} = \frac{1}{2} \gamma H^2 K_{AE} \quad (1)$$

where K_{AE} is an earth pressure coefficient for combined gravity plus seismic loading. More recent experimental studies have shown that the seismic component of earth pressure is relatively larger near the top than near the base of the wall so that the line of action of the total lateral force would be somewhat higher than the lower third point. Nevertheless the total gravity plus seismic earth force on conventional retaining walls is apparently well expressed by Eq. 1 where K_{AE} is evaluated by the Mononobe Okabe equations.

As a point of reference for subsequent studies, the Mononobe-Okabe equations were evaluated for the conditions to be used in the later model tests; vertical wall, medium dense sand backfill and horizontal sinusoidal shaking. The predicted location of the failure wedge boundary for various base accelerations are shown in Fig. 1. Note that the wedge becomes flatter with increasing base acceleration. The theoretical values for K_{AE} are shown in Fig. 2, indicating an increase in total earth force with increasing base acceleration.

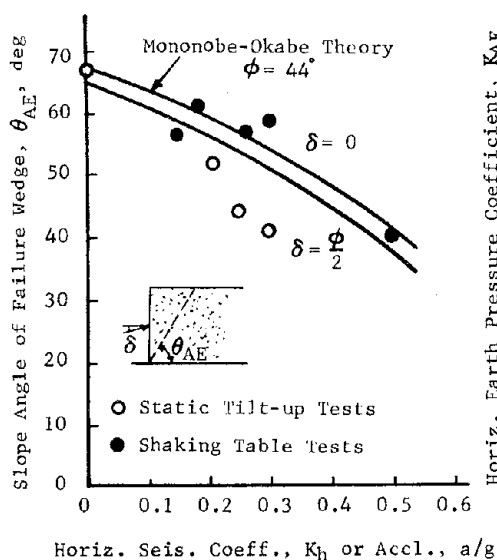


Fig. 1-Theoretical and Measured Failure Wedges

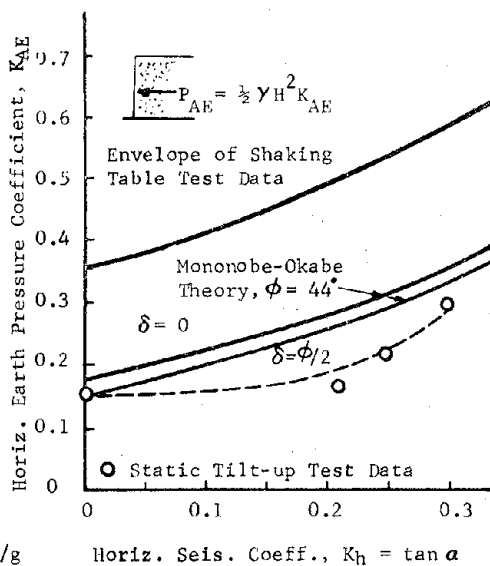


Fig. 2-Pseudo Static Seismic Earth Pressure Coefficients

The effect of a constant horizontal force component can be simulated experimentally by tilting up the rigid foundation of the model test wall. For comparatively small angles of tilt α , less than about 20 degrees,

resolution of the forces indicate that the pseudo static horizontal seismic coefficient can be closely approximated by :

$$K_h = \tan \alpha \quad (2)$$

This suggested that simple tilt up tests might be a useful experimental method of at least developing a gross understanding of the behavior of reinforced earth walls subjected to seismic loading.

Recent studies (7,8) reports the results of a large number of model tests under static loading. The same equipment was also used in the tilt up tests. The bottom of the test box was stiffened, a fixed pivot was constructed at the front, and a hydraulic jack was fixed to the back. The walls were constructed using long narrow aluminum foil strips for ties, and medium dense clean sand backfill, as used in the previous static tests. The wall heights ranged from 11 to 16 in.; and were designed for a minimum static factor of safety against tie breaking of 1.12 to 1.65.

The tests were conducted by slowly jacking up the back of the box, taking readings of relative wall displacement and tie tension force with increasing values of slope angle α . This process continued until the wall failed. After each test the slope of the failure plane was measured and the locations of the broken ties were determined. The relative outward tilt of the top just prior to failure ranged from 1.3 to 2.0 percent of the height of the wall. The measured failure plane inclinations are shown by the open dots in Fig. 1. Note that they are considerably lower than the theoretical Mononobe-Okabe predictions, especially at large values of K_h . As described previously, the failure plane under static conditions was consistently found to be closely defined by the classical equation;

$$\theta = 45^\circ + \phi/2.$$

After failure, the broken ties were consistently found in the upper third of the wall. Unfortunately the tie force instrumentation did not function well, and only a few dots were obtained for the lower ties. However, these data also indicated that the loads in the lower ties were considerably less than the ultimate strength. This is in sharp contrast to the data obtained from the static tests which showed that the tie forces increased in direct proportion to the depth, and tie breaking always occurred first at the lower ties.

The pseudo static total earth pressure coefficients are shown in Fig. 2. These were calculated by back figuring from Eq. 1, and assuming the total strength of the walls to be the same as previously found under static conditions (7). Although the data show that K_{AE} increases with increasing seismic coefficient, the indicated rate of increase is not as rapid as predicted by the Mononobe-Okabe equations.

These tests indicated that the general conclusions which have been reported elsewhere (11) for seismic earth pressure effects on regular walls may also apply in a qualitative sense to reinforced earth walls. In comparison to static conditions the seismic effects lead to a flatter failure plane, larger total lateral earth force, and a distribution of total lateral earth pressure which does not increase linearly with depth below the surface. However, it was realized that the pseudo static analytical and experimental approaches could not be expected to simulate adequately the effect of vibratory loading. Therefore no more tilt up tests were performed and the results of these pseudo static studies were used only in a qualitative sense to supplement the data from shaking table tests.

SHAKING TABLE STUDIES

The response of reinforced earth walls to seismic loading was studied in some detail by subjecting small model walls to sinusoidal vibration from a shaking table. The model walls and the box in which they were constructed were the same as used in the previous static loading study (7). The box was constructed of 3/4 in. plywood and was 30 in. wide. Most of the walls were constructed to approximately 12 inches high, and the backfill extended about 36 inches behind the wall to the rigid back of the plywood box. The sand was placed by slowly raining from a fixed height, layer by layer, as the skin and tie elements were successively added. This resulted in a dry density of 93.5 lb per cu ft, $D_r \approx 63\%$, and plane strain $\phi = 44^\circ$. The lowest skin and ties were simply placed on the floor of the box but were not attached to the box. A large glass viewing part was constructed on one side of the box to give direct visual observations of the wall and backfill deformations. Some colored sand markers were usually placed in the fill adjacent to the window.

The box was rigidly mounted on a shaking table driven by a 5 ton MTS hydraulic ram which could be controlled to any regular sinusoidal varying time and frequency deformation pattern. A photograph of the test set up is shown in Fig. 3.

Instrumentation of the wall included a control accelerometer on the table, another in the backfill, several LVDT gauges to measure the wall deformations, and several special gauges to measure the tie forces at the wall. Because of difficulties experienced in the previous static loading study (7), no buried earth pressure gauges were used and no tie force measurements were attempted at positions other than at the face of the wall. The lateral earth pressures were deduced from the tie force measurements at the wall and the tie spacings. All instruments were connected to Sanborn strip chart recorders. Because of a limited number of recorder channels

available at all times and because of some cases of instrument malfunctions, the actual number of measurements was often somewhat less than the maximum number of gauges mentioned above.

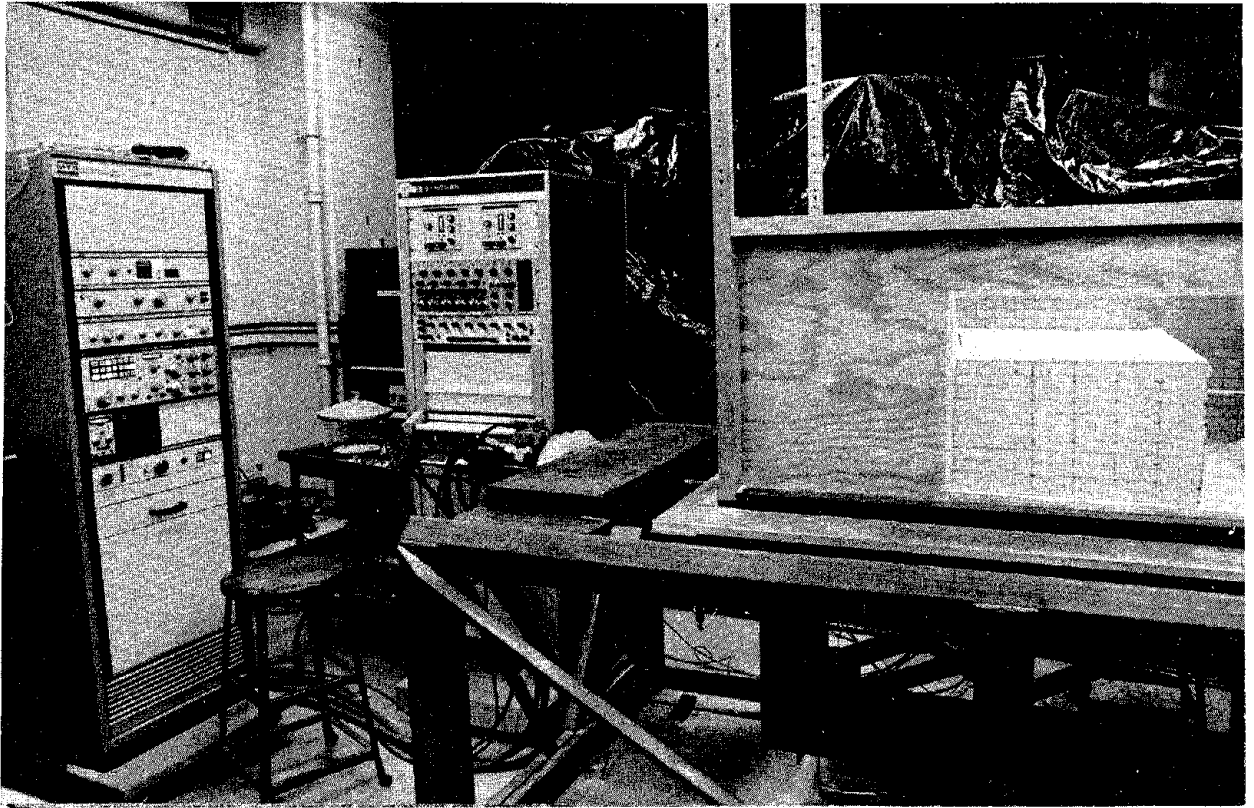


Fig. 3-Photograph of Shaking Table, Control Console and Recorder

The first series of tests were performed with the identical reinforcing materials used for the previous static tests; 1 in. high curved aluminum skin elements and 0.15 in. wide aluminum foil ties. These ties had relatively high soil-tie friction angle, $\phi_v = 31^\circ$, but a relatively weak tensile strength, about 1.1 lb. Thus, they were readily suited for studies of failure by tie breaking. During these tests the walls underwent significant outward movements and deflections before failure finally occurred. Unfortunately, the tie tension gauges in use at that time did not give reliable readings when the walls deformed enough to bend the ties. Thus the tie breaking tests gave only a qualitative and mechanistic picture of the behavior under tie breaking conditions.

The remaining tests were performed using an improved tie tension gauge, and ties which had a high tensile strength, 10 lb, but lower soil-tie friction angle, about 25° , so that when wall failures occurred it was by the ties pulling out of the sand fill. These ties were strips of 0.25 in. wide mylar magnetic recording tape.

Most of the tests were performed using one vibration frequency of

11.6 Hz . The amplitude of table movement was adjusted to give the desired base acceleration which was kept constant for each test. For the entire program, the base acceleration ranged from about 0.05g up to about 0.5g.

FAILURE MECHANISM UNDER VIBRATORY LOADING

Some of the time history records of a typical tie breaking test are shown in Fig. 4. In this test the input base acceleration was slowly increased until the wall failed. The lower two records show the table and the sand surface acceleration. Note that there is some amplification between the base and the top of the backfill. The two middle records show the relative deformations near the top and near the base of the wall, measured with respect to the rigid base of the box. The upper three records shows the tensile forces measured in a ties located in the lower third of the wall.

A study of these test records shows that during most of the vibratory loading, the top of the wall moved out progressively at a fairly uniform rate, much faster than movement at the lower part of the wall. The tie forces oscillated at a fairly constant amplitude increasing with duration of shaking and input acceleration.

Finally, when the input acceleration reached about 0.22g the force in the middle tie suddenly dropped momentarily, indicating a readjustment someplace in the backfill. Then all three tie forces began to increase rapidly, and within a few cycles the records at the lower two ties went off scale momentarily, and then dropped to near zero. The bottom of the wall then suddenly moved out well beyond the scale of the recording instrument. The ultimate load capacity of a tie was about 590 gms. and it is clear that these two ties failed. The stress in the third tie was relieved by the sudden large wall movements. Examination of the ties within the fill indicated that they had broken near the wall. In addition, a shear plane had developed in the backfill.

Several tests were performed to study the behavior under different base accelerations. In every case where the failure occurred by tie breaking, a similar deformation behavior was observed. This is illustrated on Fig. 5a which shows the observed deformed shape of the walls at various stages beginning from the static condition at t_0 , up to failure at t_5 . As the shaking started the wall began to rotate out as a plane about the toe. The rate of rotation was roughly proportional to the input base acceleration. Plane rotation continued until the top of the wall had moved about $\frac{1}{2}$ in. at which time movement at the top almost ceased, and outward movement near the base of the wall began to increase rapidly. Within a few cycles a distinctly visible bulge had developed in the lower part of the wall, and this was followed by a quick and complete collapse. For most tests,

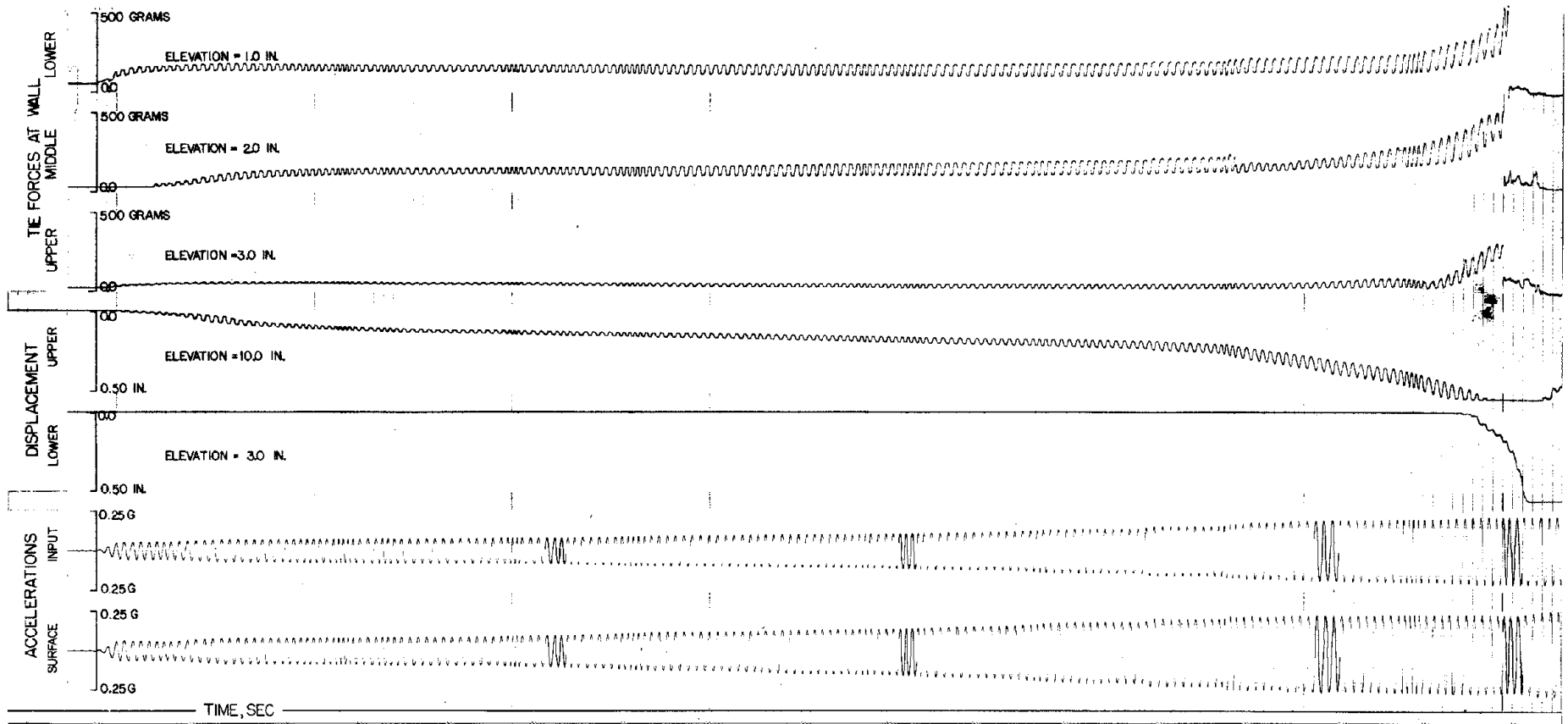


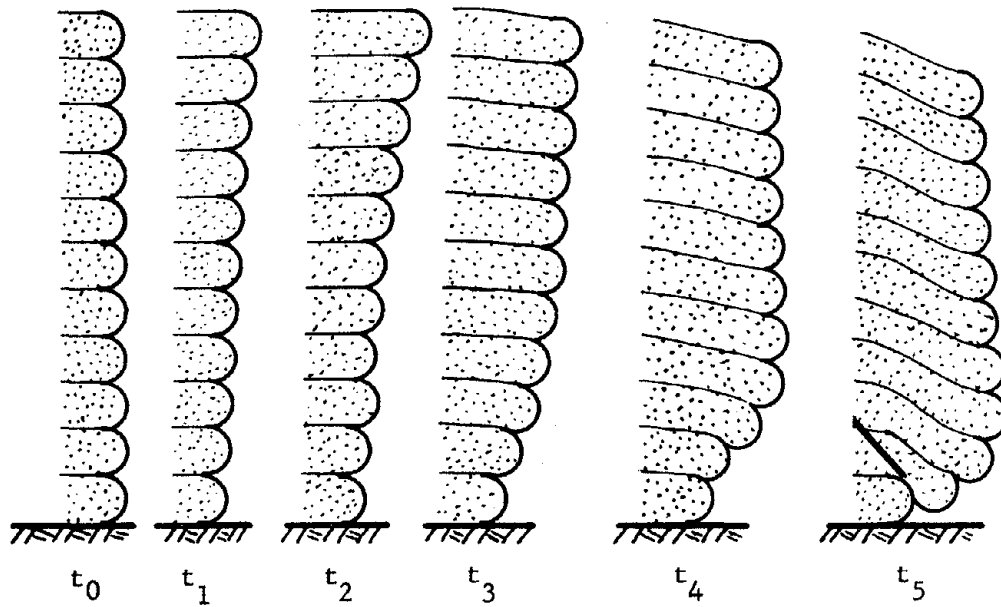
Fig. 4-Laboratory Record : Tie-Failure Test

blocks were provided to prevent excessively large movements beyond failure, so as to preserve the conditions at small strains after failure had occurred. In this way it was possible to identify that failure had occurred when the 2nd and 3rd ties from the bottom had broken, and this led to the formation of a failure plane through the backfill. In cases where the supports were omitted, the failure was always a catastrophic collapse with the skin elements breaking up and the sand backfill flowing out until it reached its angle of repose.

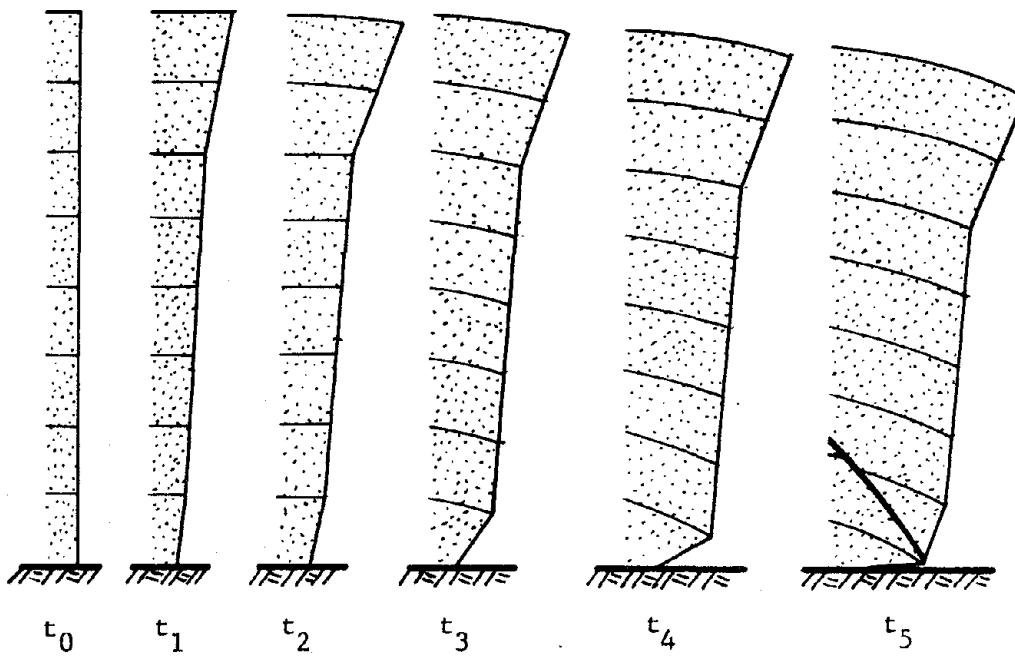
The wall design was changed slightly for the tie pullout tests. The 1 in. high curved skin elements were replaced by 1½ in. high flat thin sheets of aluminum. The weak but frictional aluminum foil ties were replaced by strong and smoother magnetic recorder tape. The sequential wall displacements consistently observed in these tests are shown in Fig. 5b, beginning with the initial static condition at t_0 . Initially the largest wall movements were at the surface, but after a short time the entire wall began to move out almost uniformly, except for the lowest skin element which rotated as if attached to the base. (The only attachment was friction of the lowest ties.) This deformation pattern continued for as long as the shaking lasted. Observations from many tests indicated that the rate of movement was approximately proportional to the base acceleration and decreased with increasing length of ties. If shaking continued long enough, the lowest skin element rotated a full 90 degrees to lay flat on the floor of the box, and then the same movement pattern continued with the next higher skin element rotating, and so on. If at any time the shaking were stopped, the wall was found to be stable and sufficiently strong to support a heavy weight applied to the backfill. Thus the walls invariably behaved in a ductile manner, and a complete catastrophic type failure was never observed.

In some tests a shear plane was observed at the end of the test, but only after very large deformations had developed. A sketch of the observed movements of marker dots in the sand backfill for one such test is shown in Fig. 6. Note that there had been considerable permanent movement at all locations even before the failure plane had developed.

As a result of these failure mechanism observations, it was concluded that reinforced earth walls should always be designed for a lower factor of safety with respect to tie pull out than for tie breaking. Then in the unfortunate event of overstressing from the effects of a large earthquake, the wall would deform in a ductile manner by yielding a small amount with each strong cycle of load, rather to develop a sudden complete collapse under one strong load pulse.



(a) Failure by Ties Breaking



(b) Failure by Ties Pulling Out

Fig. 5-Observed Failure Mechanisms

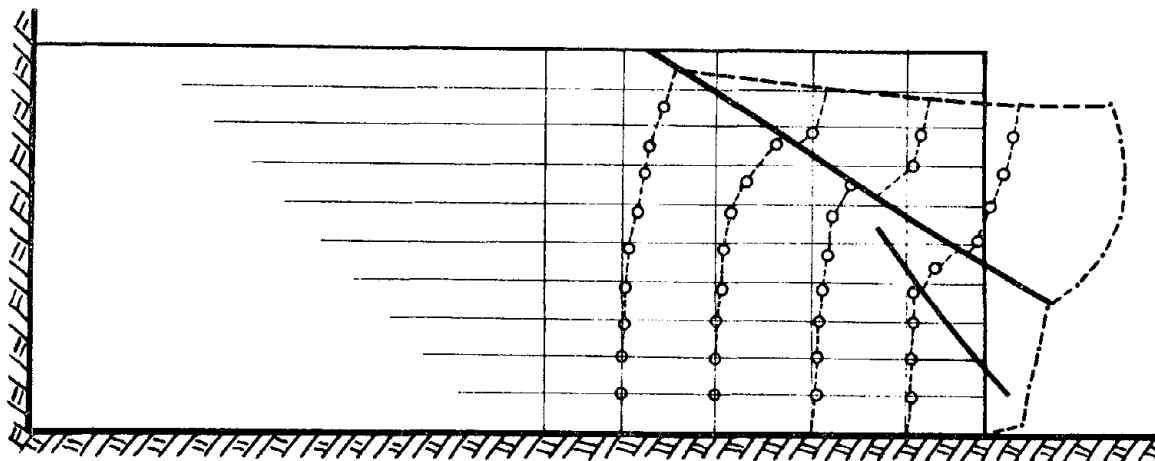


Fig. 6-Observed Deformations in the Sand Backfill at Failure

The next priority items to be studied were the soil-tie frictional strength, and the tie forces developed under seismic loading conditions. The important problem of rate and amount of progressive deformation has not been studied thus far. It is felt that useful results can be obtained following a double integration method of the acceleration time history as has been previously used by Newmark (9) and Goodman and Seed (3).

SOIL-TIE FRICTIONAL RESISTANCE

The soil-tie friction angle ϕ_v reported by Lee et al. (7) was determined by sliding a large, sand weighted sheet of the aluminum foil over a sand base. The studies reported herein used mylar magnetic recorder tape for all tie pull out wall designs. The soil-tie frictional characteristics for this tie material were determined by pulling out selected free ties which had been buried in the sand backfill during construction of actual test walls. Test ties were all 12 in. long. They were located at several depths below the surface, and at three lateral positions: adjacent to the wall; middle of the backfill; and adjacent to the back of the wooden box. For the middle locations, the portion of the tie extending to the outside of the box was insulated from the sand by a small tube.

The tests were performed by pulling on the tie at a constant rate while measuring the developed load and deformation. A typical test record is shown in Fig. 7. Note that there is a quick smooth rise in a pull out force to a peak value which occurs at a very small deformation. Continued pulling beyond the peak results in a considerable amount of stick-slip chatter, with a slow but steady reduction in load to a low residual value.

Tests were performed under three conditions: as constructed (static); during light shaking ($a = 0.05g$); and aftershaking (static). Similar load deformation curves were obtained in all cases with a weakly observed

tendency for the peak to develop earlier for the static tests than for the dynamic tests. However, in all cases the peak developed before the 12 in. long ties had pulled out $\frac{1}{2}$ in. A fairly steady residual load had developed after about $1\frac{1}{2}$ in. pull out. Further reduction beyond this represented the decrease in contact length.

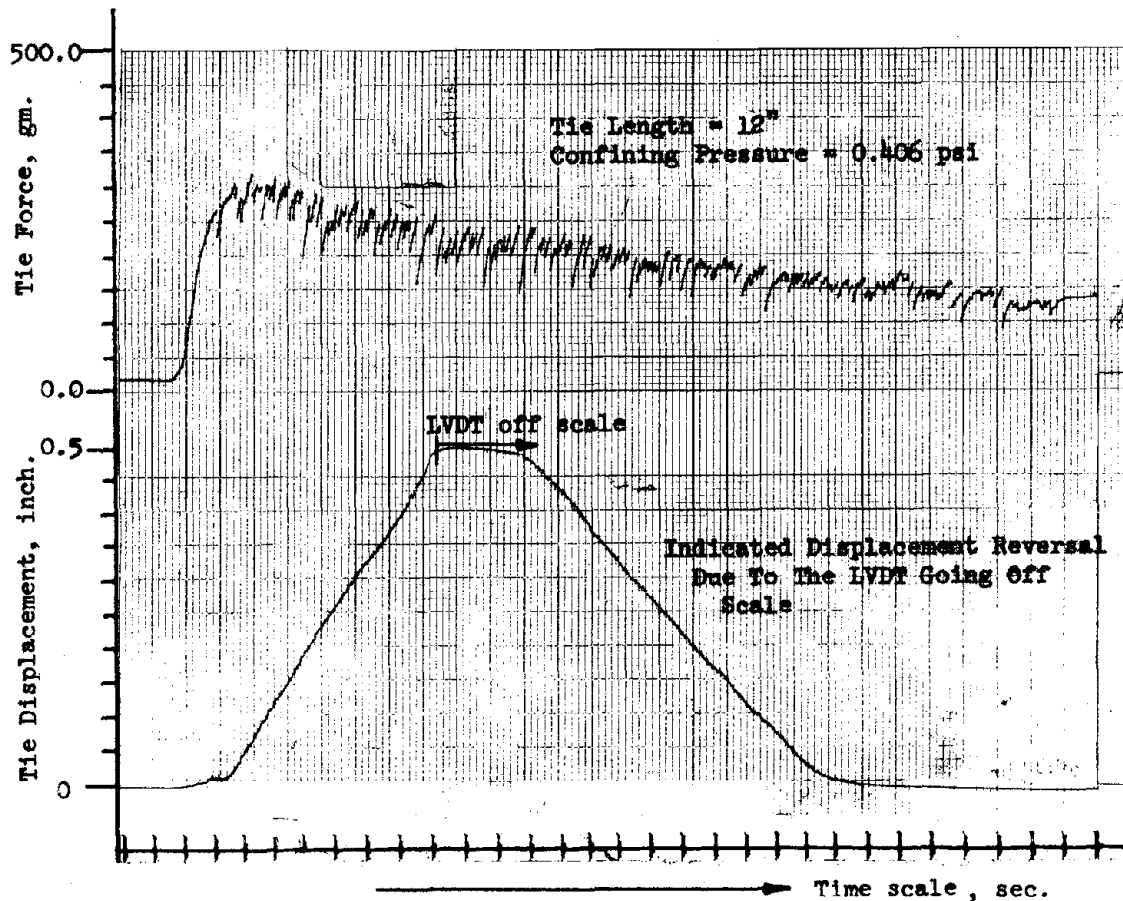


Fig. 7-Record of Pullout Test to Determine Tie Friction

The results of these tests are conveniently expressed in terms of peak and residual normal and sliding stress on the soil-tie interfaces as shown in Fig. 8 for the middle-of-the-box tests. Note that there is a fairly large scatter in the data, especially for the peak conditions. Similar data with a similar amount of scatter were also obtained for the other tests pulling out from the wall face and the back of the box (10). No consistent pattern was found in the scatter, and no completely satisfying explanation was found for it.

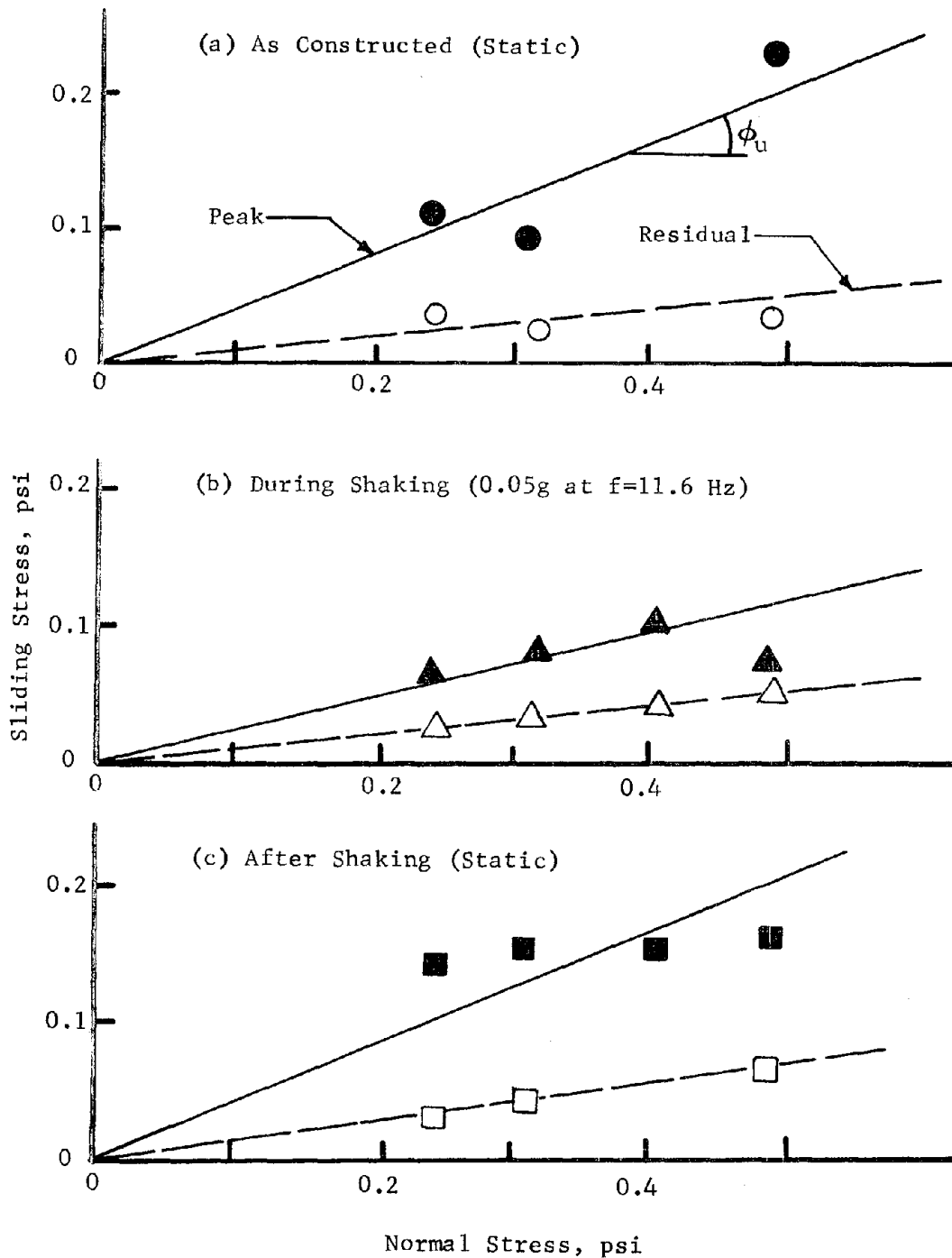


Fig. 8-Results of Tie Pull Out Tests from Middle of Box

Approximate best fit straight lines were drawn by inspection through each set of data to define the soil-tie friction angle. These data are summarized in Fig. 9. Note here also that there is either a peculiar variation, or scatter in the average peak values of ϕ_u , as compared to the fairly consistent residual values.

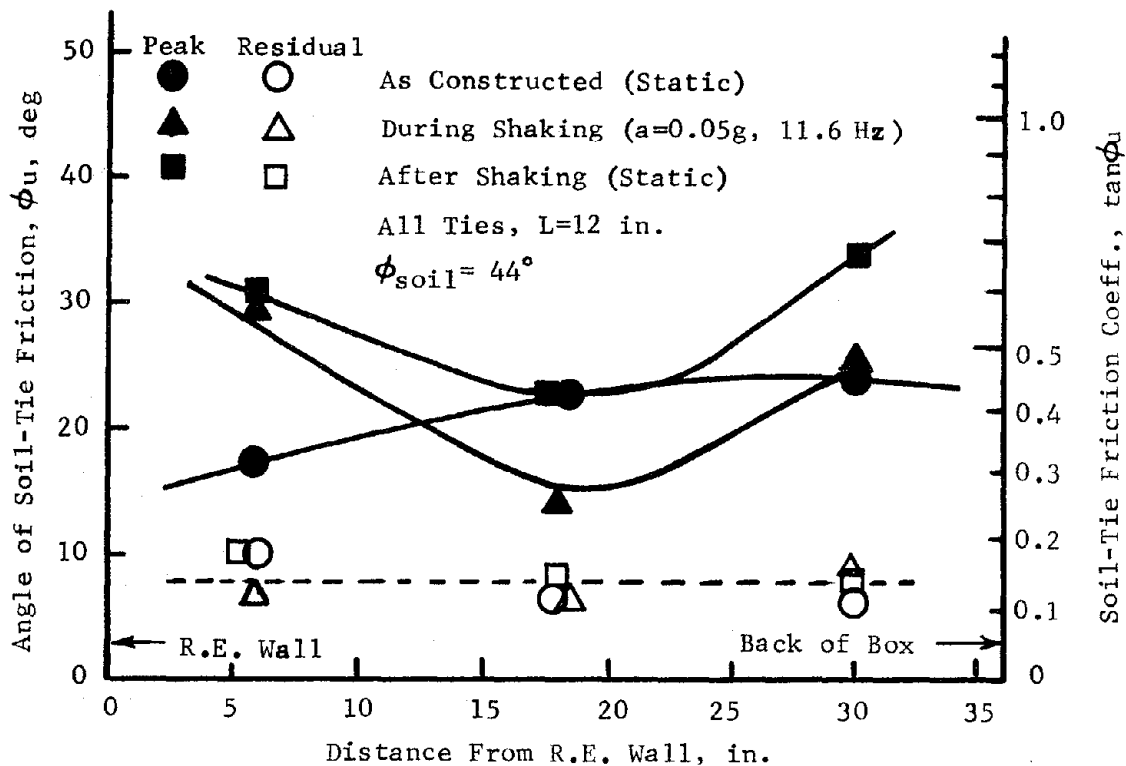


Fig. 9-Summary of Soil-Tie Friction Data

There was a considerable reduction in frictional resistance going from peak to residual. This reduction was not observed in the former tests performed by sliding a large sheet of reinforcing material over the sand. The low residual frictional resistance of the narrow ties suggests the existence of a stress arch in the sand around the ties which prevents the full overburden pressure from developing once the original frictional bond has been broken.

It is of interest to note that similar scatter, and comparatively low residual strengths were also observed in tie pull out tests performed on a full scale Highway 39 wall under static conditions (1). This led the authors of that study to recommend a factor of safety of 4.0 for designs against tie pull out where the factor of safety is based on the peak measured values of $\tan \phi_u$. Reference to Fig. 9 indicates that for these data this would be approximately equivalent to using a factor of safety of 1.0 on the residual pullout strength.

The pull out tests performed thus far during vibratory loading were limited to vibration accelerations of only 0.05g. It was observed that for the vibration frequency used (11.6 Hz) this appeared to be a threshold value marking the limit where measured tensile forces in the tie showed a significant seismic effect. However, it is realized that more work is required to more completely define the soil-tie frictional characteristics under various static and seismic loading conditions.

MEASURED TIE FORCES

Tie forces developed at the wall face were measured at various ties by means of small and light weight specially constructed load cells. Data obtained from one typical test are shown in Fig. 10. Tie force measurements made during construction are shown by the open dots. Note that the forces build up progressively with increasing height of backfill.

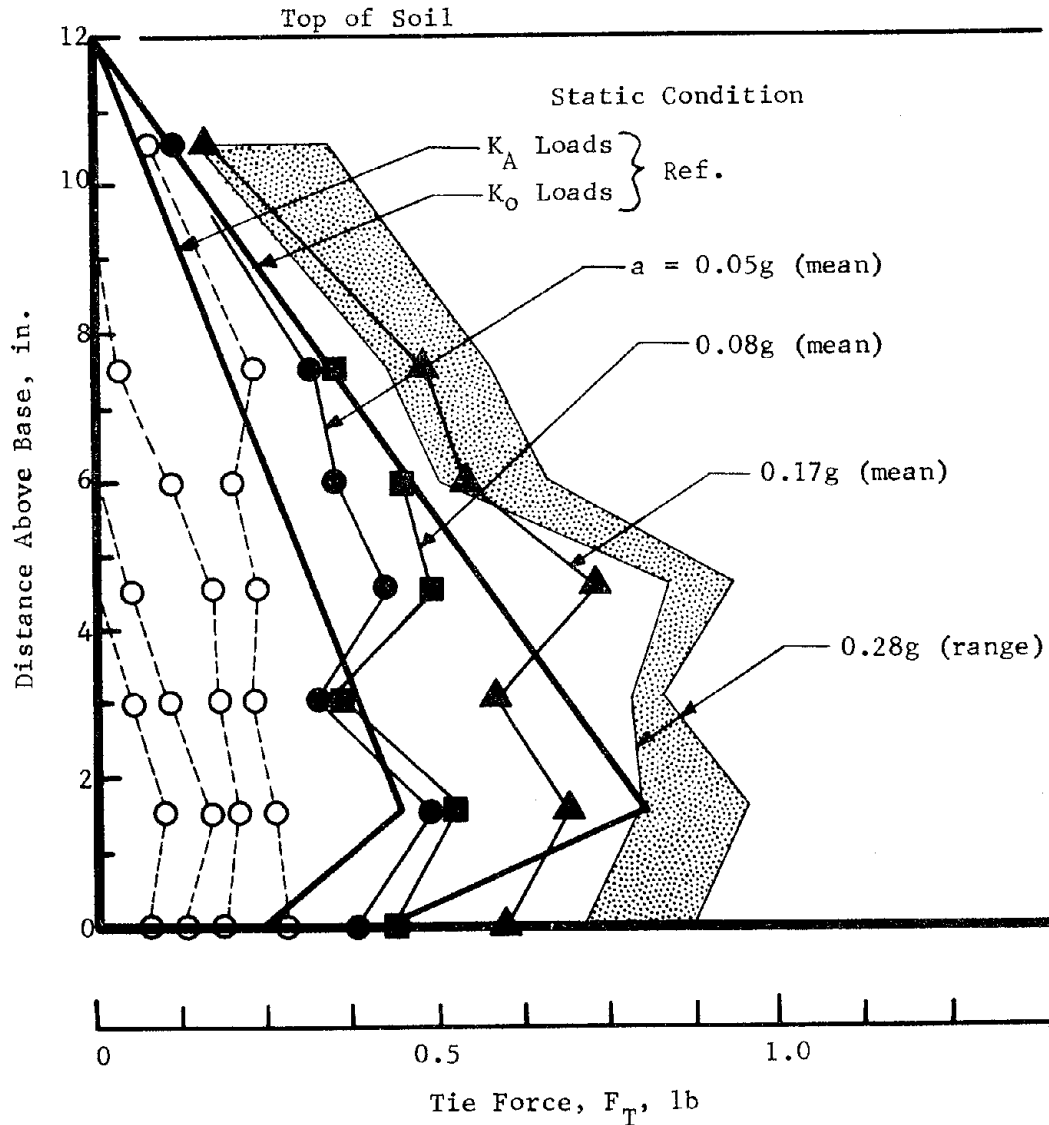


Fig. 10-Measured Tie Forces for Various Accelerations

For reference, the calculated distribution of tie forces, assuming an active Rankine or an at-rest linear earth pressure distribution, is shown by solid heavy lines. These calculations were made assuming:

Active Rankine: $\sigma_h = \gamma h K_A$ (3)

At-rest: $\sigma_h = \gamma h K_0$

where $K_A = \tan^2 (45 - \phi/2)$ (4)

$K_0 = 1 - \sin \phi$ (5)

and h is the depth below the surface of the sand. The tie force is found from

$$F_T = \sigma_h T_A \quad (6)$$

where T_A is the tributary area or area of the wall which must be supported by the tie. The theoretical line of tie force distributions calculated from Eq. 6 have a kink at the last tie above the base because T_A for the lowest tie (on the floor of the box) is only half the value of T_A for the other ties. Note that the measured maximum static as constructed tie forces are approximately defined by this theoretical K_A line.

Other tests gave similar results (10) except that there was usually more erratic scatter in the data from tie to tie and from test to test than indicated by the static data on Fig. 10. It was felt that this scatter related to such things as localized pre-stress induced at various individual ties during construction or possible effects of inflexible skin elements. In some zones the measured forces were less than the K_A line, but the location of these zones varied erratically from test to test. The maximum measured tie forces never exceeded the K_A line by more than the small amount shown in Fig. 10. In these respects the static construction tie forces are similar to that obtained in earlier studies (7).

An example of the dynamic variation in tie forces during a typical vibratory loading has been shown in Fig. 4. The forces varied sinusoidally with time about some mean value. In tests when the vibrations were stopped before failure, the residual tie force at-rest was approximately equal to the mean of the range of tie forces developed during the vibratory loading.

Values of the mean vibratory tie forces developed in a typical test at different levels of base acceleration are shown by the solid data points on Fig. 10. The range of tie forces developed for the maximum acceleration used on this wall (0.28g) is shown by a shaded area. These data are typical of all the tests performed. Taken together the data lead to several tentative conclusions.

The tie forces increase with increasing accelerations. The earth pressure at rest or K_0 line is an approximate envelope for the stresses developed at a $\approx 0.05g$. It is recalled that the static construction procedure involved raining the sand into place with careful attention to avoid any vibration or localized wall disturbance. However in the field there will always be some vibrations or other disturbance due to construction. Also in seismically active areas, accelerations as low as 0.05g may be anticipated fairly frequently. Thus the data suggests that static designs be based on an at-rest linear earth pressure increase with depth. This is in agreement with the recommendations based on recent field measurements

on the 50 ft. Highway 39 wall.(1).

The measured seismic tie forces also show a somewhat erratic variation superimposed on an overall increase with increasing depth, but being greater than zero at the ground surface. The patterns shown in Fig. 10 is typical of all the tests although the erratic nature of the scatter varied from test to test. Combining the diagrams of measured seismic tie forces, indicated that for each base acceleration the maximum tie forces at different locations could be conveniently defined by a simple linear envelope which had a non zero value at the ground surface and increased linearly with depth. Converting these maximum expected tie force envelopes into lateral pressures by Eq. 6 led to a simple relation between maximum expected lateral earth pressure and input acceleration. This envelope and the scaling factors for different input accelerations are shown in Fig. 11. This envelope is tentatively recommended as a basis for estimating the maximum probable tie forces in a reinforced earth wall during vibratory loading.

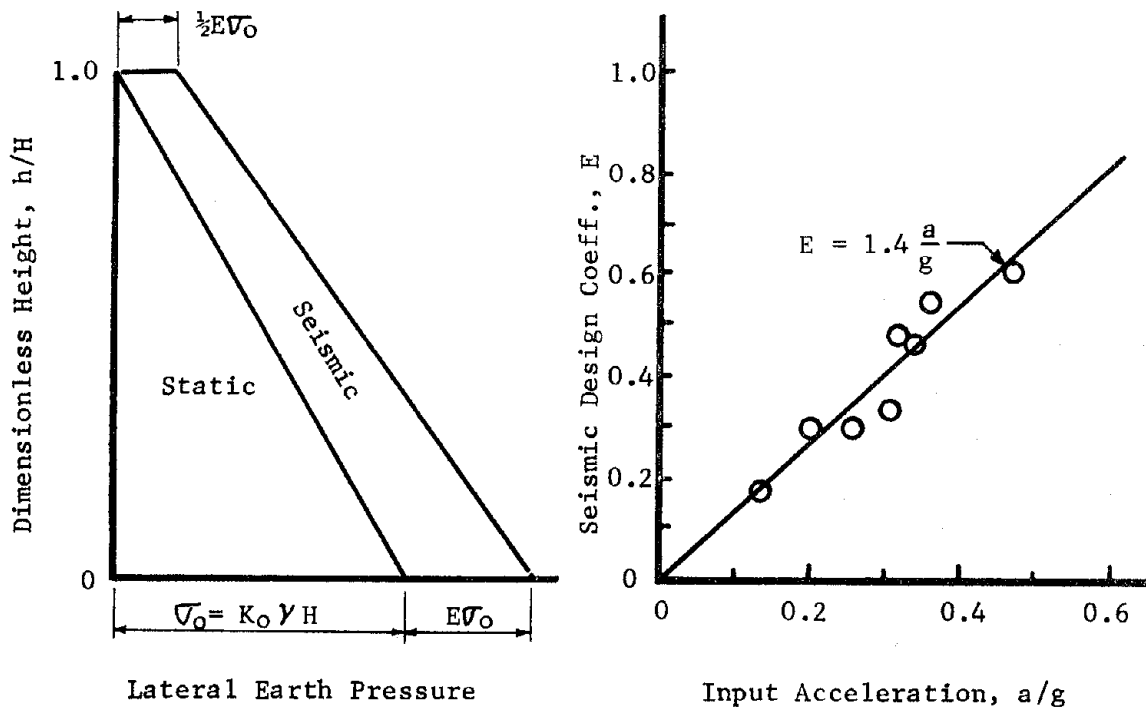


Fig. 11-Envelope of Maximum Seismic Earth Pressures

As a side consideration, the total static plus dynamic forces indicated by the envelope in Fig. 11 were calculated for several input accelerations, converted to an equivalent horizontal earth pressure coefficient K_{AE} by Eq. 1 and plotted on Fig. 2. The values are considerably larger than measured by the static tilt up tests, or calculated by the pseudo static Mononobe-Okabe equations.

INFLUENCE OF VIBRATION FREQUENCY

The model shaking table tests described thus far have been performed using various input base accelerations; all with a 12 in. high wall and a vibration frequency of 11.6 Hz. These studies indicated, as shown in Fig. 4, that there was some magnification of acceleration between the top and the bottom of the sand backfill. This magnification was greatest at the wall face and decreased towards the back of the wooden box. The amount of magnification varied with increasing base acceleration, which indicated that the soil backfill was not behaving linearly.

To further investigate the dynamic response of this model reinforced earth system, a 15 in. high wall was constructed and subjected to a wide variation of base accelerations and frequencies. An accelerometer set in the sand near the fill surface, and 8 in. behind the wall was used to indicate the magnification at that location. In addition, a sensitive LVDT was used to measure the vibratory amplitude of the wall relative to the base.

A series of tests were conducted, each at a different constant base acceleration, but using different frequencies. The results are shown in Fig. 12. Note that at every level of base acceleration the wall responded as a damped single mode elastic oscillator, giving a well defined frequency distribution curve. Spot checks indicated that data points were quite reproducible even after several other tests at different conditions. The only difficulty encountered was some background noise from equipment harmonics which tended to enter in some cases at frequencies ranging between about 15 and 19 Hz. This may have slightly influenced some of the data points in this range.

An ideal system with linear elastic and damping properties would be expected to show one unique magnification curve, independent of the input acceleration. However, as might be expected from the wealth of data available on sand (11), the different response curves for different levels of excitation indicate definite non-linear characteristics. The higher base accelerations cause higher stresses and strains as indicated in Fig. 12b. The frequency response characteristics indicated in Fig. 12a follow qualitatively the well-known trend for sands that increasing strains leads to decreasing modulus and increasing damping.

Quantatively, an estimate of the variation in modulus and damping at different acceleration levels in these tests may be made by comparing the results with ideal theory. For medium to low damping the critical damping ratio λ , may be approximately computed from

$$\lambda \approx \frac{1}{2 MF} \quad (7)$$

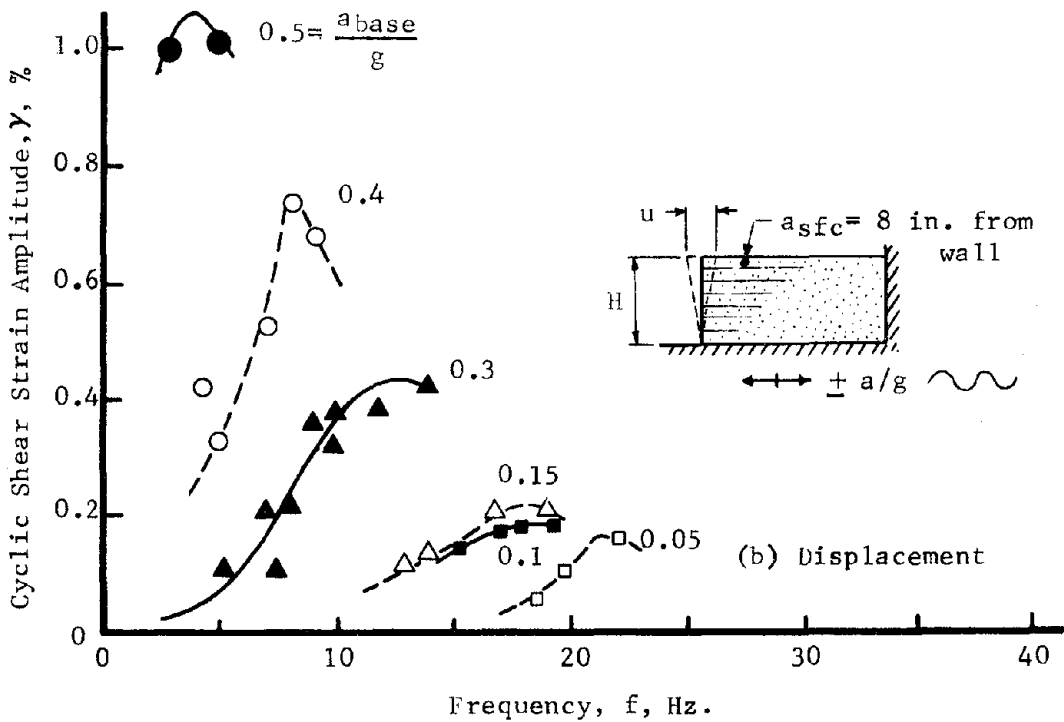
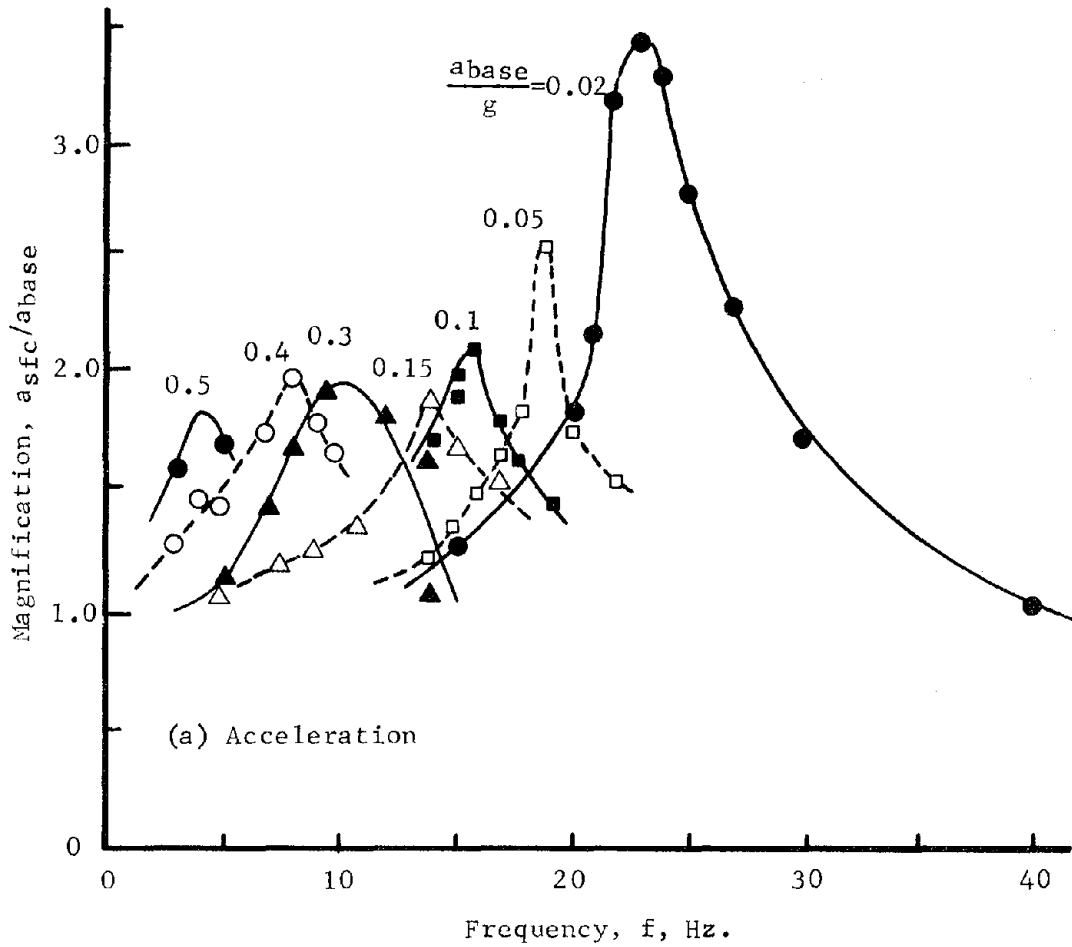


Fig. 12-Resonance Response of Model Reinforced Earth Wall

where MF is the magnification factor which may be defined as the ratio of the surface to base acceleration at resonance (13). From wave propagation theory the shear modulus G, at resonance may be computed from (5)

$$G = \frac{16 H^2 \rho}{T^2} \quad (8)$$

where ρ is the mass density of the soil, H is the thickness and T is the fundamental period of the layer.

Both T and MF are well defined in Fig. 12 for each different base acceleration so that G and λ can be computed directly from Eqs. 7 and 8. The shear strain at resonance was measured for all but the lowest base acceleration, and it was estimated by extrapolation to be about 0.08%. Thus the variation between modulus, damping and shear strain was readily obtained.

For calculation purposes, it has been found convenient to express the dynamic shear modulus as a function of mean normal stress σ_m and a coefficient K_2 (11).

$$G = 1000 K_2 \sigma_m^{\frac{1}{2}} \text{ psf} \quad (9)$$

Following this procedure the calculated shear modulus factor K_2 , is shown as a function of shear strain amplitude in Fig. 13a. The damping vs. shear strain is shown in Fig. 13b. Also for reference the range of data suggested by Seed and Idriss (11) for sand at this density ($D_r \approx 60\%$) is also shown. The damping data fall within the Seed-Idriss range, but the K_2 data are much lower. This discrepancy is probably due to the extremely low confining pressure involved in these model tests as compared to that for the usual studies, and would not be expected to be found in an actual full scale wall.

FINITE ELEMENT ANALYSES

A limited number of finite element analyses have been performed thus far in this overall study. The Berkeley computer program QUAD-4 (6) which includes strain dependent modulus and damping, was modified to include elastic tension-compression bar elements for the reinforcing (QUAD4B). The 12 x 36 in. long sand box was modeled by 64 elements, 1.5 in. high corresponding to each strain element and construction layer. The element lengths ranged from 3 to 6 inches. The bottom and back of the box was assumed to be rigid. Horizontal bar elements were placed between each nodal point along the lengths of the actual tie elements in the model tests. The density of the soil, and the stiffness of the reinforcing bar elements were made equal to the actual measured values. The input base motion was a sine wave at a frequency of 11.6 Hz and maximum acceleration of 0.1g.

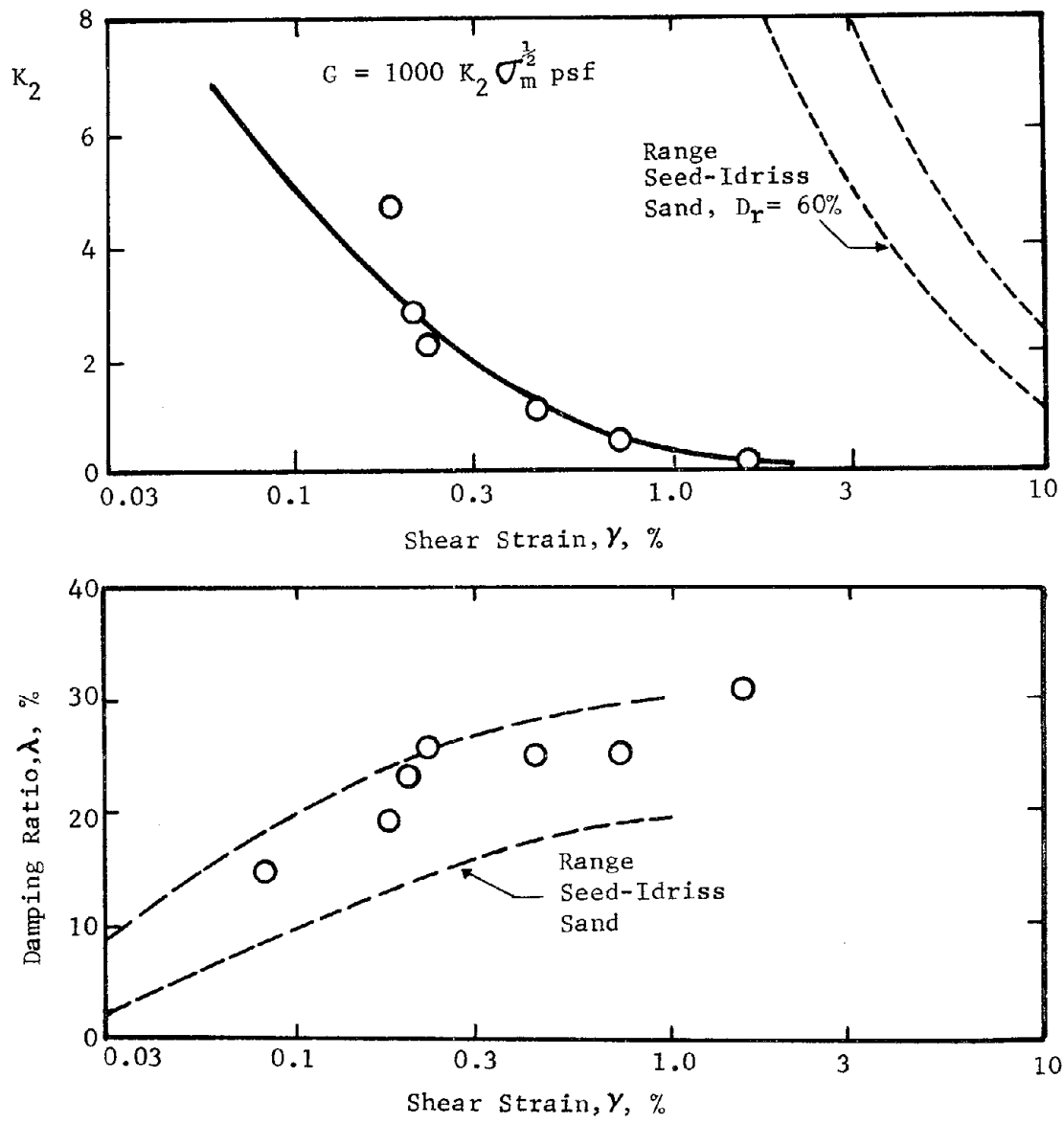


Fig. 13-Dynamic Modulus and Damping from Shaking Table Tests

Three analyses were performed and the results are shown in Fig. 14. The first analysis used the Seed-Idriss (11) strain dependent modulus and damping relations built into the program. The calculated stresses were much lower than indicated by the measured data, and the calculated average damping indicated after iteration to convergence was only about 2.8%. The second analysis reduced the maximum value of K_2 by a factor of 10 and initial estimate of damping 16%, and allowed the program to iterate to an approximate convergence. The calculated tie forces were much larger than for the first case and much closer to the actual envelope of maximum measured tie force envelope, but the final damping after iteration was only 3.1%. The final case used only one iteration with $K_2 = 5.4$ and damping set to 18%. These data corresponded approximately to the measured data shown in Fig. 13. The maximum calculated seismic tie forces for this trial were reasonably close to the measured peak force envelope.

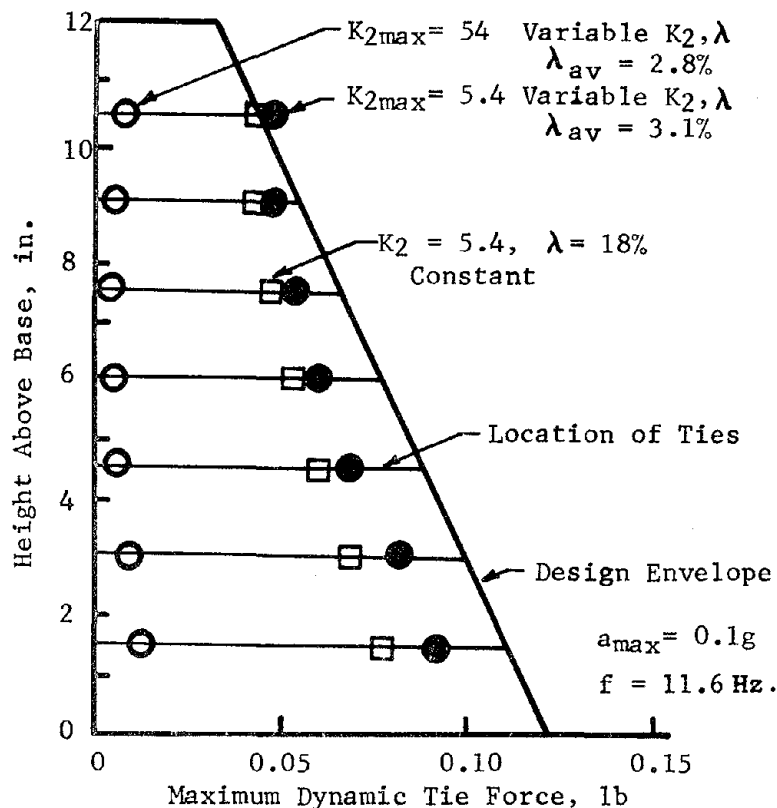


Fig. 14-Results of Finite Element Analysis of 12 in. Wall; Maximum Seismic Forces Only

The results of this study suggest that if modulus and damping factors for the sand backfill are reasonably well known, the QUAD4B computer program will predict fairly accurate tie forces. However, the calculated tie forces are quite sensitive to the soil properties, especially the dynamic shear modulus and therefore unless correct values are used, including the non-linear strain effects, inaccurate values are likely to result. Although the measured shear modulus data did not agree well with the Seed-Idriss curves because of the great differences in confining pressure, there is no reason to believe that the published curves should not be adequate for full scale structures.

A final comment on the results of finite element analyses is that the results consistently showed the seismic component of tie force at the lower ties to be a maximum at the wall, and to extend back only a short distance into the soil. For successively higher ties the distribution of seismic tie forces extended further back from the wall. For the upper ties the maximum tie force was located some distance into the backfill and was up to 100% greater than at the wall. The calculated variation of acceleration along the ground surface agreed reasonably well with the measured data.

DESIGN PROCEDURES FOR AN ACTUAL EARTHQUAKE

All of the data and comments thus far have applied only to a continuous sinusoidal input base acceleration. Design for earthquake loading poses the additional complication of erratic dynamic motion. At this writing, two possible methods are suggested to calculate the maximum tie forces to be used for design. One method is direct calculation by the QUAD4B computer program using the Seed-Idriss non-linear strain dependent modulus and damping properties. An alternative method is to use the seismic design envelope shown in Fig. 11 in conjunction with a single design acceleration obtained from response spectra and modal analysis techniques. Since response spectra for actual earthquake motions, and artificial design spectra are frequently published, the response spectra modal analysis technique probably will not require a computer and therefore may be preferred in many cases. Both methods are illustrated by an example design of a 21 ft. high reinforced earth wall with a 2 ft. surcharge.

The design earthquake selected for this illustrative example was an artificial accelerogram shown in Fig. 15a having a duration of 15 sec. and a maximum acceleration of 0.2g. An acceleration response spectrum was calculated from this motion for 12 percent of critical damping and is shown in Fig. 15b. This damping was chosen as being representative of the damping expected in a sand fill, and corresponds to the average damping from the seismic finite element analysis which was also performed.

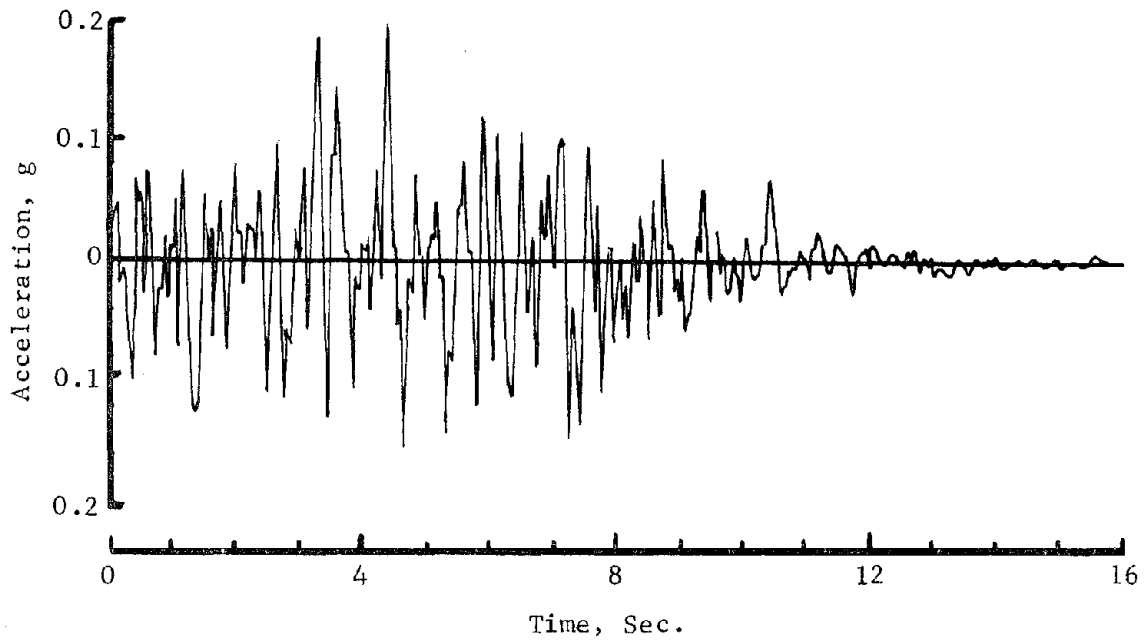
To use the design envelope technique on Fig. 11, it is necessary first of all to obtain a value for design acceleration for this earthquake motion. This is done using the response spectra on Fig. 15b and modal participation factors (2,4). The modal participation factors Γ_n are calculated from structural analysis techniques and represent the contribution of each modes to the total maximum earthquake forces acting on a structure.

For this analysis the soil backfill was assumed to be represented by 10 lumped masses, making a total of $n = 10$ possible modes. However, since the effects of the higher modes are small, only the first two modes were considered. The calculated modal participation factors for this lumped mass idealization were $\Gamma_1 = 1.25$ and $\Gamma_2 = 0.5$. The overall single value of design acceleration was therefore

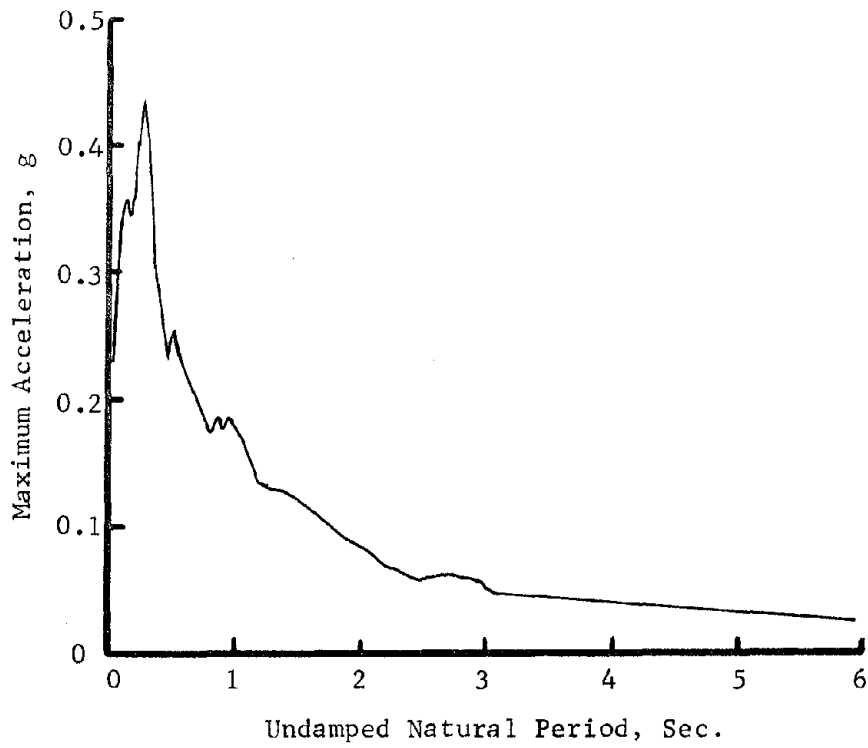
$$A_{des} = 1.25 S_{a1} + 0.5 S_{a2} \quad (10)$$

where S_{a1} and S_{a2} are the values of spectral acceleration for the periods corresponding to the first and second modes.

From wave propagation theory, the fundamental or first mode period of vibration for a layer of soil is given by rearranging Eq. 8. Using realistic



(a) Accelerograph



(b) Acceleration Response Spectra

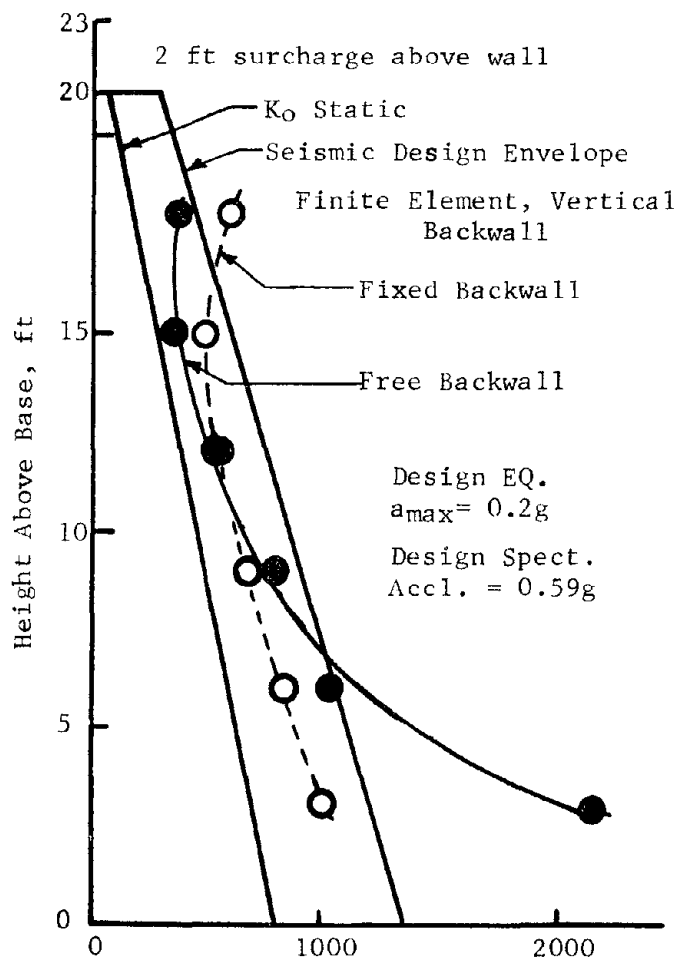
Fig. 15-Earthquake Motion Used for Design Example

values of shear modulus for medium strain levels given by Seed and Idriss (11), as well as results calculated from QUAD4B, for various cases, it was found that the first period of a reinforced earth backfill with a level surface would usually be within the range

$$T_1 = (0.006 \text{ to } 0.10) H \quad (11)$$

when T_1 is in units of seconds/cycle and H is height of backfill in ft. From wave propagation theory (5), it follows that the second mode period will be $T_2 = T / 3$. For design purposes it is recommended to use S_{d1} and S_{d2} equal to the maximum spectral response values within these respective period ranges.

Based on these considerations, and reference to Fig. 15b, the first two spectral accelerations are 0.38g and 0.22g, and the design acceleration is therefore 0.59g. Entering Fig. 11 leads to the required numerical values for the factors to construct the design static plus seismic earth pressure diagram shown in Fig. 16. Using this diagram and the appropriate tributary areas for any desired tie spacing, Eq. 6 leads directly to the maximum design force in each tie.



Static and Seismic Lateral Earth Pressure, psf
 Fig. 16-Results of Finite Element and Simplified Spectral-Modal Analysis for 21 ft wall

As an alternative approach a direct calculation was made of the tie forces using the computer program QUAD4B with the time history accelerogram on Fig. 15a and the unmodified Seed-Idriss modulus and damping factors. The finite element arrangement assumed a rectangular backfill section of the same relative shape as used in the model tests. In an actual case the backfill will likely be sloping, and have a rigidity somewhere between rigid rock and soft soil. Thus two finite element calculations were made. One with the back boundary assumed to be rigid and moving with the level rigid base, and a second with the back boundary assumed to be free.

The program QUAD4B gives only the seismic components of the tie forces. The total design requires these to be added to the static K_0 components. When this is done, the total tie forces can then be reduced to equivalent lateral earth pressures. These calculated data are also shown in Fig. 16 where they can be compared directly with the design envelope.

Only in special cases such as bridge abutments would the assumption of a free back boundary be valid. Furthermore the design force envelope was not developed for a free back boundary. In most cases, the back boundary would more likely approach a fixed condition where the results from the two design methods are in fairly good agreement.

SPECIAL DESIGN CONSIDERATION

In addition to calculating the maximum tie forces, it is necessary to decide on the tie size, spacing, and lengths, all of which requires use of an appropriate factor of safety. Of course the skin elements must be designed, allowance must be made for possible corrosion, and the foundation stability must also be checked. Space permits only a few comments dealing with dimensioning and factors of safety for the tie designs. Further details are available elsewhere (10).

Failure by tie breaking is prevented by using ties and connections sufficiently strong to resist the design forces including a safety factor. If mild steel is used for the ties, a safety factor of 2.0 on the yield strength seems appropriate to assure safety against tie breaking or connection failure. This automatically includes an additional hidden factor of safety of about 1.9 on the ultimate strength. Failure by tie pull out is prevented by providing sufficient horizontal surface area. A factor of safety of 4 on the peak soil-tie sliding friction coefficient is suggested. This recommendation includes consideration of the several features of reinforced earth behavior described herein. It is not exactly clear what portions of the ties may be effective in resisting the pull out forces. However, based on the observed response of the model walls, it is recommended that the effective length of the ties be measured for an assumed

failure plane which slopes at 60 degrees from the horizontal. If the actual seismic failure plane is somewhat flatter, this may lead to a little more actual deformation during an earthquake, but not to a catastrophic collapse.

It is important to note that two governing design considerations must be satisfied at every level of ties; pullout and breaking. It is doubtful that a truly balanced design will be practical at all levels. In general, the design of the lower ties will be governed by tie breaking considerations. The design of the upper ties will be governed by tie pull out resistance, and these will be affected most by the effects of seismic loading.

An indication of the importance of seismic loading to the cost of a reinforced earth project was estimated from the quantities of reinforcing materials required for the static and the seismic design of the 21 ft. high example wall. The quantity of steel tie material required for the seismic design was about twice that required only for static loads. However, considering the total cost of soil, skin, ties and labor, this would amount to an increase in total job cost of about 15 to 20 percent.

CONCLUSIONS

Observations and analyses of the behavior of reinforced earth retaining walls under laboratory seismic loading conditions have led to the following tentative conclusions regarding earthquake resistant designs for reinforced earth walls:

1. The Mononobe-Okabe pseudo static seismic coefficient method gives reasonable predictions of the location of the failure plane in the back-fill, but seriously under estimates the magnitude of the maximum tie forces developed under seismic loading.
2. Although under carefully controlled laboratory conditions, the maximum as-constructed static tie forces will be closely defined by an active Rankine lateral earth pressure, very slight disturbances such as might be expected during routine field construction and compaction or small earthquakes will raise these forces to an approximate at-rest lateral earth pressure. Hence an at-rest earth pressure is recommended as a minimum for static design.
3. A seismic stress design concept was developed from model shaking table tests. It took the form of a straight line envelope which defines the maximum seismic lateral stress behind a reinforced earth wall as a function of the input acceleration.
4. Use of response spectra and modal participation techniques are recommended for obtaining the input acceleration for use with the seismic stress design envelope.

5. Dynamic finite element analyses with a program which uses bar elements for the ties, and appropriate non-linear strain dependent modulus and damping in the soil led to calculated tie forces which were in reasonable agreement with the tie forces determined from the proposed seismic design envelope.
6. Because failure by tie breaking leads to complete catastrophic collapse of the wall, whereas failure by tie pull out involves only a ductile type of lateral movement during intense shaking, it is recommended that seismic designs be made to insure that tie pull out is the most probably mode of failure. It is tentatively suggested that this may be accomplished using mild steel ties along with lateral earth pressures indicated by the proposed design stress envelope; using a factor of safety of 2.0 on the yield strength, and 4.0 on the peak soil-tie coefficient of friction; and including only the length of tie behind a 60° failure wedge as effective in resisting pull out.
7. Considerable more work is required to better define and understand most aspects of the behavior of reinforced earth under both static and seismic loading. While analytical and experimental studies on small laboratory structures offer many advantages, data from full scale structures under field conditions are also badly needed.

ACKNOWLEDGEMENTS

The computer program QUAD4 was obtained from the Geotechnical Division, University of California at Berkeley. Modification to include elements was done by Mr. Tac Udaka under the direction of Professor J. Lysmer, University of California, Berkeley. A major amount of assistance was provided by Mr. B. Patton, graduate research assistant, UCLA, during the experimental studies. The shaking table was constructed by Mr. B. D. Adams under the direction of Dr. R. B. Matthiessen, while both were at UCLA. Considerable benefit was derived from discussions with Mr. J. Chang of the California Division of Highways who also provided prepublished data from their field experimental reinforced earth wall. Financial support was provided by the National Science Foundation.

REFERENCES

1. Beaton, J. L., Forsyth, R. A. and Chang, J. C., "Design and Field Behavior of the Reinforced Earth Embankment - Road 39", Report of the California Department of Transportation, Division of Highways, Sacramento, California, Paper presented at the ASCE National Meeting, Los Angeles, California, January 1974.
2. Blume, J. A., Newmark, N. M. and Corning, L. H., "Design of Multistory Reinforced Concrete Buildings for Earthquake Motions", Portland Cement Association Publication, 1961.
3. Goodman, R. E. and Seed, H. B., "Earthquake Induced Displacements In Sand Embankments", Journal of the Soil Mechanics and Foundations Division, ASCE, Vol. 92, No. SM2, March 1966, pp. 125-146.
4. Hurty, W. C. and Rubenstein, M. F., "Dynamics of Structures", Prentice Hall, 1969.
5. Idriss, I. M. and Seed, H. B., "Seismic Response of Horizontal Soil Layers", Journal of the Soil Mechanics and Foundations Division, ASCE, Vol. 94, No. SM4, July 1968, pp. 1003-1031.
6. Idriss, I. M., Lysmer, J., Wang, R. and Seed, H. B., "QUAD-4, A Computer Program for Evaluating the Seismic Response of Soil Structures by Variable Damping", Report No. EERC 73--16, July 1973.
7. Lee, K. L., Adams, B. D. and Vagneron, J. J., "Reinforced Earth Walls", Report to the National Science Foundation, UCLA-ENG 7233, April 1972.
8. Lee, K. L., Adams, B. D. and Vagneron, J. J., "Reinforced Earth Retaining Walls", Journal of the Soil Mechanics and Foundations Division, ASCE, Vol. 99, No. SM10, October 1973, pp. 745-764.
9. Newmark, N. M., "Effects of Earthquakes on Dams and Embankments", Geotechnique, Vol. 15, No. 2, June 1965, pp. 139-173.
10. Richardson, G. N., "The Response of Reinforced Earth Walls to Vibratory Loading", Master of Science Thesis, UCLA, 1973.
11. Seed, H. B. and Idriss, I. M., "Soil Moduli and Damping Factors for Dynamic Response Analyses", Report No. EERC 70-10, University of California, Berkeley, December 1970.
12. Seed, H. B. and Whitman, R. V., "Design of Earth Retaining Structures for Dynamic Loads", ASCE Specialty Conference on Lateral Stresses, Cornell University, 1970, pp. 103-147.
13. Thomson, W. T., "Vibration Theory and Applications", Prentice-Hall, 1965.
14. Uesawa, H. et al., "A Large Scale Experiment on Reinforced Earth" (In Japanese), Publication of the Japanese National Railways Research Institute, April 1969, pp. 223-226.
15. Uesawa, H., "A Conception and Basic Experiment on Reinforced Earth Method (In Japanese), Publication of the Japanese National Railways Research Institute, April 1968, pp. 206-212.
16. Uesawa, H. and Nasu, M., "Anti-Earthquake Measures for Embankment on a Weak Ground", Proceedings 5th World Conference on Earthquake Engineering, Paper 40, Rome, 1973.

